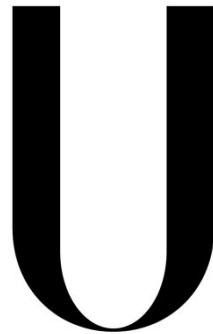


UNIVERSIDADE DE LISBOA

Faculdade de Medicina de Lisboa



LISBOA

UNIVERSIDADE
DE LISBOA

A novel role for EXP2 in invasion by *Plasmodium* sporozoites

João Tiago Carvalho Jordão de Mello Vieira

Orientadores: Prof. Dra. Maria Manuel Dias da Mota

Dra. Vanessa Alexandra Zuzarte-Luís

**Tese especialmente elaborada para obtenção do grau de
Doutor em Ciências Biomédicas, Especialidade em Microbiologia e Parasitologia**

2020

UNIVERSIDADE DE LISBOA

Faculdade de Medicina de Lisboa



A novel role for EXP2 in invasion by *Plasmodium* sporozoites

João Tiago Carvalho Jordão de Mello Vieira

Orientadores: Prof. Dra. Maria Manuel Dias da Mota

Dra. Vanessa Alexandra Zuzarte-Luís

Tese especialmente elaborada para obtenção do grau de

Doutor em Ciências Biomédicas, Especialidade em Microbiologia e Parasitologia

Júri:

Presidente: Doutor José Augusto Gamito Melo Cristino, Professor Catedrático e Presidente do Conselho Científico da Faculdade de Medicina da Universidade de Lisboa

Vogais: Doctor Maryse Lebrun, Research Director da Université de Montpellier (France);

Doctor Olivier Silvie, Investigator e Team Leader do Centre d'Immunologie et des Maladies Infectieuses (France);

Doutora Luísa Miranda Figueiredo, Investigadora Principal do Instituto de Medicina Molecular - João Lobo Antunes, unidade de investigação associada à Faculdade de Medicina da Universidade de Lisboa;

Doutor António Manuel Barbeiro Mendes, Post doctoral Investigator do Instituto de Medicina Molecular – João Lobo Antunes, unidade de investigação associada à Faculdade de Medicina da Universidade de Lisboa;

Doutora Maria Manuel Dias da Mota, Professora Associada Convidada com Agregação da Faculdade de Medicina da Universidade de Lisboa (Orientadora)

**Financiado pela Fundação para a Ciência e a Tecnologia,
através do Programa Doutor *Lisbon BioMed*, SFRH/BPD/52226/2013**

2020

A impressão desta tese foi aprovada pelo Conselho Científico da Faculdade de Medicina de Lisboa em reunião de 17 de setembro de 2019.

As opiniões expressas nesta publicação são da exclusiva responsabilidade do seu autor.

Summary

Plasmodium parasites, the causative agents of malaria, possess a translocon that exports parasite proteins into the infected erythrocyte, beyond the confines of the parasite. The parasite pore-forming protein Exported Protein 2 (EXP2) is a component of this translocon and the pore through which proteins are exported. Although EXP2, and other translocon components, are also expressed during the mosquito and liver stages of infection, their function remains unexplored.

To study the function of EXP2 during the liver stage of infection, we used a genetically engineered *Plasmodium berghei* parasite line, generated by our collaborators. In this parasite line, the EXP2 gene is silenced during the mosquito stage, as the 3' untranslated region of the EXP2 gene is excised, generating EXP2 knock-out sporozoites. The sporozoite is the mosquito transmissible form of the parasite, that when deposited in the mammalian host, infects the liver, giving rise to the pre-erythrocytic stage of *Plasmodium* infection.

Using this transgenic parasite line, we observed that invasion of the hepatocyte by EXP2 conditional knock-out parasites is impaired, both in C57Bl/6J mice and in the hepatoma cell line HepG2, suggesting that invasion is dependent on EXP2.

Using a combination of fluorescence and electron microscopy techniques, we show that EXP2 is present in the hepatocyte-infectious sporozoite in vesicles, in the apical end of the parasite. These vesicles are important for the invasion process, as they are discharged by the sporozoite and contain proteins important for hepatocyte adhesion and entry in the host cell. Stimulating sporozoites with conditions that mimic the host cell milieu, we observed that EXP2 relocates to the surface of the mosquito-transmitted sporozoite and that it is secreted by the sporozoite.

We also observed that invasion defect of the EXP2 conditional knock-out parasites can be rescued by the exogenous administration of recombinant EXP2 or recombinant α -

Summary

hemolysin, another pore-forming protein, suggesting that the function of EXP2 is through its pore-forming ability on the membrane of the hepatocyte.

Invasion of cells via pores has been documented for a variety of intracellular pathogens, like *Trypanosoma cruzi*, *Listeria monocytogenes* and adenovirus. Importantly, the pore does not allow the parasite to cross the membrane, rather it induces changes in the host cell that make it endocytose the wounded region of the membrane. We observed that recombinant EXP2 can recapitulate the major hallmarks of the membrane repair pathway. On one hand, treating cells with recombinant EXP2 leads to influx of calcium to HepG2 cells. Moreover, invasion of *Plasmodium berghei* sporozoites is dependent of acid Sphingomyelinase and finally, the invasion defect of the EXP2 conditional knock-out sporozoites can be rescued by exogenously adding acid sphingomyelinase. This suggest that indeed EXP2 induces hepatocyte membrane repair, which plays a key role in parasite invasion.

Overall, while our data show that Plasmodium parasites uses EXP2 for divergent functions in its life cycle, it also highlights the convergent evolution of different intracellular pathogens, which have developed similar strategies to take advantage of cellular responses to membrane damage, hitchhiking their way into the host cell.

Keywords: Malaria; *Plasmodium* liver stage; Sporozoites; EXP2; Hepatocyte invasion; Membrane repair mechanisms; Acid sphingomyelinase.

Resumo

A malária é uma doença tropical, causada por parasitas do género *Plasmodium*. Estes parasitas são transmitidos pela picada de um mosquito infectado do género *Anopheles*. Quando o mosquito pica um hospedeiro não infectado, transmite esporozoítos para a corrente sanguínea, que migram até ao fígado, onde infectam um hepatócito, iniciando assim a fase hepática da infecção. Dentro desta célula, o esporozoíto diferencia-se, cresce, replica e transforma-se em merozoítos. No final da fase hepática, os merozoítos são libertados do hepatócito para a corrente sanguínea. Na corrente sanguínea, dá-se a fase sanguínea da infecção, onde os merozoítos infectam eritrócitos ciclicamente. O ciclo de vida do parasita fica completo quando um mosquito, numa refeição de sangue, ingere os gâmetas do parasita, que se fundem no estômago do mosquito dando origem a mais esporozoítos.

Durante a fase sanguínea da infecção, os parasitas modificam o eritrócito que infectam, ao exportar as suas próprias proteínas para o citosol do eritrócito. Isto é conseguido através da acção de um complexo proteico chamado *Plasmodium* Translocon of Exported Proteins (Translocção de Proteínas Exportadas de *Plasmodium* – PTEX) que é semelhante aos Sistemas Tipo 3 de Secreção de Proteínas bacterianos. Crucial para a acção do PTEX é a proteína que forma o poro na membrana, chamada Exported Protein 2 (Proteína Exportada 2 – EXP2). É através do poro de EXP2 que as proteínas são transferidas do parasita para o eritrócito. Recentemente, a EXP2 foi identificada durante a fase hepática da infecção, embora a sua função não seja conhecida.

Por isso, os 3 objectivos desta tese são:

- 1) Estudar o efeito da ausência da EXP2 durante a fase hepática da infecção;
- 2) Estudar a dinâmica de expressão e localização de EXP2 no esporozoíto;
- 3) Descrever o mecanismo de invasão dos hepatócitos pelos esporozoítos.

Para estudar a função da EXP2, usámos um parasita geneticamente modificado, em que a expressão do gene EXP2 é diminuída antes da fase hepática. Para construir este parasita transgénico foram inseridas sequências FRT na região 3' não traduzida do gene da EXP2. Estas regiões são reconhecidas pela recombinase Flp, que excisa a região 3' não

Resumo

traduzida do gene *EXP2* do DNA. Em *Plasmodium*, genes que não possuam regiões 3' não traduzidas não são expressos. Na nossa linha de parasitas, a recombinase Flp está sob controlo do promotor do gene Up-regulated in Infectious Sporozoites 4 (Sobre-regulada em esporozoítos infecciosos 4 – UIS4), que é expresso no final da fase do ciclo de vida que se passa no mosquito. Assim, conseguimos obter esporozoítos sem expressão da *EXP2*, condicional à fase hepática (*EXP2* cKO). Como controlo, utilizámos parasitas que têm a região 3' não traduzida com sequências FRT mas que não expressam a recombinase (WT).

Utilizando os parasitas *EXP2* cKO verificámos que estes causam menor infecção hepática do que parasitas WT em ratinhos C57Bl/6J. Estes resultados são reprodutíveis *in vitro*, utilizando a linha celular de hepatoma HepG2. Ao fixar estas células a vários tempos após a infecção, observámos que os parasitas *EXP2* cKO infectam menos células que os parasitas WT. Este resultado é evidente desde 2 horas após a infecção e mantém-se durante as 48 horas da infecção hepática.

Durante as 2 horas iniciais da infecção hepática, o parasita transita por três fenómenos consecutivos, motilidade, migração e invasão. Os parasitas *EXP2* cKO demonstram níveis de motilidade e de migração semelhantes aos parasitas WT, estando apenas afectados no último destes 3 fenómenos, a invasão.

Os resultados anteriores indicaram-nos que a proteína *EXP2* está envolvida no processo de invasão dos hepatócitos. Para isso, a proteína tem de ser expressa nos esporozoítos. Por isso, dissecámos esporozoítos de mosquitos infectados e fizemos imunodeteção desta proteína nos esporozoítos. Encontramos esta proteína no citosol do esporozoíto, num padrão pontuado. Utilizando microscopia electrónica, observámos que a proteína *EXP2* se encontrava dentro ou na periferia de vesículas. Estas vesículas são importantes para os parasitas do filo Apicomplexa, pois a sua secreção ordenada permite aos parasitas deste filo a invasão da sua célula alvo. Se a proteína *EXP2* está envolvida no processo de invasão, é possível fazer com que seja secretada. De facto, ao estimular os parasitas com um aumento de temperatura para 37°C e incubação com soro, os parasitas secretam a proteína *EXP2*.

Como foi explicado anteriormente, a proteína *EXP2* tem a capacidade de fazer poros em membranas e possivelmente utiliza esta função durante o processo de invasão do

hepatócito. Conhecem-se outros patogénios que utilizam proteínas que formam poros como mecanismo de invasão. O mecanismo que estes patogénios utilizam é produzir um poro na membrana da célula alvo, poro esse que permite a entrada de cálcio para a célula alvo. A entrada de cálcio leva a uma cascata de sinalização que culmina na actividade da enzima esfingomielinase ácida no lado de fora a membrana plasmática, que induz endocitose da região da membrana que tem o poro que, por conseguinte, estará ligada ao parasita. Por exemplo, este mecanismo foi descrito em *Trypanosoma cruzi*, *Listeria monocytogenes* e adenovírus.

Para confirmar se este modelo de invasão ocorre em esporozoítos de *Plasmodium*, fizemos os ensaios de invasão com parasitas WT e EXP2 cKO na presença de proteínas recombinantes que formam poros, a EXP2 de *Plasmodium falciparum* e a alfa-hemolisina de *Staphylococcus aureus*. Ambas conseguem fazer com que os parasitas EXP2 cKO invadam como os parasitas WT, revertendo a sua falha de infecção.

Por outro lado, observámos que a proteína recombinante EXP2 tem a capacidade de elevar os níveis de cálcio intracelular, quando as células HepG2 são expostas a ela.

Finalmente, ao repetir os ensaios de invasão na presença de esfingomielinase ácida, conseguimos novamente converter os parasitas EXP2 cKO para níveis de invasão dos parasitas WT.

Resumindo, parasitas que não possuam a proteína EXP2 têm dificuldades em invadir hepatócitos. Estas dificuldades podem ser supridas se a proteína EXP2 for adicionada exogenamente durante a invasão. Numa infecção normal, pensamos que a proteína poderá ser secretada pelo esporozoíto para a membrana do hepatócito. Sabemos que esta proteína tem capacidade de fazer poros em membranas, com capacidade de entrada de cálcio. Isto activa um processo de reparação de membrana, via endocitose da porção da membrana que tem o poro, que facilita a invasão do parasita.

Para concluir, é interessante referir que este mecanismo de invasão não é único na Natureza, sendo por isso interessante a evolução convergente de vários patogénios para utilizar o mecanismo de reparação de membrana como modo de entrada em células humanas. De facto, tanto os níveis de invasão do parasita *Trypanosoma cruzi* como

Resumo

Plasmodium berghei, são afectados com a utilização de desipramina, um inibidor da enzima esfingomielinase ácida, o culminar do processo de reparação da membrana. É por isso um mecanismo importante, que pode ser visto como um alvo farmacológico de grande espectro.

Palavras-chave: Malária; Fase hepática de *Plasmodium*; Esporozoítos; EXP2; Invasão de hepatócitos; Mecanismos de Reparação de Membranas; Esfingomielinase ácida.

Acknowledgements

I would like to thank many people for this work:

Ana Parreira and Sofia Marques for all the help in the lab and with the mosquitos.

All the PhD students from the lab, especially Sara Baptista, Viriato M'bana, Aparajita Lahree and Inês Marreiros, for all the help with the major and minor details of protocols, such as Western Blots, specifically the order of the gel and the membrane.

Special thanks to the post-docs of the lab, such as Ângelo Chora, Inês Bento, Ksenija Slavic, for always pushing me to go deeper and more thorough into my results, conclusions and crazy ideas.

The IMM technicians: Andreia Pinto for all her Electron Microscopy work on sporozoites, António Temudo and Ana Margarida Nascimento for all their help with fluorescence microscopes.

Other students at IMM, such as Margarida Ruivo, Francisco Aresta-Branco, Jorge Santos, Maurice Itoe, for setting the bar and for showing me how a PhD is conducted.

I thank also my family and friends, who accepted all the perks of the PhD, such as working late, on weekends, on birthday parties (sometimes all three at the same time) and for being moody and tired most of the times I did not have to work.

Finally, I would like to thank 3 people.

Many thanks to Maria Mota, my supervisor, who accepted me in the lab, when I knew nothing of malaria and working with parasites and mice... Somehow, she had faith in me!

Many thanks to Patrícia Meireles, who was always at my side, on the good days and the bad days, who helped me transform the latter into the former.

Many thanks to Vanessa Zuzarte-Luís, who taught me everything I know about malaria and about being a scientist (I think I turned out fine, right?). I was privileged to have done the PhD with your supervision.

Table of Contents

Summary	i
Resumo	iii
Acknowledgements	vii
Figure and Table Index	xi
Abbreviations.....	xiii
Chapter I – Introduction	1
1. Malaria	3
2. The life cycle of <i>Plasmodium</i> parasites.....	13
3. The invasion of mammalian cells by <i>Plasmodium</i> parasites.....	19
4. Living beyond of the vacuole.....	30
Chapter II – Aims	37
Chapter III – Materials and Methods	41
1. Parasites	43
2. Recombinant Protein production and purification	44
3. Chemicals and Proteins	45
4. Infection of <i>Mus musculus</i> and parasite burden determination in mice.....	45
5. Infection of human hepatoma cell line HepG2 and live cell imaging	47
6. Immunofluorescence microscopy assays.....	48
7. Flow Cytometry assays	51
8. Nucleic acid extraction and analysis	53
9. Proteins extraction and analysis	54
10. Electron Microscopy	56
11. Statistical analysis.....	56
Chapter IV – Results	61
1. EXP2 is necessary for the invasion of hepatocytes by <i>Plasmodium</i> sporozoites	63
2. Dynamics of EXP2 protein in the sporozoite	81
3. Membrane repair pathway as a mechanism of entry	89
Chapter V – Discussion	111
References	123
<i>Curriculum Vitae</i> and Publications.....	151

Figure and Table Index

Figure 1 - Malaria endemic countries in 2016	5
Figure 2 - Drawings by Alphonse Laveran of erythrocytes infected with <i>P. falciparum</i> parasites	13
Figure 3 - Drawings of Battista Grassi of <i>P. falciparum</i> sporulating oocyst in the midgut of <i>Anopheles</i> spp mosquitos	14
Figure 4 - First images of <i>P. falciparum</i> infected hepatocytes	15
Figure 5 - Cladogram of the phylogeny of <i>Plasmodium</i> and related parasites	17
Figure 6 - Mechanisms of invasion by bacteria	19
Figure 7 – The apical complex of Apicomplexan parasites	21
Figure 8 - Invasion of erythrocytes by <i>Plasmodium falciparum</i> merozoites	24
Figure 9 - Host receptors and parasite ligands involved in red blood cell invasion by <i>P. vivax</i> (left) and <i>P. falciparum</i> (right)	26
Figure 10 - Liver invasion by <i>Plasmodium</i> sporozoites	27
Figure 11 - Protein export and erythrocyte remodelling by <i>Plasmodium</i> parasites	31
Figure 12 - Structure of the PTEX complex and of its proteins	33
Figure 13 - Protein and membrane export in hepatic stages of malaria infection	36
Figure 14- Example of the strategy used to analyze invasion and traversal of HepG2 cells at 2h after infection	52
Figure 15 - Example of the strategy used to analyze cells that have a permeabilized plasma membrane.....	53
Figure 16 – Parasite liver load in infected mice at different hours after infection	64
Figure 17 – Number of infected HepG2 cells at different hours after infection.....	65
Figure 18 - EXP2 staining in WT and EXP2 cKO sporozoites	66
Figure 19 – Expression of EXP2 at EEFs at 24 and 48 hours after infection and proportion of parasites with EXP2 at different stages of infection	67
Figure 20 – Size of exoerythrocytic forms in HepG2 cells at different hours after infection.....	68
Figure 21 – Expression of EXP2, AMA1 and UIS4 genes during liver stages of <i>Plasmodium</i> infection	69
Figure 22 – Gliding motility of WT or EXP2 cKO sporozoites	71
Figure 23 – Traversal ability of WT and EXP2 cKO sporozoites.....	73
Figure 24 - Number of extracellular and intracellular sporozoites 2 hours after infection of HepG2	74
Figure 25 – Number of infected HepG2 cells at different minutes after infection	75
Figure 26 – Correlation between WT prevalence in the EXP2 cKO population and its invasion rate	76
Figure 27 – Number of infected HepG2 cells at different minutes after infection	77
Figure 28 – Expression of EXP2, GAP45 and EXP1 genes during invasion stages of <i>Plasmodium</i> liver infection.....	78
Figure 29 – Electron micrographs of sporozoites immunolabelled with EXP2.....	81
Figure 30 – EXP2 localisation in freshly dissected sporozoites	82

Resumo

Figure 31 – EXP2 localisation in activated sporozoites	83
Figure 32 – EXP2 localisation in non-permeabilized sporozoites.....	84
Figure 33 - EXP2 localization before and after activation	85
Figure 34 – Protein secretion after sporozoite activation.....	86
Figure 35– Number of infected HepG2 cells following rEXP2 treatment	90
Figure 36 – Number of infected HepG2 cells following different regimens of rEXP2 treatment .	91
Figure 37 – Number of infected HepG2 cells following addition of rEXP2 protein at different times after infection	92
Figure 38 – Number of infected HepG2 cells following α -HL treatment	93
Figure 39 – Number of infected HepG2 cells following rSLO treatment	94
Figure 40 – Percentage of Propidium Iodide (PI) positive cells after treatment with rEXP2	95
Figure 41 – Calcein leakage after treatment with rEXP2 protein.....	96
Figure 42 – Calcium reported Gcamp6f fluorescence variation after exposure to rEXP2.....	98
Figure 43 – Traversal and infection of HepG2 cells in different cell culture media	99
Figure 44 – Traversal and infection of HepG2 cells in DMEM with decreasing calcium concentrations	100
Figure 45 – Traversal and infection of HepG2 cells in RPMI with increasing calcium concentrations	101
Figure 46 – Traversal and infection of HepG2 cells in DMEM with increasing iron concentrations	102
Figure 47 – Number of infected cells at 2 hours after infection in the absence of calcium.....	103
Figure 48 - Gliding and traversal of WT sporozoites in the presence or absence of extracellular calcium	104
Figure 49 – Number of infected HepG2 cells following GW4869 or desipramine treatment	105
Figure 50– Number of infected HepG2 cells after acid sphingomyelinase knock-down.....	106
Figure 51– Number of infected HepG2 cells following addition of aSMase protein at different times after infection	107
Figure 52 – Number of infected HepG2 cells following acid sphingomyelinase treatment.....	108
Figure 53 - Model for the action of Plasmodium EXP2.....	113
Table 1 - Number of cells used per procedure and plate type.....	47
Table 2 - List of Primary antibodies used in this study	57
Table 3 - List of Primers used in this study.	58

Abbreviations

Full name	Abbreviation
<u>A</u> cid <u>s</u> phingom <u>y</u> elin <u>a</u> se	aSMase
<u>A</u> denosine <u>t</u> riphosphate	ATP
<u>A</u> lpha <u>h</u> emolysin	α -HL
<u>A</u> pical <u>m</u> embrane <u>a</u> ntigen <u>1</u>	AMA1
<u>A</u> pical <u>r</u> ing	APR
Arginine	R
<u>A</u> rtemisinin-based <u>c</u> ombination <u>t</u> herapies	ACTs
Aspartate	D
<u>C</u> alcium- <u>d</u> ependent <u>p</u> rotein <u>k</u> inase 4	CDPK4
<u>C</u> ell- <u>t</u> raversal protein for <u>o</u> okinete and <u>s</u> porozoite	CelTOS
<u>C</u> ircumsporozoite <u>p</u> rotein	CSP
<u>C</u> luster of <u>d</u> ifferentiation <u>81</u>	CD81
<u>c</u> onditional <u>K</u> nock- <u>O</u> t	cKO
<u>C</u> ysteine- <u>r</u> ich <u>p</u> rotective <u>a</u> ntigen	CyRPA
<u>D</u> eoxyribonucleic <u>a</u> cid	DNA
<u>E</u> thylenediaminetetraacetic <u>a</u> cid	EDTA
<u>E</u> xoerythrocytic <u>f</u> orm	EEF
<u>E</u> ndoplasmic <u>r</u> eticulum	ER
<u>E</u> phrin <u>A2</u>	EphA2
<u>E</u> rythrocyte <u>b</u> inding <u>a</u> ntigen <u>s</u>	EBAs
<u>E</u> rythrocyte <u>p</u> lasma <u>m</u> embrane	ePM
<u>E</u> xported <u>p</u> rotein- <u>i</u> nteracting <u>c</u> omplex	EPIC
<u>E</u> xported protein 2	EXP2
<u>G</u> reen <u>f</u> luorescent <u>p</u> rotein	GFP
<u>G</u> lucose- <u>6</u> - <u>p</u> hosphate <u>d</u> ehydrogenase	G6PD
Glutamate	E
Glutamine	Q
<u>G</u> reen <u>f</u> luorescent <u>p</u> rotein	GFP
<u>G</u> olgi	Go
<u>H</u> eat <u>s</u> hock <u>p</u> rotein <u>70</u>	HSP70
<u>H</u> eat <u>s</u> hock <u>p</u> rotein <u>70-x</u>	HSP70-x

Resumo

<u>H</u> eat <u>s</u> hock protein 101	HSP101
<u>H</u> emagglutinin	HA
<u>H</u> emolysin <u>E</u>	HlyE
<u>H</u> eparan <u>s</u> ulfate proteoglycans	HSPGs
<u>I</u> mmunofluorescence <u>A</u> ssay	IFA
<u>I</u> ndoor <u>r</u> esidual <u>s</u> praying	IRS
<u>I</u> nhibitor of <u>c</u> ysteine <u>p</u> roteases	ICP
<u>I</u> nn <u>e</u> r <u>m</u> embrane <u>c</u> omplex	IMC
<u>I</u> nsecticide- <u>t</u> reated bed <u>n</u> ets	ITNs
<u>I</u> ntra-erythrocytic <i>P. berghei</i> - <u>i</u> nduced <u>s</u> tructures	IBIS
<u>I</u> ntra-erythrocytic <i>P. berghei</i> - <u>i</u> nduced <u>s</u> tructures <u>p</u> rotein <u>1</u>	IBIS1
<u>L</u> eucine	L
<u>L</u> ow <u>d</u> ensity lipoprotein <u>r</u> eceptor	LDLR
<u>L</u> iver- <u>s</u> pecific protein <u>2</u>	LISP2
<u>L</u> oop-mediated isothermal <u>a</u> mplification	LAMP
<u>M</u> erozoite <u>a</u> pical <u>e</u> rythrocyte- <u>b</u> inding ligand	MAEBL
<u>M</u> erozoite <u>s</u> urface protein <u>1</u>	MSP1
<u>M</u> icronemes	Mn
<u>M</u> icrotubules	Mt
<u>N</u> ucleus	Nu
<u>N</u> uclear <u>f</u> actor <u>k</u> appa light-chain-enhancer of activated <u>B</u> cells	NF-κB
<u>P</u> arasitophorous <u>v</u> acuolar protein- <u>1</u>	PV1
<u>P</u> arasitophorous <u>v</u> acuole	PV
<u>P</u> arasitophorous <u>v</u> acuole <u>m</u> embrane	PVM
<u>P</u> hosphatidylinositol <u>3</u> - <u>p</u> hosphate	PI₃P
<u>P</u> lasma <u>m</u> embrane	PM
<i>Plasmodium</i>	<i>P.</i>
<i>Plasmodium berghei</i>	<i>Pb</i>
<i>Plasmodium falciparum</i> <u>e</u> rythrocyte <u>m</u> embrane <u>p</u> rotein <u>1</u>	<i>Pf</i>EMP1
<i>Plasmodium</i> <u>t</u> ranslocon of <u>e</u> xported proteins	PTEX
<i>Plasmodium</i> <u>t</u> ranslocon of <u>e</u> xported protein 88	PTEX88
<i>Plasmodium</i> <u>t</u> ranslocon of <u>e</u> xported protein 150	PTEX150
<u>P</u> olymerase <u>c</u> hain <u>r</u> eaction	PCR
<u>P</u> ropidium <u>I</u> odide	PI

Abbreviations

<u>P</u> rotein <u>e</u> xport <u>e</u> lement	PEXEL
<u>P</u> rotein <u>k</u> inase <u>C</u> <u>z</u> eta	PKCζ
<u>P</u> rotein <u>k</u> inase <u>G</u>	PKG
<u>R</u> ecombinant <u>a</u> lpha- <u>h</u> emolysin	rα-HL
<u>R</u> ecombinant <u>E</u> xported <u>P</u> rotein <u>2</u>	rEXP2
<u>R</u> ecombinant <u>s</u> treptolysin <u>O</u>	rSLO
<u>R</u> eticulocyte-binding <u>h</u> omologous protein	RH
<u>R</u> eticulocyte-binding <u>h</u> omologous protein <u>5</u>	RH5
<u>R</u> ibon <u>u</u> cleic <u>a</u> cid	RNA
<u>R</u> ibosomal <u>r</u> ibon <u>u</u> cleic <u>a</u> cid	rRNA
<u>R</u> hoptries	Rh
<u>R</u> hoptry- <u>a</u> ssociated <u>p</u> rotein <u>2/3</u>	RAP2/3
<u>R</u> hoptry <u>n</u> eck protein	RON
<u>R</u> hoptry <u>n</u> eck protein <u>2</u>	RON2
<u>R</u> hoptry <u>n</u> eck protein <u>4</u>	RON4
<u>R</u> hoptry <u>b</u> ulb protein	ROP
<u>S</u> cavenger <u>r</u> eceptor class <u>B</u> type <u>1</u>	SR-BI
<u>S</u> porozoite <u>p</u> rotein <u>e</u> ssential for <u>c</u> ell <u>t</u> raversal <u>1</u>	spect1
<u>S</u> porozoite <u>p</u> rotein <u>e</u> ssential for <u>c</u> ell <u>t</u> raversal <u>2</u>	spect2
<u>S</u> ulfadoxine- <u>p</u> irimethamine	SP
<u>T</u> hio <u>r</u> edoxin <u>2</u>	TRX2
<u>T</u> hrombospondin <u>r</u> elated <u>a</u> nonymous <u>p</u> rotein	TRAP
<u>T</u> ubov <u>e</u> sicular <u>n</u> etwork	TVN
<u>U</u> p-regulated in <u>i</u> nfective <u>s</u> porozoites gene <u>4</u>	UIS4
<u>W</u> ild <u>T</u> ype	WT
<u>W</u> orld <u>H</u> ealth <u>O</u> rganization	WHO

Chapter I – Introduction

1. Malaria

Malaria is an ancient disease that currently affects over 200 million people worldwide [1]. It is caused by intracellular protozoan parasites of the genus *Plasmodium*. It poses one of the biggest health concerns worldwide, being the World Health Organization (WHO) the world leader in policy making for malaria eradication and driving the standard goals for basic and applied research in the field.

These parasites are thought to exist for 40 million years and have been one of the biggest pressures for the evolution of the human genome [2]. Of the 199 *Plasmodium* (*P.*) spp [3], five cause disease in humans, being *P. falciparum* the most prevalent and deadliest of the five [1]. All of the mammalian-infectious parasites are transmitted by the bite of infected *Anopheles* female mosquitos [4].

Briefly, *Plasmodium* parasites infect humans when they are injected into the bloodstream by the bite of infected mosquitos. These parasites, at this stage termed sporozoites, home to the liver, where they infect a hepatocyte. Inside the hepatocyte, one sporozoite differentiates into thousands of merozoites, a new form of the parasite, that, when released into circulation, infects erythrocytes. Merozoites grow inside erythrocytes, producing tens of new merozoites, that infect new erythrocytes. Merozoites can create infinite cycles of infection of erythrocytes, which causes the variety of symptoms that encompass the disease malaria.

During the course of the infection, some merozoites differentiate into male and female gametocytes, that, when uptaken by uninfected mosquitos during a blood meal, fuse to produce a diploid form of the *Plasmodium* parasite, initially called zygote, that in a day transforms into a motile ookinete. The ookinete migrates to the basal lamina of the mosquito midgut, where it changes into an oocyst, that later differentiates into hundreds of sporozoites. These sporozoites can be delivered into a new host, during the next blood meal of the newly infected mosquito (reviewed in [5] and further detailed below).

I – Introduction

1.1. The symptoms and complications of *Plasmodium* blood infection

Plasmodium blood infection in a naïve individual leads invariably to fever, with other symptoms like rigors, headache, nausea and muscle pain often accompanying the disease. Fever is caused when the parasite ruptures the erythrocytes it infects, which occurs every 48h (in the case of *P. falciparum*, *P. ovale* or *P. vivax*) or 72h (in the case of *P. malariae*) [6]. If the infection is treated with the appropriate medicines, it can be cleared within a few days.

If the infection is allowed to progress unchallenged, complicated malaria can develop. All of these complications arise because of exponential parasite multiplication, parasite adherence to microvasculature (causing obstruction of blood flow), activation of endothelium (caused by the obstruction) and higher inflammatory status of the individual (induced by the activated endothelium) [7,8]. All of these events cause a vicious cycle that progressively debilitates the infected host [7,8].

In the case of *P. falciparum*, the deadliest of the malaria parasites, malarial complications include severe anemia (due to an exhaustion of red blood cells and of the bone marrow), cerebral malaria (coma caused by obstruction of capillaries in the brain, local inflammation and edema) and respiratory distress (lung tissue hypoxia caused by metabolic acidosis) [7,8]. *P. vivax* has been shown to also cause severe anemia and multi-organ failure [7]. This is, in a way, intriguing, because *P. vivax* achieves a lower parasite load, when compared to *P. falciparum*, and causes less intravascular obstruction [9].

Cases of severe malaria are more common in young children as successive infections lead to some degree of immunity by the infected individual. This correlates with progressively lower parasitaemias (presence of parasites in the blood) and less severe symptoms and complications (reviewed in [10]). The majority of protection can be attributed to circulating antibody titers against *Plasmodium* parasites [11], mostly against the *Plasmodium falciparum* erythrocyte membrane protein 1 (*PfEMP1*) protein [12]. However, there is no report of natural sterile immunity to *Plasmodium* infection.

1.2. Epidemiology of malaria

Malaria is a mosquito-borne disease, yet, despite the global distribution of the *Anopheles* mosquito, malaria transmission is currently confined to the tropical regions of the globe (**Figure 1**) [1]. 90% of the cases happen in sub-Saharan Africa (almost 30% of them in Nigeria), with the remaining 10% distributed by Southeast Asia (7%), Middle East (2%) and the Americas (1%) [1]. Most of the reported infections are caused by *P. falciparum* (96%) and the other 4% are caused *Plasmodium vivax* [1]. There are 3 other human infectious *Plasmodium* parasite strains, *P. malariae*, *P. ovale curtisi* and *P. ovale wallikeri* (the last two, although morphologically similar are in fact genetically distinct subspecies [13]) that can cause malaria in humans, but the number of malaria infections caused by them is residual and not accounted for by the WHO. There is another *Plasmodium* species, *P. knowlesi*, known to cause disease in humans through zoonosis, without confirmed human-to-human transmission [5,14].

Malaria is a treatable disease (discussed in greater detail below) yet it is still responsible for an estimated 429 000 deaths worldwide [1]. It has a global death rate of 2 deaths per 1000 cases, however 70% of total deaths were children under 5 years of age [1]. It was the seventh most common cause of death in low income countries in 2015, being

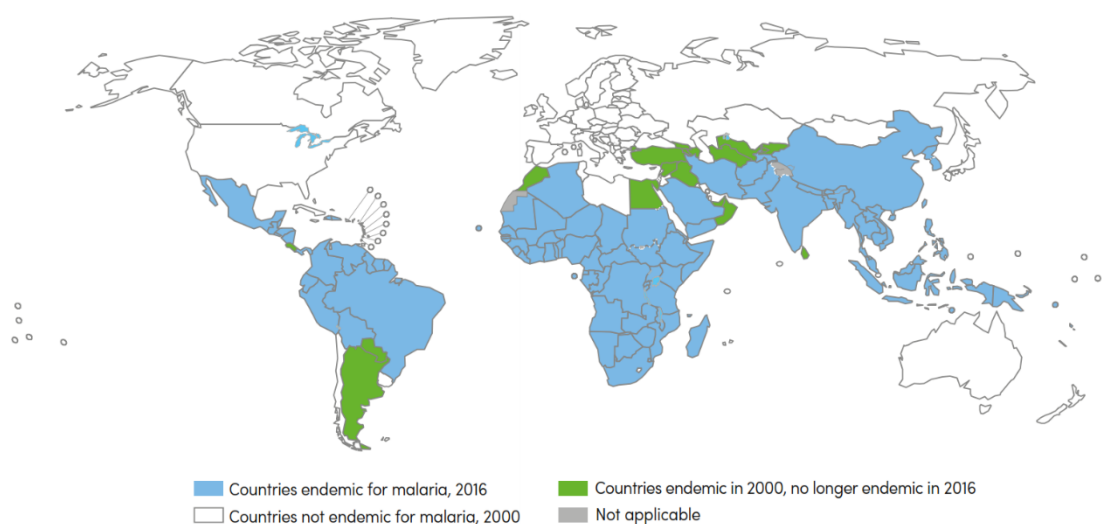


Figure 1 - Malaria endemic countries in 2016 (adapted from [1]). Blue represents countries with autoctones malaria cases. Green represents countries that were endemic for malaria in 2000 but have had no cases for at least 3 years. White represents countries without autoctone malaria cases since 2000.

I – Introduction

responsible for approximately 35 deaths per 100 000 inhabitants, similar to tuberculosis (<http://www.who.int/mediacentre/factsheets/fs310/en/index1.html>). The deadliest parasite is *P. falciparum* that is responsible for 99,3% of the fatalities [1].

1.3. Diagnosis of *Plasmodium* infection

The symptoms of malaria are non-specific and clinical suspicion relies primarily on the basis of fever or history of fever [15]. As fever can be caused by other infections and diseases, a rapid and definite diagnosis of malaria is needed before starting treatment [15].

The routine malaria diagnostic tests are microscopic analysis of Giemsa-stained blood films and the detection of circulating *Plasmodium* antigens [15–17]. Both techniques are fast (take less than 2 hours) but have disadvantages. Detection of parasites by blood film has a high limit of detection (>4-20 parasite/ μ L for a trained microscopist with high quality equipment) [18] and is time consuming (requires imaging of at least 100 fields of view) [16], giving rise to false negatives. Antigen detection is faster yet, has an even higher limit of detection [19] and it can detect antigens up to 28 days after the infection is cleared [20], giving rise to false positives.

The most sensitive and specific tests currently available are polymerase chain reaction (PCR) based techniques (reviewed in [21]), that mostly rely on the detection of species-specific 18S ribosomal ribonucleic acid (rRNA) in the blood of patients [22]. Molecular diagnostic tests take longer time to process (they require the extraction of deoxyribonucleic or ribonucleic acids, DNA or RNA, from patient samples, the PCR reaction and the readout of the result) and require the use of specialized equipment (thermocyclers for the PCR reaction) that are often absent in resource limited settings.

1.4. Treatment and chemoprevention of *Plasmodium* infections

Malaria treatment has been the subject of research for many years (reviewed in [23]). It reached a great importance when Bayer created chloroquine [24], a derivative from quinine (an old remedy against the disease made from the bark of the cinchona tree). This

drug kills the parasite during the blood stage and was the first line anti-malarial treatment in the 1950s and 60s [24]. However, the very polymorphic nature of the *Plasmodium* parasites meant that resistance appeared in the 1950s and spread to the entire world in the next years [25].

After the failure of chloroquine, several other anti-malarials were discovered/created yet resistance quickly ensued [23]. The discovery of artemisinin by Nobel laureate Tu Youyou in 1972 (reviewed in [26]) created new hope for malaria control and eradication. This drug and its derivatives are the fastest acting anti-malaria available [27] and were recommended as first-line treatment for malaria in 2006 [28]. Since artemisinin has a short half-life in circulation [29,30], malaria treatment consists of an artemisinin combination therapies (ACTs) that balance the short half-life of artemisinins with partner drugs with longer half-lives [15]. ACTs consist 5 combinations of an artemisinin derivative (dihydroartemisinin, artesunate or artemether) with a partner drug (amodiaquine, mefloquine, piperaquine, sulfadoxine-pyrimethamine (SP) or lumefantrine – all with longer half-lives), given for 3 days [15]. Some regions of the globe still harbor chloroquine sensitive strains of *P. vivax*, *ovale*, *malariae* and *knowlesi*, which should be treated with chloroquine to avoid the selection of parasites resistant to ACTs [15].

WHO further defines special risk groups, which have abnormal pharmacokinetics because of low or high body weight and co-infection with HIV or tuberculosis [15]. In these cases, the pharmacodynamics of the anti-malarials is affected, increasing the probability of treatment failure. For this reason, ACT dosage should be altered according to WHO recommendations [15]. Also, there is the risk that ACTs are teratogenic, even though recent data shows no cause for alarm [31]. The recommended treatment in the first trimester of pregnancy is quinine and clindamycin [15]. Treatment over the second and third trimester with ACTs is considered safe by the WHO [15].

Chemoprevention is a strategy designed by the WHO that should be provided to certain risk groups, such as pregnant women and young children. In women having their first or second pregnancy, SP should be given every month, starting in the second trimester of pregnancy [15,32]. For children under 1 year of age, SP should be given twice in the first year of life [15,33] and for children under 6 years of age, amodiaquine+SP treatment should

I – Introduction

be given monthly throughout transmission season [15,34]. Non-immune travelers should also perform chemoprevention with compounds that target the erythrocytic stage of disease prior, during and after travelling to malaria endemic regions [15,35,36].

To eliminate the disease in areas of low transmission, the gametocidal drug primaquine should also be given to infected individuals [15,37,38]. This reduces transmission burden in these regions, making local eradication possible.

Primaquine also has the advantage of killing hypnozoites from *P. vivax* and *P. ovale* in the liver of infected individuals [39], which are quiescent parasites forms that do not cause disease [40,41]. However, they can re-activate at a given time and start a new blood infection, causing a relapse in the patient [42–45]. However, primaquine is toxic to individuals with glucose-6-phosphate dehydrogenase (G6PD) deficiency [46], a common trait in malaria endemic regions, as it confers some degree of protection to malaria [47]. These patients can take primaquine but at a lower dose and should be monitored throughout the 14 days of treatment [15,48].

1.5. Anti-plasmodial vaccine

For successful malaria eradication, a vaccine against *Plasmodium* parasites is key. However, that has not been possible yet. The biggest challenge so far has been the high variability of its most immunogenic antigens and the low immunogenicity of the conserved sites/proteins [5,10].

The oldest studies that achieved complete sterile protection were based on the infection of human volunteers with radiation attenuated sporozoites [49], whose immunodominant antigen is the circumsporozoite protein (CSP) [50]. This started a collaboration between the Walter Reed Army Institute of Research and GlaxoSmithKline, that took more than 30 years to produce a vaccine candidate (reviewed in [51,52]). The RTS,S vaccine is a subunit vaccine based on CSP, in combination with Hepatitis B soluble Antigen and a liposome-based adjuvant. The vaccine entered clinical trials in 2009, where it was given to children between 6 weeks and 17 months old. The first results were published in 2011 [53] and RTS,S was only able to reduce clinical malaria cases by 28%,

conferring protection for only 18 months [53–60]. Despite the sub-par effect, RTS,S provides the benchmark against which new vaccine candidates can be compared to. RTS,S achieved European Medicines Agency approval in 2015 [61] and is being tested in a pilot experiment during the neonatal vaccination plan in some malaria endemic regions in sub-Saharan Africa [62].

1.6. New tools are needed to eradicate malaria

Malaria was eliminated from developed countries in the end of the 1970s, as a combination of increased national and personal wealth, swamp drainage, insecticide spraying and improved sanitation that created an unfavorable environment for malaria transmission [63]. However, despite past insecticide spraying campaigns in Europe, several *Anopheles* spp. capable of transmitting malaria are indigenous to most European countries [63]. Re-introduction of malaria was thought to be impossible, because of the harsh winters that happen in this continent, which are too cold for the development of *Plasmodium* parasites in the mosquito [63]. However, the risk of reintroduction of malaria in Europe was evident by an outbreak of *P. vivax* in 2011, where 40 autochthonous cases of malaria were reported in southern Greece [64,65]. Despite this anecdotal evidence, global warming, could, hypothetically, create milder winters, providing appropriate conditions for seasonal *P. vivax* transmission [63].

The biggest contributor to the success of malaria eradication campaigns in the 70s was the control of vector population. Indeed, insecticide-treated bed nets (ITNs) and indoor residual spraying (IRS), which eliminate *Anopheles* spp. mosquitos, were thought to contribute to 80% of the observed reduction in malaria infections since the year 2000 [66]. In the year 2015, these two actions are estimated to have averted over 500 million cases [66]. However, since ITN and IRS have become widespread and common, mosquito resistant strains are starting to appear [67], creating the fear that the current trend of malaria elimination will be reverted.

As discussed above, current diagnostic tests for *Plasmodium* infection are either fast but imprecise or precise but slow and expensive. There is the need for new diagnostic

I – Introduction

strategies that are *Plasmodium* species-specific, cheaper and easy to work with. A new tool of molecular malaria diagnostic is loop-mediated isothermal amplification (LAMP) [68], where 4 pairs of primers are used to amplify 6 sequences and detection is done using the fluorescence or turbidity of the solution [69,70]. This technique is as sensitive as conventional molecular methods [21] and has the advantage that no thermocycler is needed, bringing this technique closer to the point-of-care.

Artemisinins, as discussed above, are the current first-line treatment against malaria. Expectably, as for the every other anti-malarial, resistance to artemisinin has been reported [71]. Resistant parasites are as sensitive as the susceptible strains to artemisinins, yet, show a longer half-life when compared to susceptible strains when exposed to artemisinin treatment [72]. Because of these contradictory pieces of information, there is still some controversy whether these parasites are truly resistant. Regardless, this delayed-death phenotype has been associated with *kelch13* polymorphism [73], which is spreading throughout Southeast Asia [74,75]. This highlights the need for new anti-malarial compounds in the market, which have been the subject of research by pharmaceutical companies and academia over the last decade (reviewed in [23]).

The main focus on anti-malarial drug development has been on both improving known anti-malarial, such as chloroquine or artemisinin derivatives, as well as creating new chemotypes and leads for anti-malarial drug research [23]. The goal is to create a single-dose anti-malarial treatment, that could block the liver, blood and transmission stages of the disease [23,76,77].

KAF156 is an attractive compound that fits all of the above, as it showed anti-malarial properties against all of the stages of *Plasmodium* parasites in the mammalian host [78]. It is currently in Phase II clinical trials [79]. A similar drug candidate is DSM265, that also shows anti-malarial activity against the pre-erythrocytic stage of infection [80,81], cleared Phase I clinical trials recently [82,83], with the idea of being used as both chemoprevention agent [82] and partner drug to artemisinin [83].

The most advanced and promising anti-malarial is KAE609, or cipargamin, that can kill blood stage parasites and affect parasite transmission with a single dose [84–86]. It is

currently the fastest plasmodicidal drug available [87], having cleared Phase II clinical trials in 2014 [88].

OZ439, or artefenomel, is an artemisinin derivative with longer circulation time both in mice [89] and in humans [90], that can be given in a single dose treatment profile to clear *P. falciparum* infection [90]. Interestingly, despite being an artemisinin derivative, OZ439 does not show the delayed-death phenotype observed in the artemisinin resistance strains [91–93], making this drug useful for use in Southeast Asia.

Some focus has similarly been given to anti-relapse drugs against *P. vivax* and *P. ovale* hypnozoites, which are needed for eradication. Currently, only primaquine is used to prevent relapse, which requires strict compliance to a long 14 day treatment indication [15]. Moreover, people with G6PD deficiency develop toxicity to the excessive oxidative stress created in the detoxification of primaquine [47]. So far, the only alternative to primaquine is tafenoquine, which showed promising results in phase II clinical trials [94]. Tafenoquine, being a derivative of primaquine, is still toxic for people deficient for G6PD, highlighting the requirement for the development of new anti-relapse drugs that circumvent the need for G6PD detoxification. Advances have so far been limited, because there are few tools to study hypnozoite biology and there is currently no way of obtaining large quantities of *P. vivax* sporozoites needed for drug screening assays [95].

An effective vaccine is also needed for the control of malaria. WHO also is closely monitoring other vaccine candidates and their progression through clinical trials in a project entitled “The Rainbow Tables” [96], prospecting higher protection than the one afforded by the recent RTS,S vaccine. Currently, 37 vaccine candidates are available on the web page, with 21 in Phase II or III of clinical trials. These vaccine pipeline is very diverse, ranging from subunit-based vaccines (reviewed in [97]), whole-sporozoite vaccination (reviewed in [98]) to live *P. falciparum* sporozoite inoculation under chloroquine chemoprophylaxis [99–101]. Some of these strategies also contemplate *P. vivax* antigens [102], increasing the coverage of the vaccination strategies.

Despite the worrisome evidences detailed above, there have been great advances in tackling this disease. There has been a decrease of over 20% in the number of cases and of 50% in fatalities worldwide since the year 2000 [1], in line with the WHO Millennium

I – Introduction

Development Goals, which aimed to halve malaria cases by 2015. Malaria eradication is seen as an attainable goal for this generation [103,104]. Past results were possible with roughly 3 billion US\$ spent yearly on malaria control and eradication and 600 million US\$ spent yearly on basic research [1] and further strategies will have an estimated cost of 8,5 billion dollars over the next 15 years [105]. Moreover, better diagnostic and therapeutic options need to be developed [106]. Success will ultimately depend on the willingness of each country to adhere to WHO policy and to fund these strategies.

2. The life cycle of *Plasmodium* parasites

The earliest reports of malaria date back the Chinese documents from about 3000 BC [107], where malaria had always been associated with poor health, fevers and an enlarged spleen. Initially, it was thought as a consequence of unhealthy miasmas rising from swamps. Only in the second half of the last century did the scientific community unveil the complete life cycle of the malaria parasites, that is divided between development inside the human liver [108] and blood [109,110] and in the *Anopheles* spp female mosquito vector [111].

2.1. The discovery of *Plasmodium* parasites and its life cycle

The causative agent of malaria was only described in 1881 by Alphonse Laveran, a French physician working in Algeria [109,110]. On patients with malaria, Laveran discovered the presence of pigmented bodies in the erythrocytes (**Figure 2A-C**). These pigmented bodies, he deduced, would infect an erythrocyte (**Figure 2A**), develop into larger bodies with numerous pigmented structures (**Figure 2B, C**) and rupture the red blood cell, releasing the smaller pigmented bodies into the bloodstream, that would invade new erythrocytes, starting the cycle anew [109]. Italian physician Camillo Golgi added that the

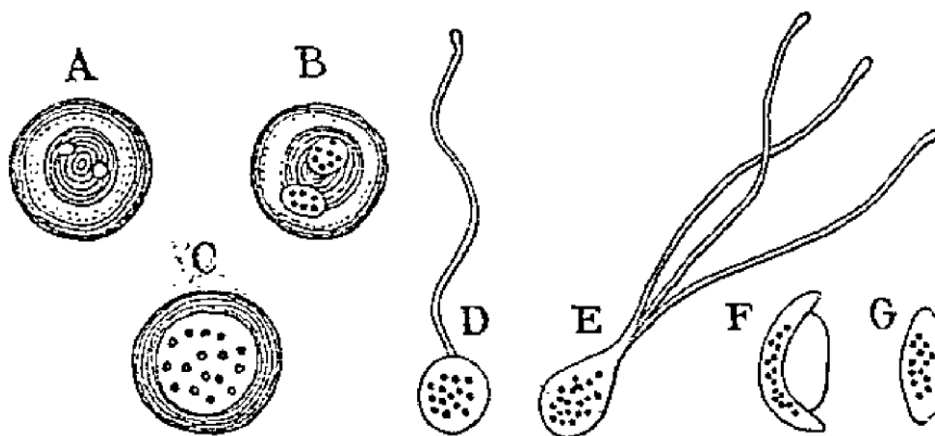


Figure 2 - Drawings by Alphonse Laveran of erythrocytes infected with *P. falciparum* parasites (adapted from [290]). A-C) erythrocytes infected with *Plasmodium* parasites in order of maturation (A early, B, intermediate, C final forms); D and E) infected erythrocytes with flagellar protusions; F and G) crescent-shaped forms.

I – Introduction

fevers associated with malaria occur when the parasites burst out of the red blood cell, before invading a new one [6].

One of the most puzzling observations made by Laveran were some crescent shaped pigmented bodies in the blood of infected patients, which, after some time, would create motile protrusions (**Figure 2D-G**) [109]. Unbeknownst to Laveran, he had found the male form of the *Plasmodium* parasite. Patrick Manson was the first to postulate that these protrusions might be a sexual transmissible form, destined for a “suctorial insect” [112]. This was found to be true when Ronald Ross and Battista Grassi, in the 1890s, established that female *Anopheles* mosquitos are the vectors that transmits malaria [4,111]. They discovered circular bodies (oocysts) in the basal lamina of the midgut of infected mosquitos, which grow in size, eventually differentiating into numerous new parasites termed sporozoites (**Figure 3**). These sporozoites then migrate into the mosquito salivary glands and are able to infect a new host during the next bite of the mosquito.

For the next 50 years, the biology of the malaria parasites was thought to be completely understood. Yet, no one knew why people bitten by infected mosquitos only developed a blood infection one week (or more) later. Some physicians thought that it simply took one week for the parasite to reach enough biomass to produce a patent infection, where others thought that the parasite would be hidden in one organ, replicating and differentiating into a blood infectious form. The latter (and correct) concept was only proved in 1948 and 1949, when Shortt and Garnham experimentally infected human volunteers by mosquito bite and biopsied a portion of their livers. There, they discovered

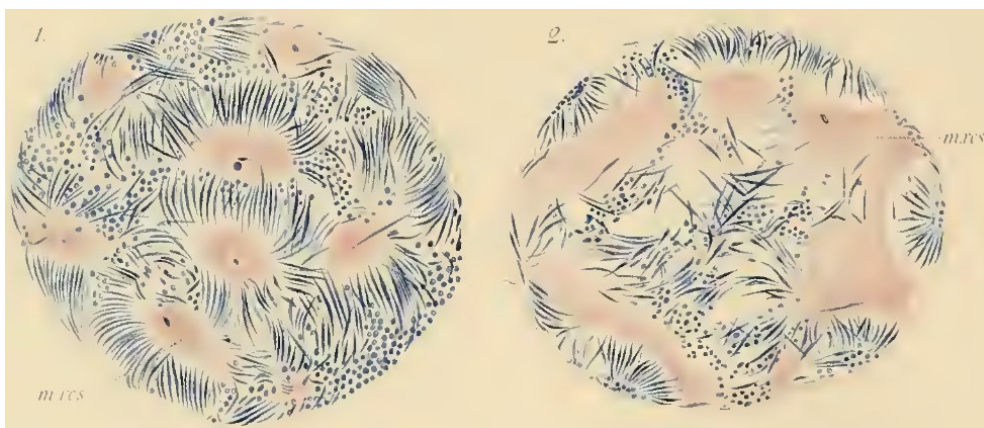


Figure 3 - Drawings of Battista Grassi of *P. falciparum* sporulating oocyst in the midgut of *Anopheles spp* mosquitos (adapted from [4]).

“plasmodial masses undergoing schizogony” (**Figure 4**) [108,113,114]. The last piece of the puzzle was added when it was discovered that *Plasmodium vivax* is able to form dormant forms in the liver, these forms infect the hepatocyte, stay in an arrested form for days, months or even years, before finalizing schizogony and establishing a blood infection[40,41].

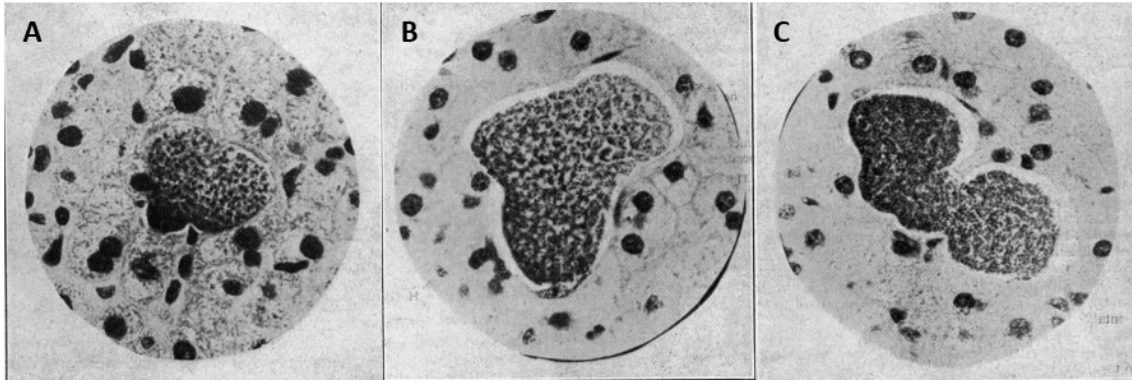


Figure 4 - First images of *P. falciparum* infected hepatocytes (adapted from [108]). Giemsa-stained liver slices of a human volunteer submitted to mosquito bites from *P. falciparum* infected mosquitos for 3 consecutive days (an estimated 770 mosquito bites in total). Three types of parasites were observed and divided into different stages of infection. A) Five-day old parasite; B) Six-day old parasite; C) Seven-day old parasite.

2.2. The phylogeny and evolution of *Plasmodium* parasites

Plasmodium parasites are single celled protozoan organisms that belong to the phylum Apicomplexa, thought to have existed for 1000 to 400 million years [115]. Every species of this phylum has an apical complex, hence the name Apicomplexa, consisting of three secretory organelles, important for invasion of the host cell. Many apicomplexans also possess a characteristic organelle, called apicoplast (first discovered in the 1970s [116–118]), which seems to be essential [119,120]. This organelle is of plastid origin [121] and is thought to be the result of an secondary endosymbiosis of an ancestral predatory eukaryotic free-living cell with a red algae [122]. Throughout time, the plastid lost the ability to make photosynthesis [122,123], yet, it is still responsible for a number of metabolic pathways [124], namely the essential FAS II pathway [125–129].

Along evolution, some apicomplexans lost a structure of their apical complex, a microtubule complex called the conoid [130,131]. This is coincident with the ability to

I – Introduction

invade cells of the blood, especially erythrocytes, giving rise to the class Hematozoa. Hematozoa are the only Apicomplexans with a dioxenic life cycle, being transmitted from host to host by blood sucking vectors. Some Hematozoa evolved both a pre-erythrocytic stage when inside the vertebrate host and way of digesting hemoglobin when inside the red blood cell, creating the order of Haemosporidian parasites [3]. Most Haemosporidian parasites only use the blood stage of infection to perform sexual commitment or differentiation, with the *Plasmodium* parasite genus the only exception to this rule, as they can replicate asexually in erythrocytes [3]. This characteristic is thought to have appeared 60 to 45 million years ago [132], in the early Cenozoic era.

The *Plasmodium* genus encompasses 199 different species, which infect birds, reptiles and mammals [3]. Indeed, the original host of *Plasmodium* parasites are thought to have been birds [132]. They are all characterized by a pre-erythrocytic stage, the invasion of erythrocytes, multiplication by schizogony (cellular division where the nucleus divides several times and then the cell divides into as many parts as there are nuclei) and the presence of a pigment (hemozoin) in the infected cell. This genus also carried the specialization of mosquitos (family *Culicidae*) as vectors of *Plasmodium* parasites [3,132].

The *Plasmodium* genus is separated into 13 different clades, depending on the type of host they infect, the number of merozoites each parasite produces inside the red blood cell and on the shape of its gametocytes. Even though all *Plasmodium* parasites are spread by the bite of infected mosquitos, only the mammalian infectious parasites are transmitted by mosquitos of the genus *Anopheles* [3]. Of the 13 clades, only three are infectious to mammals (*Laverania*, *Plasmodium* and *Vinckeia*) and are thought to exist for over 40 million years [133], with the emergence of the liver stage as the pre-erythrocytic stage.

Speciation of the *Laverania* clade is thought happen shortly after (42 to 30 million years ago [132]). These parasites are able to infect primates and are characterize by a unique genes families that code for variable surface antigens, such as the *var* genes [134,135]. Most of the *Laveriania* species have a synthenic segment of 4 genes, two of which are essential for invasion of the red blood cell, the genes that code for reticulocyte binding-like homologous protein 5 (RH5) and Cysteine-rich protective antigen (CyRPA) proteins [136]. More recently, 10 000 years ago [136,137], an infection of a human being

with a gorilla parasite is thought to have been event that lead to the speciation of *P. falciparum* [137]. Somehow this zoonotic parasite evolved a protein to bind a version of sialic acid, *N*-glycolylneuraminic acid, that is present in greater amounts in human erythrocytes [138], making human infection possible.

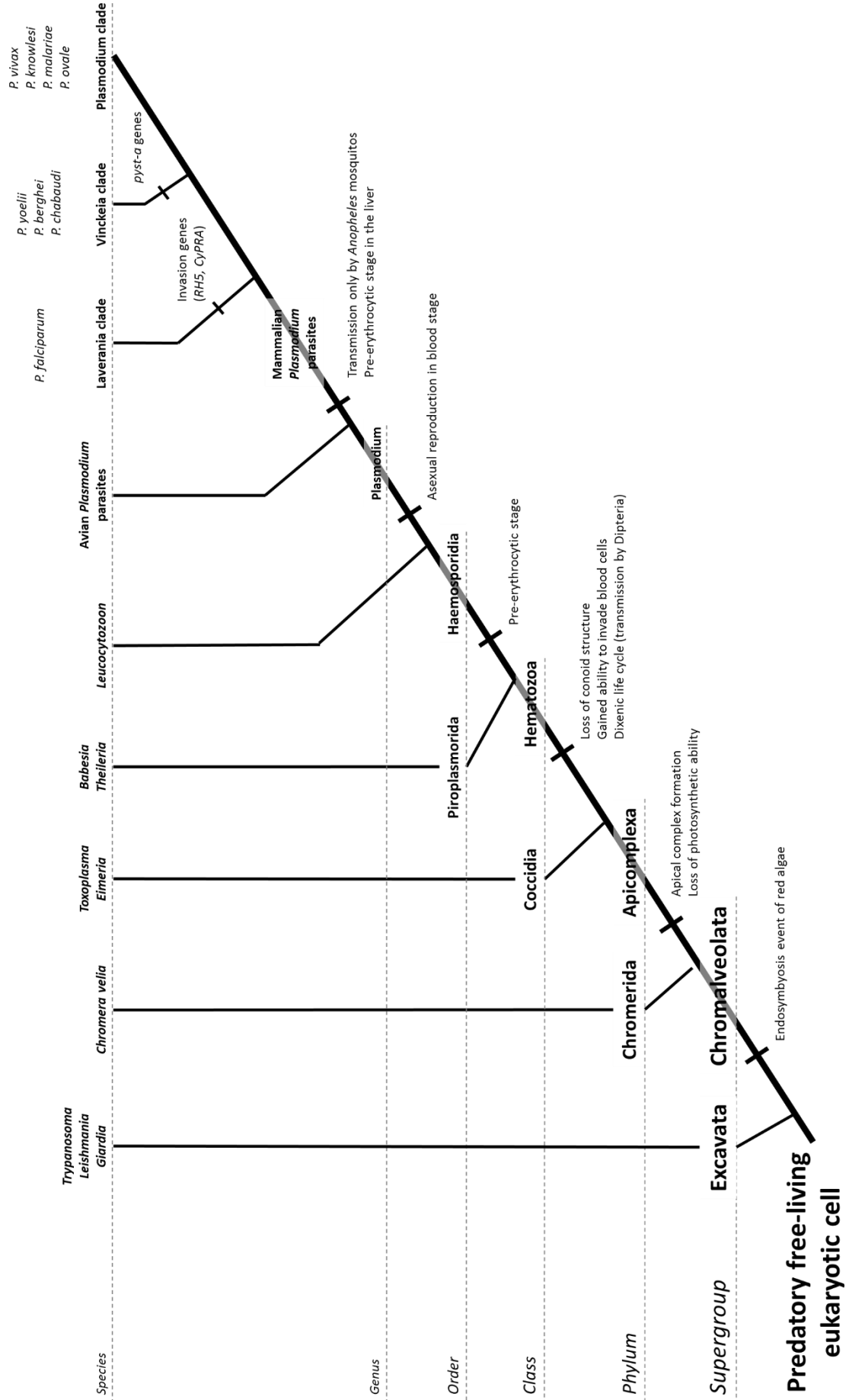
The remaining two clades have a gene family of variable surface antigens known as the *pir* gene family [134,139] and do not possess the syntenic segment of 4 genes that are important for invasion in the *Laverania* clade.

The *Vinckeia* clade (40 to 30 million years old [133]) includes all the *Plasmodium* parasites that infect non-human primates, including rodent malaria parasites, that have an estimated age of 16 million years [133]. The rodent *Plasmodium* parasites are the only to possess an expansion of the gene family called the *pyst-a* [140], thought to have a role in cholesterol uptake by the parasite [134].

In the *Plasmodium* clade, the leap to human infection happened about 400 000 years ago in the case of *P. vivax* [141] in Africa [142]. This is intriguing, because *P. vivax* is nowadays largely absent from the African continent, being only endemic in the Americas and in Asia [1]. This exclusion from Africa happens because *P. vivax* infection of the erythrocyte requires the expression of Duffy antigen receptor for chemokines on the surface of the erythrocyte for the host to become susceptible to infection [143]. Africans have a mutation on this gene [144], rendering them almost complete protection from *P. vivax* infection. The *P. vivax* lineage we currently observe is one that escaped out of Africa [145], possibly during the selection of the Duffy-negative trait in the human genome.

Figure 5 - Cladogram of the phylogeny of *Plasmodium* and related parasites. The evolution of *Plasmodium* parasites can be traced back to a once photosynthetic predatory eukaryotic cell. Eventually, this organism evolved an apical complex and gained the ability to invade blood cells and be transmitted between two organisms, one of them being female *Anopheles* mosquitos. The establishment of a pre-erythrocytic stage, further specialized in *Plasmodium* parasites, with the mammalian branch the only with the ability to invade the liver. (Image on the next page).

I – Introduction



3. The invasion of mammalian cells by *Plasmodium* parasites

Plasmodium parasites are one of many obligatory intracellular pathogens of the Apicomplexa phylum, meaning that getting inside a host cell is very important for their development. Different pathogens have evolved different strategies to enter cells, most of which can be divided into two mechanisms: the zipper or the trigger (reviewed in [146,147]). In the zipper mechanism, most studied in *Listeria monocytogenes*, surface proteins of the pathogen bind to plasma membrane receptors on the host cell, such as cadherins and integrins, in such a way that mimics cell-cell or cell-matrix connections. These engaged receptors lead to the recruitment of other host factors, like myosin and catenins, that reorganize the cytoskeleton of the host cell, forcing the host cell to advance pseudopods to engulf the pathogen. These pseudopods contain more host cell receptors that bind to the surface proteins of the pathogen, progressively covering the pathogen with host cell plasma membrane (**Figure 6**, left panel). In the trigger mechanism, the pathogen secretes its own proteins into the cytosol of the host cell, normally through type 3 secretion

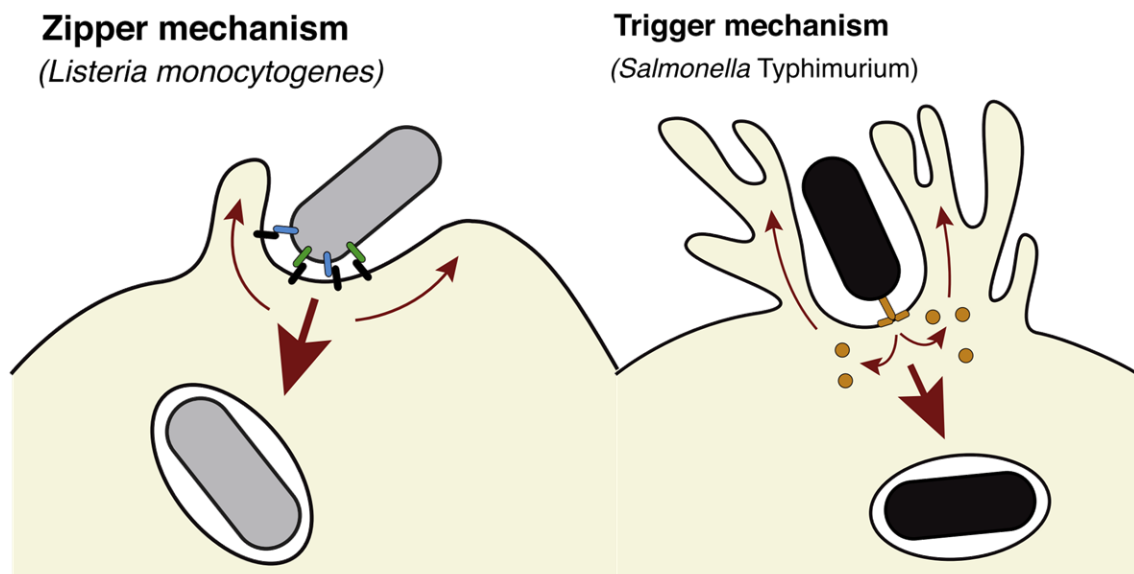


Figure 6 - Mechanisms of invasion by bacteria. Invasion by intracellular Bacteria can be divided in two categories, zipper (left) where the bacterium engages with host cell receptors and trigger (right), where the bacterium inserts its own proteins into the host cell cytoplasm. Both these interactions lead to changes in the cytoskeleton of the host cell, leading the engulfment of the bacterium. Adapted from [147].

I – Introduction

systems, which is the case for bacteria from the genus *Salmonella*. These proteins interact with cytoskeleton modifying proteins, creating ruffles in the membrane of the host cell, that fold over the pathogen, fusing around it (**Figure 6**, right panel). In essence, both types of invasion result in the same, misleading the host cell to allow for the entrance of the pathogen.

Of importance to this thesis is a particular type of trigger mechanism, involving host plasma membrane repair pathways. Briefly, the invading pathogen exports a pore-forming protein to the host cell plasma membrane, that leads to the influx of calcium ions into the host cell [148–150]. This triggers the exocytosis of acid sphingomyelinase to the outside of the host cell [151], inducing membrane invagination at the site of the pore [152]. This invagination, in turn, induces host cell endocytosis of the lesioned membrane, taking the invading microbe into the cell [148]. This mechanism was initially established for the intracellular parasite *Trypanosoma cruzi* [150] but has since been expanded to other bacteria, *Listeria monocytogenes* [148,149,153], *Neisseria gonorrhoeae* [154] and *Neisseria meningitidis* [155], as well as human adenovirus [156].

3.1. The apical complex that controls Apicomplexan invasion

Apicomplexan parasites seem to follow a different type of strategy, where the host cell seems to be passive. These intracellular parasites always develop inside a cell, enveloped by a parasitophorous vacuole (PV) and its membrane (PVM) [157]. This vacuole is created during the invasion process and its membrane is of host cell origin [158–160]. In general, the process of invasion relies on host cell receptors binding to specific parasite ligands, compartmentalized on parasite organelles, that only surface at critical points during the invasion process.

All parasites from the phylum Apicomplexa share a set of secretory organelles important for the invasion process [161] (**Figure 7**). These are created during the intracellular stages of the life-cycle of the parasites, loaded with specific proteins via a specialized route of the secretory pathway [162]. All these organelles coexist in the apical

part of the motile parasite, the zoite, nonetheless, their secretion is a tightly timed and controlled process [163,164].

The first set of organelles to get discharged are the micronemes (Mn in **Figure 7**), that are loaded with adhesins, crucial for cell tropism and proper orientation of the zoite [165]. They are the smallest of these apical vesicles and their number correlates with the motility of zoite [166].

The next set discharged are the rhoptries (Rh in **Figure 7**), an elongated pear-shaped organelle. The number and size of rhoptry organelles varies between different apicomplexans, with the size of the zoite being proportional to the size and number of rhoptries [166,167]. Yet, rhoptries seem to have a dual role during the invasion process [168,169], being spatially partitioned into two regions. The first part of the rhoptries to be discharged is called the rhoptry neck, which is closest to the apical end of the zoite. Proteins

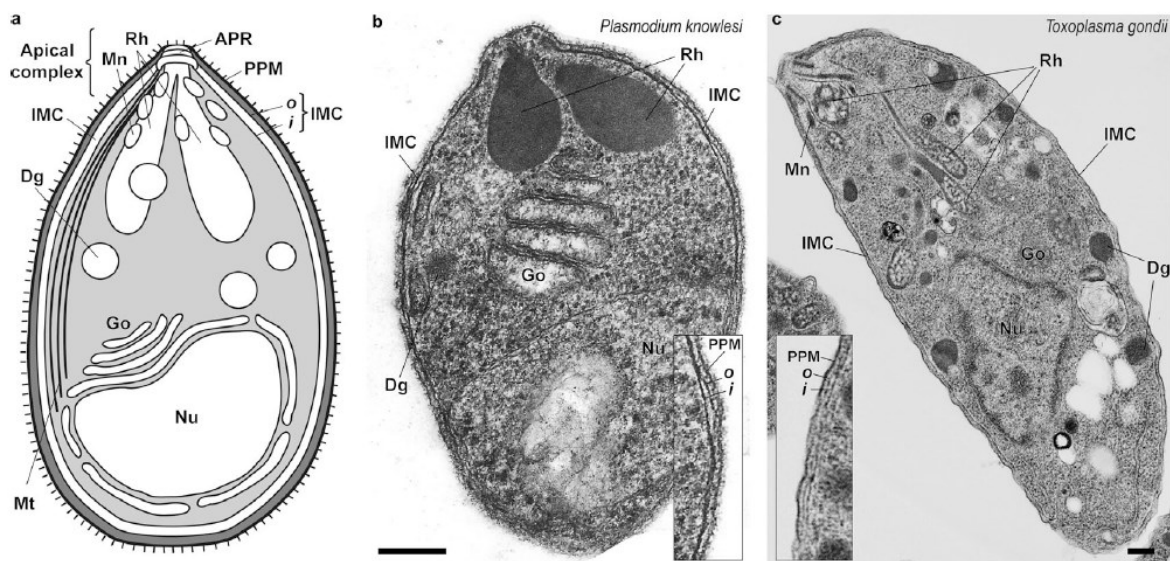


Figure 7 – The apical complex of Apicomplexan parasites. (adapted from [175]). A) Schematic representation of a *Plasmodium knowlesi* merozoite, showing the apical complex, populated with rhoptries (Rh), micronemes (Mn) topped by the apical ring (APR). The parasite plasma membrane (PPM) encases this complex as well as the inner-membrane complex (IMC), with its outer (*o*) and inner (*i*) layers. Dense granules (Dg) exist both in the apical region as well as in the parasite cell body, beneath the microtubules (Mt), that cover the IMC. The basal side of the parasite contains the Golgi apparatus (Go) as well as the nucleus (Nu). B and C) Electron micrograph of both *P. knowlesi* merozoite as well as *Toxoplasma gondii* tachyzoite showing the same compartments, highlighted.

I – Introduction

that belong to the rhoptry neck are called Rhoptry Neck Proteins (RONs) and are both adhesion-like molecules, that further tighten the grip of the parasite to the host cell, as well as invasins that propel the parasite into the host cell [168]. Several RONs are conserved between apicomplexan parasites, hinting towards divergent evolution driven by cell tropism [170]. After the rhoptry neck is secreted, the rhoptry bulb follows. The set of proteins that inhabit the bulb of the rhoptry are called ROPs and are important to prepare the host cell for the presence of the parasite [168,169]. ROPs are poorly characterized in *Plasmodium* parasites. They seem to be deposited at the membrane of the infected cells after invasion has finished [168]. In *Toxoplasma* parasites, ROP proteins are injected into the host cell cytoplasm, where they affect host cell signaling pathways [169]. The study of ROP proteins has been challenging because no homology is seen between ROPs of the different apicomplexan parasites [168], hinting that different parasites subvert cells differently.

The final granules to be discharged are the dense granules (Dg in **Figure 7**), loaded with proteins that populate the PV space, the PVM or that are injected into the host cell cytosol [167]. Dense granules are similar to micronemes (in terms of size) and to rhoptries (in terms of density when observed by Electron Microscopy), so their presence in all Apicomplexans requires further confirmation. Unlike the two previous vesicles, dense granules are not secreted through the apical end of the parasite, yet seem to fuse with the parasite plasma membrane throughout the cell body of the parasite [171–173]. The proteins that are known to constitute the dense granules are crucial for the proper establishment of the infection, as they shape the PV and PVM, the point of contact of the parasite to the infected cell [174].

All of these processes rely on the another component of the parasites, the inner-membrane complex (IMC) [175,176]. The IMC is composed of flattened membrane sacs supported by a subpellicular network of intermediate filaments, that encircles the parasite from the apical to the posterior end [177–179], with an opening at the very apical tip of the parasite, through which micronemes and rhoptries are secreted [180]. The IMC is rich with proteins that link it to both the parasite plasma membrane and to its actin cytoskeleton [181]. This allows for the forward movement of the parasite, crucial for both gliding motility as well as invasion of the host cell [182–184].

3.2. Invasion of the erythrocyte by *Plasmodium* merozoites

The invasion of the erythrocyte has mostly been studied using *P. falciparum*, with the general mechanism being conserved between different species and even with *Toxoplasma gondii*, another Apicomplexa parasite [185]. Red blood cell invasion is a fast process (taking less than 1 minute) that can be divided into 4 phases (reviewed in [186,187]).

On the first phase, pre-invasion, the merozoites attach to the surface of the RBC, via the binding of merozoite surface protein 1 (MSP1) to RBC surface proteins, such as band 3 and glycophorin A [188–190] (**Figure 8**). It is also thought that the surface protein MSP1 serves as a scaffold for other *P. falciparum* proteins needed to interact with the RBC [191].

I – Introduction

The second step of invasion starts with the release of parasite proteins from the micronemes. These include erythrocyte binding antigens (EBAs) and reticulocyte-binding homologous proteins (RH proteins), which bind to glycoporphins [192] and Complement Receptor 1 [193] respectively, on the surface of the RBC. These two groups of proteins show functional redundancy [194–197] and their binding leads to the rise of cytosolic Ca^{2+} in the parasite [198], releasing even more parasite proteins from the micronemes and rhoptries in the apical end [199–201]. This creates a gradient of binding that re-orientates the parasites in an energy-independent manner, with the apical end of the parasite facing the membrane of the erythrocyte [202].

After this reorientation, the interaction between *Pf*RH5 and basigin is essential [203–208]. The binding of these two proteins induces Ca^{2+} influx into the parasite and into the

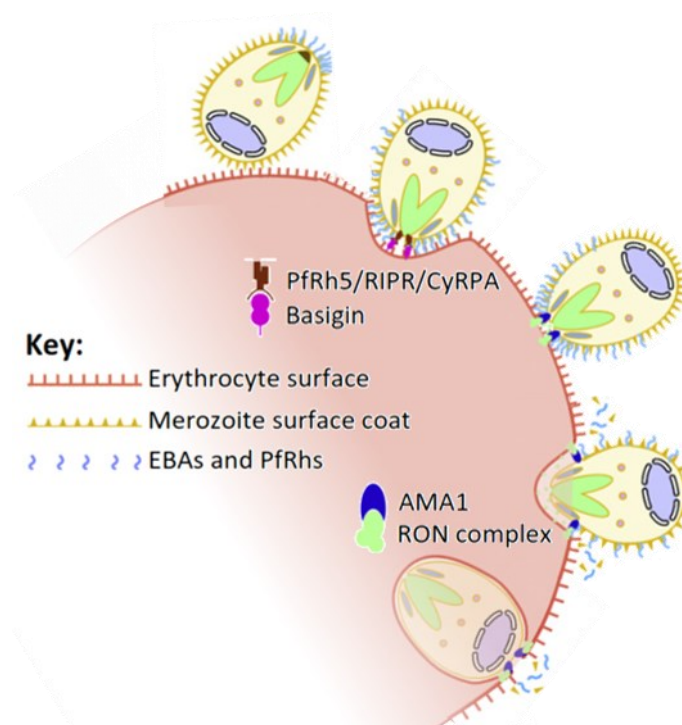


Figure 8 - Invasion of erythrocytes by Plasmodium falciparum merozoites (adapted from [187]).

As the merozoites are released, they attached to an uninfected erythrocyte via the interaction its membrane coat (especially MSP1) to the surface of the erythrocyte. This causes both the reorientation of the merozoite as well as the release of rhoptry proteins (importantly *Pf*RH5). After RH5 binding to basigin, AMA1 and the RON proteins are released, leading to the formation of the moving junction and the ensuing burrowing of the parasite into the erythrocyte. This process takes approximately 20 seconds.

RBC [209], signaling the release of more parasite proteins, committing the parasite for invasion of the RBC [199,210] (**Figure 8**).

The release of rhoptries proteins triggers the fourth and final phase of invasion, active invasion [211]. The Rhoptry Neck protein 2 (RON2) protein released from the rhoptries of the merozoite are incorporated into the RBC membrane and serves as a binding site for the Apical Membrane Antigen 1 (AMA1) protein, present at the surface of the parasite [212–215]. *PfAMA1* is also linked to the actin-myosin motor of the parasites [214,216], which propels the merozoite forward, into the RBC [217,218]. The AMA1-RON complex travels along the merozoite, from the apical to the basal end of the parasite, along with the movement of the parasite motor [217,218], being often referred to as the moving junction (**Figure 8**).

After the merozoite is completely engulfed into the RBC (**Figure 8**), and surrounded by the PVM, the RBC shrinks and forms spiky protrusions, in a process known as echinocytosis. This is a transient phenomenon, from which the RBC recovers [209].

Invasion by *P. vivax* parasites seems to follow the same molecular mechanism of the moving junction, nonetheless, it is not completely solved (**Figure 9**) [219,220]. The major deterrent has been the lack of a continuous *in vitro* culture system for *P. vivax* [220]. It has been known that *P. vivax* merozoites require binding to the Duffy Antigen Receptor for Chemokines for invasion to happen [143,144,221,222]. The absolute need for this receptor on erythrocytes is being challenged because of reports of *P. vivax* infections in Duffy-negative individuals [219,223–226]. Recently, Transferrin receptor has also been found to play a role in attachment to the erythrocyte [227,228]. Apart from these two receptors, few other *P. vivax* proteins are known to be involved in invasion although no host receptor is known (**Figure 9**).

All these models of erythrocyte invasion follow a concept of the red blood cells as a “passive host cell”, where the erythrocyte contributes (or fights back) very little to the invading parasite. Remarkably, the local state of the plasma membrane of the soon-to-be-infected erythrocytes modulates the success of invasion, namely changes in lipid rafts [229,230], cytoskeleton malleability [231–236] and calcium-dependent post-translational modification of proteins [237–243].

3.3. Invasion of the hepatocyte – two (too many) things happening at the same time

The invasion of the hepatocyte has been more challenging to describe because of one particularity of the sporozoite, its ability to cross several hepatocytes before finally infecting one [244,245]. As such, it has been challenging to decouple events that are important for cell traversal and cell invasion. Yet, a chronogram of events as well as relevant sporozoite proteins are increasingly being described (reviewed in [246]).

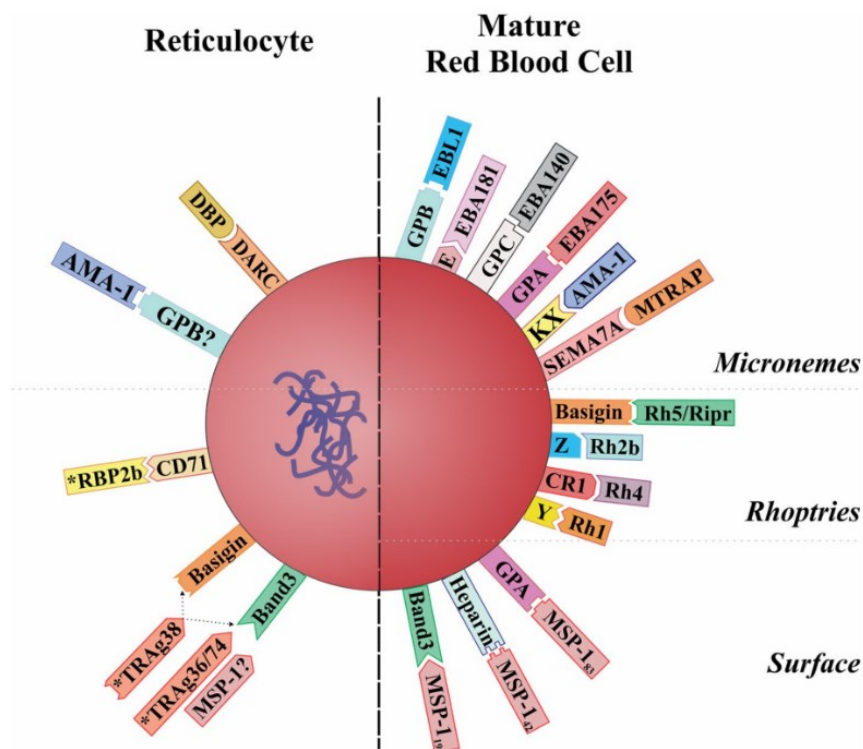


Figure 9 - Host receptors and parasite ligands involved in red blood cell invasion by *P. vivax* (left) and *P. falciparum* (right) (adapted from [220]). *P. vivax* merozoites infect preferentially reticulocytes using unknown receptors on the surface of this cell. This is stark contrast to the invasion mechanics of *P. falciparum*, where at least 9 receptors are known and 14 parasite ligands have been characterized.

Sporozoite colonization of the host starts in the skin, where sporozoites are deposited by the bite of infected mosquitos [247]. There, the sporozoites migrate until it breaches into a blood vessel, accessing the bloodstream [248–250]. The sporozoites are taken up by the hosts circulatory system, until reaching the liver, where the sporozoites attach to the heparan sulfate proteoglycans (HSPGs) of hepatocytes, protruding out of the liver parenchyma [251]. Much like MSP1 binding to erythrocytic surface proteins, binding to HSPGs is accomplished with the major surface protein of the sporozoite, CSP [251–255], and also thrombospondin related anonymous protein (TRAP) [256,257] (**Figure 10**).

The arrested sporozoite then traverses Kuppfer cells (liver-specific macrophages), making holes in the plasma membrane of the cell, through which the parasite crosses, reaching the liver parenchyma on the other side of the cell [258,259]. This process is thought to happen again to several hepatocytes, until the parasite invades. So far, four parasite proteins have been described as essential for the traversal process, sporozoite protein essential for cell traversal 1 and 2 (spect1, spect2) [260,261], perforin-like protein 1 [262] and cell-traversal protein for ookinete and sporozoite (CeITOS) [263]. These proteins are thought to form pores in the cellular membranes, wide enough to fit the parasite [264]. It is unclear why does the parasite traverse cells, it is possibly a mechanism

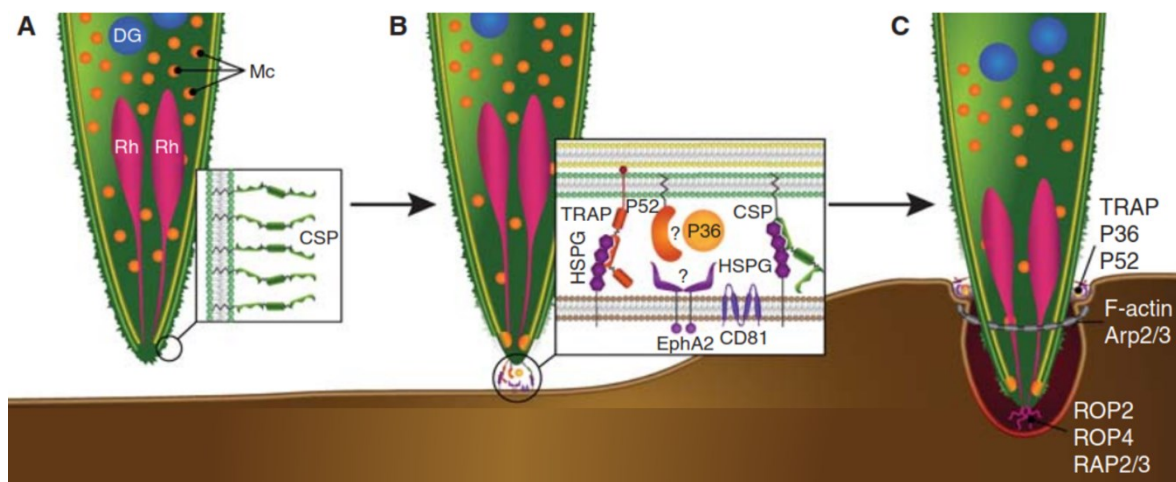


Figure 10 - Liver invasion by Plasmodium sporozoites (adapted from [246]). A) *Plasmodium* sporozoites have CSP as their main surface protein. B) As CSP binds HSPGs at the surface of hepatocytes, it causes the release of micronemes (Mc) to interact with the hepatocyte. Micronemal proteins TRAP, P52 and P36 interact with CD81 and or EphA2 leading to the release of the contents of Rh. C) Rhoptry proteins ROP2, ROP4 and RAP2/3 are secreted as the moving junction is formed, allowing for the invasion of *Plasmodium* sporozoites.

I – Introduction

to get access to the liver parenchyma. This hypothesis is supported by the fact that invasion of spect1 and spect2 knock-out parasites is enhanced when Kupffer cells are depleted from livers of mice [260,261]. Theoretically, this creates a freer barrier, through which the ability of knock-out sporozoites to cross into the parenchyma is restored.

In culture systems, it is estimated that traversal lasts for one hour and that invasion starts after it [265]. However, traversal has been a hindrance to study of the “pure” invasion because parasites are desynchronized when they start traversing, desynchronizing the start of invasion.

Regardless of the timing and physiological role of traversal, it is not an essential mechanism. Both spect1 and spect2 knock-out parasites can invade *in vitro* as well as wild-type parasites [260,261] and traversal can be bypassed by manipulating sporozoites [245,266]. This is accomplished by incubating sporozoites with sera and/or ionophores at 37°C, mimicking the conditions found by the parasite in the mammalian body. This stimulation, or activation, causes changes in the transcription [267] of the parasite and the discharge of sporozoite micronemes and rhoptries [268,269].

Several discharged proteins play a role in invasion, such as P36 and P36P (two 6-cys proteins) [270] and P52 [271], whose function remains unknown. Nonetheless, the moving junction mechanism of invasion is thought to happen exactly as in the blood stages as both AMA1 [268] and Rhoptry Neck Protein 4 (RON4) [272] are essential for host cell invasion. Merozoite apical erythrocyte-binding ligand (MAEBL) is another example of an important protein during both erythrocyte and hepatocyte invasion [273].

The regulation of apical protein discharge is still uncertain, however, several signaling molecules of the parasite have been implicated in hepatocyte invasion, namely, calcineurin [210], calcium-dependent protein kinase 4 (CDPK4) and Protein Kinase G (PKG) [274]. These proteins respond to calcium levels, highlighting the importance of this ion as a secondary messenger for the sporozoite. Recently, the host factor cluster of differentiation 81 (CD81) has been shown to be important for discharge of RON2, RON4 e Rhoptry-associated protein 2/3 (RAP2/3) by *Plasmodium* sporozoites.

More host factors also regulate invasion of the mammalian host, namely the low density lipoprotein receptor (LDLR, which binds to CSP) [252,275], CD81 [276–278], scavenger receptor class B type 1 (SR-BI) [279–281] (both binding to an unknown sporozoite ligand), Ephrin A2 receptor (EphA2) [282] (possibly binding to P36), cholesterol levels at the membrane of the hepatocyte [283,284], protein kinase C zeta (PKC ζ) [285] and actin polymerization [286] (some of these factors are shown in **Figure 10**). This suggests that the “passive host cell” model does not hold either for the invasion of the hepatocyte.

Interestingly, conflicting reports suggest different role of specific parasite and host proteins depending on the *Plasmodium* parasite used. Especially the role of host cell receptors CD81 and SR-BI seem to be species-specific and determined by the P36 molecule [281]. This suggests a conserved mechanism of hepatocyte entry with specific triggers operating for specific *Plasmodium* species (**Figure 10**).

4. Living beyond of the vacuole

During the invasion process, the parasite is surrounded by a host derived membrane, called the PVM. The membrane of the PVM and the parasite proteins that populate it, help the parasite escape cell autonomous responses, such as autophagy [287], yet, it also blocks the access of parasite to nutrients and the release of toxic by-products. Not surprisingly, the parasite evolved mechanisms to overcome this.

4.1. Remodelling the erythrocyte

As discussed in a previous section, the main cause for severe cases of malaria is the adherence to the endothelium by the infected erythrocytes [7,8,288]. This feature had been observed by many physicians throughout history, namely in the spleen, the liver and in the kidneys [4,6,109,110,289,290]. Moreover, *Plasmodium* infected erythrocytes have different morphological characteristics when compared to uninfected erythrocytes (reviewed in [291]). Notably, the surface of the RBC shows knob-like protrusions which causes cytoadherence to the endothelial wall of blood vessels and other erythrocytes [135,292–294], increased rigidity [295,296] and increased permeability at the plasma membrane [297–299]. Whereas the first two changes affect the way the parasitized RBC escape the immune system, the latter reflects the need of the parasite to access nutrients.

All these alterations are only possible because the parasite is able to place its proteins outside of the PV and at the surface of the RBC. To achieve this, the parasite evolved a complex system of signals, protein-protein interactions and an exomembrane system (**Figure 11**, reviewed in [300–302]).

For a protein to be exported, it first needs to be directed to the secretory pathway of the parasite, meaning it needs to be co-translated in the endoplasmic reticulum (ER) via the Sec61 complex [303–305] (**Figure 11**). All proteins that are to be exported to the parasite vacuolar space share a hydrophobic region after the ER signal peptide [303,306].

Some exported proteins also share a sequence motif downstream of the ER signal peptide, which targets for protein export [307,308]. The *Plasmodium* Export Element (PEXEL) motif is composed of 5 amino acid residues, RxLxE/Q/D (x represents an uncharged residue) and is present in most of the *Plasmodium* species [309]. It seems that the Arginine (R) and Leucine (L) residues are important for sorting out of the ER and the fifth residue (E

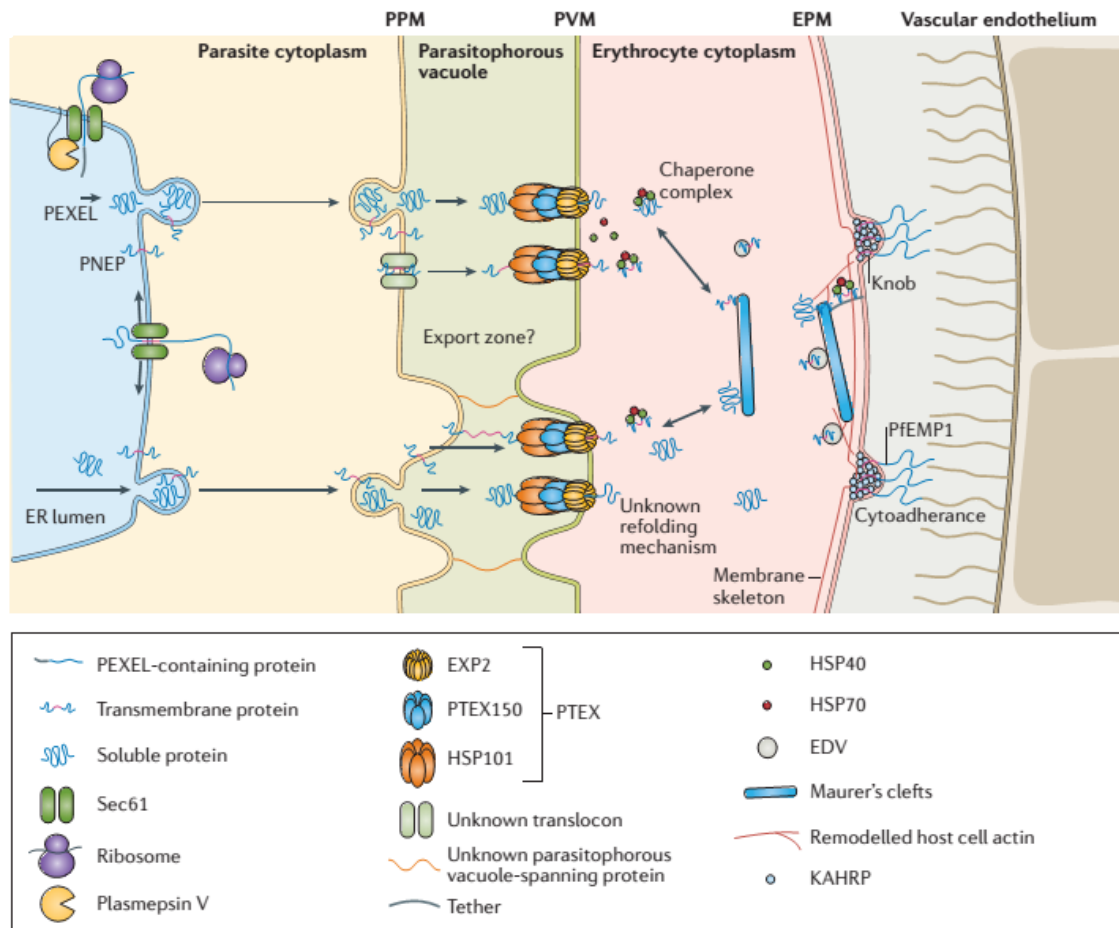


Figure 11 - Protein export and erythrocyte remodelling by Plasmodium parasites (adapted from [302]). Exported proteins are co-transcribed into the ER. There, PEXEL-positive proteins are cleaved by Plasmepsin V, whereas PEXEL Negative Exported Proteins (PNEPs) are not. Both types of exported proteins are packaged into secretory vesicles and secreted out of the parasite plasma membrane (PPM), to the parasitophorous vacuole space. Once in the vacuolar space, exported proteins are unfolded and exported through the *Plasmodium* Translocon of Exported Proteins (PTEX) complex, which sits at the parasitophorous vacuole membrane (PVM). They are re-folded in the erythrocyte cytosol by already exported chaperones and fed to the Maurer's clefts (and later to the erythrocyte membrane) or directly to the plasma membrane of the erythrocyte (EPM). Exposed proteins, such as PfEMP1, can interact with the endothelium, causing the parasitized erythrocyte to adhere to the microvasculature.

I – Introduction

or Q or D) is important to direct the protein to the outside of the PVM [307,310]. This motif serves as the proteolytic cleavage site for an ER-resident aspartyl protease, Plasmeprin V (PMV) [310,311], that cleaves the PEXEL motif at the leucine residue, creating a protein with an acetylated N-terminus [312,313] (**Figure 11**).

Some of the exported proteins do not have a PEXEL motif [314], however, they share a hydrophobic amino acid sequences in the N-terminus [314,315], with PEXEL-positive proteins. This suggests that they might converge into the same trafficking pathway [314–317] (**Figure 11**). Recent analysis suggests that over 450 *P. falciparum* proteins are predicted to have a PEXEL motif, and thus, predicted to be exported by the parasite [318] nevertheless, if we consider the existence of PEXEL-negative proteins, that total can increase to 550 proteins [319].

After the ER, exported proteins are then trafficked in secretory vesicles until fusing with the parasite plasma membrane (pPM), being released into the vacuolar space [320] or, in the case of trans-membrane proteins, being incorporated into the pPM [316,321,322] (**Figure 11**).

Despite the knowledge of some of the export elements, it is still unclear how the parasite manages to distinguish between proteins destined for other organelles, such as the apicoplast, or proteins destined for the vacuolar space. The involvement of specialized lipids – phosphatidylinositol 3-phosphate (PI₃P) – for sorting purposes was proposed to act as the signature for exported cargo [323] but has been challenged by more recent results that show that protein export is PI₃P-independent [324] and that PI₃P only accumulates around the food vacuole of the parasite [325]. The emerging model suggests that all secretory vesicles follow the same pathway until the Golgi Aparatus [326,327], where they can be sorted from secretory into exported vesicles [301].

Once at the vacuolar space, exported proteins need to be unfolded [328] and require energy to cross the PVM [329]. To achieve this, exported proteins interact with the *Plasmodium* translocon of exported proteins (PTEX) multiprotein complex [330]. The complex is composed of five different proteins: an AAA+-ATPase heat shock protein 101 (HSP101), Exported Protein 2 (EXP2), PTEX150, PTEX88 and thioredoxin 2 (TRX2) [330,331] (**Figure 11**). The precise stoichiometry and structure of the complex has already been

resolved [332], showing that this complex forms a structure with close to 1000 kDa. HSP101 and PTEX150 are each expected to associate as hexamers (each with 600 kDa) with 7 EXP2 proteins forming the pore of the complex (approximately 210 kDa), on the interface with the PVM (**Figure 12**) [332].

HSP101, EXP2 and PTEX150 are considered the core components of the PTEX, since no genetic deletion of these genes has been possible during the blood stages of infection [330,333,334]. However, conditional knock-down approaches of both HSP101 [335] and PTEX150 [336] have shown that these proteins are responsible for the export of *Plasmodium* proteins (both PEXEL positive or negative) and that protein export is important for parasite viability.

So far, the study of individual components of the PTEX complex has yielded a mode of action for the complex that is remarkably similar to bacterial secretion systems [337]. Exported proteins are unfolded by the HSP101 protein, in an ATP-dependent manner, which are channelled through PTEX150 [338] until crossing the membrane pore created by the EXP2 protein [322,339]. The EXP2 protein shares homology to Hemolysin E (HlyE) from bacteria [331] and can mediate the conductance of small molecules [339–341]. The functions of TRX2 and PTEX88 are not yet known but seem not to be required for protein export [333,334,342]. However, gene deletion of both TRX2 [336] and PTEX88

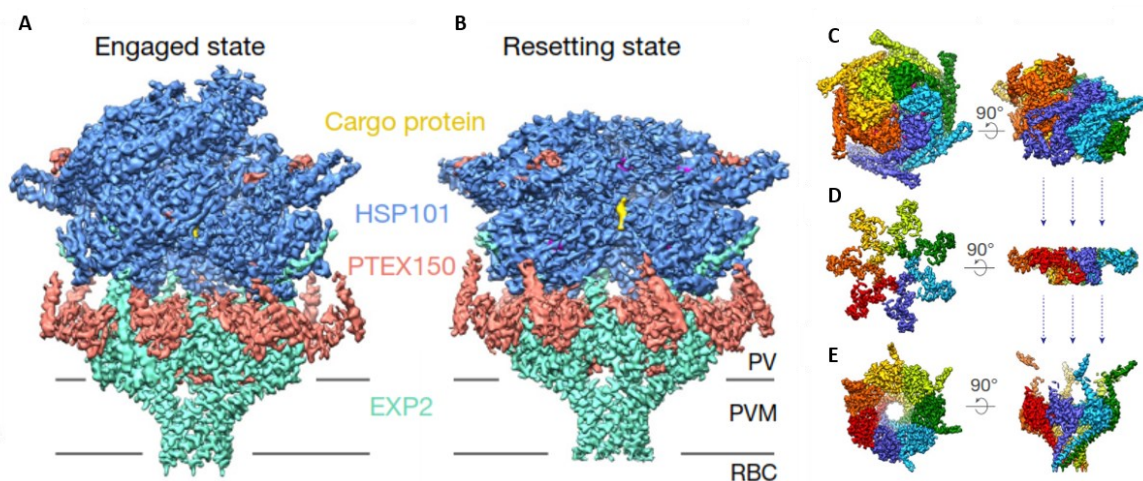


Figure 12 - Structure of the PTEX complex and of its proteins (adapted from [332]). PTEX complex in reference to the vacuolar space and erythrocyte cytosol, through the PVM with a cargo protein in the engaged (A) and resetting (B) stages. Individual proteins of the PTEX, at side (left) and top (right) view, each monomer is labelled with a different colour: C – HSP101; D – PTEX150; E – EXP2.

I – Introduction

[333,334,342,343] lead to a decrease in parasite proteins in the surface of the infected erythrocyte, and an overall lower virulence.

Imaging the PTEX complex at the PVM has shown that these proteins form discrete foci in blood stage parasites [321] hinting that the PV or PVM can be functionally partitioned [344] into “export zones” [300,345] (**Figure 11**).

Another group of proteins has been shown to interact with the PTEX, albeit, in a transient manner. *Pf*PV1 [346,347], Pf113 and HSP70-x form the Exported Protein Interacting Complex (EPIC) [338]. It is proposed that the EPIC acts as an intermediate between the vacuolar space and the PTEX complex [348]. Of these 3 proteins, all of them can be deleted in rodent malaria parasites without an effect in parasite viability [349] but in *P. falciparum*, only HSP-70x can be deleted.

Once exported proteins cross the PVM, in an unfolded state, they need to be refolded via chaperone-containing structures called J-dots [350], composed of HSP70-x and several DNAj co-chaperones [351] (**Figure 11**). It is also thought that erythrocytic chaperones help the re-folding of exported cargo [329]. A total of 18 DNAj chaperones are exported by *P. falciparum* [351], highlighting the importance of protein re-folding in the RBC cytoplasm.

Some of the exported proteins need to find their way into the erythrocyte plasma membrane (ePM) and *Plasmodium* parasites have evolved a way to solve this problem by creating an exomembrane system within the host cell cytoplasm. In *P. falciparum*, the system is called Maurer’s Clefts. Maurer’s Clefts are formed after invasion of the erythrocyte [352] and mature into stacks of unilamellar membranes [353], which are tethered to the ePM by the cytoskeleton [354] (**Figure 11**). These structures have been shown to traffic *Pf*EMP1, knob-associated histidine-rich protein (KAHRP) and other surface proteins to the ePM [303,355–357]. There is still no consensus on how exported proteins enter the Maurer’s Clefts [320,358,359], yet the current model proposes they are internalized in chaperone-associated complexes [301]. Once in the Maurer’s Clefts, exported proteins fold and interact, creating the multi-protein complexes seen at the ePM. Protein-filled vesicles bud off from the Maurer’s Clefts, migrate through cytoskeleton filaments and merge with the ePM to form the knobs [354,360] (**Figure 11**). Interestingly, seven of the exported DNAj

proteins also have cytoskeleton binding motifs, suggesting they can be involved in sorting of exported proteins to and from the Maurer's Clefts [361].

To uncover function of exported proteins several groups tried to knock-out a total of 51 genes for exported proteins. Only a quarter was shown to be essential for *in vitro* culture of blood stages [362], however several proteins are known to be dispensable for *in vitro* culture but essential in the context of an *in vivo* infection.

4.2. Does the hepatocyte also get remodeled?

Several proteins of the PTEX complex described above were recently observed to also be present during the liver stages of infection [363–365], raising the possibility of protein export to the hepatocyte cytoplasm. Surprisingly, the motor protein of the complex, HSP101, is not detected during this stage [364], and a PEXEL-positive GFP fusion protein was shown not to be exported during the liver stages [365].

Nonetheless, we appreciate that the infected hepatocyte changes because of the presence of the parasite [366]: apoptosis is blocked [367,368], AMPK phosphorylation is repressed [369], there is an unfolded protein response and ER stress in the hepatocyte [370] and hepatic glucose transporters are re-localized to the plasma membrane [371]. Still, the parasite effector(s) that causes these changes remains elusive. To date, only three parasite proteins in the cytosol of the infected hepatocyte [372].

The first parasite protein detected in the cytoplasm of hepatocytes was CSP [373–376]. There, it is suggested that CSP interacts with hepatic ribosomes, ER and the nuclear envelope [374] (**Figure 13**), inhibiting protein translation [375] and preventing Nuclear Factor Kappa light-chain-enhancer of activated B cells (NF- κ B) translocation to host cell nucleus [376]. CSP amino acid sequence endorses these reports as it possesses both a PEXEL motif and a nuclear localization sequence [376]. Despite all of these reports, the presence of CSP in the host cell cytosol remains controversial as other laboratories fail to replicate these findings [377,378].

I – Introduction

In 2010, the protein Inhibitor of Cysteine Proteases (ICP) was identified in the cytosol of hepatocytes in the early stages of liver infection and is thought to block host cell autophagy [379].

The last protein to be discovered in the cytosol of infected hepatocytes was liver-specific protein (LISP2) [380], playing an unclear role in merozoite formation (**Figure 13**).

Apart from protein export, in the infected hepatocyte, *Plasmodium* parasites have been observed to emanate proteins and membranes from the PVM, creating a tubovesicular network (TVN, **Figure 13**) [381]. Some of these structures are physically separated from the PV and PVM, yet, are of PVM origin, containing UIS4 and Intra-erythrocytic *P. berghei*-Induced Structures Protein 1 (IBIS1) [381]. These protrusions are thought to be parasite driven, a way of the parasite to discard unwanted host material [382].

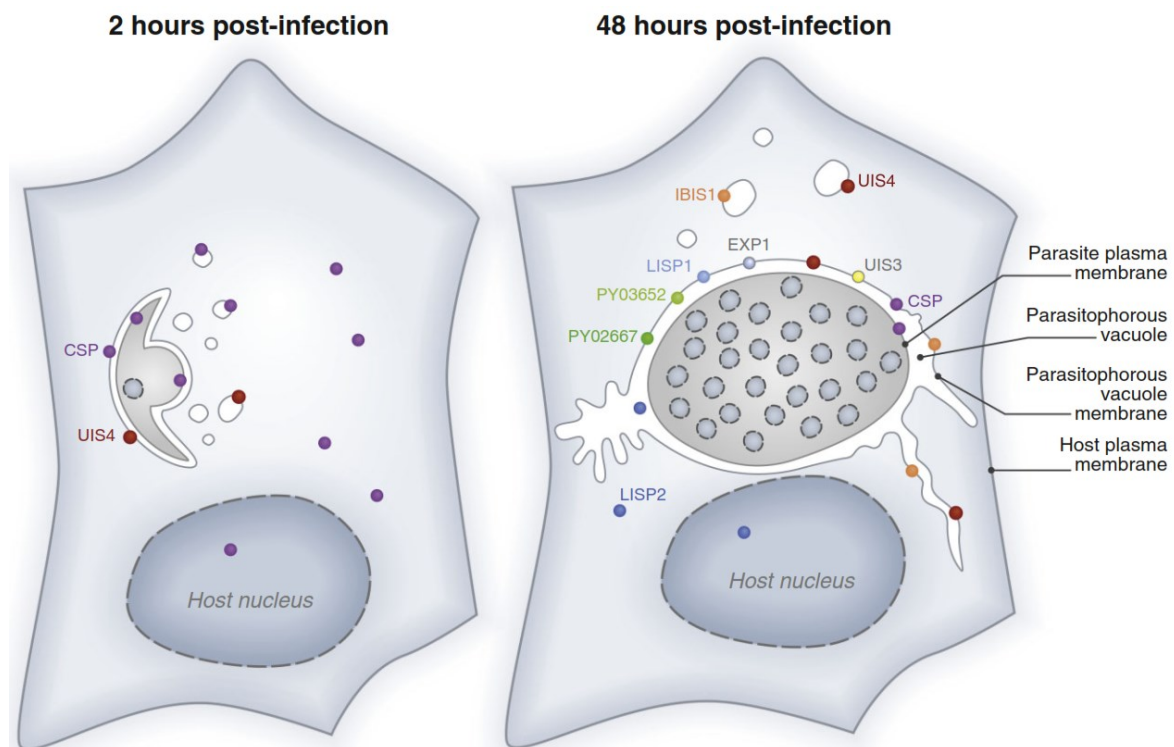


Figure 13 - Protein and membrane export in hepatic stages of malaria infection (adapted from [372]). After invasion by *Plasmodium* sporozoites, CSP (soluble) and UIS4 (in vesicles) are found in the cytoplasm of the infected cell (left panel). As the infection advances, more proteins populate the cytoplasm of the infected cell, namely IBIS1 (at the TVN) and LISP2 (soluble). The PVM of the parasites also protrudes into the host cell, in tubules termed TVN.

Chapter II – Aims

Exported protein 2 (EXP2) is a *Plasmodium* parasite protein that is expressed throughout its life cycle [333,364,383]. It shares sequence homology to bacterial pore-forming protein HlyE [330] and works as such in the PTEX complex during the blood stage of infection [332].

Recent reports suggest that it might serve another purpose for the parasite. Primarily, its expression pattern is different from other PTEX proteins [331,333,364]. Additionally, it is observed at the membrane of the PVM in the absence of other proteins of the PTEX [321]. Finally, EXP2 by itself in membranes allows the flow of molecules across the membrane [340,341].

However, the expression of EXP2 is not restricted to the blood stage of infection, where all the of previous works were focused. EXP2 has been reported to be also present during the liver stage of infection, where its function is still unknown [363,364]. The difficulty in assessing the function of EXP2 had been that genetic modification of *Plasmodium* parasites is only possible during the blood stage of infection, where EXP2 is essential for parasite propagation [384]. As such, we cannot generate liver stage parasites that lack the EXP2 gene or protein as we cannot propagate parasites through its life cycle.

Recently, a conditional knock-out parasite line (cKO), that does not express EXP2 during the liver stage of infection was produced [365]. It is based on the flippase (FLP) and Flippase Recognition Target (FRT) sequences system [385,386]. The authors replaced the 3' untranslated region (UTR) of the EXP2 gene by a generic 3'UTR that was flanked by FRT sequences. The FLP gene was inserted downstream of the UIS4 promoter, resulting in expression of FLP at the later stages of sporozoite development. This would result in the excision of the 3'UTR of EXP2 and silencing of the gene at the sporozoite stage [365]. Using this parasite, Ming Kalanon and colleagues, were able to infect mice and detect that the lack of the EXP2 expression lead to a decrease in the parasite liver burden in these mice [365]. Interestingly, since there is no protein export during the liver stage, this hints at the possibility of a new role for EXP2 during the liver stage.

II - Aims

Taking this into consideration, we aimed to decipher the role of EXP2 during the liver stages. In particular, we proposed to:

- 1) Study the effect of the absence of EXP2 during the liver stages of infection;

We will use the EXP2 cKO parasite line to infect both C57Bl/6J mice and HepG2 cells, analyze the number of infected cells as well as the size of the parasite, as a proxy for its development. Moreover, we will test if EXP2 cKO sporozoites show impaired gliding motility or cell traversal ability.

- 2) Study the dynamics of EXP2 during the sporozoite stage;

Using EXP2 antibodies or an EXP2-HA tagged line, we want to study the dynamic of EXP2 protein expression and localization in the sporozoite stage of the *Plasmodium berghei* life cycle. We will complement these observations by studying the dynamics of EXP2 mRNA expression.

Given the results obtained with the two previous aims, we added another unexpected aim:

- 3) Understand the mechanism of *Plasmodium* sporozoite invasion of hepatocytes.

As will be explained below, the EXP2 cKO sporozoites showed impaired invasion, when compared to the WT sporozoites. This leads us to study the mechanisms by which *Plasmodium* sporozoites invade hepatocytes. Briefly, we propose that *Plasmodium* sporozoites invade by triggering a membrane repair mechanism in the host cell. As such, we will test whether several steps in this mechanism are required for invasion by *Plasmodium* sporozoites to invade hepatocytes.

Chapter III – Materials and Methods

1. Parasites

1.1 Parasite lines

The following parasite lines were used in this study:

- GFP-expressing *P. berghei* ANKA (clone 259cl2) [387]
- *P. berghei* NK65 EXP2 FRT [365]
- *P. berghei* NK65 EXP2 FRT UIS4 FLP Recombinase [365]
- *P. berghei* NK65 EXP2 FRT TRAP FLP Recombinase [365]
- *P. berghei* NK65 EXP2-HA [333]

The first was a kind gift from Professor Chris Janse from Leiden University Medical Center from Leiden, The Netherlands, the others were a kind gift from Professor Tania de Koning-Ward from Deakin University in Melbourne, Australia.

Parasites were stored in frozen blood vials, containing 10^7 blood stage parasites, and kept at -80°C in our laboratory.

1.2 Mosquito dissection

To obtain sporozoites, blood vials were injected into a BALB/c wild-type mouse. After 5 days of infection, exflagellation of the male gametes in the blood of infected mice was observed under a light microscope. If more than 5 events per field of view were observed, the infected mouse would be used to feed naïve *Anopheles stephensi* mosquitos, bred in the Insectary of the Instituto de Medicina Molecular João Lobo Antunes (iMM JLA), for 30min. 22-35 days after the mosquito blood meal, salivary glands, containing *P. berghei* sporozoites, were dissected from of infected female *Anopheles stephensi* mosquitoes into DMEM medium and collected into an Eppendorf tube (Eppendorf, Hamburg, Germany). Salivary glands would be smashed with a plastic pestle and filtered through a 40- μm Falcon cell-strainer (Thermo Fisher Scientific, Waltham, Massachusetts, United States) to release sporozoites. Sporozoites were counted using a hemocytometer (Marienfeld Superior, Lauda-Königshofen, Germany).

2. Recombinant Protein production and purification

Recombinant EXP2 protein (rEXP2) was a kind gift from Professor Masafumi Yohda from Tokyo University of Agriculture and Technology from Tokyo, Japan. rEXP2 was expressed and purified as per manufacturer's instructions [339].

Briefly, a parasite expressing a truncated version of the EXP2 protein fused to Glutathione S-transferase (GST) protein creating the plasmid pGEX-3X-HRV3C-EXP2. This plasmid was used to transform *E. coli* B21, a gift from the laboratory of Gonçalo Bernardes at IMM JLA. Transformed bacteria were grown in suspension in LB broth supplemented with 100 µg/mL ampicillin at 37°C and 220 rotations per minute. Optical density (OD₆₀₀) of the culture was measured at 600 nm using a portable spectrophotometer. When OD₆₀₀ reached 0.5, the broth was supplemented with isopropyl b-D-1thiogalactopyranoside (IPTG) to a final concentration of 0.5 mM. Transformed bacteria were kept for 24 hours at 18°C, after which they were pelleted and stored at -20°C.

Lysis and protein purification were performed by Francisco J. Enguita, at IMM JLA as described previously [339]. The pelleted bacteria were resuspended in PBS containing 137 mM NaCl (Sigma); 2.7 mM KCl (Sigma); 1 mM EDTA (Sigma) and 0.15 mM phenylmethylsulfonyl fluoride (Sigma) and disrupted by sonication. Cell debris was eliminated by centrifugation at 14,000 g, the supernatant collected and filtered through a membrane with 0.45 µm pore size and incubated with 0.05% n-dodecyl-b-D-maltopyranoside (DDM, Sigma) at 4°C for 1 h prior to loading onto a 1 mL GST Hitrap FF column (GE Healthcare, Chicago, IL, USA). The column was then washed with a 10-fold volume of washing buffer (PBS with 0.02% DDM). To release rEXP2, HRV 3C protease (Takara Bio, Shiga, Japan) in 50 mM Tris-HCl, 200 mM NaCl and 0.02% DDM was applied to the column. After a 16 h incubation at 4°C, rEXP2 was eluted from the column with PBS buffer. All the purification steps were performed in an AKTA Explorer chromatographic system (GE Healthcare, Chicago, IL, USA). rEXP2 concentration was estimated using Pierce BCA Protein Assay Kit (Thermo Fisher Scientific).

3. Chemicals and Proteins

Desipramine, alpha-Hemolysin from *Staphylococcus aureus* and Sphingomyelinase from *Bacillus cereus* were purchased from Sigma (Kawasaki, Japan); GW4869 was purchased from Santa Cruz Biotechnology (Dallas, Texas, United States).

4. Infection of *Mus musculus* and parasite burden determination in mice

4.1. Mice

Male C57BL/6J and BALB/c wild-type mice, aged 4-8 weeks, were purchased from Charles River Laboratories (Saint-Germain-sur-l'Arbresle, France). Mice were housed in the facilities of the IMM JLA, in specific pathogen-free environment and given water and food *ad libitum*. All *in vivo* protocols were approved by the ORBEA committee of the IMM JLA and were performed according to national and European regulations.

4.2. Infection

To infect mice using sporozoites, 20,000 parasites were suspended in 200 μ L of simple DMEM and injected retro-orbitally into mice. To infect using blood transfusion, 200 μ L of blood containing 10^6 infected red blood cells were injected intra-peritoneally.

4.3. Liver load determination

At different time points after sporozoite infection (6h, 24, 48h after infection), livers of infected mice were collected into 3 mL of denaturing solution. Livers were then mechanically homogenized using 1 mm diameter silica beads (BioSpec Products,

III – Materials and Methods

Bartlesville, Oklahoma, United States) in MiniBeadBeater homogenizer (BioSpec Products) for 2min.

Denaturing solution is composed of 4 M Guanidium Thiocyanite (Sigma), 25 mM Sodium Citrate (Sigma), 0.5% Sarcosyl (Sigma) in MilliQ water treated with DEPC (Sigma).

After mechanical disruption of the tissue, 100 µL of homogenate was used to extract RNA, using NZY Total RNA Isolation Kit (NZYTech), as per manufacturer's instructions. 1 µg of extracted RNA was converted into cDNA using NZY First-Strand cDNA Synthesis Kit (NZYTech), as per manufacturer's instructions. cDNA was then used for quantitative Polymerase Chain Reaction (qPCR), by measuring the abundance of *Pb18S* RNA, compared to *MmHprt* RNA.

4.4. Pre-patency determination

For the detection of pre-patency of cKO parasites blood infection, mice were infected with 20,000 sporozoites and blood smears of these mice were checked every day for infected red blood cells until every mouse had a patent blood infection.

4.5. Parasitemia determination

Peripheral blood parasitemia was determined by thin blood smear (described in [388]). Briefly, a drop of blood from an infected mouse was smeared onto a glass slide (Marienfeld Superior). The blood smear was fixed in methanol (Merck Millipore, Burlington, Massachusetts, United States) for 30 seconds and air dried. Afterwards, the fixed blood smear was stained with 10% Giemsa stain solution (Sigma) for 5min, after which it was washed with water. Stained slides were examined in a bright-field microscopic (Olympus CX41, Olympus, Tokyo, Japan) to determine the number of infected red blood cells in at least 2.000 total red blood cells. Parasitemia was calculated as the percentage of infected red blood cells.

5. Infection of human hepatoma cell line HepG2 and live cell imaging

5.1. Cells

HepG2 (obtained from American Type Culture Collection) cells were cultured at 37°C, with a 5% CO₂ atmosphere, in Dulbecco's Modified Eagles Medium (DMEM, Gibco, Thermo Fisher Scientific), supplemented with 10% Fetal Bovine Serum (Gibco), 1% glutamine (Gibco) and 1% penicillin/streptomycin (Gibco).

For experimental setups, cells were rinsed with sterile Phosphate Buffered Saline (PBS, Gibco) and detached with TrypLEExpress solution (Gibco) for 5min at 37°C. Trypsin activity was stopped by adding complete DMEM, where cells were suspended. Cells were filtered through a 40-µm Falcon cell-strainer (Thermo Fisher Scientific) and recovered by centrifuging at 1,200 rpm for 5min in a bench top centrifuge (Eppendorf 5810R, Eppendorf). Cells were suspended in DMEM and counted in an hemocytometer. The number of seeded cells varied depending on the experimental procedure and the type of plate used (**Table 1**). When 24-well plates (Thermo Fisher Scientific) were used, No. 1 grade 12 mm diameter glass coverslips (VWR, Radnor, Pennsylvania, United States) were added to the well before cells were plated. After plating, cells were incubated at 37°C, with a 5% CO₂ atmosphere.

Table 1 - Number of cells used per procedure and plate type.

Procedure	Type of plate	Number of cells	Other
Traversal and/or invasion assay	24-well plate	100,000 cells	Coverslip optional
Invasion assay	Black 96-well plate	20,000 cells	n/a
Time course	24-well plate	50,000 cells	Coverslip was used
Time course	Black 96-well plate	10,000 cells	n/a
Calcium influx	8 well ibidi plates	20,000 cells	n/a

III – Materials and Methods

5.2. Infection of cells

To infect cells, the appropriate number of sporozoites were suspended in complete DMEM and incubate with cells and centrifuged for 5min at 3,000 rpm. Cells were incubated for 2 hours at 37°C, with a 5% CO₂ atmosphere, after which the medium was replaced by complete DMEM supplemented with 0.3% Fungizone (Gibco).

For some experiments, drugs or rEXP2 protein was added during infection step. These materials were either added to the cells concomitantly with sporozoites or added to the cells 1 hour after the sporozoites.

5.3. Transfection of cells and live imaging

To image calcium entry, HepG2 cells were transfected with the Gcamp6f, a calcium reporter fluorescent plasmid (Addgene Plasmid #40755, Watertown, MA, USA), using FuGene 6 HD (Promega, Madison, WI, USA) and OptiMEM (Gibco). 48 h after transfection, cells were imaged in Zeiss Cell Observer widefield fluorescent microscope for 3min. After an initial 30s of imaging, the appropriate concentration of rEXP2 or vehicle control was added to the culture medium and cells were imaged for another 150s. Fluorescence signal through time was normalized to the fluorescence at time -30s (F_i/F_0).

6. Immunofluorescence microscopy assays

6.1. Time Course analysis

To process cells and parasites for immunofluorescence assays, experiments are performed either on black glass-bottom 96-well plates (Greiner Bio-One, Kremsmünster, Austria), or on No. 1 grade 12 mm diameter glass coverslips. Cells and parasites were fixed at the appropriate time point in 4% paraformaldehyde (Santa Cruz Biotechnology)

for 10-20min at room temperature. Cell and parasite fixed material was then blocked and permeabilized with 5% Bovine Serum Albumin (BSA, NZYTech) 0.2% Saponin (Sigma) in PBS for, at least, 30min at room temperature. Cells and parasites were stained with the appropriate primary antibodies (**Table 2**), diluted in 5% BSA 0.2% Saponin, for 2 hours, at room temperature in a humid chamber. Samples were washed 3 times with PBS for 10min. After washing, samples were stained with appropriate fluorescent secondary antibodies (Thermo Fisher Scientific), with 1 mg/mL Hoechst 33342 (Thermo Fisher Scientific), diluted in 5% BSA 0.2% Saponin, for 1 hour at room temperature in a humid chamber. Stained samples were washed 3 times with PBS for 10min. After the final wash, coverslips were mounted on glass slides using a drop of Fluoromount-G (Thermo Fisher Scientific). If black glass-bottom 96-well plates were being used, 50 μ L of Fluoromount G would be placed on the stained well.

For time course analysis, samples were imaged using either Leica DM5000B, Zeiss Axiovert 200M, Zeiss Cell Observer, all widefield fluorescence microscopes, using a 20x dry objective.

6.2. Sporozoite staining

To stain for EXP2, 50,000 sporozoites were incubated in DMEM medium containing or not FBS at 37°C on glass coverslips. After 30min of incubation, sporozoites were fixed in 4% paraformaldehyde for 10-20min at room temperature. Fixed sporozoites were permeabilized using ice-cold methanol for 5min at -20°C. After washing, sporozoites were blocked and stained as described before.

Coverslips were imaged using Zeiss LSM 880 confocal point-scanning fluorescence microscope (Zeiss, Oberkochen, Germany), using 63x oil objective, GaAsP and Airyscan detectors.

III – Materials and Methods

6.3. Gliding assay

For gliding assays 50,000 sporozoites were incubated in complete DMEM medium at 37°C on glass coverslips. After 30min of incubation, sporozoites were fixed in 4% paraformaldehyde for 10-20min at room temperature. Fixed sporozoites were blocked as described before and only stained with α CSP antibody (clone 3D11) [389] and an anti-mouse secondary antibody and Hoechst. Coverslips were imaged using a Leica DM5000B widefield fluorescence microscope (Leica, Wetzlar, Germany) and 40x dry objective.

Since CSP is shed in a circular fashion during sporozoite gliding, sporozoite motility can be quantified by counting the circles of CSP produced by each individual sporozoite. Sporozoites were divided into 3 groups (no trails; 1-10 trails; >10 trails) based on the number of CSP circles, termed trails, that it would display.

6.4. In/out staining

For invasion determination, sporozoites were incubated with cells for, at most, 2 hours in complete DMEM medium at 37°C. At the appropriate time point, cells were fixed. Differently from the protocol explained before, fixed cells and parasites preparation were blocked using 5% BSA in PBS, without any permeabilizing agent. Samples were incubated with α CSP antibody (clone 3D11) [389] for 2h in humid chamber at 37°C, followed by washing with PBS. Afterwards, samples were permeabilized using 5% BSA 0.2% Saponin for 30min and incubated with α UIS4 antibody (Sicgen, Cantanhede, Portugal) for 2h in humid chamber at 37°C. After washing with PBS, samples were incubated with appropriate secondary antibodies for 1h in humid chamber. Samples were washed and mounted as described before.

For in/out staining analysis, samples were imaged using either Leica DM5000B, Zeiss Axiovert 200M, Zeiss Cell Observer, all widefield fluorescence microscopes, using a 40x dry objective.

6.5. Image analysis

All images were processed using FIJI software, version 1.52i [390] and macros written for each analysis to automate it.

7. Flow Cytometry assays

7.1. Invasion quantification

To quantify invasion and/or traversal of *P. berghei*, 100,000 HepG2 cells were plated in 24-well plates. One day later, they were incubated with 50,000 sporozoites complete DMEM or RPMI at 37°C. Ethylenediaminetetraacetic acid (EDTA) or Calcium chloride were added to alter calcium concentration in the media. After two hours of incubation, cells were washed with PBS, and detached using TrypLEExpress solution for 5min at 37°C. Trypsin activity was stopped by adding 20% FBS in PBS and the suspension of cells was collected into 1.5 mL Eppendorf tubes (Eppendorf) or in Flow Cytometry tubes (Thermo Fisher Scientific). Cells were kept on ice, until being analyzed by Flow Cytometry, either in BD Accuri C6 or in BD LSR Fortessa Cytometers (Becton Dickinson, Franklin Lakes, New Jersey, United States).

Invasion of the parasite was ascertained by Flow Cytometry only when GFP-expressing sporozoites were used. Infected cells are detected because of the GFP has Excitation/Emission maxima at 488/510nm, as described in [391] (an example of the gating strategy used is in **Figure 14**).

7.2. Traversal quantification

To quantify the level of traversal, HepG2 cells and sporozoites were incubated in the presence of 0.5 mg/mL of 10,000 kDa Dextran-Rhodamine (Thermo Fisher Scientific) in complete DMEM or RPMI at 37°C. EDTA or Calcium chloride were added to alter

III – Materials and Methods

calcium concentration in the media. The dextran molecule is passively taken up by cells that have been traversed and is detected because of the Rhodamine dye, that has Excitation/Emission maxima at 570/590nm, as previously described in [244,391] (an example of the gating strategy used is in **Figure 14**).

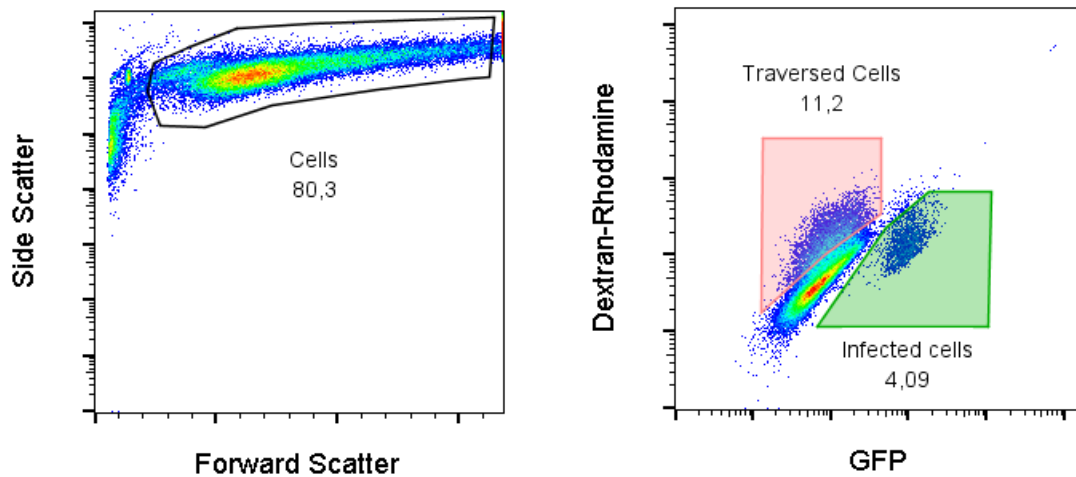


Figure 14- Example of the strategy used to analyze invasion and traversal of HepG2 cells at 2h after infection. This sample was acquired in the BD Accuri C6 cytometer and analyzed in FlowJo V10.

7.3. Permeability assay

To address the pore-forming ability of rEXP2 protein, we optimized a protocol based on [151,392–394]. Briefly, 50.000 HepG2 cells are suspended in Calcium-complete DMEM in the presence or absence of 2.5 mM EDTA or in Calcium-free DMEM. rEXP2 is added to the cells, at different concentrations, while on ice. Cells are incubated with protein on ice for 5min. After these 5min, Propidium Iodide or ToPro-3 (Thermo Fisher Scientific) were added to the sample, at final concentration of 50 µg/mL, and cells are transferred to 37°C for 10min. After this incubation, cells are put back on ice, until analysis by Flow Cytometry, on either BD Accuri C6 or in BD LSR Fortessa Cytometers (example of the gating strategy in **Figure 15**).

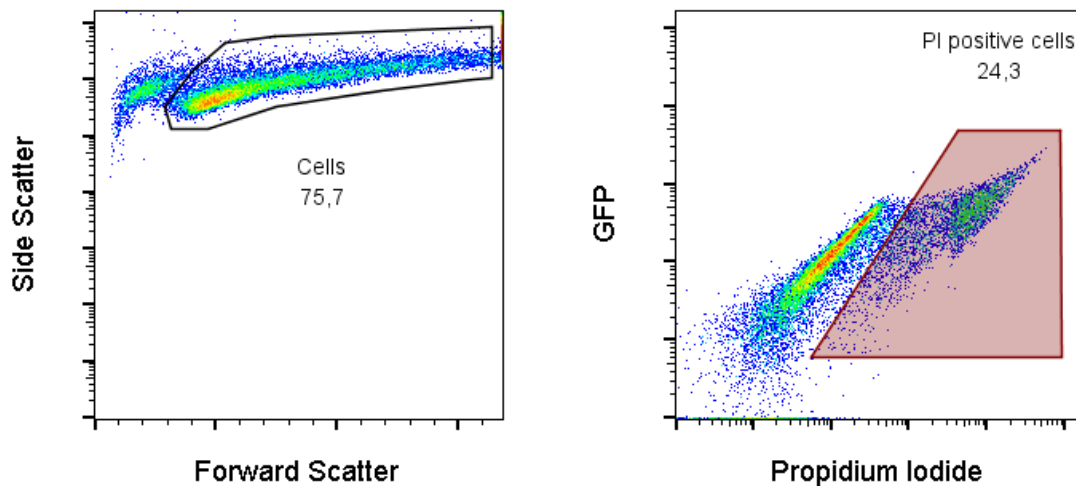


Figure 15 - Example of the strategy used to analyze cells that have a permeabilized plasma membrane. This sample was acquired in the BD Accuri C6 cytometer and analyzed in FlowJo V10.

7.4. Analysis of Flow Cytometer data

Analysis was performed using FlowJo software, version 10 (FlowJo LLC, Ashland, Oregon, United States).

8. Nucleic acid extraction and analysis

8.1. RNA extraction from cultures cells and cDNA synthesis

At the appropriate point of the experiment, cells were washed with PBS, and detached using TrypLEExpress solution for 5min at 37°C. Trypsin activity was stopped by adding complete DMEM the suspension of cells was collected into 1.5 mL Eppendorf tubes and pelleted by centrifugation at 2,000 rpm for 5min. Pelleted cells were then lysed and RNA was extracted using NZY Total RNA Isolation Kit (NZYTech), as per manufacturer's instructions. 1 µg of extracted RNA was converted into cDNA using NZY

III – Materials and Methods

First-Strand cDNA Synthesis Kit (NZYTech), as per manufacturer's instructions. cDNA was then used for quantitative Polymerase Chain Reaction (qPCR).

8.2. Sporozoite gDNA extraction

After sporozoite dissection from salivary glands, these would be pelleted by centrifugation in a tabletop centrifuge (Eppendorf) at maximum speed for 15min. Genomic DNA was purified using NZY Blood gDNA Isolation kit (NZYTech).

8.3. Gene abundance analysis

cDNA and gDNA abundance were analyzed using either ViiA 7 (384-well plates) or 7500Fast (96-well plates) Real-Time PCR Systems (Thermo Fisher Scientific) using iTaq Universal SYBR Green Supermix (Bio Rad). Analysis of results was performed using the $\Delta\Delta C_T$ method:

$$\Delta C_t = C_t^{Gene\ of\ interest} - C_t^{Housekeeping}$$

$$\Delta\Delta C_t = \Delta C_t^{Experimental} - \Delta C_t^{Control}$$

$$Relative\ Gene\ expression = 2^{[\Delta\Delta C_t]}$$

9. Proteins extraction and analysis

For preparation of samples from blood stages, BALB/c mice were infected with either GFP-expressing *P. berghei* ANKA (*PbGFP*) or with *P. berghei* NK65 EXP2-HA (*PbEXP2-HA*) and parasites were allowed to multiply until reaching a parasitemia of approximately 10%. Mice were sacrificed using isoflurane overdose and blood was removed by heart puncture. Red blood cells were suspended in PBS and pelleted by centrifugation at 450g for 5min without break. Pelleted red blood cells were lysed using

0.05% Saponin with cOmplete Protease Inhibitor Cocktail (Sigma) in PBS for 5min of ice. Parasites were pelleted at 2500g for 5min and were lysed in 500 μ L of RIPA buffer with 1% SDS for 2h on ice.

For sporozoite stage samples, sporozoites were dissected as described before and purified using a protocol described in [395]. Briefly, dissected sporozoites were purified from mosquito debris by performing a gradient centrifugation in 17% Accudenz (Progen, Heidelberg, Germany) solution at 2,500g for 20min without break. After the centrifugation, parasites (less dense than Accudenz) are retained at the top of solution, whereas debris (denser than Accudenz) are pelleted to the bottom of the tube. Sporozoites were collected and centrifuged to remove excess Accudenz at max speed for 10min.

Purified sporozoites would be counted and stimulated with or without fetal calf serum (FCS) at 37°C or would be kept on ice. Sporozoites and secreted proteins would be separated by a centrifugation at max speed for 10min and sporozoites were lysed with RIPA buffer with 1% SDS for 1h on ice.

RIPA buffer with 1% SDS was composed of 50 mM Tris-HCl (NZYTech), 150 mM NaCl (Sigma), 5 mM EDTA (Sigma), 10 mM NaF (Sigma), 1% Triton X-100 (USB Corporation, Cleveland, Ohio, United States), 0.5% Sodium Deoxycholate (AppliChem, Maryland Heights, Missouri, United States), 1% SDS (Sigma). Following lysis, NuPAGE loading dye (Thermo Fisher Scientific) and β -mercaptoethanol (to a final concentration of 10%, Sigma) were added to all samples.

Samples were separated by 8-12% in Acrylamide gels and transferred to 0.2 μ m pore-sized Nitrocellulose membranes (Bio-Rad, Warszawa, Poland). Membranes were placed inside Falcon tubes and blocked with 5% skim-milk (Nestle, Vevey, Switzerland) overnight at 4°C, on a tube roller. Membranes were then incubated with the appropriate primary antibodies, diluted in 5% skim milk, for 1 hour at room temperature. Membranes were washed with 0.1% Tween 20 (sigma) in PBS 5 times for 5 minutes. Membranes were then incubated with the appropriate secondary antibodies, conjugated to Horseradish Peroxidase (Jackson ImmunoResearch Laboratories, West Grove, Pennsylvania, United States), diluted in 5% skim milk, for 1 hour at room

III – Materials and Methods

temperature, after which they were washed again 5 times for 5 minutes. Western blots were revealed using Amersham ECL Prime Blotting Detection Reagent (GE Healthcare, Little Chalfont, United Kingdom) on the ChemiDoc XRS+ system (Bio-Rad).

10. Electron Microscopy

Immuno-electron microscopy of purified parasites was performed according to Tokuyasu technique. Briefly, the pellet was chemically fixed in 0.1 M phosphate buffer containing 2% formaldehyde and 0.2% glutaraldehyde, embedded in food-grade gelatine and cryopreserved in 2.3 M sucrose. Gelatine blocks were shaped in cubes and froze in liquid nitrogen and sectioned at -110°C using a cryo-ultramicrotome (UC7 and FC7, Leica) to generate 70 nm sections. Sections were collected and thawed in a mixture of 2.3M sucrose and 2% methylcellulose. Immuno-labelling was done in 1% Bovine Serum Albumin and 0.8% gelatine from cold water fish skin in PBS with rabbit α EXP2 primary antibody (1:500) and 15nm gold coupled Protein A (CMC Utrecht, The Netherlands, 1:50). After immuno-labelling, the sections were stained and mounted in a mixture of 3% (aq.) uranyl acetate and 2% methylcellulose. Images were recorded using a Hitachi H-7650 electron microscope (Hitachi, Tokyo, Japan) at 100 kV acceleration. Electron Microscopy

11. Statistical analysis

Statistical analysis was performed using GraphPad Prism 8 software. Student *t*-test was used to assess significance of differences observed between two groups. Non-linear regression was performed to assess Desipramine and GW4869 inhibitory effects on invasion.

Primary Antibody Table

Table 2 - List of Primary antibodies used in this study. When an antibody was not used for a given technique, its dilution will say non-applicable (n/a).

Antibody against...	Raised in ...	Clone	Dilution used in...			Reference	Obtained from...
			IFA	WB	ImmunoEM		
<i>PbCSP</i>	Mouse	3D11	1:300	1:2000	n/a	[389]	The Malaria Research and Reference Reagent Resource (MR4)
<i>PbHSP70</i>	Mouse	2E6	1:300	1:1000	n/a	[396]	MR4
<i>PfEXP2</i>	Mouse	7.7	1:500	n/a	n/a	[383]	European Malaria Reagent Repository
<i>PfEXP2</i>	Rabbit	Polyclonal	1:1000	n/a	1:500	[330]	Gift from the laboratory of Tania de Koning-Ward
<i>PbUIS4</i>	Goat	Polyclonal	1:1000	n/a	n/a	n/a	Sicgen
<i>PbTRAP</i>	Rabbit	Polyclonal	1:1000	1:2000	n/a	n/a	Gift from the laboratory of Joana Tavares
<i>PfRON4</i>	Mouse	Monoclonal	1:100	n/a	n/a	n/a	Gift from the laboratory of Margarida Ruivo
<i>PbBiP</i>	Rabbit	Polyclonal	n/a	1:2000	n/a	[397]	GeneScript

III – Materials and Methods

Primer List

Table 3 - List of Primers used in this study. All primers were ordered from Sigma and were suspended to 100 µM in RNase- and DNase-free water.

Number	Sequence (5' --> 3')	Species	Target gene	Reference	Application
P01	AAGCATTAAATAAAGCGAATACATCCTTAC	<i>P. berghei</i>	<i>18s</i>	[279]	Liver load determination
P02	GGAGATTGGTTTTGACGTTTATGTG	<i>P. berghei</i>	<i>18s</i>	[279]	Liver load determination
P03	TTTGCTGACCTGCTGGATTAC	<i>H. sapiens / M. musculus</i>	<i>HPRT/Hprt</i>	[398]	Liver load determination
P04	CAAGACATTCTTTCCAGTTAAAGTTG	<i>H. sapiens / M. musculus</i>	<i>HPRT/Hprt</i>	[398]	Liver load determination
P05	GTTGGTTCGCTAAACTGCATC	<i>H. sapiens</i>	<i>DHFR</i>	[399]	SSR genotyping
P06	CTGTTTACCTTCTACTGAAGAGG	<i>H. sapiens</i>	<i>DHFR</i>	[399]	SSR genotyping
P07	TGCAGCAGATAATCAAACCTC	<i>P. berghei</i>	<i>hsp70</i>	[399]	SSR genotyping
P08	ACTTCAATTTGTGGAACACC	<i>P. berghei</i>	<i>hsp70</i>	[399]	SSR genotyping
P09	ACGATCCAGGTTTGATTG	<i>P. berghei</i>	<i>exp2</i>	[400]	Expression (qPCR)
P10	TGGTAATAGTGGGACATTC	<i>P. berghei</i>	<i>exp2</i>	[400]	Expression (qPCR)
P11	ATTGCTCAACCTTATCAAACCTG	<i>P. berghei</i>	<i>serine tRNA ligase</i>	[401]	Expression (qPCR)
P12	AGCCACATCTGAACAACCG	<i>P. berghei</i>	<i>serine tRNA ligase</i>	[401]	Expression (qPCR)
P13	GGCCCACATTTGGGAAAGTT	<i>H. sapiens</i>	<i>SMPD1</i>	this study	Expression (qPCR)
P14	TTCACCGGATGATCTTGCCT	<i>H. sapiens</i>	<i>SMPD1</i>	this study	Expression (qPCR)
P15	GTGGAGTAGTCTTTAAGG	<i>P. berghei</i>	<i>gap45</i>	[400]	Expression (qPCR)
P16	GTGGAGTAGTCTTTAAGG	<i>P. berghei</i>	<i>gap45</i>	[400]	Expression (qPCR)
P17	TGCCTCATAAAATAAACCCA	<i>P. berghei</i>	<i>adenylosuccinate lyase</i>	[401]	Expression (qPCR)
P18	TCGTAAACTGTTGAATCGG	<i>P. berghei</i>	<i>adenylosuccinate lyase</i>	[401]	Expression (qPCR)
P19	CCAAACCAAGCGATCATAACAG	<i>P. berghei</i>	<i>uis4</i>	[400]	Expression (qPCR)
P20	CTTCACCCACTAAATCGCTTAATTC	<i>P. berghei</i>	<i>uis4</i>	[400]	Expression (qPCR)
P21	ATTTGGGTTGATGGTTATTG	<i>P. berghei</i>	<i>ama1</i>	[402]	Expression (qPCR)
P22	TCCTTGTCGAAATTTGGTAG	<i>P. berghei</i>	<i>ama1</i>	[402]	Expression (qPCR)

P23	AGGGAAGACATCCATTCCAATTGG	<i>P. berghei</i>	<i>exp1</i>	[400]	Expression (qPCR)
P24	TGAAGATTTGGCATGTTAAGTGGTG	<i>P. berghei</i>	<i>exp1</i>	[400]	Expression (qPCR)

Chapter IV – Results

1. EXP2 is necessary for the invasion of hepatocytes by *Plasmodium* sporozoites

The liver stage of infection is a complex stage of the life cycle of *Plasmodium* parasites. It is the transition phase between the mosquito vector and the blood stage of infection and, for the newly formed sporozoites it is crucial that invasion and colonization of the liver is successful. Moreover, once inside the hepatocyte, the parasite must change first from the long and slender sporozoite to the spherical exoerythrocytic form and later to the blood infections merozoites. To assess the function of EXP2 during the liver stages of *Plasmodium* infection, we used a conditional gene deletion system, where the deletion of the EXP2 gene happens during the mosquito stages of *Plasmodium* infection [365], the stage that precedes the liver stage. These parasites express a Flp recombinase from yeast under the control of the mosquito and liver stage gene, Up-regulated in Infective Sporozoites 4 (UIS4) [385,386]. Also, the EXP2 locus of these parasites has been altered to feature FRT sequences on its 3' untranslated region of the locus, achieving the EXP2 conditional Knock-Out parasite line (EXP2 cKO). Using this system, we expect to achieve an EXP2 locus that lacks its final region, causing it to stop being expressed. Effectively, we will obtain EXP2 KO sporozoites, that will enable us to study the liver stages. As a control, we will use a parasite line that has its EXP2 locus featuring the FRT sequences but that does not express the Flp Recombinase (WT parasites).

1.1. EXP2 is important during the liver stage, yet, not for parasite maturation

To question whether EXP2 would be important during the liver stages of *Plasmodium* infection, we infected C57Bl6/c mice with either WT or EXP2 cKO sporozoites, dissected from infected mosquitos. At 6 hours, 24 hours and 48 hours after infection, we sacrificed the infected mice and collected their livers. RNA was extracted from these livers and the relative abundance of *Pb18s* rRNA compared to the mouse hypoxanthine-guanine phosphoribosyltransferase (*MmHprt*) housekeeping gene. When compared to infection with WT parasites, the EXP2 cKO parasites show reduced liver infection, starting at 6 hours

IV - Results

after infection until 48 hours after infection (**Figure 16**). The decrease in liver load for the first time point, 6 hours after infection, suggests that EXP2 cKO parasites might have a defect in colonization of the host liver (**Figure 16** – left graph). This can be explained by a defect in the infection of hepatocytes. Another possibility might be that parasites lacking EXP2, might lack the function the PTEX complex, which in the blood stage is responsible for the export of parasite proteins to the cytoplasm and membrane of erythrocytes [330]. During the liver stage, the PTEX could export proteins that prevent parasite elimination by the immune system of the infected mice or by the cell autonomous response of the infected cell.

To ascertain if the parasites were being eliminated by the immune system, we used WT and EXP2 cKO sporozoites to infect HepG2 cells, in an *in vitro* culture system [403]. After infection, we fixed the HepG2 cells, stained the parasites using the PVM marker UIS4 [404], and counted the number of infected cells at each time point. We fixed the cells as early as

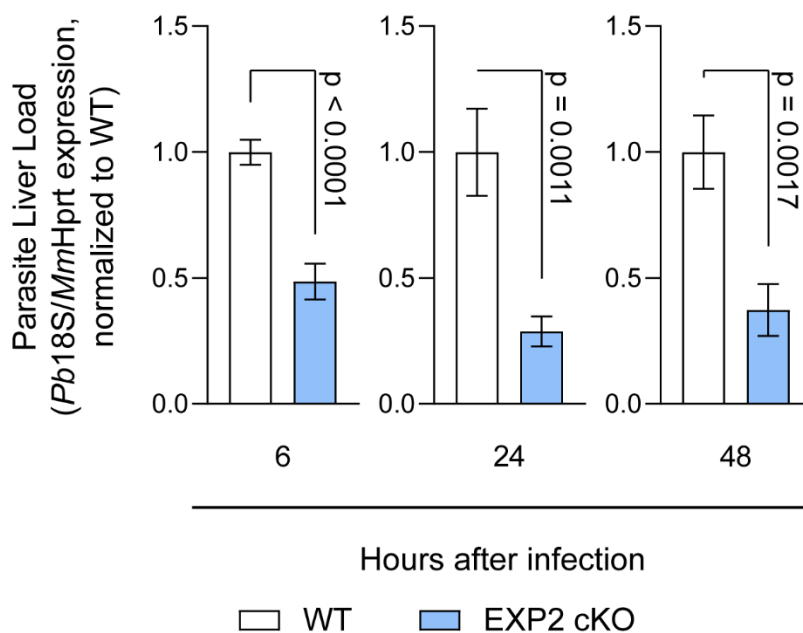


Figure 16 – Parasite liver load in infected mice at different hours after infection. C57Bl/6c mice were infected with 20,000 WT (white bars) or EXP2 cKO (blue bars) sporozoites and sacrificed at different hours after infection. RNA was extracted from livers of infected mice and parasite liver load was assessed by qPCR for *Pb18s* rRNA, compared to *MmHprt*. For each time point, the parasite liver load was normalized to the values obtained for infections using WT parasites. (N=10 for 6 hours after infection, N=15 for the other time points, mean \pm standard error of the mean (sem)).

2 hours after infection to account for the invasion of HepG2 cells; 12 and 24 hours after infection to account for sporozoite differentiation from long and slender sporozoite to spherical EEF; and finally we fixed cells at 48 and 55 hours after infection to verify if parasites were replicating normally. We observe that the number of infected cells is reduced from 2 hours after infection, by approximately 50% (**Figure 17** – left panel). Interestingly, this reduction in infected cells is kept constant during the remainder of the liver stage (**Figure 17** – remaining panels). This suggests that the EXP2 cKO parasites might pass through a selection barrier early during the infection process, that once crossed, is not able to affect the parasite EXP2 cKO parasites anymore. These results are comparable to the ones obtained during the infection of C57Bl/6c mice (**Figure 16**). The *in vitro* experiments also suggest that the immune system might not be needed for the elimination of these parasites, as the immune system is absent in *in vitro* experiments.

Such an early defect in establishment of infection by EXP2 cKO parasites, hints at a function of EXP2 in the sporozoite. As such, we decided to quantify the proportion of EXP2

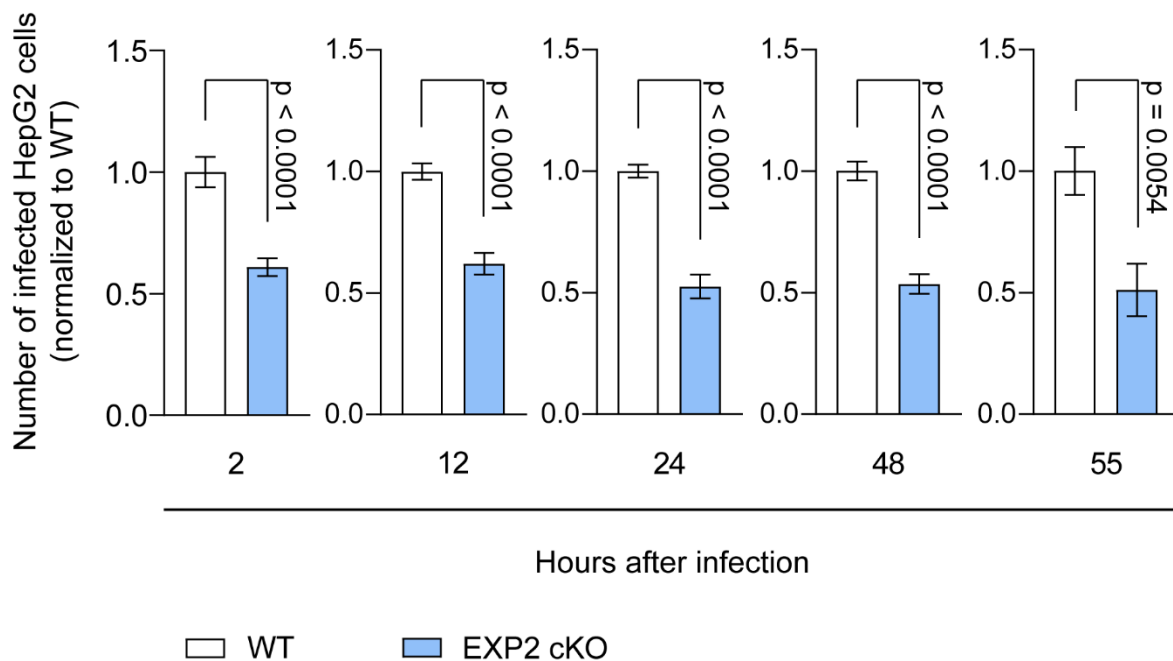


Figure 17 – Number of infected HepG2 cells at different hours after infection. HepG2 cells were infected with WT (white bars) or EXP2 cKO (blue bars) sporozoites, fixed, stained for the PVM marker UIS4, and the number of infected cells was counted for different hours after infection using widefield fluorescence microscopy. For each time point, the number of infected cells was normalized to the values obtained for infections using WT parasites. (N=5, mean \pm sem).

IV - Results

cKO parasites that would still express the EXP2 protein. For this, we dissected WT and EXP2 cKO sporozoites and performed immunofluorescence analysis (IFA), staining for the EXP2 protein. When analyzing WT sporozoites, we observed that EXP2 is present in the cytosol of the sporozoite, in a punctuated pattern (**Figure 18** – top panels). On the EXP2 cKO parasites, interestingly, we observe that approximately 50% of the EXP2 cKO sporozoites show EXP2 staining similar to WT parasites (**Figure 18**– middle panel) and that 50% of the EXP2 cKO sporozoites show no EXP2 staining (**Figure 18**– bottom panel). This indicates that the FRT/Flp system is not very efficient considering that only 50% of the sporozoites are effectively KO for EXP2. Curiously, these 50% of WT parasites in the EXP2 cKO population might be the same fraction of parasites that are observed developing inside HepG2 cells (**Figure 17** – left panel).

Interestingly, the EXP2 cKO population become increasingly enriched in parasites lacking EXP2 protein (as detected by IFA) as the liver stage progresses. Whereas 50% of EXP2 cKO sporozoites show EXP2 protein, only less than 5% of the exoerythrocytic forms

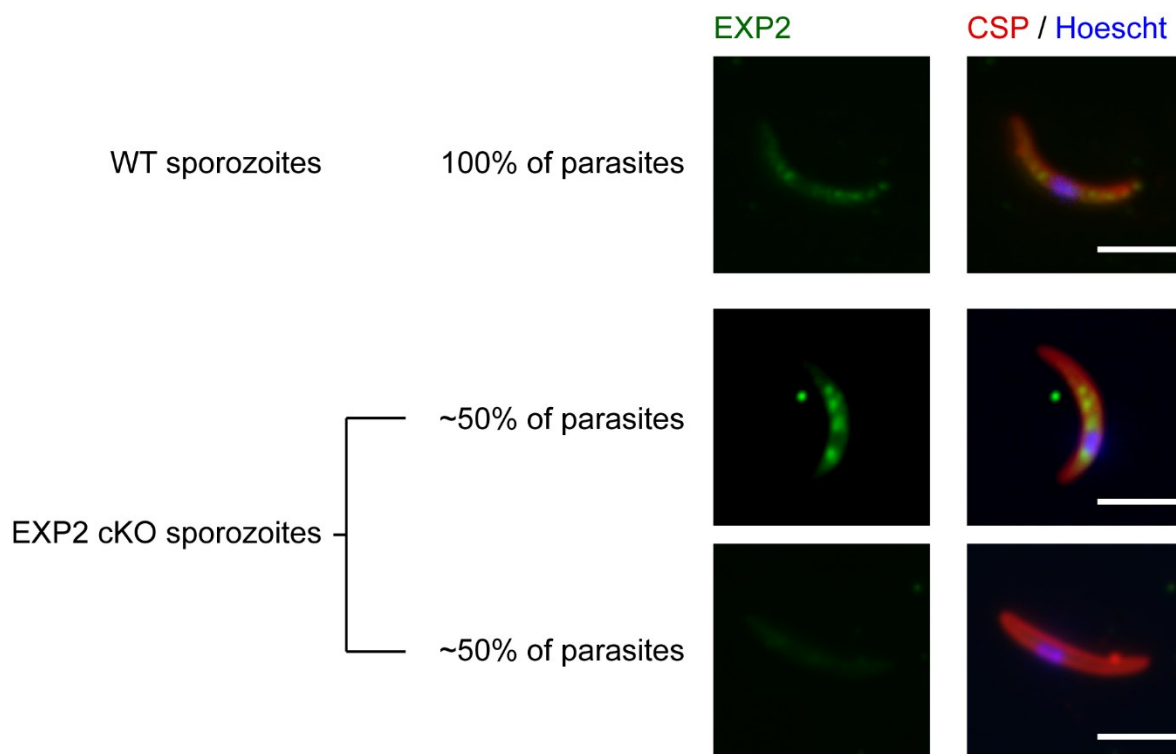


Figure 18 - EXP2 staining in WT and EXP2 cKO sporozoites. Freshly dissected sporozoites were fixed and permeabilized with ice-cold methanol at -20°C for 5 minutes. Sporozoites were stained with anti-EXP2 (green) and anti-CSP antibodies (red) and the DNA dye Hoechst (blue). (Scale bars: 5 μ m).

observed at 24 hours and 48 hours after infection are positive for the EXP2 protein when developing inside HepG2 cells (**Figure 19**). These results show that the conditional deletion system is leaky at the sporozoite stage and that it continues throughout the liver stage (**Figure 19**). This progressive deletion of the EXP2 locus can be explained by the expression of the UIS4 gene, which starts at the sporozoite stage [405] and is kept during the liver stage [404].

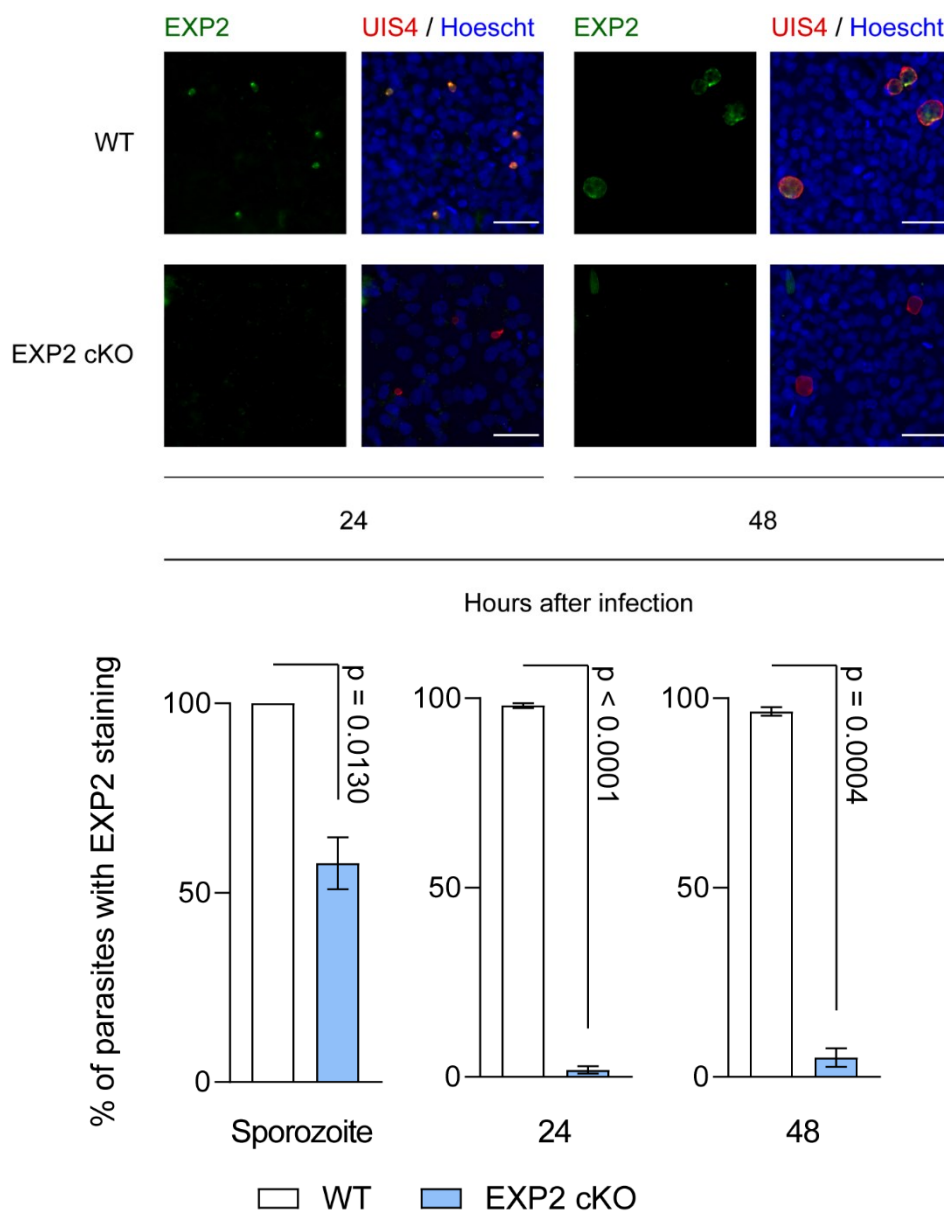


Figure 19 – Expression of EXP2 at EEFs at 24 and 48 hours after infection and proportion of parasites with EXP2 at different stages of infection. Top, HepG2 cells were infected with either WT or EXP2 cKO sporozoites, fixed at 24h and 48 hours after infection and were stained with anti-UIS4 (red) and anti-EXP2 (green) antibody. (Scale bar: 50 μ m). Bottom, proportion of WT (white bars) or EXP2 cKO (blue bars) parasites with EXP2 protein at different stages of infection. (N=3, mean \pm sem).

IV - Results

However, the lack of the EXP2 protein do not seem to hinder the development of EXP2 cKO parasites. Indeed, from 24 hours to 48 hours after infection, most EXP2 cKO EEFs develop normally inside the infected cell, both in terms of number (**Figure 17**) and also in terms of growth. EXP2 cKO parasites grow to the same extent as the WT parasites during the same time interval (from $80 \mu\text{m}^2$ to $400 \mu\text{m}^2$, **Figure 20**) as quantified by measuring the PVM area (delimited by UIS4 staining) in infected cells. This suggests that parasites lacking EXP2 during the liver stage develop normally inside a cell.

This raises the question if there is any protein export during the liver stage. Two possibilities arise. First, protein export might not be needed during the liver stages. The parasite are infecting a nucleated cell, with ability to respond to a number of alterations induced by the parasite. As such, there might be no need for the parasite to alter the surface of the hepatocyte nor its metabolic pathways, the major alterations during the blood stage of infection [302]. Secondly, protein export might still happen but through a different mechanism. The current understanding of protein export during the blood stages

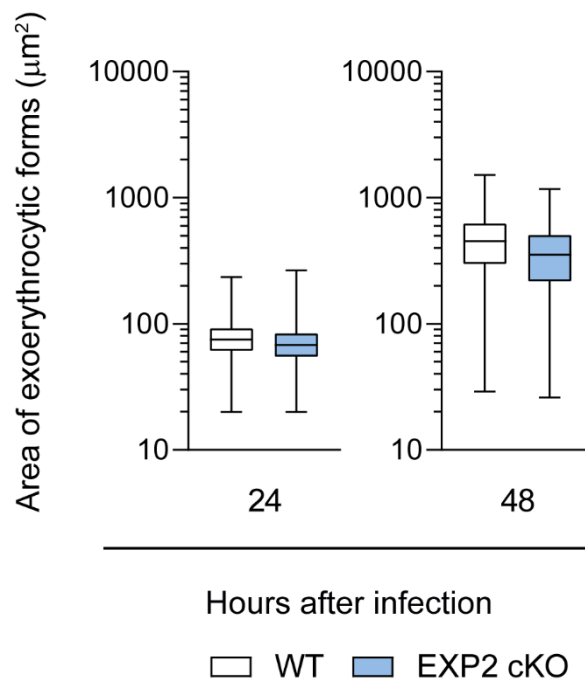


Figure 20 – Size of exoerythrocytic forms in HepG2 cells at different hours after infection. HepG2 cells were infected with WT (white boxplots) or EXP2 cKO (blue boxplots) sporozoites, fixed, stained for the PVM marker UIS4, and the size of parasites, in μm^2 , was measured for different hours after infection using widefield fluorescence microscopy. (N=5, boxplot represent the 25%, 50% and 75% quartile, with the minimum and maximum values shown by the bars).

suggests that the PTEX, and the EXP2 pore, is the only mechanism *Plasmodium* parasites possess to export proteins [322]. It is possible that protein export during the liver stages happens through a different molecular mechanism. The lack of knowledge about protein export during the liver stages makes it difficult to study what are the consequences of EXP2 deletion as there are no known exported protein to verify.

Apart from these two hypothesis, these results suggest that EXP2 is not needed during the liver stage, apart from the initial stages of infection. In fact, we measured EXP2 mRNA expression during the liver stages of *Plasmodium* infection, and we observed that the EXP2 gene is progressively down-regulated during the liver stage, only peaking at the last time point measured, 55 hours after infection (**Figure 21** – left panel). This last time point is probably more related to the preparation of the parasite to the ensuing blood stage, rather than development during the liver stage. AMA1, an important protein for the invasion of merozoites, follows a similar pattern to EXP2, as it is down-regulated during the liver stage, peaking at 55 hours after infection (**Figure 21** – middle panel). On the other hand, UIS4, the PVM marker, is progressively down-regulated during the liver stage, not

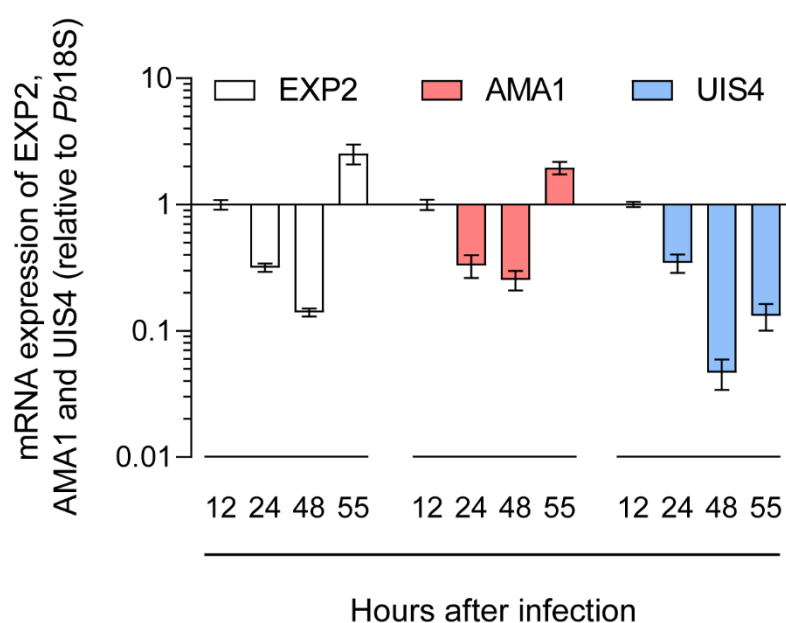


Figure 21 – Expression of EXP2, AMA1 and UIS4 genes during liver stages of *Plasmodium* infection. EXP2 (white bars), AMA1 (red bars) and UIS4 (blue bars) gene expression was analysed by qPCR, compared to the expression of 3 *Plasmodium* genes (*18s*, *serine-tRNA-ligase* and *adenylosuccinate lyase*) for HepG2 cells infected with WT parasites at different hours after infection. Expression values for each gene were normalized to expression at 12 hours after infection. (N=2, mean \pm sem).

IV - Results

peaking at the end of the liver stage as it happens with the other two proteins (**Figure 21** – right panel).

Concluding, EXP2 seems to be important during the initial stages of *Plasmodium berghei* liver stages, as its deletion compromises the colonization of both livers of mice and the HepG2 cell line. However, *Plasmodium* parasites lacking EXP2 protein develop normally inside HepG2 cells and possibly in the livers of infected mice as well.

1.2. EXP2 is important for cell invasion, but not for either gliding motility or traversal

On the previous section, we have established that parasites lacking EXP2 are hindered in their ability to infect the HepG2 cell line. However, the ability to infect a cell is a blend of three different phenomena, gliding motility, traversal capacity and invasion itself. If the parasite is defective on one (or more) of these characteristics, it might explain its difficulty in infecting a cell or the mouse liver.

The first ability of the sporozoite we tested was the gliding motility. Apicomplexan parasites show a type of motility, termed gliding, due to the glideosome, a protein complex that links the cytoskeleton to the IMC and to the plasma membrane of the parasite [184]. This protein complex is responsible for moving surface proteins of the parasite from the apical end of the sporozoite to the basal end. These bind to a variety of substrates, including glass and plastics used in cell culture tools, and, once they reach the basal end of the parasite, are released and remain adherent to the substrate [406] (**Figure 22**, left panel).

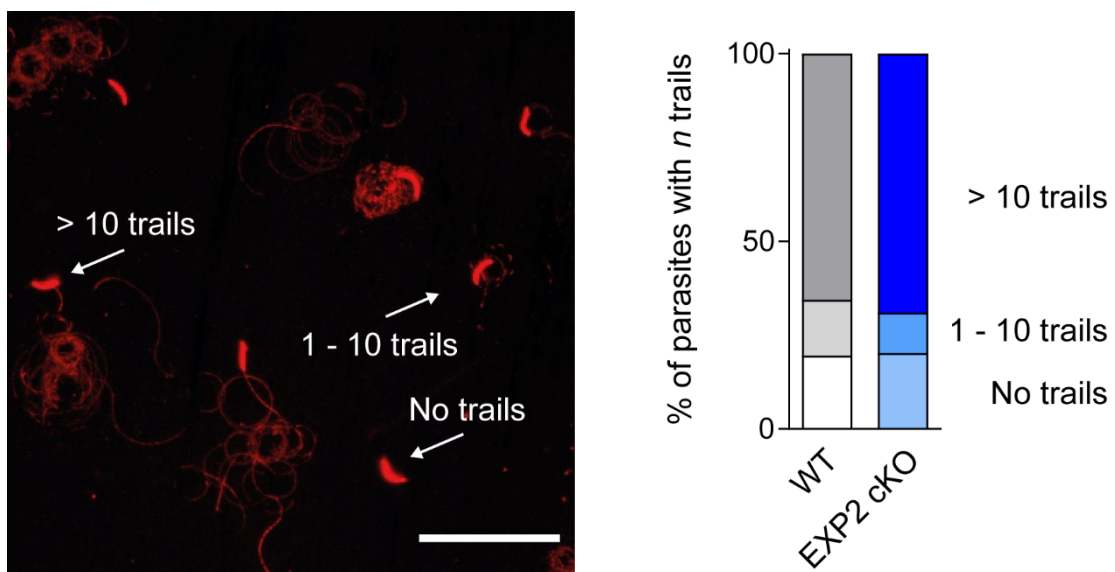


Figure 22 – Gliding motility of WT or EXP2 cKO sporozoites. Freshly dissected salivary gland WT (white and different shades of grey bars) or EXP2 cKO (different shades of blue bars) sporozoites were incubated in a glass coverslip at 37°C in the presence of complete DMEM medium. After 30 minutes of incubation, coverslips were stained using α PbCSP antibody, to detect trails of this protein on the glass coverslip. Sporozoites and trails were imaged using widefield fluorescence microscopy. Parasites were stratified into groups of parasites that showed no trails of CSP (bottom bars), 1 to 10 trails (middle bar) and more than 10 trails of CSP (top bars) as shown on the micrograph on the right (scale bar 50 μ m). (Representative image of 3 independent experiments).

IV - Results

In the case of *Plasmodium* sporozoites, the major surface protein is CSP protein, which is released by the sporozoite as it glides [407]. Because sporozoites have a concave shape, their motility is circular. As such, sporozoites leave behind circles of CSP protein, which can be imaged and counted to identify how much the parasite moved or glided (**Figure 22**, left panel). We decided to divide the motility of parasites into three categories: parasites that did no glide (no trails were counted), parasites that showed 1 to 10 circles of CSP (1 – 10 trails) or parasites that showed more than 10 circles of CSP (> 10 trails).

When we compared WT parasites to EXP2 cKO parasites, we can observe that the proportions of sporozoites that fit into one of these three categories is similar between the two parasite lines (**Figure 22**, right panel), suggesting that gliding motility is unaffected by the lack of EXP2 this protein. This was expected since the proteins that make up the glideosome have been studied in detail without any documentation of EXP2.

The next process the sporozoite needs to perform for infection is the traversal of cells. This process is unique to *Plasmodium* parasites, where the parasite passes through a cell, wounding the membrane of the cell, without infecting it [244,265]. To test if WT or EXP2 cKO parasites have the same capacity to traverse HepG2 cells, we incubated these parasites with cells in the presence of a fluorescent dextran molecule [391]. A normal cellular membrane is impermeable to this fluorescent dextran, with a molecular weight of 10,000 kiloDaltons, which can only be uptaken by a cell through membrane damage. After flow cytometry analysis, we detected almost no difference in the number of traversed cells by either WT or EXP2 cKO parasites (**Figure 23**).

There seems to be a slight increase in the number of traversed cells when cells are exposed to EXP2 cKO sporozoites, but this increase fails to be statistically significant. Importantly, it is reminiscent of earlier reports of P36 and P36p knock-out parasites, that showed a correlation between a lower number of infected cells to an increased number of traversed cells [270].

To conclude, the first two phenomena that precede invasion of the hepatocyte by *Plasmodium* sporozoites are normal in the EXP2 cKO parasite line, when compared to WT parasites.

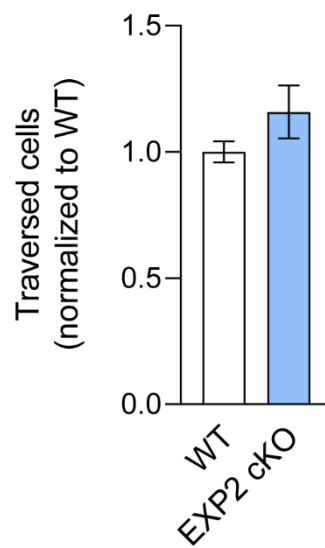


Figure 23 – Traversal ability of WT and EXP2 cKO sporozoites. Freshly dissected salivary gland WT (white bar) or EXP2 cKO (blue bar) sporozoites were allowed to traverse HepG2 cells at 37°C in the presence of complete DMEM medium supplemented with 0.5 mg/mL dextran-rhodamine. After 2 hours of incubation, HepG2 were trypsinized and analysed by flow cytometry for the staining of rhodamine. At least 20,000 cells were analysed for each experiment. (N=9, mean \pm sem).

IV - Results

1.3. EXP2 is critical for the invasion of the hepatocyte

The last of the three phenomena that culminate in infection of the hepatocyte is the invasion of the soon-to-be-infected cell. To assess if EXP2 cKO sporozoites were defective in the invasion step, we incubated WT or EXP2 cKO sporozoites with HepG2 cells and fixed them at 2 hours after infection. To assess invasion of sporozoites, we stained the samples using two sets of parasite markers, one for the membrane of the sporozoite (CSP) and another for the PVM marker (UIS4) (**Figure 24**, right panels). This allows us to distinguish from the total sporozoite population (observed using CSP staining), which sporozoites had in fact invaded HepG2 cells, as these would show staining for both UIS4 and CSP proteins (termed intracellular). When comparing the number of extracellular sporozoites (**Figure 24**, left panel), we observe that 75% of EXP2 cKO sporozoites were found outside cells, showing only CSP staining, when compared to only 50% WT sporozoites. Conversely, whereas approximately 50% of total WT sporozoites were found inside HepG2 cells, surrounded by the PVM marker UIS4, only 25% of total EXP2 cKO sporozoites were found with the UIS4 marker around. This suggests that EXP2 cKO sporozoites are unable to invade HepG2 cells.

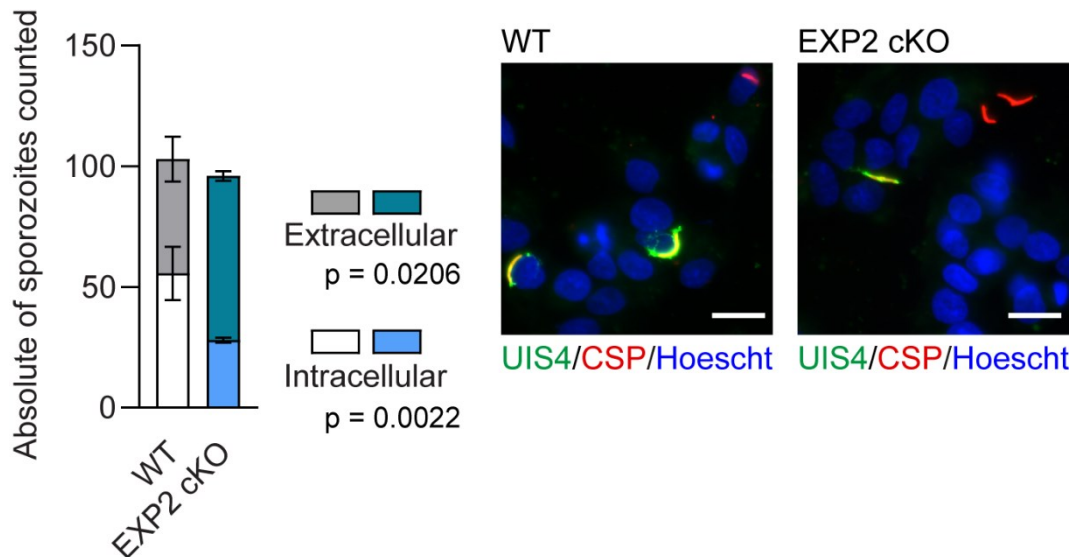


Figure 24 - Number of extracellular and intracellular sporozoites 2 hours after infection of HepG2. HepG2 cells were infected with WT (white and gray bars) or EXP2 cKO (light blue and darker blue bars) sporozoites, fixed, stained for the PVM marker UIS4 and the sporozoites membrane marker CSP, and the number of extracellular (only CSP positive sporozoites, darker bars) and intracellular (both CSP and UIS4 positive sporozoites, lighter bars) were counted using widefield fluorescence microscopy, as shown in the representative micrographs on the right. (N=3, mean \pm sem).

To better assess the temporal resolution of the possible defect in invasion, we incubated WT or EXP2 cKO parasites with HepG2 cells and fixed them at different time points after infection, until 2 hours or 120 minutes. This time interval has been shown to be when sporozoites invade cells *in vitro* [265]. As before, we consider that a parasite has invaded if it has a PVM surrounding itself, which we can visualize by staining for the PVM-resident protein UIS4.

When comparing WT or EXP2 cKO parasites, we observe that the WT parasite invades cells to a higher extent than the EXP2 cKO parasites (**Figure 25**). Indeed, the difference between these two parasite lines is already visible at 60 minutes after infection and is kept throughout time, until the end of the invasion step.

To further validate that the lack of EXP2 would be responsible for a defect in invasion of HepG2 cells, we took advantage of the leakiness of the FRT/Flp conditional knock-out system. For every sporozoite dissection and invasion assay, we have a different level of excision of the *EXP2* locus, which we can quantify by qPCR, by analyzing the genomic DNA of the sporozoites used in each experiment.

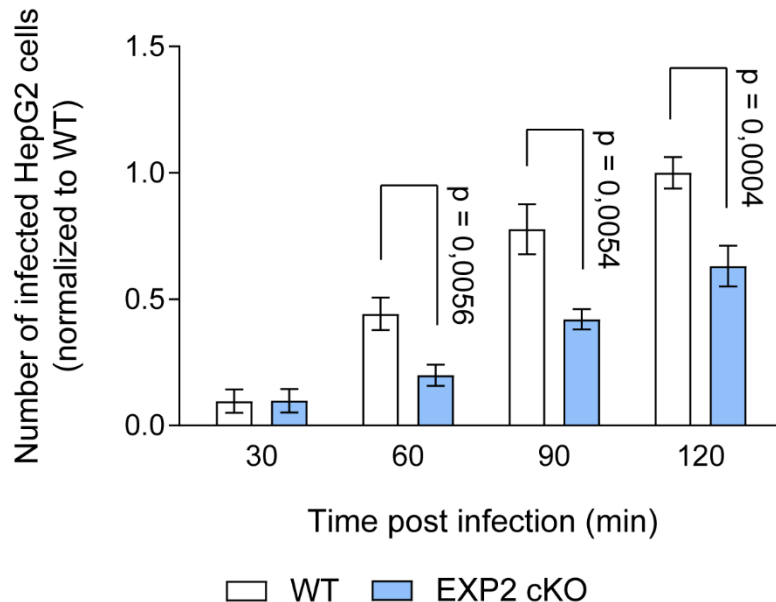


Figure 25 – Number of infected HepG2 cells at different minutes after infection. HepG2 cells were infected with WT (white bars) or EXP2 cKO (blue bars) sporozoites, fixed, stained for the PVM marker UIS4, and the number of infected cells was counted for different minutes after infection using widefield fluorescence microscopy. The number of infected cells at each time was normalized to values obtained using WT parasites at 120 minutes after infection. (N=3, mean \pm sem).

IV - Results

We decided to test if the level of excision of the *EXP2* locus would correlate to the levels of invasion observed in by the *EXP2* cKO parasites. We observe that there is a linear correlation between the levels of unexcised sporozoites in the *EXP2* cKO population with the invasion capacity of the parasites (**Figure 26**). This means that if *EXP2* cKO parasite population has more WT parasites, it is more invasive. Conversely, if *EXP2* cKO parasite population has more KO parasites, the less invasive it becomes (**Figure 26**). Interestingly, the correlation values are not 1 (perfect correlation) and the plotted curve cannot fully explain the invasion rate of *EXP2* cKO parasites using the gDNA quantification alone. This means that some *EXP2* *genetically*-KO parasites might still retain their invasive capacity, possibly due to a build up to *EXP2* mRNA or protein before the excision event took place, that makes the parasite *functionally*-WT.

It is curious to note that only a small fraction of parasites (for WT and *EXP2* cKO parasite lines) invade cells after 30 minutes of incubation, only committing to invasion from 60

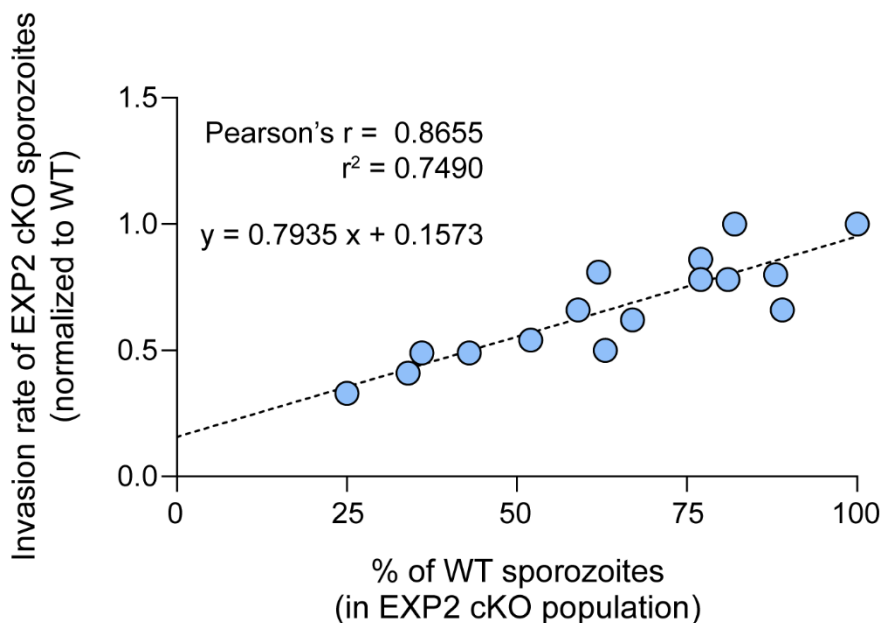


Figure 26 – Correlation between WT prevalence in the *EXP2* cKO population and its invasion rate.

Genomic DNA was extracted from WT and *EXP2* cKO parasites during each experiment and the proportion of unexcised parasites in the *EXP2* cKO sporozoite population was assessed by qPCR. These proportions (X-axis) are plotted to invasion rate of *EXP2* cKO parasites, when compared to WT parasites (Y-axis) for each experiment. The equation on the figure represents the equation of the linear regression performed on the data (shown as a dashed line). (Each dot represents one independent experiment, N=16).

minutes onwards (**Figure 25**). To assess if this would be an off-target of manipulating the *EXP2* locus, we performed the same experiment with another *P. berghei* parasite line, that has an unperturbed *EXP2* locus [387]. To our reassurance, this *P. berghei* parasite line follows the same temporal dynamics of infection as do the WT and *EXP2* cKO parasite lines (**Figure 27** – left side of the graph), few parasites infected cells before 45 minutes after incubation of parasites with cells. This result is in line with previous results that show that *Plasmodium* sporozoite traverse cells during their first hour in contact with them, only committing to invasion afterwards [265]. To examine if cell traversal is indeed delaying invasion of HepG2 cells, we repeated the same experiment with *SPECT1* KO parasites that, despite not being able to traverse cells, are as effective as WT parasites in invading them [260]. To our surprise we observe that *SPECT1* KO sporozoites follow the same temporal dynamics as all the parasite lines tested by us (**Figure 27** – right side of the graph). For the first 45 minutes of incubation, very few parasites invade cells; this event only starts at 45 minutes and lasts until 90 minutes.

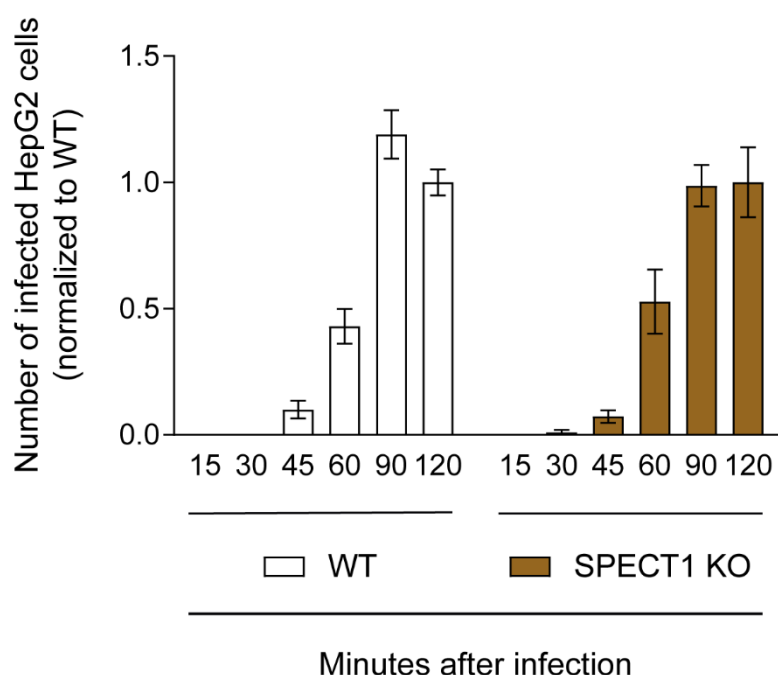


Figure 27 – Number of infected HepG2 cells at different minutes after infection. HepG2 cells were infected with WT (white bars) or *Spect1* KO (dark yellow bars) sporozoites, fixed, stained for the PVM marker UIS4, the number of infected cells was counted for different minutes after infection using widefield fluorescence microscopy. For each parasite line, the number of infected cells was normalized to the values obtained for infections at 120 minutes after infection. (N=3, mean \pm sem).

IV - Results

To understand if EXP2 would be playing a role in this *delayed* invasion phenomenon, the decided to analyze EXP2 mRNA expression by qPCR in sporozoites during the invasion time frame. We decided to focus on 3 time points: 30 minutes post incubation with cells (very little invasion), 60 minutes post incubation (invasion starts) and 120 minutes post incubation (invasion has finished). EXP2 mRNA dynamics seems to precisely follow the dynamics of invasion, peaking at 60 minutes post incubation and decreasing at the last time point (**Figure 28**). This dynamic is unexpected and does not follow other invasion related proteins. For example, glideosome-associated protein 45 (GAP45) mRNA levels are kept constant during the first steps (there is possibly sufficient levels of this gene in the sporozoite when it resides the salivary gland) is down-regulated only at the end of the invasion process (**Figure 28**). This down-regulation is expected given that the IMC is destroyed by the parasite, after invasion of the cell [408]. On the other hand, exported protein 1 (EXP1) mRNA expression is steadily upregulated has invasion starts and the parasites is effectively inside the host cell (**Figure 28**). This also correlates with the possible

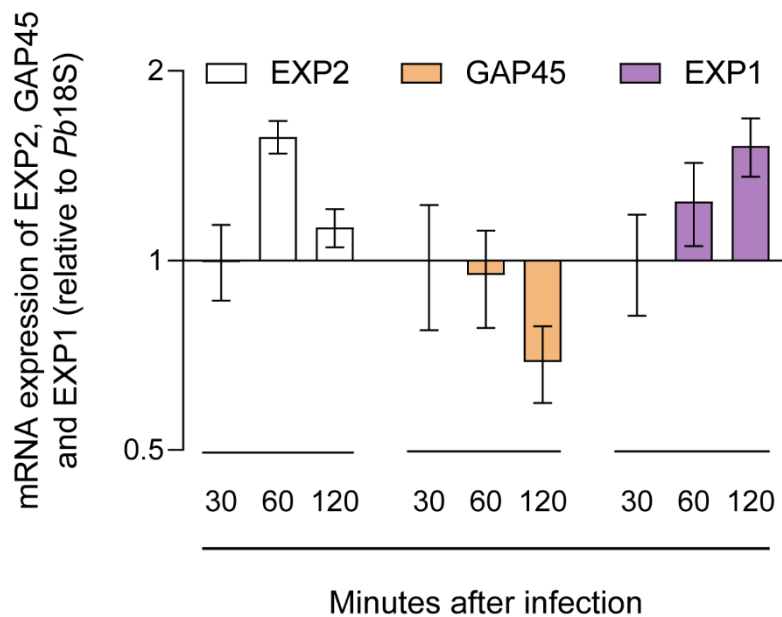


Figure 28 – Expression of EXP2, GAP45 and EXP1 genes during invasion stages of *Plasmodium* liver infection. EXP2 (white bars), GAP45 (orange bars) and EXP1 (purple bars) gene expression was analysed by qPCR, compared to the expression of 3 *Plasmodium* genes (*18s*, *serine-tRNA-ligase* and *adenylosuccinate lyase*), for HepG2 cells infected with WT parasites at different minutes after infection. Expression values for each gene were normalized to expression at 30 minutes after infection. (N=3, mean \pm sem).

importance of EXP1 during the liver stages, where it is found in the PVM of the parasite [363,409].

The peak of EXP2 expression at 1 hour after interaction with cells, together with the fact that levels EXP2 correlate with invasion, firmly support the fact that parasites require EXP2 to successfully invade cells. Once inside, parasites seem not to require EXP2 for parasite growth and multiplication.

To conclude the first section, we have established that sporozoites require EXP2 protein for invasion of the hepatocytes. Levels of EXP2 mRNA positively correlate with invasion rate of the EXP2 cKO parasite population. Moreover, once EXP2 cKO parasites are inside cells, EXP2 does not seem to be necessary for the development and maturation of the parasite inside hepatocytes.

2. Dynamics of EXP2 protein in the sporozoite

From the previous section, we ascertained that EXP2 is important for invasion of *Plasmodium berghei* sporozoites. The corollary of this results is that EXP2 must be present at the sporozoite stage, which has been previously observed (**Figure 18**) [333,364].

To better localize EXP2 in the sporozoites, we performed electron microscopy on freshly dissected sporozoites (**Figure 29**). Using a gold-labelled secondary antibody, we detect EXP2 along the cell body of the parasite (**Figure 29** – sagittal view) and at higher

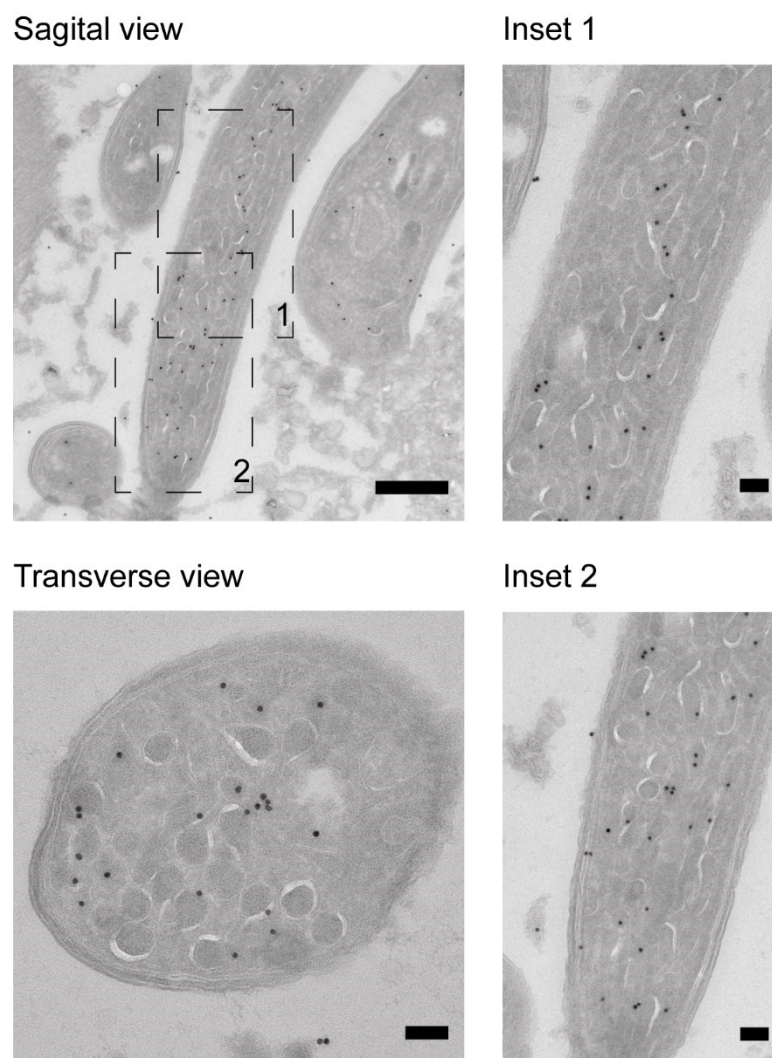


Figure 29 – Electron micrographs of sporozoites immunolabelled with EXP2. Freshly dissected sporozoites were immunolabelled with EXP2 (black dots). (Scale bars: Sagittal view 500nm; Transverse view and Insets 100 nm.)

IV - Results

magnification, we observe that EXP2 staining is close to, or even inside vesicles (**Figure 29** – inset 1 and 2 and transverse views).

These numerous puncta suggest that EXP2 can be present in vesicular structures in the cell body of the parasite. To discriminate if EXP2 is present in micronemes, rhoptries or dense granules of the parasite, we performed IFA for EXP2 and TRAP (present in micronemes), RON4 (rhoptries) and UIS4 (located in an unidentified population of vesicles, possibly dense granules). From analyzing confocal micrographs, we do not see co-localization of EXP2 with any of the other 3 proteins used (**Figure 30**). It is noteworthy that we observe two types of staining for TRAP (the micronemal protein), vesicular and membranar (**Figure 30** – top panel). This shows that some micronemes might have already been secreted by the parasite during the manipulation of the sporozoite, from the dissection of the salivary glands to the fixation, which takes 15 to 30 minutes.

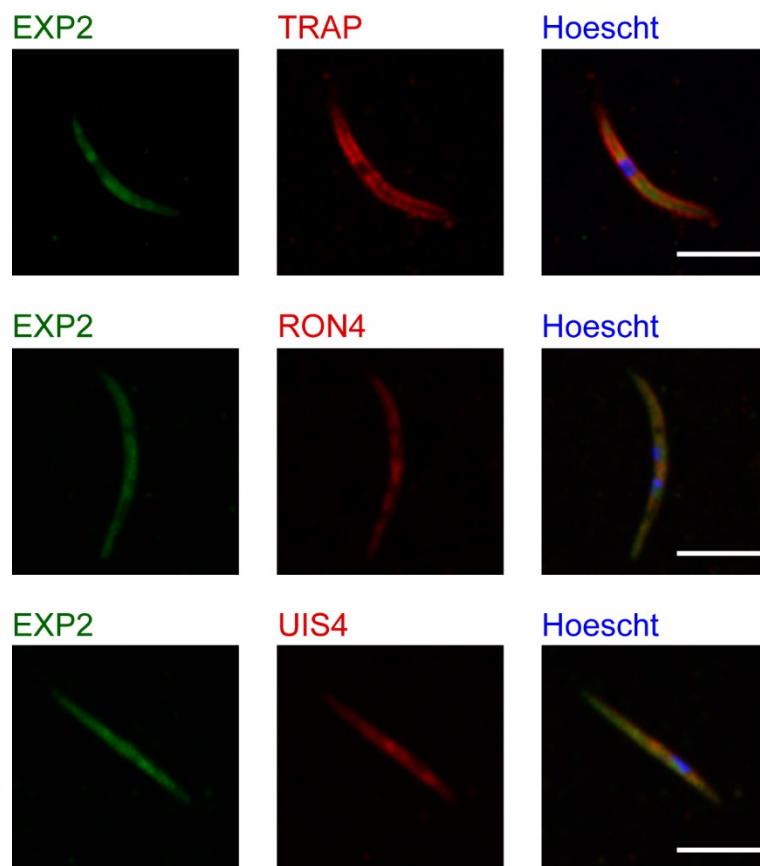


Figure 30 – EXP2 localisation in freshly dissected sporozoites. Sporozoites were fixed immediately after dissection, were permeabilized using ice cold methanol for 5 minutes at -20°C and were stained for EXP2 protein (green), TRAP, RON4 or UIS4 (red) and Hoechst (blue). (Scale bars: $5\ \mu\text{m}$).

The secretion of micronemes lead us to hypothesize that vesicular EXP2 might also be secreted by the parasite, during the invasion process. To test for this, we stimulated freshly dissected sporozoites with fetal calf serum (FCS) for 30 minutes at 37°C (**Figure 31**). These stimuli have been used to mimic the conditions sporozoites encounter in the blood stream of the mammalian host and that has been shown to activate *Plasmodium* sporozoites [268,270,410] and merozoites [200], as well as *T. gondii* tachyzoites [411], inducing exocytosis of apical vesicles.

As expected, membranar staining of TRAP protein is increased following activation (**Figure 31** – top panel) and we even observe trails of TRAP protein. Importantly, this activation is also able to induce the translocation of EXP2 from the cytosolic vesicles to the surface of the sporozoite (**Figure 31** – left panels). Both RON4 and UIS4 protein do not show any change in location following stimulation (**Figure 31** – middle and bottom panels, respectively). This was expected as RON4 has been shown to be secreted after the

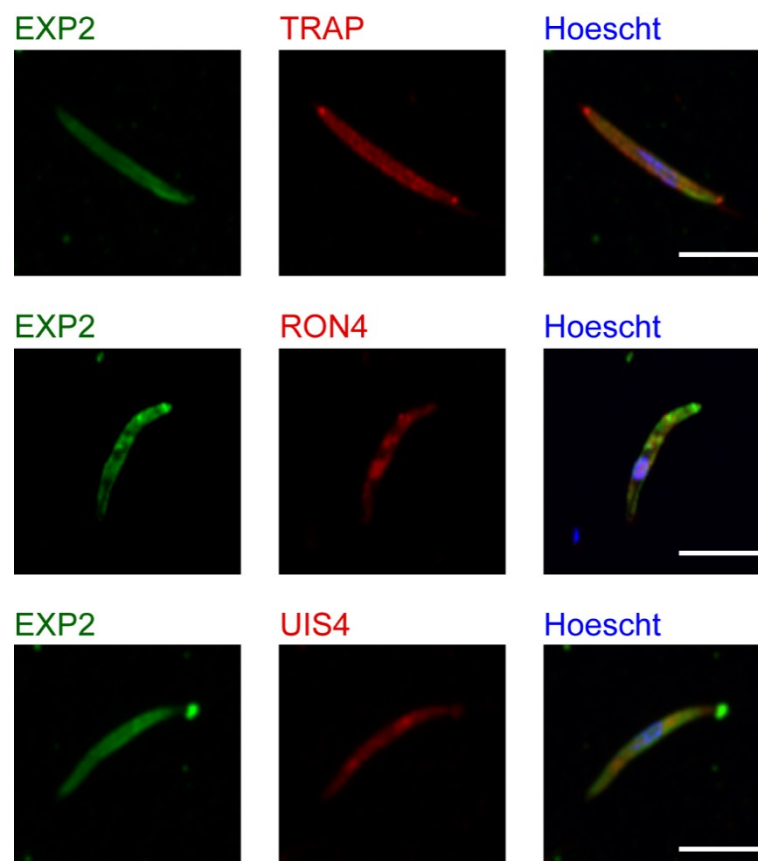


Figure 31 – EXP2 localisation in activated sporozoites. Sporozoites were fixed after being incubated for 30min, at 37°C in complete DMEM medium containing fetal calf serum. Sporozoites were permeabilized using ice cold methanol for 5 minutes at -20°C and were stained for EXP2 protein (green), TRAP, RON4 or UIS4 (red) and Hoechst (blue). (Scale bars: 5 µm).

IV - Results

sporozoites engage with host cell receptor CD81 [412] and UIS4 is only secreted at the end of the invasion process [404].

To further confirm that EXP2 protein is present at the surface of the sporozoite, we performed the previous staining procedure without permeabilization of the sporozoites. As before, only TRAP and EXP2 proteins are detected on activated sporozoites (**Figure 32**).

Importantly, not all sporozoites showed a change in EXP2 location following activation. We observed EXP2 at the membrane in 50% of activated sporozoites (**Figure 33**, left panel), whereas 40% of activated sporozoites still showed EXP2 in the cytosol (**Figure 33**, central panel). Notably, in 10% of activated sporozoites, EXP2 was observed to be concentrated in the apical end of the sporozoites, capping the parasite (**Figure 33**, right panel). This has been previously observed for TRAP [413] and suggests that EXP2 could be secreted by sporozoites during activation.

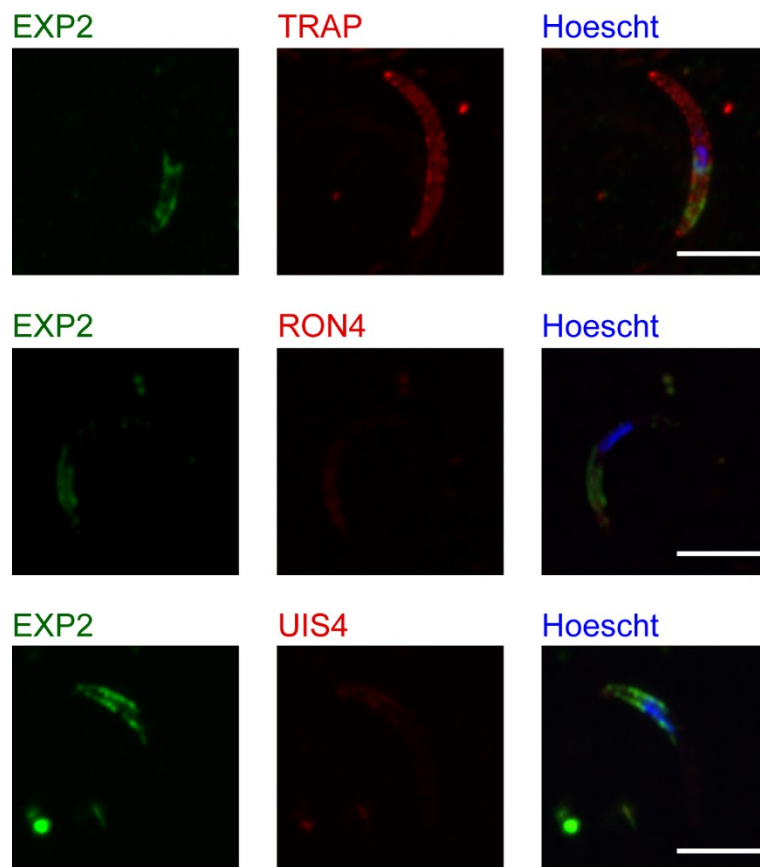
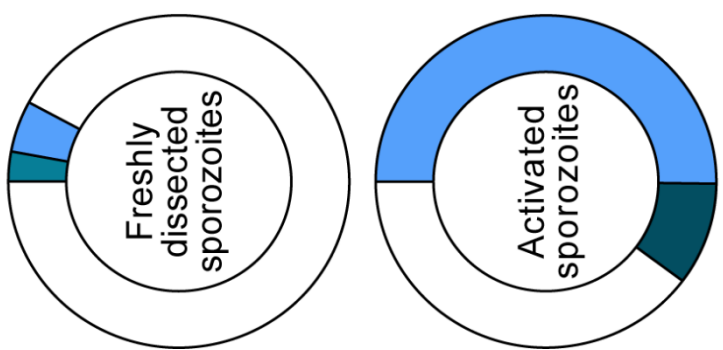
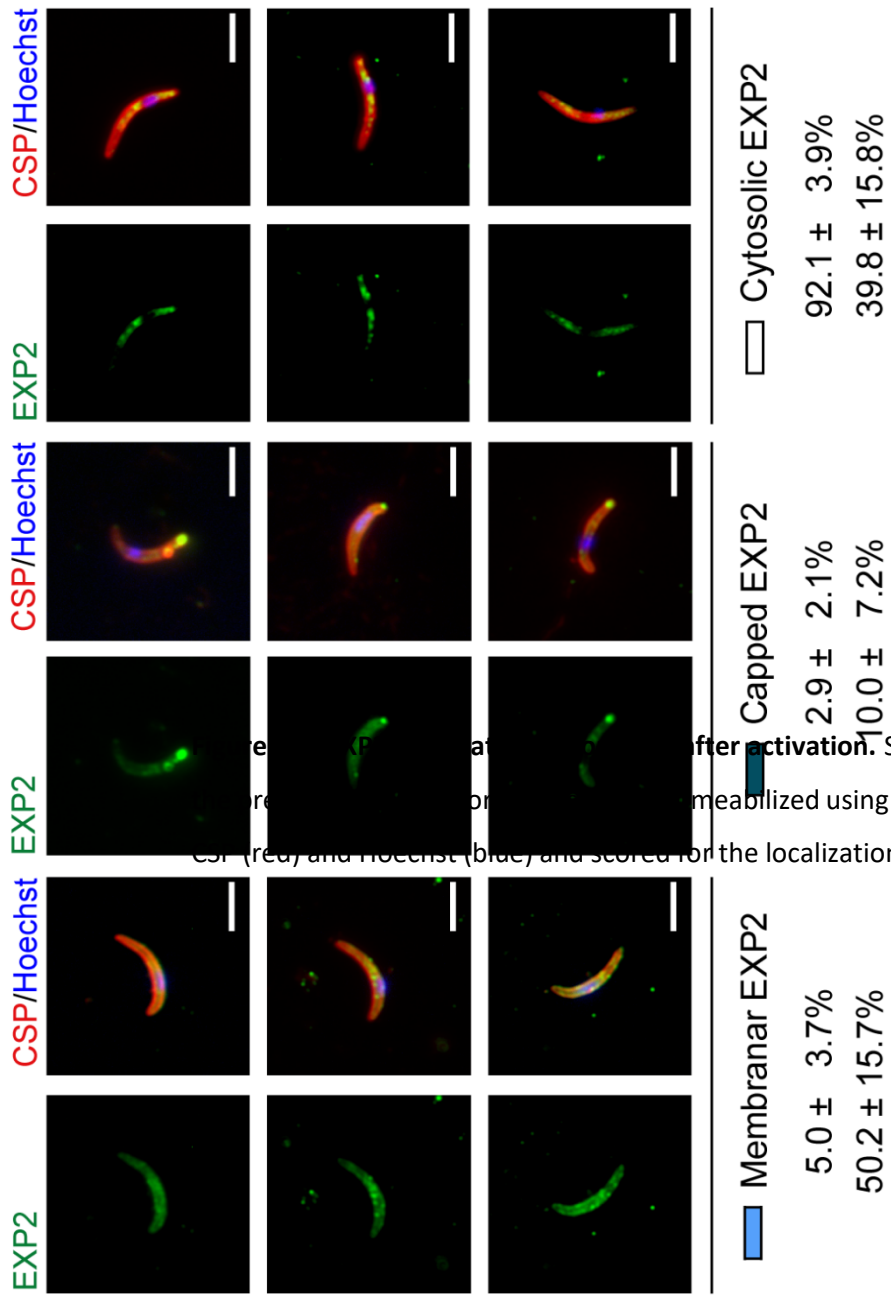


Figure 32 – EXP2 localisation in non-permeabilized sporozoites. Sporozoites were fixed after being incubated for 30min, at 37°C in complete DMEM medium containing fetal calf serum (FCS, bottom panel). Sporozoites were not permeabilized before antibody incubation and were stained for EXP2 protein (green), TRAP, RON4 or UIS4 (red) or Hoechst (blue). (Scale bars: 5 µm).



Freshly dissected:
Activated:

after activation. Sporozoites were dissect and either fixed or permeabilized using ice cold methanol for 5 minutes at -20°C. Stained with anti-EXP2 (green), anti-CSP (red) and Hoechst (blue) and scored for the localization of EXP2, which could be cytoplasmatic

IV - Results

Indeed, sporozoite activation has been shown to induce exocytosis of proteins, not only to the surface of the sporozoite but also to the medium surrounding the sporozoite [268]. To facilitate the detection of EXP2 in the medium, we used a *P. berghei* parasite line that possesses a HA-tagged EXP2 [333]. To further increase the detection, we purified the sporozoites after dissection by gradient purification, using the Nycodenz polymer [395]. These two modifications allowed us to achieve very concentrated sporozoite mixtures (for example, 500,000 sporozoites in 25 μ L) and better detection of the protein of interest (antibodies against HA-tag have more affinity than those available against *Plasmodium* EXP2).

To test if EXP2-HA would be secreted the same way as TRAP, we activated sporozoites and after 30 minutes of incubation, separated the sporozoite from the media by centrifugation. We assayed both the sporozoites as well as the media for the EXP2-HA protein by SDS-PAGE followed by Western Blot. We observe that the HA-tagged EXP2 is present in the pellet fraction (sporozoites) in all conditions as is in lysates of mixed blood stages (BS, **Figure 34**– bottom panel). As hypothesized, the EXP2-HA is also and only detected in the medium of sporozoites that were incubated at 37°C and in the presence of FCS (**Figure 34**– bottom panel).

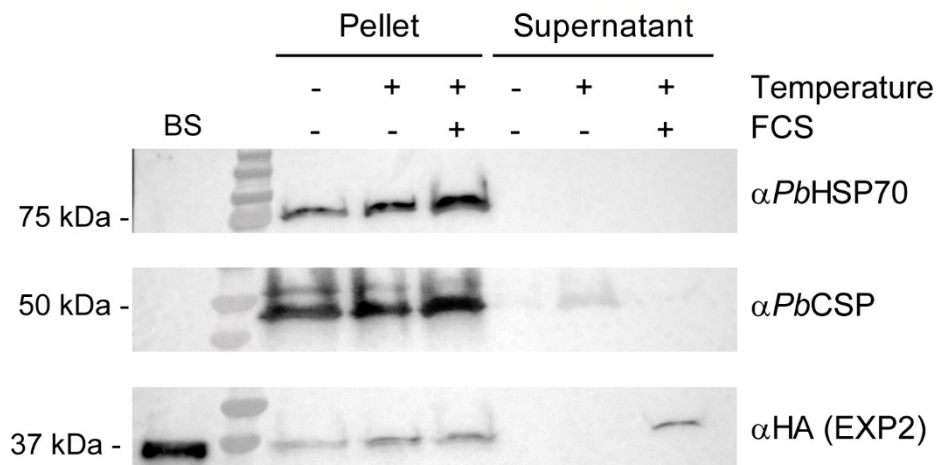


Figure 34 – Protein secretion after sporozoite activation. Freshly dissected sporozoites were purified using 17% Accudenz. After recovery, sporozoites were kept at 4°C or stimulated at 37°C in the absence or presence of FCS for 30 minutes. Sporozoites were pelleted, lysed and the supernatants were recovered. Both pellet and supernatant fractions were assayed for presence of HA-tagged EXP2, CSP and HSP70 by Western Blot. As a control, lysate of a blood stage (BS) infection using EXP2-HA parasites was used. (Representative Western Blot of 6 independent experiments).

To control for the input of sporozoites, we also assayed for CSP and we only detect this surface protein on the sporozoite fractions (**Figure 34**– middle panel). An important source of EXP2-HA in the supernatant fractions of the sporozoites could be unwanted lysis of the sporozoites because of the addition of serum to the sample. This does not seem to be the case as the cytosol protein HSP70 is only detected in the sporozoite fraction, showing that secreted EXP2 does not originate from lysed sporozoites (**Figure 34**– top panel).

To conclude, we have shown that sporozoites express the EXP2 protein, initially localized in vesicles. Upon stimulation with serum and temperature, EXP2 is translocated to the surface of the sporozoite and secreted to the medium.

3. Membrane repair pathway as a mechanism of entry

We have established on the previous section that EXP2 is secreted by Plasmodium sporozoites after stimulation with temperature and serum. We have also established before that EXP2 is critical for the invasion of hepatocytes by the sporozoite. How can EXP2 be involved in an invasion mechanism?

We know that EXP2 is a pore-forming protein and that there are numerous examples of pathogens that use pore-forming proteins to invade their target cell. Importantly, such pathogens do not enter the cell through the pore their proteins make, rather, the pore created in the membrane of the target cell, activates a membrane repair pathway that is used by the parasite to get inside [148–156].

3.1. EXP2 is required at an intermediate stage of the invasion timeframe

If EXP2 is playing a role in the invasion mechanism and is secreted during by the activated sporozoite, we wondered if we could rescue the invasion defect of EXP2 cKO parasites by adding exogenous EXP2 protein during the invasion step. Therefore, we produced recombinant EXP2 protein (rEXP2) [339] and used it to supplement both WT and EXP2 cKO sporozoites during the invasion step. We decided to add rEXP2 1 hour after sporozoites were incubated with cells, as it was the time point at which we saw up-regulation of the EXP2 mRNA (**Figure 28**). We fixed cells 2 hours after infection and counted the number of infected cells. We observed that the addition of rEXP2 protein rescued the defect of the EXP2 gene in a dose dependent manner, increasing the level of infection of the EXP2 cKO parasites to levels comparable to the ones observed with WT parasites (**Figure 35** – top panel). Importantly, if we wash out the rEXP2 protein at 2 hours after infection (end of invasion step) and allow invaded parasites to progress with the infection, we observe that the number of infected cells at 48 hours after infection is comparable to the number of cells infected with WT parasites (**Figure 35** – bottom panel). This means that once the EXP2 cKO parasites overcome the invasion defect, they mature normally. It is noteworthy to point out that we achieve the rescue with diminutive amounts of rEXP2, in

IV - Results

the nanomolar range. These concentrations are similar to the ones used to study the invasion mechanism described by other pathogens.

We had observed that the EXP2 protein is at the membrane of the sporozoites (**Figure 31-Figure 33**) and this could possibly mean that the EXP2 protein is acting on the sporozoite, possibly inducing changes in the permeability of the sporozoite membrane, facilitating the

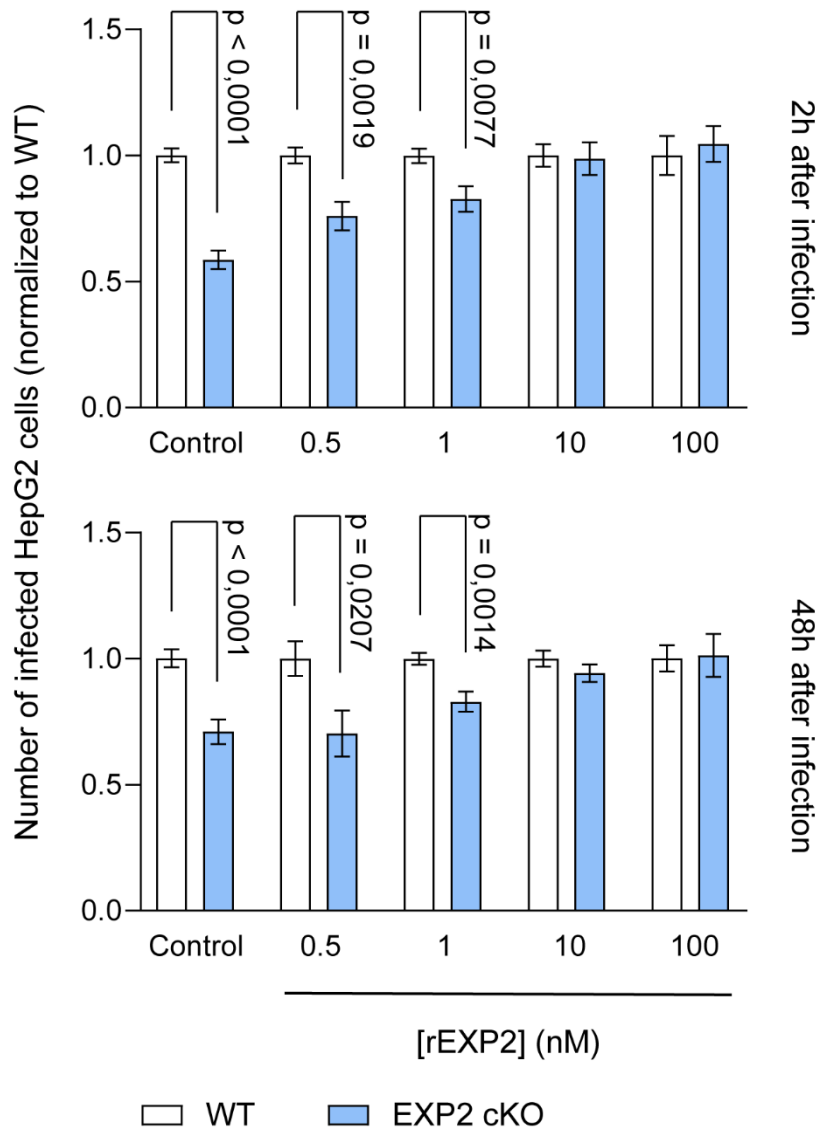


Figure 35– Number of infected HepG2 cells following rEXP2 treatment. HepG2 cells were infected with WT (white bars) or EXP2 cKO (blue bars) sporozoites and treated with increasing concentrations of rEXP2, starting at 1 hour after infection until 2 hours after infection. Cells were fixed either at 2 hours after infection (top) or at 48 hours after infection (bottom), stained for the PVM marker UIS4, and the number of infected cells was counted for different hours after infection using widefield fluorescence microscopy. For each concentration of rEXP2, the number of infected cells was normalized to the values obtained for infections using WT parasites. (N=5, mean \pm sem).

entry of ions that might be critical for sporozoite activation [410]. Indeed, it has been shown that after stimulation of sporozoites to high concentrations of potassium ions, sporozoites tend to invade cells faster [266]. These potassium ions could be entering through EXP2 pores. To test if EXP2 could be acting in the sporozoite alone, we decided to dissect sporozoites and incubate them with rEXP2 protein, in the absence of hepatoma cells. When we added the treated sporozoites to cells, we did not observe any rescue of the invasion defect (**Figure 36**, second set from the left). Also, we added rEXP2 protein at the same time that we added sporozoites to the hepatoma cells. Again, when rEXP2 is added at time zero, no rescue is observed (**Figure 36**, third set from the left). We only observed rescue, when rEXP2 is added at 1 hour after invasion (**Figure 36**, fourth set from the left).

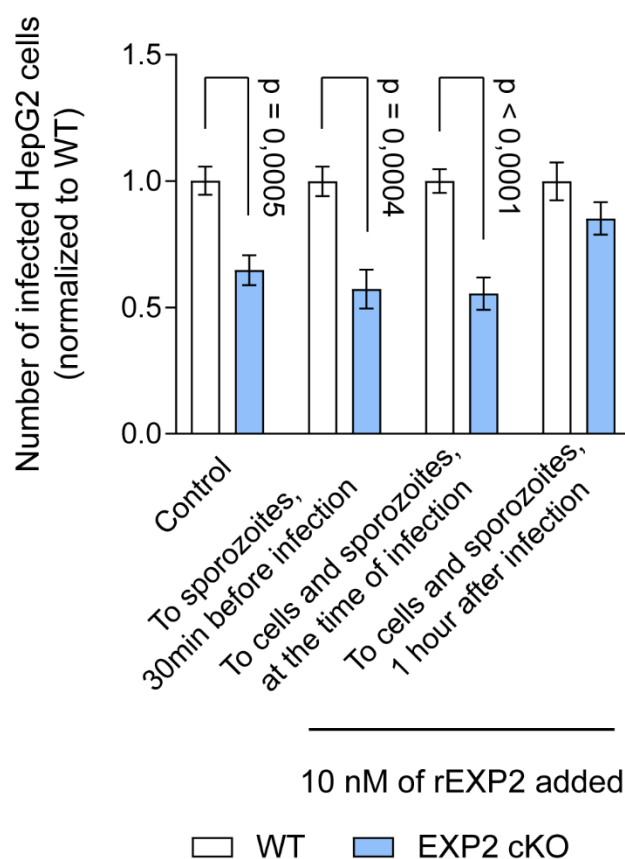


Figure 36 – Number of infected HepG2 cells following different regimens of rEXP2 treatment. HepG2 cells were infected with WT (white bars) or EXP2 cKO (blue bars) sporozoites and treated with 10 nM of rEXP2 protein in different regimens. Cells were fixed at 2 hours after infection, stained for the PVM marker UIS4, and the number of infected cells was counted for each condition using widefield fluorescence microscopy. The number of infected cells was normalized to the values obtained for infections using WT parasites. (N=3, mean ± sem).

IV - Results

Interestingly, when WT parasites were treated with rEXP2 protein, we do not observe any increase in invasion. To assess if WT parasites are affected by treatment with rEXP2 protein, we treated WT parasite with rEXP2 protein at different time intervals after incubation with cells. We tested two different concentrations of rEXP2 protein, which enhance invasion of EXP2 cKO parasite, 1 and 10 nM. As observed before, no effect on the number of infected cells was observed, at any of the treatment regimens with rEXP2 protein (**Figure 37**). The possible explanation of this result is that each EXP2-expressing sporozoite secretes enough amount of EXP2 protein to achieve its own invasion, meaning that extra EXP2 protein is not needed. When EXP2 is lacking in the EXP2 cKO sporozoite, the added EXP2 protein does indeed make a difference.

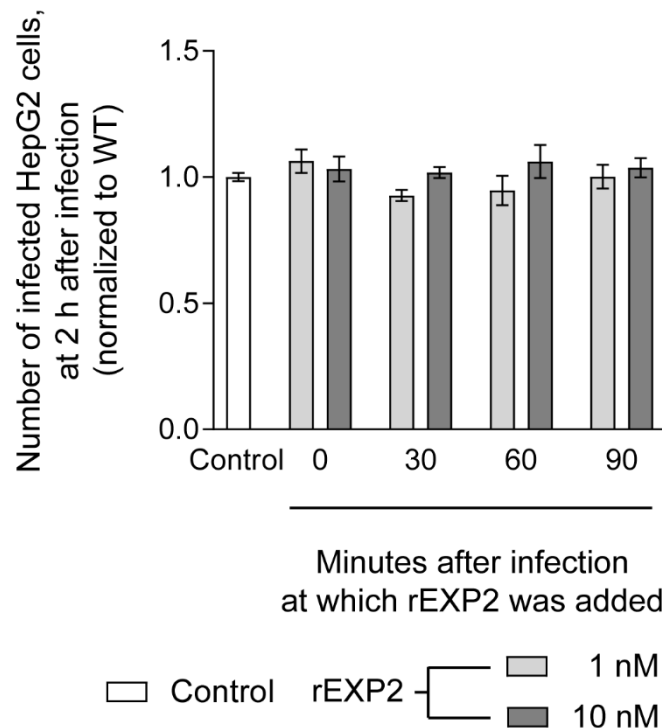


Figure 37 – Number of infected HepG2 cells following addition of rEXP2 protein at different times after infection. HepG2 cells were infected with WT sporozoites exposed to 1 nM (light grey) or 10 nM (dark grey) of rEXP2 at different minutes after incubation of sporozoites with cells. Cells were fixed at 2 hours after infection, stained for the PVM marker UIS4, and the number of infected cells was counted using widefield fluorescence microscopy. For each concentration of rEXP2, number of infected cells was normalized to values obtained where no rEXP2 was used. (N=3, mean \pm sem).

3.2. Invasion requires a specific type of membrane pore formation

If rEXP2 can rescue the invasion defect of EXP2 cKO sporozoites, it could be because of its pore-forming ability. For this, we incubated WT and EXP2 cKO sporozoites with two other pore-forming proteins. Initially, we added recombinant α -hemolysin (α -HL) from *Staphylococcus aureus*, in increasing concentration at 1 hour after incubation with cells [414,415]. We observed that, similarly to rEXP2, the invasion defect of EXP2 cKO parasites is reverted (**Figure 38**). Interestingly, we achieve rescue at a lower concentration with α -HL than with rEXP2 and the effect of seems to be lost when α -HL concentration increases. This can be explained by the fact that α -HL is 1000 times more hemolytic [416] than rEXP2 [339], possibly leading to hepatoma cell or sporozoite lysis. The estimated pore size of α -HL is approximately 1 nm (with 7 α -HL monomers) [414,415], similar to the 1.5 nm of the EXP2 pore (7 monomers of EXP2) [332,339].

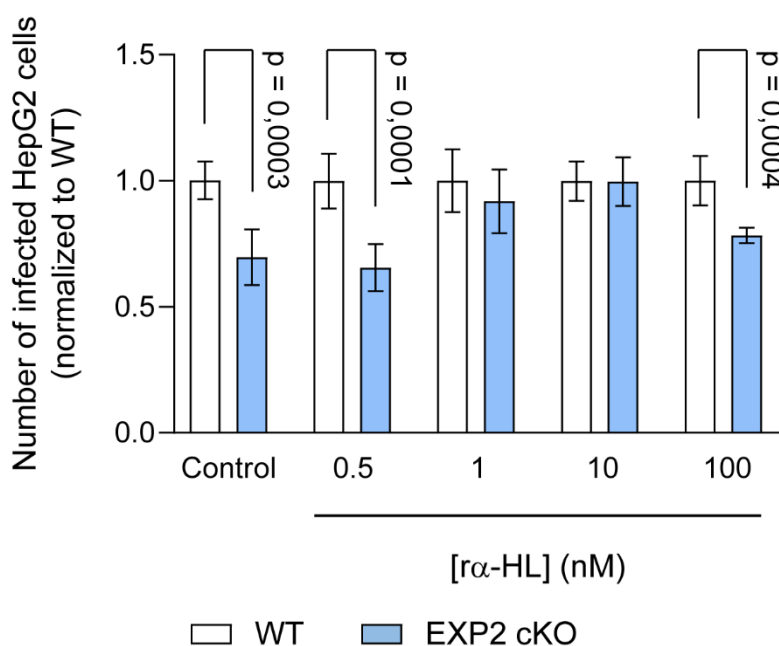


Figure 38 – Number of infected HepG2 cells following α -HL treatment. HepG2 cells were infected with WT (white bars) or EXP2 cKO (blue bars) sporozoites and treated with increasing concentrations of recombinant alpha-hemolysin (α -HL) starting at 1 hour after infection. Cells were fixed at 2 hours after infection, stained for the PVM marker UIS4, and the number of infected cells was counted using widefield fluorescence microscopy. The number of infected cells was normalized to the values obtained for infections using WT parasites. (N=3, mean \pm sem).

IV - Results

We also incubated WT or EXP2 cKO sporozoites with the recombinant pore-forming protein Streptolysin O (rSLO) from *Streptococcus pyogenes*, that creates a pore of an estimated diameter of 30 nm [417]. When SLO is used, we do not observe rescue of the EXP2 cKO sporozoites (**Figure 39**). Taken together with the previous results, it seems that there is an upper limit to the size of the pore that *Plasmodium* sporozoites use to invade.

In fact, sporozoites are also expected to use pore forming proteins during traversal. CelTOS is predicted to create pores of 50 nm in diameter [418] and spect2 has homology to human proteins with membrane attack complex [261], reported to form pores with 12 to 17 nm in diameter [419]. Both these pores are at least 10 times bigger pores than those made by EXP2 [332]. It seems that sporozoites uses two different sets of pore-forming proteins for two distinct functions. Bigger pores would disrupt membranes to traverse and smaller pores to enhance invasion.

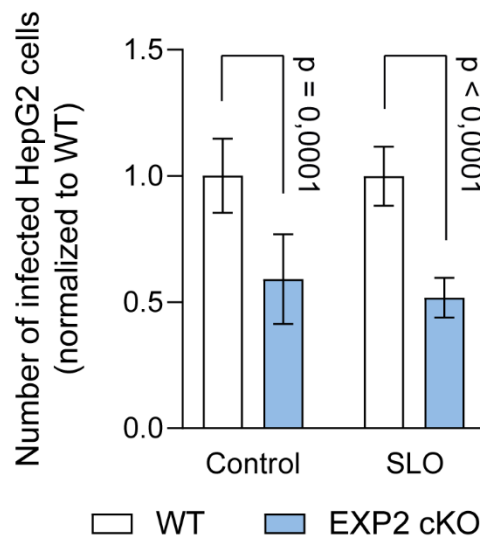


Figure 39 – Number of infected HepG2 cells following rSLO treatment. HepG2 cells were infected with WT (white bars) or EXP2 cKO (blue bars) sporozoites and treated with 10 nM of rSLO starting at 1 hour after infection. Cells were fixed at 2 hours after infection, stained for the PVM marker UIS4, and the number of infected cells was counted using widefield fluorescence microscopy. The number of infected cells was normalized to the values obtained for infections using WT parasites. (N=3, mean \pm sem).

To test if rEXP2 was indeed creating pores in the HepG2 cells, that would trigger membrane repair, we tested if the membrane of these cells would lose its characteristic impermeability.

Firstly, we tested if the nucleic acid dye Propidium Iodide (PI) would be able to enter cells treated with rEXP2 protein. Cells are normally impermeable to PI, as it cannot cross the plasma membrane, and we wondered if it could cross through the EXP2 pore. For this, we incubated HepG2 cells with 100 nM of rEXP2 protein in the presence of PI. Unfortunately, we did not observe HepG2 cells labelled with the fluorescence dye (**Figure 40** – left columns). Since pores can induce calcium influx into the cell that trigger a membrane repair pathway that seals the pore, we repeated the experiment using calcium-rich medium with ethylenediaminetetraacetic acid (EDTA), a calcium chelator, at a concentration that would chelate all the available calcium ions and also used calcium-free medium. As before, no difference was observed between cells untreated cells and cells treated with rEXP2 (**Figure 40** – middle and right columns). Curiously, the number of PI positive cells is higher in the condition where calcium-free medium is used, indicating that

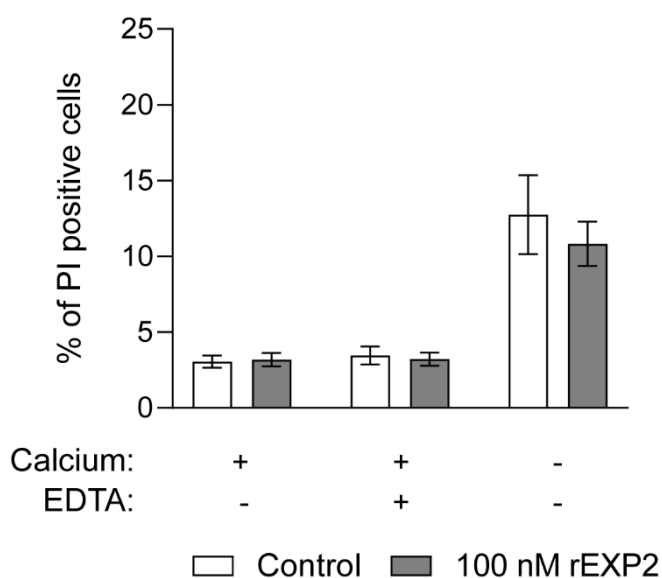


Figure 40 – Percentage of Propidium Iodide (PI) positive cells after treatment with rEXP2. HepG2 cells in suspension were treated with 100 nM of rEXP2 for 5 minutes at 37°C and labelled with DNA probe PI. Immediately after adding the dye, cells were analysed by Flow Cytometry. To prevent endocytosis of the EXP2 pore, the suspension of cells was assayed in medium with normal levels of calcium in the presence of calcium chelator EDTA or in calcium-free medium.

IV - Results

this medium might lead to a loss in cell permeability, on its own. This can be explained by the fact that we cannot supplement this media with FCS, as its calcium content would defeat the purpose of using calcium-free medium.

To better control for the role of endocytosis and membrane repair, we then tested if by incubating cells with rEXP2 protein we could cause leakage of cellular contents to the outside of the cell. To measure outflow, we loaded HepG2 cells with the fluorescent molecule Calcein Green, that is retained in the cytoplasm of cells. We then exposed cells to 1 or 10 nM of rEXP2 protein and collected the medium of the cells and measured Calcein Green fluorescence, as a surrogate for leakage of the cell. As a control, we lysed cells with Triton-X 100, that completely lyses cells and releases all the Calcein Green. We did not observe any Calcein Green leakage when cells were exposed to rEXP2 protein, at any of the concentrations tested, at any of the time points assessed (**Figure 41**).

If rEXP2 can create pores to the same size of the native EXP2 protein, its estimate pore size is of 1 nm [332]. It is plausible, that these pores are too small to fit both Calcein

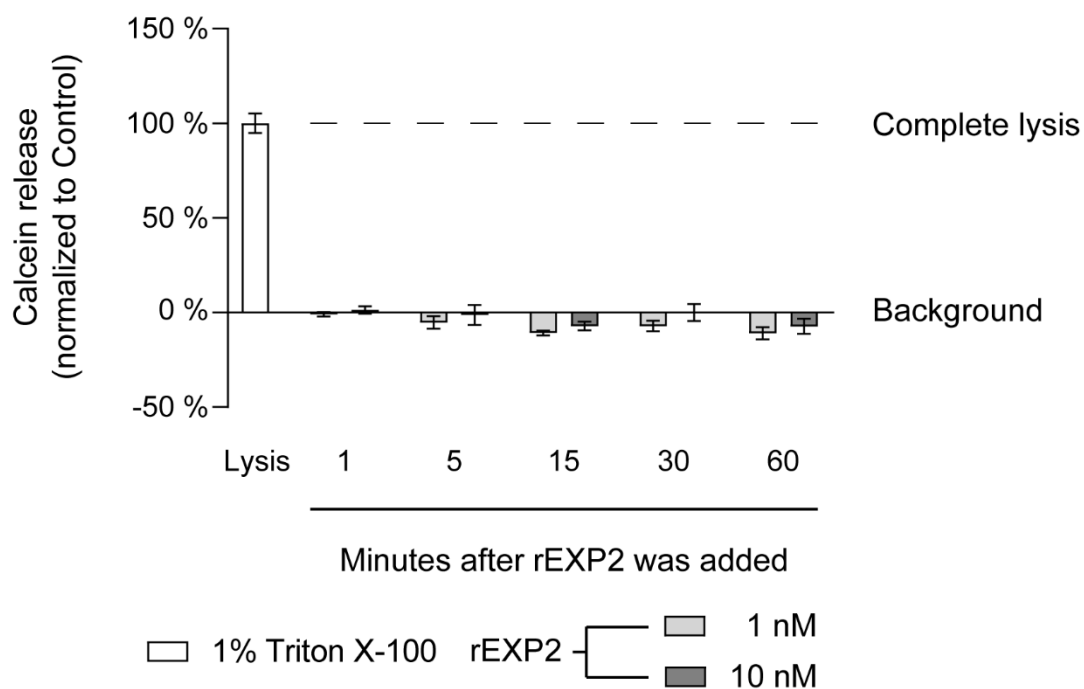


Figure 41 – Calcein leakage after treatment with rEXP2 protein. HepG2 cells were loaded with Calcein Green for 1 hour, after which they were exposed to 1 nM (light grey) or 10 nM (dark grey) of rEXP2 for up to 60 minutes. Cellular supernatant was collected at different minutes after exposure to EXP2, and Calcein Green fluorescence was assayed.

Green and PI. However, it is big enough to fit ions through it. And as such, we tested if calcium would flow into the cells. To measure calcium influx, we transfected HepG2 cells with the genetically encoded calcium sensor Gcamp6f, which is a Green fluorescent protein (GFP) that is split in two regions with a calmodulin domain between [420]. As this domain binds accessible calcium ions, it brings the two halves of the GFP protein together, leading to fluorescence emission [420]. After the cells are stably expressing this sensor, we imaged them in a widefield fluorescence microscope before and after exposure to rEXP2 protein at a frame rate of 0.3 seconds. To normalize the measured fluorescence between different cells, we normalized fluorescence of each cell observed at each timepoint (F_i) to the fluorescence of the cell at the beginning to the recording (F_0). We imaged the cells for 30 seconds, to register the basal level of fluorescence and added 100 nM of rEXP2 and imaged the cells for 150 seconds, for a total of 180 seconds. We observed that immediately after addition (at time = 0 seconds) of rEXP2 or control solution (solute of rEXP2 protein), fluorescence of the cells increase, possibly responding to the mechanical perturbation of the medium because of the added volume (**Figure 42**). However, cells treated with control solution return quickly to values registered before addition, whereas cells treated with 100 nM of rEXP2 show higher values of Gcamp6f fluorescence, taking longer to return to the initial fluorescence levels (**Figure 42**). Gcamp6f fluorescence levels return to initial values at 90 seconds after addition of rEXP2.

IV - Results

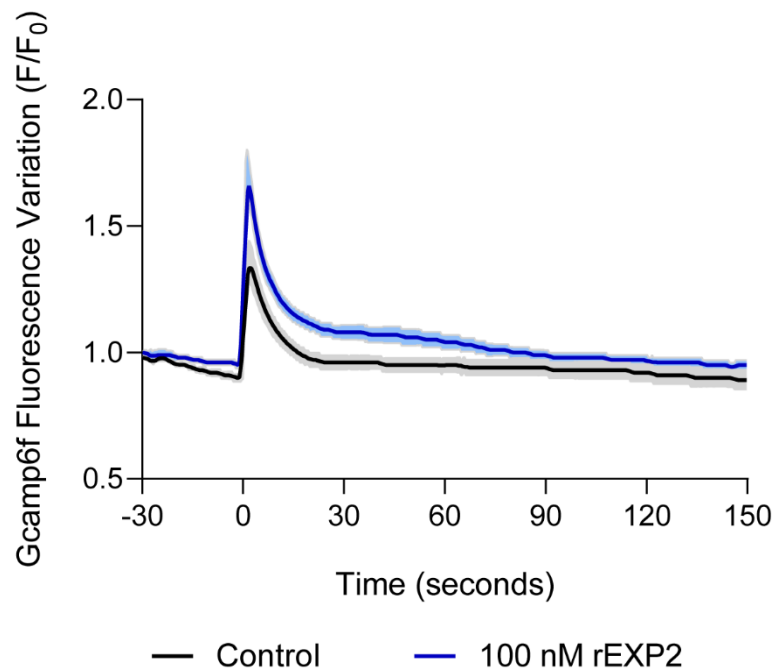


Figure 42 – Calcium reported Gcamp6f fluorescence variation after exposure to rEXP2. HepG2 cells were transfected with the genetically encoded calcium reporter fluorescent protein Gcamp6f, and exposed to 100 nM rEXP2 (dark blue line) or control (black line). Cells were imaged in a widefield fluorescence microscope 30 seconds before addition of rEXP2 to register baseline fluorescence in a total time of 180 seconds, at a frame rate of 0.3 frames/second. Gcamp6f fluorescence intensity was normalized by dividing F_i by the initial intensity value, F_0 . (N=3, at least 50 cells were imaged, shaded areas represent the 95% Confident Interval for the respective darker lines).

3.3. Invasion is tightly linked to extracellular calcium

As discussed in the previous experiment, extracellular calcium flows inside cells treated with rEXP2 protein. This means that the concentration of extracellular calcium is important for invasion of hepatocytes by *Plasmodium* sporozoites. To test this, we decided to perform a very simple experiment, where we used HepG2 cells and performed invasion assay using WT sporozoites, in either DMEM or RPMI cell culture media. Calcium concentration in DMEM is of 1.8 mM, whereas RPMI has 0.6 mM of calcium. Interestingly, when RPMI was used during the invasion step, we observed a reduction in almost half of the percentage of infected cells, as measured by flow cytometry analysis (**Figure 43** – green columns, right axis). On the other hand, the percentage of traversed cells almost doubled when cells and sporozoites were exposed to RPMI (**Figure 43** – red columns, left axis).

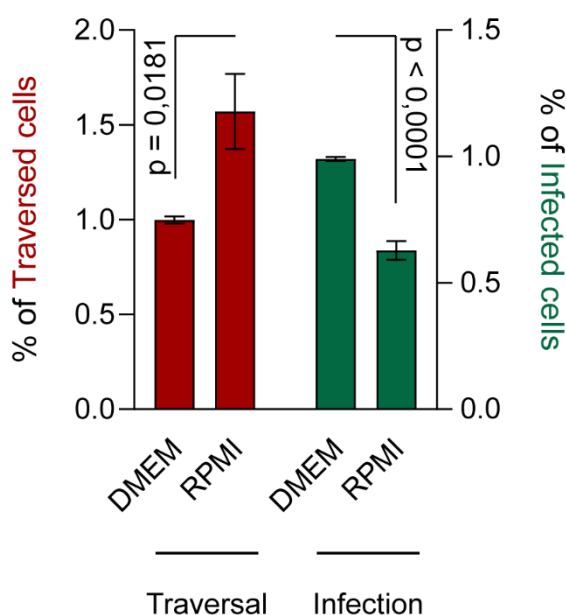


Figure 43 – Traversal and infection of HepG2 cells in different cell culture media. HepG2 cells were grown in complete DMEM medium, which was either maintained or replaced by RPMI during infection with WT parasites. During invasion step, cells were also incubated with 0.5 mg/mL of 10 kDa dextran-rhodamine dye. After 2 hours of infection, cells were trypsinized and analysed by Flow Cytometry. Traversal (left Y axis, red bars) and Infection (right Y-axis, green bars) values were normalized to those observed in DMEM medium. (N=3, mean \pm sem).

IV - Results

To test if these differences were because of the differences in calcium concentration, we wondered if we could transform the invasion efficiency observed in DMEM media into the one observed in RPMI media simply by altering calcium concentration.

To achieve this, we incubated sporozoites with cells in DMEM in the presence of increasing concentrations of EDTA, in a way to decrease the calcium content. Interestingly, when calcium concentration is decreased, the percentage of infected cells is progressively reduced (**Figure 44** – green columns, right axis). Conversely, the percentage of traversed cells increases progressively, as calcium concentration decreases (**Figure 44** – red columns, left axis). Importantly, when we achieve the lowest calcium concentration, 0.3 mM, traversal is also decreased, hinting that extracellular calcium might also be needed for the activation of the sporozoite into an invasive state.

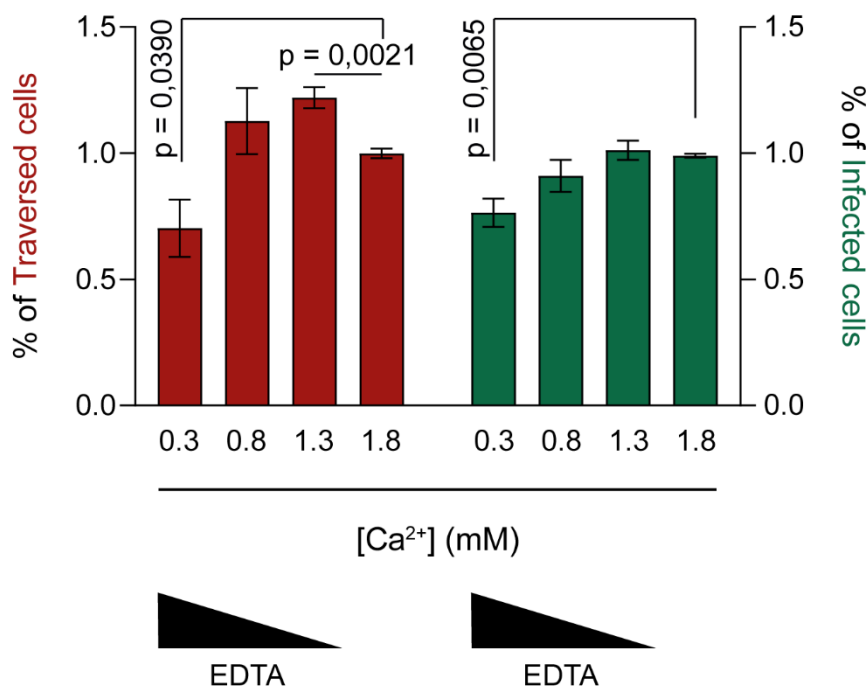


Figure 44 – Traversal and infection of HepG2 cells in DMEM with decreasing calcium concentrations. HepG2 cells were grown in complete DMEM medium, which was replaced by DMEM with increasing concentration of calcium chelator EDTA during infection with WT parasites, supplemented with 0.5 mg/mL of 10 kDa dextran-rhodamine dye. After 2 hours of infection, cells were trypsinized and analysed by Flow Cytometry. Traversal (left Y axis, red bars) and Infection (right Y-axis, green bars) values were normalized to those observed in DMEM medium with 1.8 mM of Ca²⁺ (normal level of calcium in DMEM). (N=3, mean ± sem).

On the other hand, we incubated sporozoites with cells in RPMI in the presence of increasing concentrations of calcium chloride, in a way to increase the calcium levels. As expected, when calcium concentration is increased, the percentage of infected cells is progressively increased (**Figure 45** – green columns, right axis). Conversely, the percentage of traversed cells decreases progressively, as calcium concentration increases (**Figure 45** – red columns, left axis).

Unfortunately, we could not transform RPMI into DMEM simply by changing calcium concentration, yet, only by changing one parameter, we change the magnitude of invasion and traversal. This does not seem to be an effect of solely changing the proportion of divalent ions in the media, since alterations in iron concentrations does not affect neither the percentage of invaded cells nor traversed cells (**Figure 46**).

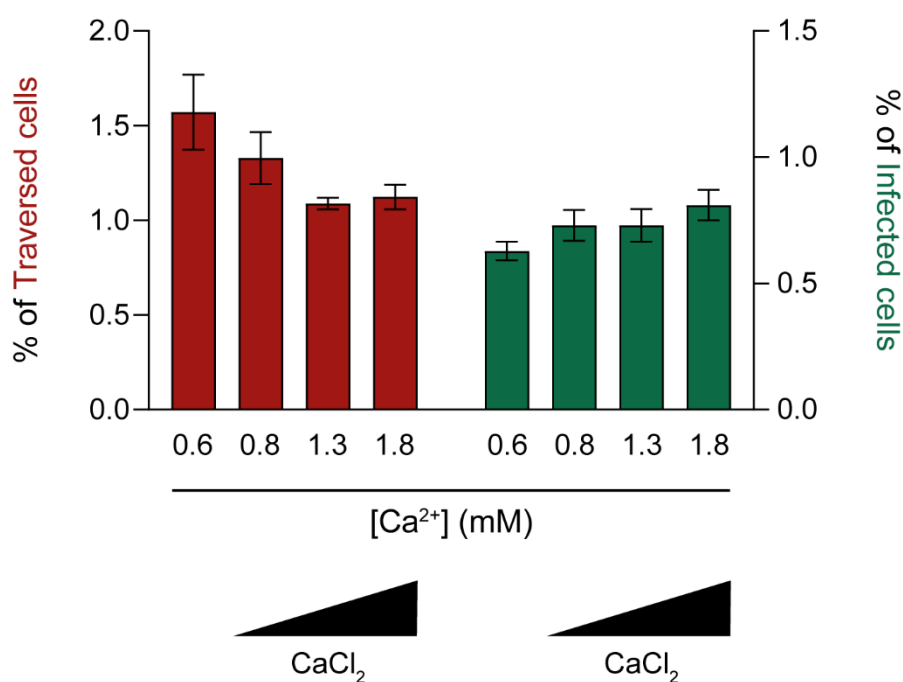


Figure 45 – Traversal and infection of HepG2 cells in RPMI with increasing calcium concentrations.

HepG2 cells were grown in complete DMEM medium, which was replaced by RPMI with increasing concentration of calcium chloride (CaCl₂) during infection with WT parasites, supplemented with 0.5 mg/mL of 10 kDa dextran-rhodamine dye. After 2 hours of infection, cells were trypsinized and analysed by Flow Cytometry. Traversal (left Y axis, red bars) and Infection (right Y-axis, green bars) values were normalized to those observed in RPMI medium with 0.6 mM of Ca²⁺ (normal level of calcium in RPMI). (N=3, mean ± sem).

IV - Results

This inverse correlation has already been described for the Plasmodium parasites KO for either *PbP36* or *PbP36p* [270], which fail to invade yet traverse more cells than the WT parasites used in that study. We also observe an increase in the proportion of traversed cells, using a parasite that has an invasion defect (**Figure 23**).

EDTA, used in a previous experiment, has the drawback of being able to detach cells from the cell culture plates. For this reason, we can never use EDTA to fully eliminate calcium in the medium. To achieve this, we used calcium-free medium, without any supplementation with FCS. As such, HepG2 cells were grown in calcium-rich medium and the medium was replaced by calcium-free medium (after washing cells three times with calcium-free medium) for infection with WT parasites. 2 hours after incubation, we measured the number of invaded cells by fluorescence microscopy. Expectedly, the number of invaded cells was decreased when parasites invaded cells in calcium-free

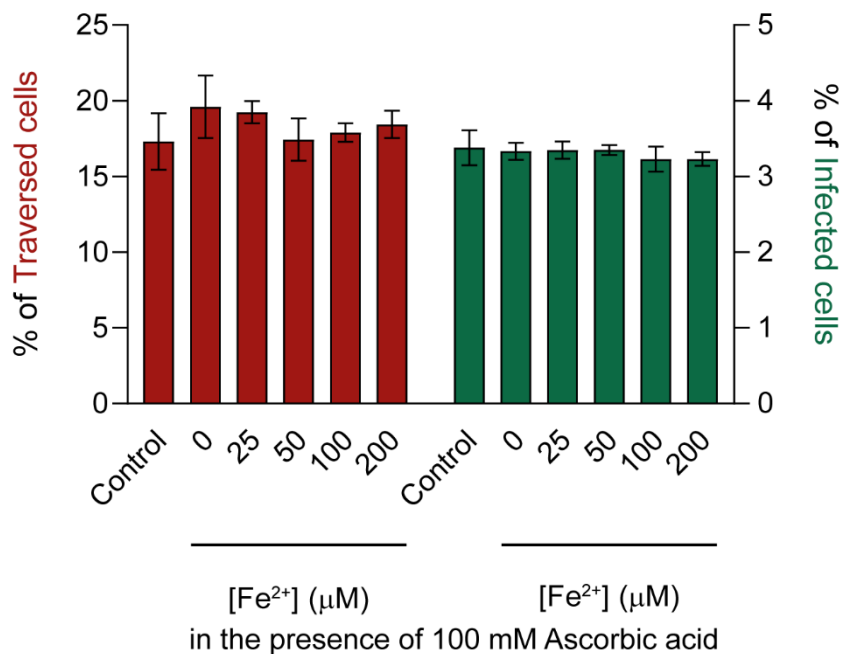


Figure 46 – Traversal and infection of HepG2 cells in DMEM with increasing iron concentrations.

HepG2 cells were grown in complete DMEM medium, which was replaced by DMEM containing 100 mM of ascorbic acid and with increasing concentrations of iron during infection with WT parasites, supplemented with 0.5 mg/mL of 10 kDa dextran-rhodamine dye. After 2 hours of infection, cells were trypsinized and analysed by Flow Cytometry. Traversal (left Y axis) and Infection (right Y-axis) values were normalized to those observed in DMEM medium without any ascorbic acid or iron added. (N=1, mean ± standard deviation).

medium (**Figure 47**, white bars). Since extracellular calcium might be involved in the motility and traversal capacity of sporozoites, we performed the previous experiments using also SPECT KO sporozoite, which do not perform traversal. Again, these sporozoites do not invade cells, to a similar extent as WT sporozoites (**Figure 47**, dark yellow bars).

We also assessed the gliding motility and traversal ability of WT sporozoites in calcium-free medium. To perform these experiments, sporozoites were dissected using calcium-free medium and were placed either in the presence or kept in the absence of calcium. Importantly, the gliding ability of sporozoites in calcium-free medium is severely impaired, as approximately 75% of sporozoites were observed to have no trails in the absence of extracellular calcium (**Figure 48**, left plot). Moreover, the traversal ability of these sporozoites was also impaired (**Figure 48**, right plot), albeit not to the same extent as invasion (**Figure 47**).

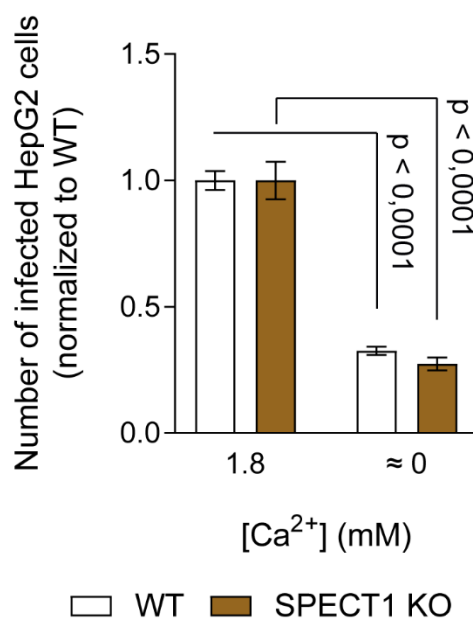


Figure 47 – Number of infected cells at 2 hours after infection in the absence of calcium. HepG2 cells were grown in complete DMEM medium, which was replaced by calcium-free DMEM containing during infection with WT (white bars) or Spect1 KO (dark yellow bars) sporozoites. After 2 hours of infection, cells were fixed, stained for the PVM marker UIS4, and the number of infected cells was counted using widefield fluorescence microscopy. For each parasite line, the number of infected cells was normalized to the values obtained for infections in calcium-rich conditions after infection. (N=3, mean ± sem).

IV - Results

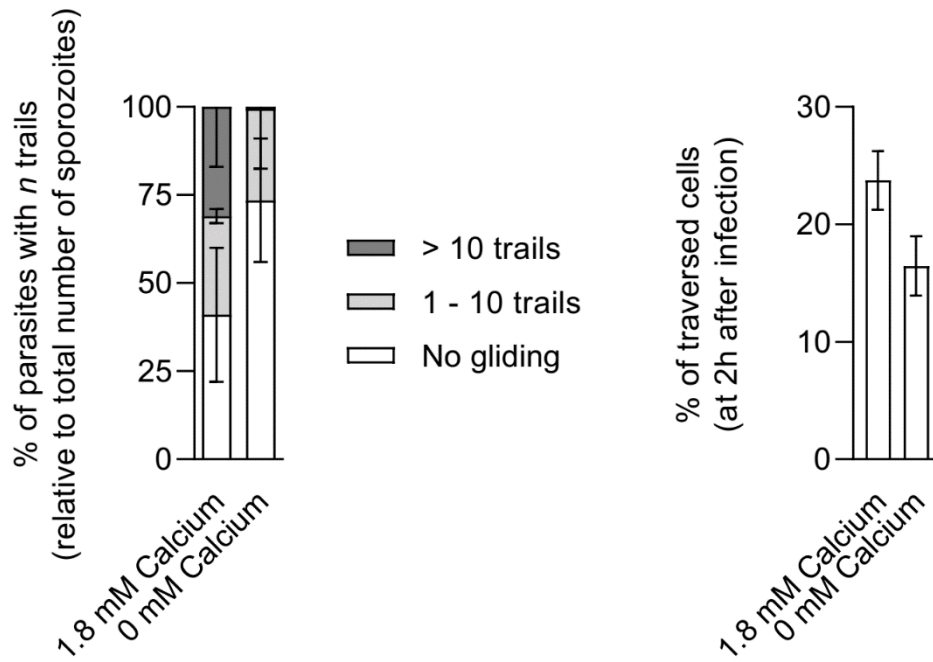


Figure 48 - Gliding and traversal of WT sporozoites in the presence or absence of extracellular calcium. WT sporozoites were dissected in calcium-free medium and their gliding (left plot) and traversal ability (right plot) were assessed as explained previously. (N=3, mean \pm sem).

To conclude, extracellular calcium seems to regulate several processes important for cell invasion, namely, gliding motility, traversal capacity and *de facto* invasion of *Plasmodium berghei* sporozoites. Given its pleotropic role in both sporozoite activation and cellular response to the invading sporozoite, its precise role for host membrane repair mechanisms could not be elucidated.

3.4. Membrane repair contributes to *Plasmodium* sporozoite invasion

The results detailed above point to the activation of the membrane repair pathway described for invasion by other pathogens. The culmination of the calcium entrance into cells is the exocytosis of lysosomes to the membrane of the host cell, that deliver sphingomyelinase to the membrane [151]. This enzyme is responsible for the hydrolysis of sphingomyelin to ceramide [421], inducing membrane curvature [152]. This activity can come from two protein in mammalian cells, the neutral sphingomyelinase and the acid sphingomyelinase (aSMase). Neutral sphingomyelinase is present in higher concentrations in the inner leaflet of the plasma membrane [422], inducing outer curvature of the membrane, responsible for outward blebbing of membranes [423]. This enzyme is pharmacologically inhibited by the compound GW4869 [424], which, when added to WT sporozoites during the invasion step, fails to inhibit sporozoite invasion (**Figure 49**). Conversely, pharmacological inhibition of aSMase by desipramine [425], reduces invasion of sporozoites in a dose dependent manner (**Figure 49**). Fitting a dose-dependent model

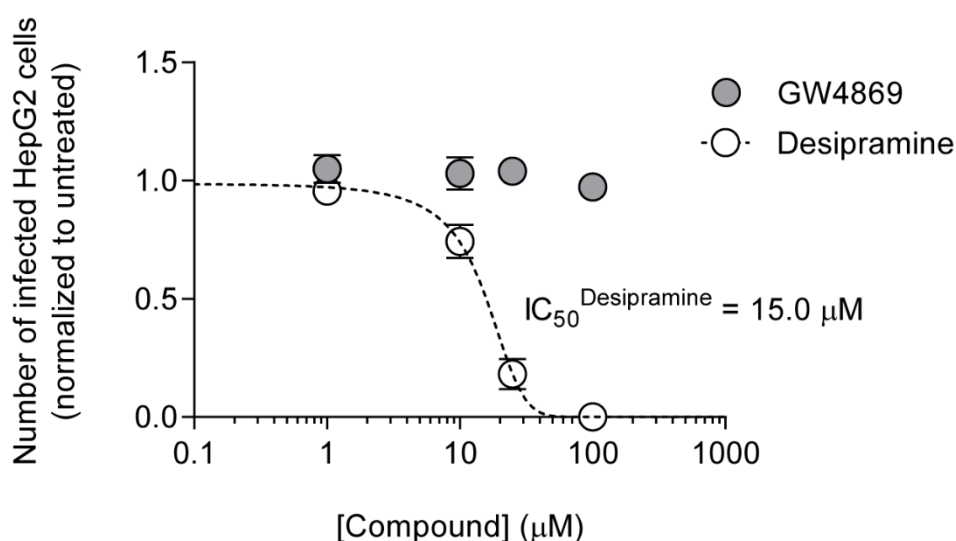


Figure 49 – Number of infected HepG2 cells following GW4869 or desipramine treatment. HepG2 cells were infected with WT sporozoites and treated with increasing concentrations of neutral (GW4869, grey circles) or acid (desipramine, white circles) sphingomyelinase inhibitors. At 2 hours after infection, cells were fixed, stained for the PVM marker UIS4, and the number of infected cells was counted using widefield fluorescence microscopy. The number of infected cells was normalized to the values obtained for infections in absence of any inhibitor. The dashed line in the figure represents the non-linear regression performed to fit an inhibition model to the data, with the fitted IC_{50} value shown. (N=3, mean \pm sem).

IV - Results

into the obtained results, we obtain an inhibitory concentration of approximately 15 μ M, similar to the ones obtained for *T. cruzi* [150]. aSMase is present mostly on lysosomes, being delivered to the outer leaflet of the host cell by exocytosis [151]. There, aSMase leads to the formation of an inward curvature of the membrane [152], that is thought to be a signal to the host cell to start an endocytic process.

To confirm the importance of aSMase in the invasion process, we used shRNA against the *SMPD1* mRNA (the gene coding for aSMase protein) and observed that decrease in expression of aSMase of approximately 40% (**Figure 50**, left plot) leads to the corresponding decrease in WT sporozoite invasion (**Figure 50**, right plot, white bars). Importantly, when sporozoites are treated with recombinant aSMase protein, this decrease in invasion is rescued (**Figure 50**, right plot, grey bars).

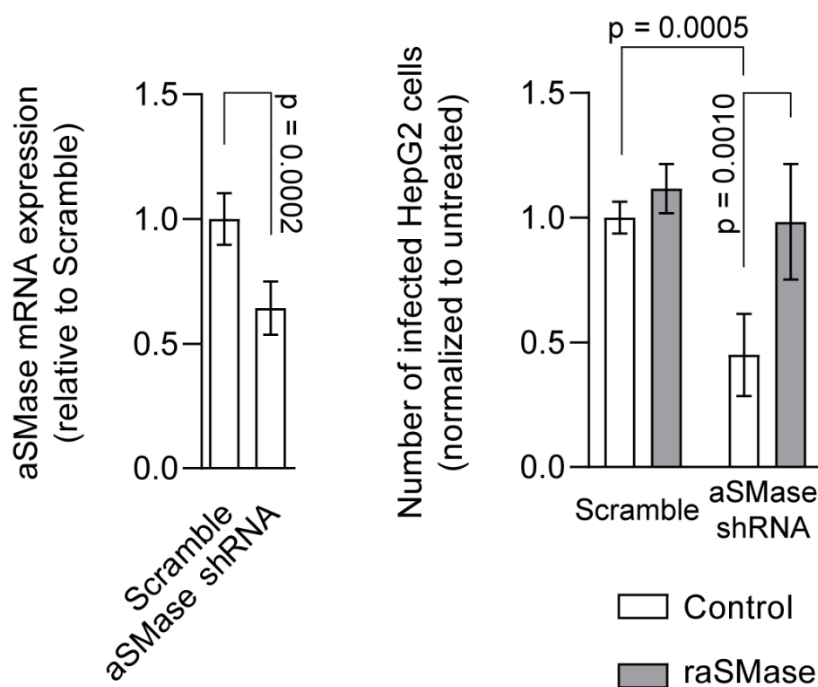


Figure 50– Number of infected HepG2 cells after acid sphingomyelinase knock-down. HepG2 cells were transfected with shRNA against the *SMPD1* mRNA or control shRNA. 48 hours after transfection, the expressing of aSMase mRNA was assessed by qCPR (left plot). Also, at 48 hours after infection, cells were infected with WT sporozoites until 2 hours after infection. Cells and sporozoites were also treated with recombinant acid sphingomyelinase at 1 hour after infection. At 2 hours after infection, cells were fixed, stained for the PVM marker UIS4, and the number of infected cells was counted using widefield fluorescence microscopy. The number of infected cells was normalized to the values obtained for infections in absence of desipramine. (N=3, mean \pm sem).

We hypothesized that the pore formed by EXP2 is a mechanism that the parasite employs to achieve endocytosis by the host cell, that facilitates its invasion. This means that aSMase addition to sporozoites would be enough to increase invasion of sporozoites. To test this hypothesis, we added recombinant aSMase from *Bacillus cereus* to WT parasites during the invasion step. Contrary to what was observed for the rEXP2 protein, addition of aSMase slightly increases the invasion of WT parasites, in a time frame comparable to the one observed with rEXP2 protein (**Figure 51**). Curiously, the later aSMase is added, the more infected cells are obtained. However, the effect is limited in time, as addition of aSMase as late as 90 minutes post incubation seems irrelevant for parasite invasion. This is in agreement with previous results as invasion starts at 45 minutes post incubation and is finished 45 minutes later, at the total time of 90 minutes (**Figure 25**).

Lastly, we tested if we could rescue the defect of EXP2 cKO sporozoites by adding aSMase during the invasion step. As previously done, aSMase was added to WT or EXP2

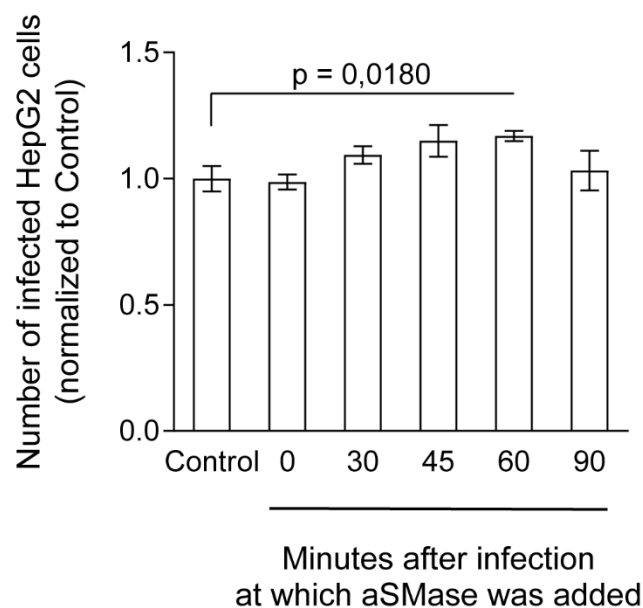


Figure 51– Number of infected HepG2 cells following addition of aSMase protein at different times after infection. HepG2 cells were infected with WT sporozoites exposed to 10 μ U/mL of raSMase protein at different minutes after incubation of sporozoites with cells. Cells were fixed at 2 hours after infection, stained for the PVM marker UIS4, and the number of infected cells was counted using widefield fluorescence microscopy. For each timing of aSMase, the number of infected cells was normalized to the values obtained where no aSMase was used (control). (N=3, mean \pm sem).

IV - Results

cKO sporozoites 1 hour after sporozoites were incubated with HepG2 cells. We again observe a rescue of the invasion defect of EXP2 cKO sporozoites at 2 hours after infection (**Figure 52**– top panel). Moreover, if we wash out the added aSMase and let the infection progress until 48 hours, the number of infected cells is again reverted in the case of EXP2 cKO parasites (**Figure 52**– bottom panel). This means, once again, that once EXP2 cKO sporozoites invade cells, their ability to mature is not hindered by the lack of the EXP2 protein.

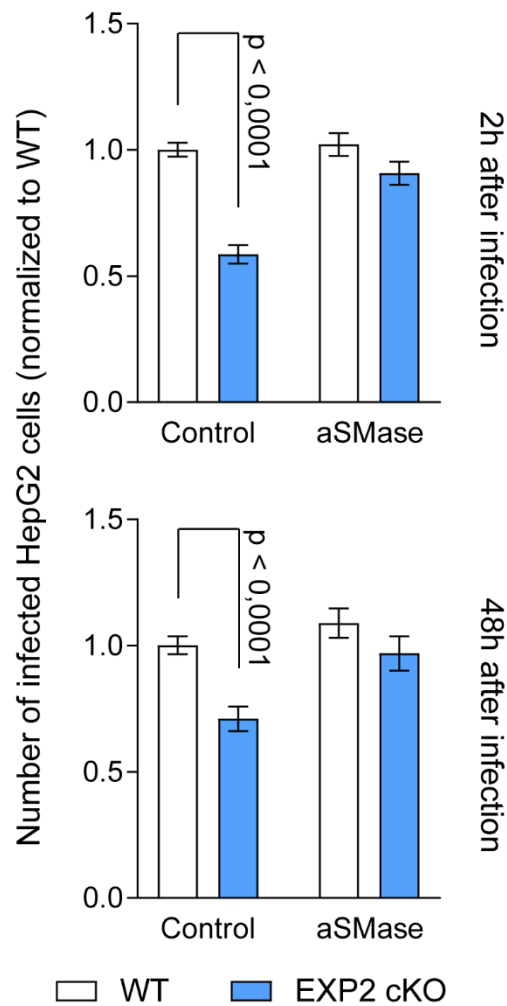


Figure 52 – Number of infected HepG2 cells following acid sphingomyelinase treatment. HepG2 cells were infected with WT (white bars) or EXP2 cKO (blue bars) sporozoites, and treated with 10 μ U/mL of raSMase recombinant protein starting at 1 hour after infection until 2 hours after infection. Cells were fixed either at 2 hours after infection (top panel) or at 48 hours after infection (bottom panel), stained for the PVM marker UIS4, and the number of infected cells was counted using widefield fluorescence microscopy. The number of infected cells was normalized to the values obtained for infections using WT parasites and no raSMase. (N=5, mean \pm sem).

In the previous sections, we showed that the lack EXP2 at the sporozoites stage can be overcome by addition of pore-forming protein, that form pores of approximately 1 nm in diameter. This pore seems to be able to allow the flow of calcium ions but not of much else solutes. This influx of calcium leads to the changes in the host cell that might coalesces into the activity of aSMase. This protein is involved in endocytosis and possibly makes the host cell permissive to invasion by *Plasmodium* sporozoites.

Chapter V – Discussion

The results in this thesis suggest a novel role for the EXP2 protein during the sporozoite stage, especially during its invasion of the hepatocyte (**Figure 53**). We have shown that the protein is present at the sporozoite stage and that it is secreted by the sporozoite when exposed to conditions that mimic the host cell milieu. We propose that the secreted EXP2 protein produces pores in the membrane of the hepatocyte, that lead to the influx of calcium. This increase in intracellular calcium, should trigger the exocytosis of aSMase-containing vesicles that, once secreted, cause the formation of ceramide rich lipid domains that promote endocytosis.

One of the cornerstones of this model is the interaction of a *Plasmodium* protein with lipid membranes, rather than host cell receptors. Moreover, the proposed model sheds light into some of the unexplained roles of host factors for the invasion of *Plasmodium* sporozoites as explained below.

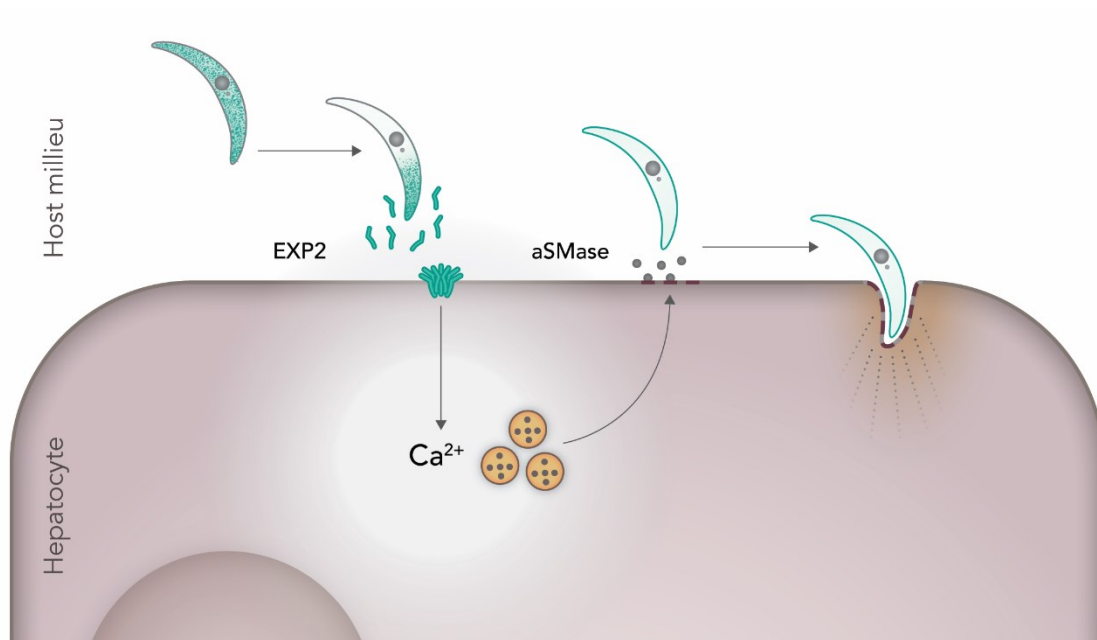


Figure 53 - Model for the action of *Plasmodium* EXP2. EXP2 is secreted by the sporozoite once stimulated by the host cell milieu conditions (increase in temperature and FCS). EXP2 forms pores at the membrane of hepatocytes, allowing the influx of calcium. This leads to the release of aSMase-containing vesicles that create ceramide-rich domains at the membrane of the soon-to-be-infected hepatocyte. This domain is endocytosed by the cell, which is taken advantage for by the invading parasite.

1. EXP2 is present at the sporozoite and secreted following stimulation

EXP2 had previously been identified during the sporozoite stage of *Plasmodium berghei* [333,364], where it was also observed to be present in a punctuate pattern (**Figure 18, Figure 29 and Figure 30**). Interestingly, when EXP2 is fused to a reporter protein [364], the fluorescent signal seems to aggregate in only one punctum, as opposed to multiple vesicles. This might be explained by the fusion of the EXP2 protein to the reporter, that can affect the proper sorting of the EXP2 protein into its final vesicular destination. Regardless of the difference in localization, EXP2-mCherry parasites still progressed through the life cycle normally [364]. Moreover, the detection of EXP2 during the sporozoite stage is not restricted to *Plasmodium berghei*. Indeed, EXP2 transcription is also found to be up-regulated by *Plasmodium falciparum* sporozoites when exposed to conditions that mimic the host milieu [267]. This corroborates the up-regulation we observed during the invasion kinetics (**Figure 28**).

Surprisingly, EXP2 is not detected when proteomics of salivary gland sporozoites were performed [426,427]. This can be explained by the low abundance of the EXP2 protein during the sporozoite stage, when compared to members of the glideosome complex, for example. Also, if EXP2 requires 1 hour of stimulation for its expression to peak, the authors of the proteomes might have not assayed the sporozoite at the appropriate time to detect the EXP2 protein.

This can also mean that the levels of EXP2 protein build up during the invasion kinetics (via transcription and translation). This can account for the *delayed* invasion kinetics, where parasites wait for 1 hour to successfully invade hepatocytes (**Figure 25-Figure 27**).

This *delayed* invasion phenotype seems to happen *in vivo*, yet, the time delay is much smaller. For instance, *P. berghei* sporozoites were observed inside hepatocytes within minutes of their inoculation in the skin [428,429]. Moreover, the traversal of hepatocytes was recorded to take up to 15 minutes in a mouse liver [429] whereas it takes approximately 1 hour in plated cells [265]. This can be explained by a shortcoming of the *in vitro* system, which lacks blood flow, the three-dimensional architecture of hepatocytes, as

well as other types of cells and matrix components that encompass a normal liver. It is possible that the missing components signal to the sporozoite in a more intense fashion than a monolayer of hepatoma cells does. In fact, in the calcium experiments using DMEM and RPMI, we can never convert one medium to the other (**Figure 43-Figure 45**), suggesting that more cues than extracellular calcium regulates the invasion of the sporozoite.

Another cause for the *delayed* invasion kinetics is the secretion of the EXP2 protein. EXP2 is seen in vesicles yet these do not seem to be any of the typical vesicles. In terms of size, they seem micronemes or dense granules and in terms of density, they seem to be micronemes [166]. Yet, EXP2 does not co-localize with TRAP (**Figure 30**). This can possibly mean that two (or more) types of micronemes exist, one that are released faster (containing TRAP) and another set that is released later, in response to certain stimuli (containing EXP2). This is not completely new, as the cysteine proteases P36 and P36p are secreted after stimulation with temperature and serum [270], similarly to EXP2 (**Figure 31-Figure 33**). The 1 hour delay, might be the time it takes the sporozoite to produce, sort and export EXP2 protein and others through the apical end.

2. EXP2 goes to the hepatocyte membrane and allows the influx of calcium

We hypothesize that the secreted EXP2 protein forms pores in the membrane of the hepatocyte. We tested if the pore would be big enough to fit PI or Calcein Green (**Figure 40 and Figure 41**). Both molecules have an atomic weight of approximately 700 and 1000 Da, respectively. Considering the pore size of EXP2 has a radius of 1 nm in its smallest point [332], there is no possibility that either of these molecules would fit into the pore.

On the other hand, calcium ions have an approximate size of 40 Da and would fit perfectly in the pores created by EXP2. Moreover, besides fitting calcium, EXP2 pores would also allow for the efflux of potassium ions from cells as well as the influx of sodium or

Chapter V -Discussion

chloride ions. It is unclear what would be the potential of these ions for invasion, but potassium efflux is correlated with inflammasome activation [430] and possible elimination of the infected cell (reviewed in [431]). This defense mechanism for protection against intracellular infections would be damaging to the invading pathogens, and possibly for this reason, some bacterial toxins have evolved the ability to “select” the type of ions can go through (reviewed in [432]). It would be interesting to understand if the EXP2 pore also possesses this type ion selectivity. This can be the case as inflammasome activation has not been reported during *Plasmodium* liver stage. Yet, infection by sporozoites does start an apoptotic program by the host cell [433], that is inhibited by the sporozoite [367,368]. The sporozoite also induces an autophagic response against the exoerythrocytic forms of the parasite that is blocked and ultimately advantageous for the parasite [287,434].

We also show that the invasion ability of EXP2 cKO parasites can be rescued using the α -HL but not SLO (**Figure 38 and Figure 39**). This result suggests that there is an upper limit of pore size, as pores made up of SLO allow the flow of both PI [150]. We can consider that EXP2 is more similar to α -HL, both in terms of pore size (approximately 1 to 2 nm) and stoichiometry (heptameric pores) [414,415]. As such, it is possible that EXP2 shares with α -HL the selectivity for ions.

After the EXP2 pore is placed on the membrane, we see calcium influx into HepG2 cells (**Figure 42**). Our results show a very little and transient calcium increase in treated cells and again this correlates with the smaller pore size of EXP2 than that of SLO. Interestingly, when calcium is removed from the medium, invasion is reduced but not completely inhibited (**Figure 47**). Membrane repair mechanisms have been reported to happen with as little as 1 μ M of extracellular calcium [435]. It is possible that our removal of calcium was insufficient as the normal medium has almost 2 mM of calcium (2,000 times more). Also, it is possible that as the parasite traverses cells, it causes leakage of intracellular calcium into the medium.

3. EXP2 pore activates membrane repair

The pore created by EXP2 is repaired by aSMase-dependent mechanisms that ultimately are used by the parasite to invade the hepatocyte. This is similar to other pathogens, that take advantage of this strategy to infect the cell [148–156].

The creation of ceramide-rich membrane domains might serve two roles. On one hand, ceramide has been shown to activate PKC ζ [436,437], an inducer of endocytosis [438] and of *Plasmodium* sporozoite invasion [285]. On the other hand, it creates a scaffold where transmembrane receptors such as CD81 and SR-BI can aggregate because of the higher membrane order [439]. This aggregation of CD81 and SR-BI and its proximity to the parasite, might be enough to induce exocytosis of rhoptry proteins, such as RON4, RON2 and AMA1 [412] that make up the moving junction. Indeed, *artificial* aggregation of CD81 can be induced by adding cholesterol (increasing membrane viscosity) and this has been shown to increase invasion of sporozoites [283]. Finally, engagement of CD81 has been proposed to change actin polymerization [440,441], which has been described to be important for the invasion of the parasite [286].

4. Lipid rafts as target for anti-Plasmodial strategies

If indeed *Plasmodium* parasites rely on the generation of lipid rafts for invasion, preventing the formation of these lipid domains should prevent invasion of this parasite. Lipid rafts pose an advantage to several pathogens as they can be platforms where host cell receptors are aggregated (reviewed in [442]). Importantly, cholesterol, a major component of lipid rafts, has been shown to be a positive modulator of invasion, as it aggregates CD81 molecules needed by the parasite [283]. The timing to disruption of the lipid raft is critical as its their effect can be short lived. For example, while desipramine inhibits Hepatitis C virus [443] invasion of hepatocytes (as it prevents ceramide generation

Chapter V -Discussion

and host cell receptor clustering), increased ceramide generation before invasion can also inhibit invasion of Hepatitis C virus [439] (as it removes host cell receptors from the surface of the host cell). Hence, the timing of manipulation of lipid rafts seems critical, which is a problem in terms of prophylaxis, because our anti-raft compound would have to be present at all times, without affecting natural host cell signalling.

The reliance of *Plasmodium* parasites on membrane repair is an *intelligent* option, given that the host cell has little option but to repair its wounded membrane. This strategy has the added bonus of relying on no protein receptor. This gives the cell very little ability to generate mutations to prevent invasion. The only protein involved in membrane wound repair is acid sphingomyelinase. This poses an interesting question as *Plasmodium* parasites have had an enormous ability to change the human genome. Traits such as sickle cell [360] and G6PD deficiency [47] have been selected for by evolution because they confer these individuals with an extra fitness when dealing with *Plasmodium* infection. Why have not mutations of the acid sphingomyelinase gene been more prevalent in malaria endemic regions? Acid sphingomyelinase is encoded by the *SPMD1* gene and mutations to this gene gives rise to a disease called Niemann-Pick [444] that has two types of variant, type A and B. Both patients suffer from hepatosplenomegaly yet differ in lesions in the central nervous system (type A disease is also neurodegenerative). Both types of Niemann-Pick are characterized by excess sphingomyelin in lysosomes and plasma membrane [421]. Conversely, patients show a lack of ceramides [445], which are potent lipid messengers, and their loss might lead to abnormal signalling cascades [446]. This leads to impaired liver and spleen function, affecting normal plasma lipid and haematological parameters [444]. Most type A Niemann-Pick patients die in 2 to 3 years of age, while type B patients are more diverse with symptoms appearing between childhood and adulthood and progressively worsening along life, leading to liver failure and respiratory complications [444]. As evidenced by the consequences of Niemann-Pick disease, the loss of this protein is possibly too much for an organism to handle, giving *Plasmodium* parasites a double evolutionary advantage against the host cell.

5. EXP2 is not needed during the liver stage

One of the most surprising results of this project is that the lack of EXP2 during the liver stage does not affect the development of the parasite (**Figure 19 and Figure 20**). EXP2 is needed during the blood stage of infection [365], where it is part of the PTEX complex, crucial for exporting proteins to the cytosol of the erythrocyte (reviewed in [302]). Moreover, EXP2 is becoming increasingly recognized as a nutrient channel [321,340,341] besides its function in protein export. Yet, during the liver stages, parasites lacking EXP2 in the vacuole grow and differentiate to the same extent as do WT parasites.

This result has two possible interpretations. On one hand, it can mean that protein export is not needed during the liver stage of infection. Indeed, parasite proteins that interact with host cell proteins are always found in the PVM. This is the case of the interaction between *Plasmodium* EXP1 and host Apolipoprotein H [409] and *Plasmodium* UIS3 to host autophagy effector protein LC3 [287]. Moreover, there might be no need for the parasite to change a nucleated cell as it needs to change the barren erythrocyte.

On the other hand, alterations in the host cell metabolism caused by the parasite have been reported [366]. As discussed before, host cell apoptosis is inhibited in infected cells [368]. Also, host AMPK is found to be less active during *Plasmodium* infection [369] and host glucose transporter Glut1 is deployed to the membrane following *Plasmodium* infection [371]. These alterations are driven by the presence of the parasite and might be caused by a parasite effector. As such, parasite proteins should be able to exit the liver schizont in an EXP2-independent manner, meaning that protein export during the liver stage can be caused by a different mechanism with different proteins.

Chapter V -Discussion

To conclude, we have surprisingly observed that a blood stage protein, has a moonlighting function as a facilitator of invasion during the liver stage. Even though EXP2 is still making a pore in a membrane, the different timings and location of action dictates very different outcomes. On the blood stage, EXP2 exports proteins and in the liver stage, it makes ions flow into the host cell. This induces a cascade of events in the hepatocyte that ultimately leads to the endocytosis of the parasite.

With this work, we have achieved a new perspective on the mechanism of *Plasmodium* sporozoite invasion. This can potentially lead to new anti-malarial strategies. It also establishes that *Plasmodium* parasites have reached a point of convergent evolution with other pathogens, from other eukaryotic parasites, bacteria and virus.

[...]

Rust: There wasn't much to do besides walk around, explore...

Marty: And... and look up at the sky and make up stories. Like what?

Rust: [...] It's just one story. The oldest.

Marty: What's that?

Rust: Light versus dark.

Marty: [...] Appears to me that the dark has a lot more territory.

[...]

Rust: You're looking at it wrong, the sky thing.

Marty: How's that?

Rust: Once there was only dark. If you ask me, the lights winning.

True Detective

References

1. WHO. World Malaria Report [Internet]. World Health Organization. Geneva; 2016. doi:10.4135/9781452276151.n221
2. Loy DE, Liu W, Li Y, Learn GH, Plenderleith LJ, Sundararaman SA, et al. Out of Africa: origins and evolution of the human malaria parasites *Plasmodium falciparum* and *Plasmodium vivax*. *Int J Parasitol*. The Author(s); 2017;47: 87–97. doi:10.1016/j.ijpara.2016.05.008
3. Martinsen ES, Perkins SL, Schall JJ. A three-genome phylogeny of malaria parasites (*Plasmodium* and closely related genera): Evolution of life-history traits and host switches. *Mol Phylogenet Evol*. 2008;47: 261–273. doi:10.1016/j.ympev.2007.11.012
4. Grassi B. Studi di uno Zoologo sulla Malaria. 2nd Editio. Roma: Reale Accademia dei Lincei; 1901.
5. Cowman AF, Healer J, Marapana D, Marsh K. Malaria: Biology and Disease. Cell. Elsevier Inc.; 2016;167: 610–624. doi:10.1016/j.cell.2016.07.055
6. Golgi C. Sulla infezione malarica. *Arch Sci Med Torino*. 1886;10: 109–135.
7. Wassmer SC, Taylor TE, Rathod PK, Mishra SK, Mohanty S, Arevalo-Herrera M, et al. Investigating the pathogenesis of severe malaria: A multidisciplinary and cross-geographical approach. *Am J Trop Med Hyg*. 2015;93: 42–56. doi:10.4269/ajtmh.14-0841
8. Wassmer SC, Grau GER. Severe malaria: what's new on the pathogenesis front? *Int J Parasitol*. 2017;47: 145–152. doi:10.1016/j.ijpara.2016.08.002
9. Costa FTM, Lopes SC, Ferrer M, Leite JA, Martin-Jaular L, Bernabeu M, et al. On cytoadhesion of *Plasmodium vivax*: Raison d'être? *Mem Inst Oswaldo Cruz*. 2011;106: 79–84. doi:S0074-02762011000900010 [pii]
10. Langhorne J, Ndungu FM, Sponaas A-M, Marsh K. Immunity to malaria: more questions than answers. *Nat Immunol*. 2008;9: 725–732. doi:10.1038/ni.f.205
11. Cohen S, McGregor I, Carrington S. Gamma-Globulin and Acquired Immunity to Human Malaria. *Nature*. 1961;192: 733–737. doi:10.1038/192733a0
12. Bull PC, Lowe BS, Kortok M, Molyneux CS, Newbold CI, Marsh K. Parasite antigens on the infected red cell surface are targets for naturally acquired immunity to malaria. *Nat Med*. 1998;4: 358–360. doi:10.1038/nm0398-358
13. Sutherland CJ, Tanomsing N, Nolder D, Oguike M, Jennison C, Pukrittayakamee S, et al. Two Nonrecombining Sympatric Forms of the Human Malaria Parasite *Plasmodium ovale* Occur Globally. *J Infect Dis*. 2010;201: 1544–1550. doi:10.1086/652240
14. Ng OT, Eng EO, Cheng CL, Piao JL, Lee CN, Pei SW, et al. Naturally acquired human *Plasmodium knowlesi* infection, Singapore. *Emerg Infect Dis*. 2008;14: 814–816. doi:10.3201/eid1405.070863
15. World Health Organization. Guidelines for the Treatment of Malaria. 3rd ed. World Health Organization, editor. Geneva; 2015. doi:10.1016/0035-9203(91)90261-V
16. World Health Organization. Basic Malaria Microscopy. 2nd Editio. Geneva; 2010.
17. World Health Organization. The use of malaria rapid diagnostic tests. 2nd Editio. Geneva; 2006. doi:10.1093/cid/cis228
18. Raghavan K. Statistical considerations in the microscopical diagnosis of Malaria, with special reference to the role of cross-checking. *Bull World Health Organ*. 1966;34: 788–791.
19. Wongsrichanalai C, Barcus MJ, Muth S, Sutamihardja A, Wernsdorfer WH. A review of malaria diagnostic tools: Microscopy and rapid diagnostic test (RDT). *Am J Trop Med Hyg*. 2007;77: 119–127. doi:10.3126/ajms.v1i2.2965
20. Kain KC, Pillai D, Ohrt C, Harrington MA, Humar A. ParaSight®F Test Compared with the Polymerase Chain Reaction and Microscopy for the Diagnosis of *Plasmodium falciparum* Malaria in Travelers. *Am J Trop Med Hyg*. 1997;56: 44–48. doi:10.4269/ajtmh.1997.56.44
21. Roth JM, Korevaar DA, Leeflang MMG, Mens PF. Molecular malaria diagnostics: A systematic review and meta-analysis. *Crit Rev Clin Lab Sci*. 2016;53: 87–105. doi:10.3109/10408363.2015.1084991

References

22. Snounou G, Viriyakosol S, Jarra W, Thaithong S, Brown KN. Identification of the four human malaria parasite species in field samples by the polymerase chain reaction and detection of a high prevalence of mixed infections. *Mol Biochem Parasitol*. 1993;58: 283–92. doi:10.1016/0166-6851(93)90050-8
23. Wells TNC, van Huijsduijnen RH, Van Voorhis WC. Malaria medicines: a glass half full? *Nat Rev Drug Discov*. 2015;14: 424–442. doi:10.1038/nrd4573
24. Krafts K, Hempelmann E, Skórska-Stania A. From methylene blue to chloroquine: A brief review of the development of an antimalarial therapy. *Parasitol Res*. 2012;111: 1–6. doi:10.1007/s00436-012-2886-x
25. Wongsrichanalai C, Pickard AL, Wernsdorfer WH, Meshnick SR. Epidemiology of drug-resistant malaria. *Lancet Infect Dis*. 2002;2: 209–218. doi:10.1016/S1473-3099(02)00239-6
26. Su X-Z, Miller LH. The discovery of artemisinin and the Nobel Prize in Physiology or Medicine. *Sci China Life Sci*. 2015;58: 1175–1179. doi:10.1007/s11427-015-4948-7
27. White NJ. Assessment of the pharmacodynamic properties of antimalarial drugs in vivo. *Antimicrob Agents Chemother*. 1997;41: 1413–1422.
28. World Health Organization. Guidelines for the treatment of malaria. 1st Editio. Geneva; 2006. doi:WHO Library Cataloguing-in-Publication Data
29. Alin MH, Ashton M, Kihamia CM, Mtey GJ, Bjorkman A. Multiple dose pharmacokinetics of oral artemisinin and comparison of its efficacy with that of oral artesunate in *falciparum* malaria patients. *TransRSocTropMedHyg*. 1996;90: 61–65.
30. Gordi T, Huong DX, Hai TN, Nieu T, Ashton M, Nieu NT. Artemisinin Pharmacokinetics and Efficacy in Uncomplicated-Malaria Patients Treated with Two Different Dosage Regimens. *Antimicrob agents Chemother*. 2002;46: 1026–1031. doi:10.1128/AAC.46.4.1026
31. Mosha D, Mazuguni F, Mrema S, Sevene E, Abdulla S, Genton B. Safety of artemether-lumefantrine exposure in first trimester of pregnancy: an observational cohort. *Malar J*. 2014;13: 197. doi:10.1186/1475-2875-13-197
32. Kayentao K, Garner P, Maria van Eijk A, Naidoo I, Roper C, Mulokozi A, et al. Intermittent Preventive Therapy for Malaria During Pregnancy Using 2 vs 3 or More Doses of Sulfadoxine-Pyrimethamine and Risk of Low Birth Weight in Africa. *Jama*. 2013;309: 594. doi:10.1001/jama.2012.216231
33. Aponte JJ, Schellenberg D, Egan A, Breckenridge A, Carneiro I, Critchley J, et al. Efficacy and safety of intermittent preventive treatment with sulfadoxine-pyrimethamine for malaria in African infants: a pooled analysis of six randomised, placebo-controlled trials. *Lancet*. Elsevier Ltd; 2009;374: 1533–1542. doi:10.1016/S0140-6736(09)61258-7
34. Meremikwu Martin M, Donegan S, Sinclair D, Esu E, Oringanje C. Intermittent preventive treatment for malaria in children living in areas with seasonal transmission. *Cochrane Database Syst Rev*. 2012; 10–12. doi:10.1002/14651858.CD003756.pub4
35. World Health Organization. International travel and health. World Health Organization. Geneva; 2012. doi:10.1136/bmj.2.6190.610-b
36. World Health Organization. Malaria. International Travel And Health. Geneva; 2016. Available: http://www.who.int/ith/ITH_chapter_7.pdf
37. Graves PM, Gelband H, Garner P. Primaquine or other 8-aminoquinoline for reducing *P. falciparum* transmission. *Cochrane Database Syst Rev*. 2014; doi:10.1002/14651858.CD008152.pub3
38. Eziefula AC, Bousema T, Yeung S, Kanya M, Owaraganise A, Gabagaya G, et al. Single dose primaquine for clearance of *Plasmodium falciparum* gametocytes in children with uncomplicated malaria in Uganda: A randomised, controlled, double-blind, dose-ranging trial. *Lancet Infect Dis*. Eziefula et al. Open Access article distributed under the terms of CC BY-NC-ND; 2014;14: 130–139. doi:10.1016/S1473-3099(13)70268-8
39. Galappaththy GN, Tharyan P, Kirubakaran R. Primaquine for preventing relapse in people with

- Plasmodium vivax* malaria treated with chloroquine. Cochrane Database Syst Rev. 2013; doi:10.1002/14651858.CD004389.pub3
40. Krotoski WA, Krotoski DM, Garnham PC, Bray RS, Killick-Kendrick R, Draper CC, et al. Relapses in primate malaria: discovery of two populations of exoerythrocytic stages. Preliminary note. Br Med J. 1980;280: 153–154. doi:10.1136/bmj.280.6208.153-a
 41. Krotoski WA, Collins WE, Bray RS, Garnham PCC, Cogswell FB, Gwadz RW, et al. Demonstration of Hypnozoites in Sporozoite-Transmitted *Plasmodium vivax* Infection. Am J Trop Med Hyg. 1982;31: 1291–1293. Available: http://www.ncbi.nlm.nih.gov/entrez/query.fcgi?cmd=Retrieve&db=PubMed&dopt=Citation&list_uids=6816080
 42. Chen N, Auliff A, Rieckmann K, Gatton M, Cheng Q. Relapses of *Plasmodium vivax* infection result from clonal hypnozoites activated at predetermined intervals. J Infect Dis. 2007;195: 934–41. doi:10.1086/512242
 43. Imwong M, Snounou G, Pukrittayakamee S, Tanomsing N, Kim JR, Nandy A, et al. Relapses of *Plasmodium vivax* Infection Usually Result from Activation of Heterologous Hypnozoites. J Infect Dis. 2007;195: 927–933. doi:10.1086/512241
 44. de Araujo FCF, de Rezende AM, Fontes CJF, Carvalho LH, Alves de Brito CF. Multiple-Clone Activation of Hypnozoites Is the Leading Cause of Relapse in *Plasmodium vivax* Infection. PLoS One. 2012;7: 1–9. doi:10.1371/journal.pone.0049871
 45. Imwong M, Boel MHE, Pagornrat W, Pimanpanarak M, McGready R, Day NPJ, et al. The first *Plasmodium vivax* relapses of life are usually genetically homologous. J Infect Dis. 2012;205: 680–683. doi:10.1093/infdis/jir806
 46. Bolchoz LJ, Budinsky R a, McMillan DC, Jollow DJ. Primaquine-induced hemolytic anemia: formation and hemotoxicity of the arylhydroxylamine metabolite 6-methoxy-8-hydroxylaminoquinoline. J Pharmacol Exp Ther. 2001;297: 509–515.
 47. Luzzatto L, Nannelli C, Notaro R. Glucose-6-Phosphate Dehydrogenase Deficiency. Hematol Oncol Clin North Am. Elsevier Inc; 2016;30: 373–393. doi:10.1016/j.hoc.2015.11.006
 48. White NJ, Qiao L, Qi G, Luzzatto L. Rationale for recommending a lower dose of primaquine as a *Plasmodium falciparum* gametocytocide in populations where G6PD deficiency is common. Malar J. 2012;11: 418. doi:10.1186/1475-2875-11-418
 49. Nussenzweig V, Nussenzweig RS. Rationale for the Development of an Engineered Sporozoite Malaria Vaccine. Adv Immunol. 1989;45: 283–334. doi:10.1016/S0065-2776(08)60695-1
 50. Arun Kumar K, Sano G, Boscardin S, Nussenzweig RS, Nussenzweig MC, Zavala F, et al. The circumsporozoite protein is an immunodominant protective antigen in irradiated sporozoites. Nature. 2006;444: 937–940. doi:10.1038/nature05361
 51. Kaslow DC, Biernaux S. RTS, S: Toward a first landmark on the Malaria Vaccine Technology Roadmap. Vaccine. Elsevier Ltd; 2015;33: 7425–7432. doi:10.1016/j.vaccine.2015.09.061
 52. Cohen J, Nussenzweig V, Vekemans J, Leach A. From the circumsporozoite protein to the RTS,S/AS candidate vaccine. Hum Vaccin. 2010;6: 90–96. doi:10.4161/hv.6.1.9677
 53. RTSS Clinical Trials Partnership. A Phase 3 Trial of RTS,S/AS01 Malaria Vaccine in African Infants. N Engl J Med. 2012;365: 2284–2295. doi:10.1056/NEJMoa1208394
 54. RTSS Clinical Trials Partnership. Efficacy and safety of RTS,S/AS01 malaria vaccine with or without a booster dose in infants and children in Africa: final results of a phase 3, individually randomised, controlled trial. Lancet. Elsevier Ltd; 2015;386: 31–45. doi:10.1016/S0140-6736(15)60721-8
 55. Umeh R, Oguiche S, Oguonu T, Pitmang S, Shu E, Onyia JT, et al. Immunogenicity and safety of the candidate RTS,S/AS01 vaccine in young Nigerian children: A randomized, double-blind, lot-to-lot consistency trial. Vaccine. 2014;32: 6556–6562. doi:10.1016/j.vaccine.2014.07.067
 56. RTSS Clinical Trials Partnership. Efficacy and safety of the RTS,S/AS01 malaria vaccine during 18

References

- months after vaccination: a phase 3 randomized, controlled trial in children and young infants at 11 African sites. *PLoS Med.* 2014;11: e1001685. doi:10.1371/journal.pmed.1001685
57. Swysen C, Vekemans J, Bruls M, Oyakhirome S, Drakeley C, Kremsner P, et al. Development of standardized laboratory methods and quality processes for a phase III study of the RTS, S/AS01 candidate malaria vaccine. *Malar J.* 2011;10: 223. doi:10.1186/1475-2875-10-223
58. Amanda, L.; Johan, V.; Lievens, M.; Ofori-Anyinam, O.; Cahill, C.; Owusu-Agyei, S.; Abdulla, S.; Macete, E.; Njuguna, N.; Savarese, B.; Loucq, L. and Ballou WR. Design of a phase III multicenter trial to evaluate the efficacy of the RTS,S/AS01 malaria vaccine in children across diverse transmission settings in Africa. *Malar J.* 2011;10: 224. doi:10.1186/1475-2875-10-224
59. Vekemans J, Marsh K, Greenwood B, Leach A, Kabore W. Assessment of severe malaria in a multicenter , phase III , RTS , S / AS01 malaria candidate vaccine trial : case definition , standardization of data collection and patient care Assessment of severe malaria in a multicenter , phase III , RTS , S / AS01 m. *Malar J.* 2011;221.
60. Lievens M, Aponte JJ, Williamson J, Mmbando B, Mohamed A, Bejon P, et al. Statistical methodology for the evaluation of vaccine efficacy in a phase III multi-centre trial of the RTS,S/AS01 malaria vaccine in African children. *Malar J.* 2011;10: 222. doi:10.1186/1475-2875-10-222
61. European Medicines Agency. Assessment Report of Mosquirix. 2015.
62. World Health Organization. Malaria vaccine: WHO position paper-January 2016 [Internet]. *Weekly Epidemiological Record.* 2016. doi:10.1371/jour
63. Piperaki ET, Daikos GL. Malaria in Europe: emerging threat or minor nuisance? *Clin Microbiol Infect.* Elsevier Ltd; 2016;22: 487–493. doi:10.1016/j.cmi.2016.04.023
64. Hellenic Centre for Disease Control and Prevention. Epidemiological Surveillance Report [Internet]. 2011. Available: http://www.cdc.gov/healthyweight/losing_weight/index.html
65. Spanakos G, Alifrangis M, Schousboe ML, Patsoula E, Tegos N, Hansson HH, et al. Genotyping *Plasmodium vivax* isolates from the 2011 outbreak in Greece. *Malar J.* 2013;12: 463. doi:10.1186/1475-2875-12-463
66. Bhatt S, Weiss DJ, Mappin B, Dalrymple U, Cameron E, Bisanzio D, et al. Coverage and system efficiencies of insecticide-treated nets in Africa from 2000 to 2017. *Elife.* 2015;4: 1–37. doi:10.7554/eLife.09672
67. Toé KH, Jones CM, N’fale S, Ismaï HM, Dabiré RK, Ranson H. Increased pyrethroid resistance in malaria vectors and decreased bed net effectiveness Burkina Faso. *Emerg Infect Dis.* 2014;20: 1691–1696. doi:10.3201/eid2010.140619
68. Notomi T, Okayama H, Masubuchi H, Yonekawa T, Watanabe K, Amino N, et al. Loop-mediated isothermal amplification of DNA. *Nucleic Acids Res.* 2000;28: E63. doi:10.1093/nar/28.12.e63
69. Polley SD, Mori Y, Watson J, Perkins MD, González IJ, Notomi T, et al. Mitochondrial DNA targets increase sensitivity of malaria detection using loop-mediated isothermal amplification. *J Clin Microbiol.* 2010;48: 2866–2871. doi:10.1128/JCM.00355-10
70. Hopkins H, González IJ, Polley SD, Angutoko P, Ategeka J, Asiimwe C, et al. Highly sensitive detection of malaria parasitemia in a malaria-endemic setting: Performance of a new loop-mediated isothermal amplification kit in a remote clinic in Uganda. *J Infect Dis.* 2013;208: 645–652. doi:10.1093/infdis/jit184
71. Noedl H, Se Y, Schaecher K, Smith BL, Socheat D, Fukuda MM. Evidence of Artemisinin-Resistant Malaria in Western Cambodia. *N Engl J Med.* 2008;359: 2619–2620. doi:10.1056/NEJMc0805011
72. Witkowski B, Amaratunga C, Khim N, Sreng S, Chim P, Kim S, et al. Novel phenotypic assays for the detection of artemisinin-resistant *Plasmodium falciparum* malaria in Cambodia: *in-vitro* and *ex-vivo* drug-response studies. *Lancet Infect Dis.* Elsevier Ltd; 2013;3099: 1–7. doi:10.1016/S1473-3099(13)70252-4
73. Ariev F, Witkowski B, Amaratunga C, Beghain J, Langlois A-C, Khim N, et al. The resistance gene in

- malaria parasite identified. *Nature*. 2014;505: 50–55. doi:10.1038/nature12876
74. Phyo AP, Nkhoma S, Stepniewska K, Ashley EA, Nair S, McGready R, et al. Emergence of artemisinin-resistant malaria on the western border of Thailand: A longitudinal study. *Lancet*. Elsevier Ltd; 2012;379: 1960–1966. doi:10.1016/S0140-6736(12)60484-X
 75. Ashley EA, Dhorda M, Fairhurst RM, Amaratunga C, Lim P, Suon S, et al. Spread of Artemisinin Resistance in *Plasmodium falciparum* Malaria. *N Engl J Med*. 2014;371: 411–423. doi:10.1056/NEJMoa1314981
 76. Mishra M, Mishra VK, Kashaw V, Iyer AK, Kashaw SK. Comprehensive review on various strategies for antimalarial drug discovery. *Eur J Med Chem*. Elsevier Masson SAS; 2017;125: 1300–1320. doi:10.1016/j.ejmech.2016.11.025
 77. Hemingway J, Shretta R, Wells TNC, Bell D, Djimdé AA, Achee N, et al. Tools and Strategies for Malaria Control and Elimination: What Do We Need to Achieve a Grand Convergence in Malaria? *PLoS Biol*. 2016;14: 1–14. doi:10.1371/journal.pbio.1002380
 78. Kuhen KL, Chatterjee AK, Rottmann M, Gagaring K, Borboa R, Buenviaje J, et al. KAF156 is an antimalarial clinical candidate with potential for use in prophylaxis, treatment, and prevention of disease transmission. *Antimicrob Agents Chemother*. 2014;58: 5060–5067. doi:10.1128/AAC.02727-13
 79. White NJ, Duong TT, Uthaisin C, Nosten F, Phyo AP, Hanboonkunupakarn B, et al. Antimalarial Activity of KAF156 in *Falciparum* and *Vivax* Malaria. *N Engl J Med*. 2016;375: 1152–1160. doi:10.1056/NEJMoa1602250
 80. Coteron JM, Esquivias J, Deng X, White KL, White J, Koltun M, et al. Structure-Guided Lead Optimization of Triazolopyrimidine-Ring Substituents Identifies Potent *Plasmodium falciparum* Dihydroorotate Dehydrogenase Inhibitors with Clinical Candidate Potential. *J Med Chem*. 2011;54: 5540–5561. doi:10.1021/jm200592f
 81. Phillips MA, Lotharius J, Marsh K, White J, Dayan A, White KL, et al. A long-duration dihydroorotate dehydrogenase inhibitor (DSM265) for prevention and treatment of malaria. *Sci Transl Med*. 2015;7: 296ra111-296ra111. doi:10.1126/scitranslmed.aaa6645
 82. Sulyok M, Rückle T, Roth A, Mürbeth RE, Chalon S, Kerr N, et al. DSM265 for *Plasmodium falciparum* chemoprophylaxis: A randomised, double blinded, phase 1 trial with controlled human malaria infection. *Lancet Infect Dis*. 2017;17. doi:10.1016/S1473-3099(17)30139-1
 83. McCarthy JS, Lotharius J, Rückle T, Chalon S, Phillips MA, Elliott S, et al. Safety, tolerability, pharmacokinetics, and activity of the novel long-acting antimalarial DSM265: A two-part first-in-human phase 1a/1b randomised study. *Lancet Infect Dis*. 2017;17. doi:10.1016/S1473-3099(17)30171-8
 84. Rottmann M, McNamara C, Yeung BKS, Lee MCS, Zou B, Russell B, et al. Spiroindolones, a Potent Compound Class for the Treatment of Malaria. *Science*. 2010;329: 1175–1180. doi:10.1126/science.1193225
 85. Van Pelt-Koops JC, Pett HE, Graumans W, Van Der Vegte-Bolmer M, Van Gemert GJ, Rottmann M, et al. The spiroindolone drug candidate NITD609 potently inhibits gametocytogenesis and blocks *Plasmodium falciparum* transmission to *Anopheles* mosquito vector. *Antimicrob Agents Chemother*. 2012;56: 3544–3548. doi:10.1128/AAC.06377-11
 86. Upton LM, Brock PM, Churcher TS, Ghani AC, Gething PW, Delves MJ, et al. Lead clinical and preclinical antimalarial drugs can significantly reduce sporozoite transmission to vertebrate populations. *Antimicrob Agents Chemother*. 2015;59: 490–497. doi:10.1128/AAC.03942-14
 87. Chavchich M, Van Breda K, Rowcliffe K, Diagana TT, Edstein MD. The spiroindolone KAE609 does not induce dormant ring stages in *Plasmodium falciparum* parasites. *Antimicrob Agents Chemother*. 2016;60: 5167–5174. doi:10.1128/AAC.02838-15
 88. White NJ, Pukrittayakamee S, Phyo AP, Rueangweerayut R, Nosten F, Jittamala P, et al. Spiroindolone KAE609 for *Falciparum* and *Vivax* Malaria. *N Engl J Med*. 2014;371: 403–410.

References

- doi:10.1056/NEJMoa1315860
89. Charman SA, Arbe-Barnes S, Bathurst IC, Brun R, Campbell M, Charman WN, et al. Synthetic ozonide drug candidate OZ439 offers new hope for a single-dose cure of uncomplicated malaria. *Proc Natl Acad Sci*. 2011;108: 4400–4405. doi:10.1073/pnas.1015762108
 90. Phyo AP, Jittamala P, Nosten FH, Pukrittayakamee S, Imwong M, White NJ, et al. Antimalarial activity of artefenomel (OZ439), a novel synthetic antimalarial endoperoxide, in patients with *Plasmodium falciparum* and *Plasmodium vivax* malaria: an open-label phase 2 trial. *Lancet Infect Dis*. 2016;16: 61–69. doi:10.1016/S1473-3099(15)00320-5
 91. Straimer J, Gnädig NF, Stokes BH, Ehrenberger M, Crane AA, Fidock A. *Plasmodium falciparum* K13 Mutations Differentially Impact Ozonide Susceptibility and Parasite Fitness In Vitro. *MBio*. 2017;8: 1–12.
 92. Baumgärtner F, Jourdan J, Scheurer C, Blasco B, Campo B, Mäser P, et al. In vitro activity of anti-malarial ozonides against an artemisinin-resistant isolate. *Malar J*. *BioMed Central*; 2017;16: 45. doi:10.1186/s12936-017-1696-0
 93. Yang T, Xie SC, Cao P, Giannangelo C, McCaw J, Creek DJ, et al. Comparison of the exposure time dependence of the activities of synthetic ozonide antimalarials and dihydroartemisinin against K13 wild-type and mutant *Plasmodium falciparum* Strains. *Antimicrob Agents Chemother*. 2016;60: 4501–4510. doi:10.1128/AAC.00574-16
 94. Rajapakse S, Rodrigo C, Fernando SD. Tafenoquine for preventing relapse in people with *Plasmodium vivax* malaria. *Cochrane Database Syst Rev*. 2015; doi:10.1002/14651858.CD010458.pub2
 95. Campo B, Vandal O, Wesche DL, Burrows JN. Killing the hypnozoite – drug discovery approaches to prevent relapse in *Plasmodium vivax*. *Pathog Glob Health*. 2015;109: 107–122. doi:10.1179/2047773215Y.0000000013
 96. Schwartz L, Brown G V, Genton B, Moorthy VS. A review of malaria vaccine clinical projects based on the WHO rainbow table. *Malar J*. 2012;11: 11. doi:10.1186/1475-2875-11-11
 97. Draper SJ, Angov E, Horii T, Miller LH, Srinivasan P, Theisen M, et al. Recent advances in recombinant protein-based malaria vaccines. *Vaccine*. Elsevier Ltd; 2015;33: 7433–7443. doi:10.1016/j.vaccine.2015.09.093
 98. Bijker EM, Borrmann S, Kappe SH, Mordmüller B, Sack BK, Khan SM. Novel approaches to whole sporozoite vaccination against malaria. *Vaccine*. Elsevier Ltd; 2015;33: 7462–7468. doi:10.1016/j.vaccine.2015.09.095
 99. Roestenberg M, McCall M, Hopman J, Wiersma J, Luty AJF, van Gemert GJ, et al. Protection against a Malaria Challenge by Sporozoite Inoculation. *N Engl J Med*. 2009;361: 468–477. doi:10.1056/NEJMoa0805832
 100. Richie TL, Billingsley PF, Sim BKL, James ER, Chakravarty S, Epstein JE, et al. Progress with *Plasmodium falciparum* sporozoite (PfSPZ)-based malaria vaccines. *Vaccine*. Elsevier Ltd; 2015;33: 7452–7461. doi:10.1016/j.vaccine.2015.09.096
 101. Mordmüller B, Surat G, Lagler H, Chakravarty S, Ishizuka AS, Lalremruata A, et al. Sterile protection against human malaria by chemoattenuated PfSPZ vaccine. *Nature*. 2017;542: 445–449. doi:10.1038/nature21060
 102. Mueller I, Shakri AR, Chitnis CE. Development of vaccines for *Plasmodium vivax* malaria. *Vaccine*. Elsevier Ltd; 2015;33: 7489–7495. doi:10.1016/j.vaccine.2015.09.060
 103. World Health Organization. Global technical strategy for malaria 2016–2030 [Internet]. 1st Editio. World Health Organization. Geneva; 2015. doi:ISBN: 978 92 4 156499 1
 104. Roll Back Malaria Partnership. Action and investment to defeat malaria 2016–2030 [Internet]. 1st Editio. Geneva; 2015. Available: http://www.rollbackmalaria.org/files/files/aim/RBM_AIM_Report_A4_EN-Sept2015.pdf

105. Newby G, Bennett A, Larson E, Cotter C, Shretta R, Phillips AA, et al. The path to eradication: A progress report on the malaria-eliminating countries. *Lancet*. Elsevier Ltd; 2016;387: 1775–1784. doi:10.1016/S0140-6736(16)00230-0
106. Alonso PL, Brown G, Arevalo-Herrera M, Binka F, Chitnis C, Collins F, et al. A research Agenda to underpin Malaria Eradication. *PLoS Med*. 2011;8. doi:10.1371/journal.pmed.1000406
107. Cox FEG. History of the discovery of the malaria parasites and their vectors. *Parasit Vectors*. 2010;3: 5. doi:10.1186/1756-3305-3-5
108. Shortt HE, Fairley NH, Covell G, Shute PG, Garnham PCC. The pre-erythrocytic stage of *Plasmodium falciparum* - a preliminary note. *Br Med J*. 1949;2: 1006–1008.
109. Laveran A. Un nouveau parasite trouvé dans le sang des malades atteints de fièvre palustre: origine parasitaire des accidents de l'impaludisme. *Bull Mem Soc Med Hop*. 1881;17: 158–164.
110. Laveran A. *Traité du paludisme*. Masson G, editor. Paris: Libraire de l'Académie de Médecine; 1898.
111. Ross R. On some Peculiar Pigmented Cells Found in two Mosquitoes fed on Malarial Blood. *Br Med J*. 1897;2: 1786–1788. doi:10.1136/bmj.2.1929.1786
112. Manson P. On the Nature and Significance of the Crescentic and Flagellated Bodies in the Malarial Blood. *Br Med J*. 1894;2: 1306–1308. doi:10.1136/bmj.2.1771.1306
113. Shortt HE, Garnham PCC. Pre-erythrocytic Stage in Mammalian Malaria Parasites. *Nature*. 1948;161: 126.
114. Shortt HE, Garnham PCC, Covell G, Shute PG. The pre-erythrocytic stage of human malaria, *Plasmodium vivax*. *Br Med J*. 1948;1: 547.
115. Escalante AA, Ayala FJ. Evolutionary origin of *Plasmodium* and other Apicomplexa based on rRNA genes. *Proc Natl Acad Sci U S A*. 1995;92: 5793–7. doi:10.1073/pnas.92.13.5793
116. Kilejian A. Cellular mitochondrial DNA from the avian malarial parasite *Plasmodium lophurae*. *Biochim Biophys Acta*. 1975;390: 276–284.
117. Borst P, Overdulve JP, Weijers PJ, Fase-Fowler F, Van den Berg M. DNA circles with cruciforms from *Isospora (Toxoplasma) gondii*. *Biochim Biophys Acta*. 1984;781: 100–111. doi:10.1016/0167-4781(84)90128-3
118. Williamson DH, Wilson RJM, Bates PA, McCready S, Perler F, Qiang B-U. Nuclear and mitochondrial DNA of the primate malarial parasite *Plasmodium knowlesi*. *Mol Biochem Parasitol*. 1985;14: 199–209.
119. He CY, Shaw MK, Pletcher CH, Striepen B, Tilney LG, Roos DS. A plastid segregation defect in the protozoan parasite *Toxoplasma gondii*. *EMBO J*. 2001;20: 330–339. doi:10.1093/emboj/20.3.330
120. Fichera ME, Roos DS. A plastid organelle as a drug target in apicomplexan parasites. *Nature*. 1997;390: 407–409. doi:10.1038/37132
121. Moore RB, Oborník M, Janoušková J, Chrudimský T, Vancová M, Green DH, et al. A photosynthetic alveolate closely related to apicomplexan parasites. *Nature*. 2008;452: 900–900. doi:10.1038/nature06871
122. Janoušková J, Horak A, Oborník M, Lukes J, Keeling PJ. A common red algal origin of the apicomplexan, dinoflagellate, and heterokont plastids. *Proc Natl Acad Sci*. 2010;107: 10949–10954. doi:10.1073/pnas.1003335107
123. Archibald JM. The Puzzle of Plastid Evolution. *Curr Biol*. Elsevier Ltd; 2009;19: R81–R88. doi:10.1016/j.cub.2008.11.067
124. Ralph SA, van Dooren GG, Waller RF, Crawford MJ, Fraunholz, Martin J, Foth BJ, et al. Metabolic maps and functions of the *Plasmodium falciparum* apicoplast. *Nat Rev Microbiol*. 2004;2: 203–216. doi:10.1111/j.1574-6976.2006.00027.x
125. Shears MJ, Botté CY, McFadden GI. Fatty acid metabolism in the *Plasmodium* apicoplast: Drugs, doubts and knockouts. *Mol Biochem Parasitol*. Elsevier B.V.; 2015;199: 34–50.

References

- doi:10.1016/j.molbiopara.2015.03.004
126. Yeh E, DeRisi JL. Chemical rescue of malaria parasites lacking an apicoplast defines organelle function in blood-stage *Plasmodium falciparum*. PLoS Biol. 2011;9. doi:10.1371/journal.pbio.1001138
 127. Yu M, Kumar TRRS, Nkrumah LJ, Coppi A, Retzlaff S, Li CD, et al. The fatty acid biosynthesis enzyme FabI plays a key role in the development of liver-stage malarial parasites. Cell Host Microbe. Elsevier Inc.; 2008;4: 567–78. doi:10.1016/j.chom.2008.11.001
 128. Vaughan AM, O’neill MT, Tarun AS, Camargo N, Phuong TM, Aly ASI, et al. Type II fatty acid synthesis is essential only for malaria parasite late liver stage development. Cell Microbiol. 2009;11: 506–520. doi:10.1111/j.1462-5822.2008.01270.x
 129. van Schaijk BCL, Santha Kumar TR, Vos MW, Richman A, van Gemert GJ, Li T, et al. Type II fatty acid biosynthesis is essential for *Plasmodium falciparum* sporozoite development in the midgut of anopheles mosquitoes. Eukaryot Cell. 2014;13: 550–559. doi:10.1128/EC.00264-13
 130. Morrisette NS, Sibley LD. Cytoskeleton of Apicomplexan Parasites. Microbiol Mol Biol Rev. 2002;66: 21–38. doi:10.1128/MMBR.66.1.21-38.2002
 131. Hu K, Roos DS, Murray JM. A novel polymer of tubulin forms the conoid of *Toxoplasma gondii*. J Cell Biol. 2002;156: 1039–1050. doi:10.1083/jcb.200112086
 132. Pacheco MA, Matta NE, Valkiūnas G, Parker PG, Mello B, Stanley CE, et al. Mode and Rate of Evolution of Haemosporidian Mitochondrial Genomes: Timing the Radiation of Avian Parasites. Mol Biol Evol. 2018;35: 383–403. doi:10.1093/molbev/msx285
 133. Pacheco MA, Battistuzzi FU, Junge RE, Cornejo OE, Williams C V, Landau I, et al. Timing the origin of human malarias: the lemur puzzle. BMC Evol Biol. 2011;11: 299. doi:10.1186/1471-2148-11-299
 134. Frech C, Chen N, Price R, Tjitra E, Guerra C, Yeung S, et al. Variant surface antigens of malaria parasites: functional and evolutionary insights from comparative gene family classification and analysis. BMC Genomics. 2013;14: 427. doi:10.1186/1471-2164-14-427
 135. Su X zhuan, Heatwole VM, Wertheimer SP, Guinet F, Herrfeldt JA, Peterson DS, et al. The large diverse gene family var encodes proteins involved in cytoadherence and antigenic variation of *Plasmodium falciparum*-infected erythrocytes. Cell. 1995;82: 89–100. doi:10.1016/0092-8674(95)90055-1
 136. Sundararaman SA, Plenderleith LJ, Liu W, Loy DE, Learn GH, Li Y, et al. Genomes of cryptic chimpanzee *Plasmodium* species reveal key evolutionary events leading to human malaria. Nat Commun. 2016;7: 11078. doi:10.1038/ncomms11078
 137. Liu W, Li Y, Learn GH, Rudicell RS, Robertson JD, Keele BF, et al. Origin of the human malaria parasite *Plasmodium falciparum* in gorillas. Nature. 2010;467: 420–425. doi:10.1038/nature09442
 138. Martin MJ, Rayner JC, Gagneux P, Barnwell JW, Varki A. Evolution of human-chimpanzee differences in malaria susceptibility: Relationship to human genetic loss of N-glycolylneuraminic acid. Proc Natl Acad Sci U S A. 2006;102: 12819–12824.
 139. Janssen CS, Phillips RS, Turner MR, Barret MP. *Plasmodium* interspersed repeats: The major multigene superfamily of malaria parasites. Nucleic Acids Res. 2004;32: 5712–5720. doi:10.1093/nar/gkh907
 140. Carlton JM, Angiuoli S V., Suh BB, Kooij TW, Perteza M, Silva JC, et al. Genome sequence and comparative analysis of the model rodent malaria parasite *Plasmodium yoelii yoelii*. Nature. 2002;419: 512–519. doi:10.1038/nature01099
 141. Cornejo OE, Escalante AA. The origin and age of *Plasmodium vivax*. Trends Parasitol. 2006;22: 558–563. doi:10.1016/j.pt.2006.09.007
 142. Liu W, Li Y, Shaw KS, Learn GH, Plenderleith LJ, Malenke JA, et al. African origin of the malaria parasite *Plasmodium vivax*. Nat Commun. 2014;5. doi:10.1038/ncomms4346
 143. Miller LH, Mason SJ, Clyde DF, McGinniss MH. The Resistance Factor to *Plasmodium vivax* in Blacks.

- N Engl J Med. 1976;295: 302–304. doi:10.1056/NEJM197608052950602
144. Tournamille C, Colin Y, Cartron JP, Kim CL Van. Disruption of a GATA motif in the Duffy gene promoter abolishes erythroid gene expression in Duffy-negative individuals. *Nat Genet.* 1995;10: 224–228. doi:10.1038/ng0695-224
 145. Loy DE, Plenderleith LJ, Sundararaman SA, Liu W, Gruszczyk J, Chen Y-J, et al. Evolutionary history of human *Plasmodium vivax* revealed by genome-wide analyses of related ape parasites. *Proc Natl Acad Sci.* 2018;115: E8450–E8459. doi:10.1073/pnas.1810053115
 146. Haglund CM, Welch MD. Pathogens and polymers: Microbe–host interactions illuminate the cytoskeleton. *J Cell Biol.* 2011;195: 7–17. doi:10.1083/jcb.201103148
 147. Ribet D, Cossart P. How bacterial pathogens colonize their hosts and invade deeper tissues. *Microbes Infect.* Elsevier Masson SAS; 2015;17: 173–183. doi:10.1016/j.micinf.2015.01.004
 148. Vadia S, Arnett E, Haghghat A-C, Wilson-Kubalek EM, Tweten RK, Seveau S. The Pore-Forming Toxin Listeriolysin O Mediates a Novel Entry Pathway of *L. monocytogenes* into Human Hepatocytes. *PLoS Pathog.* 2011;7: e1002356. doi:10.1371/journal.ppat.1002356
 149. Vadia S, Seveau S. Fluxes of Ca²⁺ and K⁺ are required for the listeriolysin O-dependent internalization pathway of *Listeria monocytogenes*. *Infect Immun.* 2014;82: 1084–1091. doi:10.1128/IAI.01067-13
 150. Fernandes MC, Cortez M, Flannery AR, Tam C, Mortara RA, Andrews NW. *Trypanosoma cruzi* subverts the sphingomyelinase-mediated plasma membrane repair pathway for cell invasion. *J Exp Med.* 2011;208: 909–21. doi:10.1084/jem.20102518
 151. Fernandes MC, Corrotte M, Miguel DC, Tam C, Andrews NW. The exocyst is required for *trypanosome* invasion and the repair of mechanical plasma membrane wounds. *J Cell Sci.* 2015;128: 27–32. doi:10.1242/jcs.150573
 152. Holopainen JM, Subramanian M, Kinnunen PKJ. Sphingomyelinase induces lipid microdomain formation in a fluid phosphatidylcholine/sphingomyelin membrane. *Biochemistry.* 1998;37: 17562–17570. doi:10.1021/bi980915e
 153. Lam JGT, Vadia S, Pathak-Sharma S, McLaughlin E, Zhang X, Swanson J, et al. Host cell perforation by listeriolysin O (LLO) activates a Ca²⁺-dependent cPKC/Rac1/Arp2/3 signaling pathway that promotes *Listeria monocytogenes* internalization independently of membrane resealing. *Mol Biol Cell.* 2018;29: 270–284. doi:10.1091/mbc.E17-09-0561
 154. Grassmé H, Gulbins E, Brenner B, Ferlinz K, Sandhoff K, Harzer K, et al. Acidic sphingomyelinase mediates entry of *N. gonorrhoeae* into nonphagocytic cells. *Cell.* 1997;91: 605–615. doi:10.1016/S0092-8674(00)80448-1
 155. Simonis A, Hebling S, Gulbins E, Schneider-Schaulies S, Schubert-Unkmeir A. Differential Activation of Acid Sphingomyelinase and Ceramide Release Determines Invasiveness of *Neisseria meningitidis* into Brain Endothelial Cells. *PLoS Pathog.* 2014;10. doi:10.1371/journal.ppat.1004160
 156. Luisoni S, Suomalainen M, Boucke K, Tanner LB, Wenk MR, Guan XL, et al. Co-option of membrane wounding enables virus penetration into cells. *Cell Host Microbe.* 2015;18: 75–85. doi:10.1016/j.chom.2015.06.006
 157. Ladda R, Aikawa M, Sprinz H. Penetration of Erythrocytes by Merozoites of Mammalian and Avian Malarial Parasites. *J Parasitol.* 1969;55: 633. doi:10.2307/3277308
 158. Ward GE, Miller LH, Dvorak JA. The origin of parasitophorous vacuole membrane lipids in malaria-infected erythrocytes. *J Cell Sci.* 1993;106 (Pt 1: 237–48. Available: <http://www.ncbi.nlm.nih.gov/pubmed/8270628>
 159. Suss-Toby E, Zimmerberg J, Ward GE. *Toxoplasma* invasion: the parasitophorous vacuole is formed from host cell plasma membrane and pinches off via a fission pore. *Proc Natl Acad Sci U S A.* 1996;93: 8413–8. doi:10.1073/pnas.93.16.8413
 160. Dluzewski AR, Mitchell GH, Fryer PR, Griffiths S, Wilson RJ, Gratzler WB. Origins of the

References

- parasitophorous vacuole membrane of the malaria parasite, *Plasmodium falciparum*, in human red blood cells. *J Cell Sci.* 1992;102 (Pt 3: 527–32. Available: <http://www.ncbi.nlm.nih.gov/pubmed/1506432> <http://jcs.biologists.org/content/102/3/527.full.pdf>
161. Sharma P, Chitnis CE. Key molecular events during host cell invasion by Apicomplexan pathogens. *Curr Opin Microbiol.* Elsevier Ltd; 2013;16: 432–437. doi:10.1016/j.mib.2013.07.004
 162. Venugopal K, Marion S. Secretory organelle trafficking in *Toxoplasma gondii*: A long story for a short travel. *Int J Med Microbiol.* 2018;308: 751–760. doi:10.1016/j.ijmm.2018.07.007
 163. Singh S, Chitnis CE. Signalling mechanisms involved in apical organelle discharge during host cell invasion by apicomplexan parasites. *Microbes Infect.* Elsevier Masson SAS; 2012;14: 820–4. doi:10.1016/j.micinf.2012.05.007
 164. Lourido S, Moreno SNJ. The calcium signaling toolkit of the Apicomplexan parasites *Toxoplasma gondii* and *Plasmodium* spp. *Cell Calcium.* Elsevier Ltd; 2015;57: 186–193. doi:10.1016/j.ceca.2014.12.010
 165. Bargieri DY, Andenmatten N, Lagal V, Thiberge S, Whitelaw J a, Tardieux I, et al. Apical membrane antigen 1 mediates apicomplexan parasite attachment but is dispensable for host cell invasion. *Nat Commun.* 2013;4: 2552. doi:10.1038/ncomms3552
 166. Scholtyseck E, Mehlhorn H. Ultrastructural study of characteristic organelles (paired organelles, micronemes, micropores) of sporozoa and related organisms. *Zeitschrift für Parasitenkd.* 1970;34: 97–127. doi:10.1007/BF00260383
 167. Blackman MJ, Bannister LH. Apical organelles of Apicomplexa: biology and isolation by subcellular fractionation. *Mol Biochem Parasitol.* 2001;117: 11–25. Available: <http://www.ncbi.nlm.nih.gov/pubmed/11551628>
 168. Counihan N a, Kalanon M, Coppel RL, de Koning-Ward TF. *Plasmodium* rhoptry proteins: why order is important. *Trends Parasitol.* Elsevier Ltd; 2013;29: 228–36. doi:10.1016/j.pt.2013.03.003
 169. Boothroyd JC, Dubremetz JF. Kiss and spit: The dual roles of *Toxoplasma* rhoptries. *Nat Rev Microbiol.* 2008;6: 79–88. doi:10.1038/nrmicro1800
 170. Proellocks NI, Coppel RL, Waller KL. Dissecting the apicomplexan rhoptry neck proteins. *Trends Parasitol.* Elsevier Ltd; 2010;26: 297–304. doi:10.1016/j.pt.2010.02.012
 171. Torii M, Adams JH, Miller LH, Aikawa M. Release of merozoite dense granules during erythrocyte invasion by *Plasmodium knowlesi*. *Infect Immun.* 1989;57: 3230–3233. doi:10.1111/j.1523-1739.2011.01708.x
 172. Leriche MA, Dubremetz JF. Exocytosis of *Toxoplasma gondii* dense granules into the parasitophorous vacuole after host cell invasion. *Parasitol Res.* 1990;76: 559–62. doi:10.1056/NEJM198506203122514
 173. Bannister LH, Mitchell GH. The Fine Structure of Secretion by *Plasmodium knowlesi* Merozoites during Red Cell Invasion. *J Protozool.* 1989;36: 362–367. doi:10.1111/j.1550-7408.1989.tb05527.x
 174. Mercier C, Adjogble KDZ, Däubener W, Delauw M-F-C. Dense granules: are they key organelles to help understand the parasitophorous vacuole of all apicomplexa parasites? *Int J Parasitol.* 2005;35: 829–49. doi:10.1016/j.ijpara.2005.03.011
 175. Tardieux I, Baum J. Reassessing the mechanics of parasite motility and host-cell invasion. *J Cell Biol.* 2016;214: 507–515. doi:10.1083/jcb.201605100
 176. Harding CR, Meissner M. The inner membrane complex through development of *Toxoplasma gondii* and *Plasmodium*. *Cellular Microbiology.* 2014. pp. 632–641. doi:10.1111/cmi.12285
 177. Kono M, Herrmann S, Loughran NB, Cabrera A, Engelberg K, Lehmann C, et al. Evolution and architecture of the inner membrane complex in asexual and sexual stages of the malaria parasite. *Mol Biol Evol.* 2012;29: 2113–32. doi:10.1093/molbev/mss081
 178. Dzierszinski F, Nishi M, Ouko L, Roos DS. Dynamics of *Toxoplasma gondii* differentiation. *Eukaryot*

- Cell. 2004;3: 992–1003. doi:10.1128/EC.3.4.992-1003.2004
179. Aikawa M. Ultrastructure of the pellicular complex of *Plasmodium fallax*. J Cell Biol. 1967;35: 103–13. doi:10.1083/jcb.35.1.103
 180. Mitchell GH, Bannister LH. Malaria parasite invasion: interactions with the red cell membrane. Crit Rev Oncol Hematol. 1988;8: 225–310. doi:10.1016/S1040-8428(88)80011-8
 181. Gaskins E, Gilk S, DeVore N, Mann T, Ward G, Beckers C. Identification of the membrane receptor of a class XIV myosin in *Toxoplasma gondii*. J Cell Biol. 2004;165: 383–93. doi:10.1083/jcb.200311137
 182. Dobrowolski JM, Sibley LD. *Toxoplasma* Invasion of Mammalian Cells Is Powered by the Actin Cytoskeleton of the Parasite. Cell. 1996;84: 933–939. doi:10.1016/S0092-8674(00)81071-5
 183. Jones ML, Kitson EL, Rayner JC. *Plasmodium falciparum* erythrocyte invasion: a conserved myosin associated complex. Mol Biochem Parasitol. 2006;147: 74–84. doi:10.1016/j.molbiopara.2006.01.009
 184. Baum J, Richard D, Healer J, Rug M, Krnajski Z, Gilberger TW, et al. A conserved molecular motor drives cell invasion and gliding motility across malaria life cycle stages and other apicomplexan parasites. J Biol Chem. 2006;281: 5197–5208. doi:10.1074/jbc.M509807200
 185. Alexander DL, Mital J, Ward GE, Bradley P, Boothroyd JC. Identification of the moving junction complex of *Toxoplasma gondii*: A collaboration between distinct secretory organelles. PLoS Pathog. 2005;1: 0137–0149. doi:10.1371/journal.ppat.0010017
 186. Koch M, Baum J. The mechanics of malaria parasite invasion of the human erythrocyte – towards a reassessment of the host cell contribution. Cell Microbiol. 2016;18: 319–329. doi:10.1111/cmi.12557
 187. Weiss GE, Crabb BS, Gilson PR. Overlaying Molecular and Temporal Aspects of Malaria Parasite Invasion. Trends Parasitol. Elsevier Ltd; 2016;32: 284–295. doi:10.1016/j.pt.2015.12.007
 188. Goel VK, Li X, Chen H, Liu S-C, Chishti AH, Oh SS. Band 3 is a host receptor binding merozoite surface protein 1 during the *Plasmodium falciparum* invasion of erythrocytes. Proc Natl Acad Sci. 2003;100: 5164–5169. doi:10.1073/pnas.0834959100
 189. Li X, Chen H, Oo TH, Daly TM, Bergman LW, Liu SC, et al. A Co-ligand Complex Anchors *Plasmodium falciparum* Merozoites to the Erythrocyte Invasion Receptor Band 3. J Biol Chem. 2004;279: 5765–5771. doi:10.1074/jbc.M308716200
 190. Baldwin MR, Li X, Hanada T, Liu SC, Chishti AH. Merozoite surface protein 1 recognition of host glycophorin a mediates malaria parasite invasion of red blood cells. Blood. 2015;125: 2704–2711. doi:10.1182/blood-2014-11-611707
 191. Kadekoppala M, Holder AA. Merozoite surface proteins of the malaria parasite: The MSP1 complex and the MSP7 family. Int J Parasitol. Australian Society for Parasitology Inc.; 2010;40: 1155–1161. doi:10.1016/j.ijpara.2010.04.008
 192. Duraisingh MT, Maier AG, Triglia T, Cowman AF. Erythrocyte-binding antigen 175 mediates invasion in *Plasmodium falciparum* utilizing sialic acid-dependent and -independent pathways. Proc Natl Acad Sci. 2003;100: 4796–4801. doi:10.1073/pnas.0730883100
 193. Tham W-H, Wilson DW, Lopaticki S, Schmidt CQ, Tetteh-Quarcoop PB, Barlow PN, et al. Complement receptor 1 is the host erythrocyte receptor for *Plasmodium falciparum* Pfrh4 invasion ligand. Proc Natl Acad Sci. 2010;107: 17327–17332. doi:10.1073/pnas.1008151107
 194. Lopaticki S, Maier AG, Thompson J, Wilson DW, Tham WH, Triglia T, et al. Reticulocyte and erythrocyte binding-like proteins function cooperatively in invasion of human erythrocytes by malaria parasites. Infect Immun. 2011;79: 1107–1117. doi:10.1128/IAI.01021-10
 195. Persson KEM, McCallum FJ, Reiling L, Lister NA, Stubbs J, Cowman AF, et al. Variation in use of erythrocyte invasion pathways by *Plasmodium falciparum* mediates evasion of human inhibitory antibodies. J Clin Invest. 2008;118: 342–351. doi:10.1172/JCI32138
 196. Gaur D, Furuya T, Mu J, Jiang L Bin, Su XZ, Miller LH. Upregulation of expression of the reticulocyte

References

- homology gene 4 in the *Plasmodium falciparum* clone Dd2 is associated with a switch in the erythrocyte invasion pathway. *Mol Biochem Parasitol.* 2006;145: 205–215. doi:10.1016/j.molbiopara.2005.10.004
197. Dolan SA, Miller LH, Wellem TE. Evidence for a switching mechanism in the invasion of erythrocytes by *Plasmodium falciparum*. *J Clin Invest.* 1990;86: 618–624. doi:10.1172/JCI114753
198. Gao X, Gunalan K, Yap SSL, Preiser PR. Triggers of key calcium signals during erythrocyte invasion by *Plasmodium falciparum*. *Nat Commun.* 2013;4: 1–11. doi:10.1038/ncomms3862
199. Paul AS, Saha S, Engelberg K, Jiang RHY, Coleman BI, Kosber AL, et al. Parasite calcineurin regulates host cell recognition and attachment by apicomplexans. *Cell Host Microbe.* Elsevier Inc.; 2015;18: 49–60. doi:10.1016/j.chom.2015.06.003
200. Singh S, Alam MM, Pal-Bhowmick I, Brzostowski JA, Chitnis CE. Distinct external signals trigger sequential release of apical organelles during erythrocyte invasion by malaria parasites. *PLoS Pathog.* 2010;6. doi:10.1371/journal.ppat.1000746
201. Singh S, More KR, Chitnis CE. Role of calcineurin and actin dynamics in regulated secretion of microneme proteins in *Plasmodium falciparum* merozoites during erythrocyte invasion. *Cell Microbiol.* 2014;16: 50–63. doi:10.1111/cmi.12177
202. Dasgupta S, Auth T, Gov NS, Satchwell TJ, Hanssen E, Zuccala ES, et al. Membrane-wrapping contributions to malaria parasite invasion of the human erythrocyte. *Biophys J. The Authors;* 2014;107: 43–54. doi:10.1016/j.bpj.2014.05.024
203. Hayton K, Gaur D, Liu A, Takahashi J, Henschen B, Singh S, et al. Erythrocyte Binding Protein PfrH5 Polymorphisms Determine Species-Specific Pathways of *Plasmodium falciparum* Invasion. *Cell Host Microbe.* 2008;4: 40–51. doi:10.1016/j.chom.2008.06.001
204. Baum J, Chen L, Healer J, Lopaticki S, Boyle M, Triglia T, et al. Reticulocyte-binding protein homologue 5 - An essential adhesin involved in invasion of human erythrocytes by *Plasmodium falciparum*. *Int J Parasitol. Australian Society for Parasitology Inc.;* 2009;39: 371–380. doi:10.1016/j.ijpara.2008.10.006
205. Chen L, Lopaticki S, Riglar DT, Dekiwadia C, Uboldi AD, Tham WH, et al. An egf-like protein forms a complex with pfrh5 and is required for invasion of human erythrocytes by *Plasmodium falciparum*. *PLoS Pathog.* 2011;7. doi:10.1371/journal.ppat.1002199
206. Crosnier C, Bustamante LY, Bartholdson SJ, Bei AK, Theron M, Uchikawa M, et al. Basigin is a receptor essential for erythrocyte invasion by *Plasmodium falciparum*. *Nature.* 2011;480: 534–537. doi:10.1038/nature10606
207. Douglas AD, Williams AR, Knuepfer E, Illingworth JJ, Furze JM, Crosnier C, et al. Neutralization of *Plasmodium falciparum* Merozoites by Antibodies against PfrH5. *J Immunol.* 2014;192: 245–258. doi:10.4049/jimmunol.1302045
208. Reddy KS, Amlabu E, Pandey AK, Mitra P, Chauhan VS, Gaur D. Multiprotein complex between the GPI-anchored CyRPA with PfrH5 and PfrRipr is crucial for *Plasmodium falciparum* erythrocyte invasion. *Proc Natl Acad Sci.* 2015;112: 1179–1184. doi:10.1073/pnas.1415466112
209. Weiss GE, Gilson PR, Taechalerpaisarn T, Tham WH, de Jong NWM, Harvey KL, et al. Revealing the Sequence and Resulting Cellular Morphology of Receptor-Ligand Interactions during *Plasmodium falciparum* Invasion of Erythrocytes. *PLoS Pathog.* 2015;11: 1–25. doi:10.1371/journal.ppat.1004670
210. Philip N, Waters AP. Conditional Degradation of *Plasmodium* Calcineurin Reveals Functions in Parasite Colonization of both Host and Vector. *Cell Host Microbe.* The Authors; 2015;18: 122–131. doi:10.1016/j.chom.2015.05.018
211. Srinivasan P, Beatty WL, Diouf A, Herrera R, Ambroggio X, Moch JK, et al. Binding of *Plasmodium* merozoite proteins RON2 and AMA1 triggers commitment to invasion. *Proc Natl Acad Sci.* 2011;108: 13275–13280. doi:10.1073/pnas.1110303108
212. Alexander DL, Arastu-Kapur S, Dubremetz JF, Boothroyd JC. *Plasmodium falciparum* AMA1 binds a rhoptry neck protein homologous to TgRON4, a component of the moving junction in *Toxoplasma*

- gondii*. Eukaryot Cell. 2006;5: 1169–1173. doi:10.1128/EC.00040-06
213. Richard D, MacRaild CA, Riglar DT, Chan JA, Foley M, Baum J, et al. Interaction between *Plasmodium falciparum* apical membrane antigen 1 and the rhoptry neck protein complex defines a key step in the erythrocyte invasion process of malaria parasites. J Biol Chem. 2010;285: 14815–14822. doi:10.1074/jbc.M109.080770
 214. Tonkin ML, Roques M, Lamarque MH, Pugnère M, Douguet D, Crawford J, et al. Host cell invasion by apicomplexan parasites: Insights from the co-structure of AMA1 with a RON2 peptide. Science. 2011;333: 463–467. doi:10.1126/science.1204988
 215. Lamarque M, Besteiro S, Papoin J, Roques M, Vulliez-Le Normand B, Morlon-Guyot J, et al. The RON2-AMA1 interaction is a critical step in moving junction-dependent invasion by apicomplexan parasites. PLoS Pathog. 2011;7. doi:10.1371/journal.ppat.1001276
 216. Treeck M, Zacherl S, Herrmann S, Cabrera A, Kono M, Struck NS, et al. Functional analysis of the leading malaria vaccine candidate AMA-1 reveals an essential role for the cytoplasmic domain in the invasion process. PLoS Pathog. 2009;5: e1000322. doi:10.1371/journal.ppat.1000322
 217. Aikawa M, Miller LH, Johnson J, Rabbege J. Erythrocyte entry by malarial parasites. J cell Biol Biol. 1978;77: 72–82. doi:10.1083/jcb.77.1.72
 218. Riglar DT, Richard D, Wilson DW, Boyle MJ, Dekiwadia C, Turnbull L, et al. Super-resolution dissection of coordinated events during malaria parasite invasion of the human erythrocyte. Cell Host Microbe. Elsevier Inc.; 2011;9: 9–20. doi:10.1016/j.chom.2010.12.003
 219. Gunalan K, Niangaly A, Thera MA, Doumbo OK, Miller LH. *Plasmodium vivax* Infections of Duffy-Negative Erythrocytes: Historically Undetected or a Recent Adaptation? Trends Parasitol. Elsevier Ltd; 2018;34: 420–429. doi:10.1016/j.pt.2018.02.006
 220. Bermúdez M, Moreno-Pérez DA, Arévalo-Pinzón G, Curtidor H, Patarroyo MA. *Plasmodium vivax* in vitro continuous culture: the spoke in the wheel. Malar J. BioMed Central; 2018;17: 301. doi:10.1186/s12936-018-2456-5
 221. Yogavel M, Chhibber-Goel J, Jamwal A, Gupta S, Sharma A. Engagement Rules That Underpin DBL-DARC Interactions for Ingress of *Plasmodium knowlesi* and *Plasmodium vivax* Into Human Erythrocytes. Front Mol Biosci. 2018;5: 1–6. doi:10.3389/fmolb.2018.00078
 222. Miller LH. Interaction between cytochalasin B-treated malarial parasites and erythrocytes. Attachment and junction formation. J Exp Med. 1979;149: 172–184. doi:10.1084/jem.149.1.172
 223. Menard D, Barnadas C, Bouchier C, Henry-Halldin C, Gray LR, Ratsimbao A, et al. *Plasmodium vivax* clinical malaria is commonly observed in Duffy-negative Malagasy people. Proc Natl Acad Sci. 2010;107: 5967–5971. doi:10.1073/pnas.0912496107
 224. Mendes C, Dias F, Figueiredo J, Mora VG, Cano J, de Sousa B, et al. Duffy negative antigen is no longer a barrier to *Plasmodium vivax* - molecular evidences from the African West Coast (Angola and Equatorial Guinea). PLoS Negl Trop Dis. 2011;5: 2–7. doi:10.1371/journal.pntd.0001192
 225. Russo G, Faggioni G, Paganotti GM, Djeunang Dongho GB, Pomponi A, De Santis R, et al. Molecular evidence of *Plasmodium vivax* infection in Duffy negative symptomatic individuals from Dschang, West Cameroon. Malar J. BioMed Central; 2017;16: 1–9. doi:10.1186/s12936-017-1722-2
 226. Ryan JR, Stoute JA, Amon J, Dunton RF, Mtalib R, Koros J, et al. Evidence for transmission of *Plasmodium vivax* among a duffy antigen negative population in Western Kenya. Am J Trop Med Hyg. 2006;75: 575–81. doi:10.4269/ajtmh.2006.75.575
 227. Gruszczyk J, Huang RK, Chan L-JJ, Menant S, Hong C, Murphy JM, et al. Cryo-EM structure of an essential *Plasmodium vivax* invasion complex. Nature. Springer US; 2018;559: 1. doi:10.1038/s41586-018-0249-1
 228. Gruszczyk J, Kanjee U, Chan LJ, Menant S, Malleret B, Lim NTY, et al. Transferrin receptor 1 is a reticulocyte-specific receptor for *Plasmodium vivax*. Science. 2018;359: 48–55. doi:10.1126/science.aan1078

References

229. Murphy SC, Fernandez-pol S, Chung PH, Murthy SNP, Stephen B, Salomao M, et al. Cytoplasmic remodeling of erythrocyte raft lipids during infection by the human malaria parasite *Plasmodium falciparum*. *Blood*. 2012;110: 2132–2139. doi:10.1182/blood-2007-04-083873
230. Samuel BU, Mohandas N, Harrison T, McManus H, Rosse W, Reid M, et al. The role of cholesterol and glycosylphosphatidylinositol-anchored proteins of erythrocyte rafts in regulating raft protein content and malarial infection. *J Biol Chem*. 2001;276: 29319–29. doi:10.1074/jbc.M101268200
231. Pasvol G, Weatherall DJ, Wilson RJM. Cellular mechanism for the protective effect of haemoglobin S against *P. falciparum* malaria. *Nature*. 1978;274: 701–703. doi:10.1038/274701a0
232. Olson JA, Kilejian A. Involvement of spectrin and atp in infection of resealed erythrocyte ghosts by the human malarial parasite, *Plasmodium falciparum*. *J Cell Biol*. 1982;95: 757–762. doi:10.1083/jcb.95.3.757
233. Dluzewski AR, Rangachari K, Gratzer WB, Wilson RJM. Inhibition of malarial invasion of red cells by chemical and immunochemical linking of spectrin molecules. *Br J Haematol*. 1983;55: 629–637. doi:10.1111/j.1365-2141.1983.tb02845.x
234. Shear HL, Roth EF, Ng C, Nagel RL. Resistance to malaria in ankyrin and spectrin deficient mice. *Br J Haematol*. 1991;78: 555–560. doi:10.1111/j.1365-2141.1991.tb04488.x
235. Liu SC, Palek J, Yi SJ, Nichols PE, Derick LH, Chiou SS, et al. Molecular basis of altered red blood cell membrane properties in Southeast Asian ovalocytosis: role of the mutant band 3 protein in band 3 oligomerization and retention by the membrane skeleton. *Blood*. 1995;86: 349–58. Available: <http://www.ncbi.nlm.nih.gov/pubmed/7795244>
236. Zuccala ES, Baum J. Cytoskeletal and membrane remodelling during malaria parasite invasion of the human erythrocyte. *Br J Haematol*. 2011;154: 680–689. doi:10.1111/j.1365-2141.2011.08766.x
237. Dluzewski AR, Rangachari K, Wilson RJM, Gratzer WB. A cytoplasmic requirement of red cells for invasion by malarial parasites. *Mol Biochem Parasitol*. 1983;9: 145–160. doi:10.1016/0166-6851(83)90106-8
238. Rangachari K, Dluzewski A, Wilson RJM, Gratzer WB. Control of malarial invasion by phosphorylation of the host cell membrane cytoskeleton. *Nature*. 1986;324: 364–365. doi:10.1038/324364a0
239. Rangachari K, Dluzewski AR, Wilson RJ, Gratzer WB. Cytoplasmic factor required for entry of malaria parasites into RBCs. *Blood*. 1987;70: 77–82. doi:10.1182/blood-2015-06-651331
240. Murray MC, Perkins ME. Phosphorylation of erythrocyte membrane and cytoskeleton proteins in cells infected with *Plasmodium falciparum*. *Mol Biochem Parasitol*. 1989;34: 229–36. Available: <http://www.ncbi.nlm.nih.gov/pubmed/2525229>
241. Wasserman M, Vernot JP, Mendoza PM. Role of calcium and erythrocyte cytoskeleton phosphorylation in the invasion of *Plasmodium falciparum*. *Parasitol Res*. 1990;76: 681–8. Available: <http://www.ncbi.nlm.nih.gov/pubmed/2251243>
242. Wasserman M, Chaparro J. Intraerythrocytic calcium chelators inhibit the invasion of *Plasmodium falciparum*. *Parasitol Res*. 1996;82: 102–107. doi:10.1007/s004360050078
243. Wu Y, Nelson MM, Quail A, Xia D, Wastling JM, Craig A. Identification of phosphorylated proteins in erythrocytes infected by the human malaria parasite *Plasmodium falciparum*. *Malar J*. 2009;8. doi:10.1186/1475-2875-8-105
244. Mota MM, Pradel G, Vanderberg JP, Hafalla JC, Frevert U, Nussenzweig RS, et al. Migration of *Plasmodium* sporozoites through cells before infection. *Science*. 2001;291: 141–4. doi:10.1126/science.291.5501.141
245. Mota MM, Hafalla JCRR, Rodriguez A. Migration through host cells activates *Plasmodium* sporozoites for infection. *Nat Med*. 2002;8: 1318–1322. doi:10.1038/nm
246. Vaughan AM, Kappe SHI. Malaria Parasite Liver Infection and Exoerythrocytic Biology. *Cold Spring Harb Perspect Med*. 2017;7: a025486. doi:10.1101/cshperspect.a025486
247. Medica DL, Sinnis P. Quantitative dynamics of *Plasmodium yoelii* sporozoite transmission by

- infected anopheline mosquitoes. *Infect Immun*. 2005;73: 4363–9. doi:10.1128/IAI.73.7.4363-4369.2005
248. Amino R, Thiberge S, Martin B, Celli S, Shorte S, Frischknecht F, et al. Quantitative imaging of *Plasmodium* transmission from mosquito to mammal. *Nat Med*. 2006;12: 220–4. doi:10.1038/nm1350
249. Jin Y, Kebaier C, Vanderberg J. Direct microscopic quantification of dynamics of *Plasmodium berghei* sporozoite transmission from mosquitoes to mice. *Infect Immun*. 2007;75: 5532–5539. doi:10.1128/IAI.00600-07
250. Yamauchi LM, Coppi A, Snounou G, Sinnis P. *Plasmodium* sporozoites trickle out of the injection site. *Cell Microbiol*. 2007;9: 1215–22. doi:10.1111/j.1462-5822.2006.00861.x
251. Pancake SJ, Holt GD, Mellouk S, Hoffman SL. Malaria Sporozoites and Circumsporozoite Proteins Bind Specifically to Sulfated Glycoconjugates. *J Cell Biol*. 1992;117: 1351–1357. doi:10.1083/jcb.117.6.1351
252. Shakibaei M, Frevert U. Dual interaction of the malaria circumsporozoite protein with the low density lipoprotein receptor-related protein (LRP) and heparan sulfate proteoglycans. *J Exp Med*. 1996;184: 1699–711. Available: <http://www.pubmedcentral.nih.gov/articlerender.fcgi?artid=2192891&tool=pmcentrez&rendertype=abstract>
253. Ying P, Shakibaei M, Patankar MS, Clavijo P, Beavis RC, Clark GF, et al. The malaria circumsporozoite protein: Interaction of the conserved regions I and II-plus with heparin-like oligosaccharides in heparan sulfate. *Exp Parasitol*. 1997;85: 168–182. doi:10.1006/expr.1996.4134
254. Pinzon-Ortiz C, Friedman J, Esko J, Sinnis P. The binding of the circumsporozoite protein to cell surface heparan sulfate proteoglycans is required for *Plasmodium* sporozoite attachment to target cells. *J Biol Chem*. 2001;276: 26784–26791. doi:10.1074/jbc.M104038200
255. Coppi A, Tewari R, Bishop JR, Bennett BL, Lawrence R, Esko JD, et al. Heparan sulfate proteoglycans provide a signal to *Plasmodium* sporozoites to stop migrating and productively invade host cells. *Cell Host Microbe*. 2007;2: 316–27. doi:10.1016/j.chom.2007.10.002
256. Müller H-M, Reckmann I, Hollingdale MR, Bujard H, Robson KJH, Crisanti A. Thrombospondin related anonymous protein (TRAP) of *Plasmodium falciparum* binds specifically to sulfated glycoconjugates and to HepG2 hepatoma cells suggesting a role for this molecule in sporozoite invasion of hepatocytes. *EMBO J*. 1993;12: 2881–2889.
257. McCormick CJ, Tuckwell DS, Crisanti A, Humphries MJ, Hollingdale MR. Identification of heparin as a ligand for the A-domain of *Plasmodium falciparum* thrombospondin-related adhesion protein. *Mol Biochem Parasitol*. 1999;100: 111–124. doi:10.1016/S0166-6851(99)00052-3
258. Baer K, Roosevelt M, Clarkson AB, Van Rooijen N, Schnieder T, Frevert U. Kupffer cells are obligatory for *Plasmodium yoelii* sporozoite infection of the liver. *Cell Microbiol*. 2007;9: 397–412. doi:10.1111/j.1462-5822.2006.00798.x
259. Tavares J, Formaglio P, Thiberge S, Mordelet E, Van Rooijen N, Medvinsky A, et al. Role of host cell traversal by the malaria sporozoite during liver infection. *J Exp Med*. 2013;210: 905–915. doi:10.1084/jem.20121130
260. Ishino T, Yano K, Chinzei Y, Yuda M. Cell-passage activity is required for the malarial parasite to cross the liver sinusoidal cell layer. *PLoS Biol*. 2004;2: E4. doi:10.1371/journal.pbio.0020004
261. Ishino T, Chinzei Y, Yuda M. A *Plasmodium* sporozoite protein with a membrane attack complex domain is required for breaching the liver sinusoidal cell layer prior to hepatocyte infection. *Cell Microbiol*. 2005;7: 199–208. doi:10.1111/j.1462-5822.2004.00447.x
262. Kaiser K, Camargo N, Coppens I, Morrisey JM, Vaidya AB, Kappe SHI. A member of a conserved *Plasmodium* protein family with membrane-attack complex/perforin (MACPF)-like domains localizes to the micronemes of sporozoites. *Mol Biochem Parasitol*. 2004;133: 15–26. doi:10.1016/j.molbiopara.2003.08.009

References

263. Kariu T, Ishino T, Yano K, Chinzei Y, Yuda M. CelTOS, a novel malarial protein that mediates transmission to mosquito and vertebrate hosts. *Mol Microbiol.* 2006;59: 1369–79. doi:10.1111/j.1365-2958.2005.05024.x
264. Jimah JR, Salinas ND, Sala-Rabanal M, Jones NG, David Sibley L, Nichols CG, et al. Malaria parasite CelTOS targets the inner leaflet of cell membranes for pore- dependent disruption. *Elife.* 2016;5: 1–17. doi:10.7554/eLife.20621
265. Risco-Castillo V, Topçu S, Marinach C, Manzoni G, Bigorgne AE, Briquet S, et al. Malaria sporozoites traverse host cells within transient vacuoles. *Cell Host Microbe.* 2015;18: 593–603. doi:10.1016/j.chom.2015.10.006
266. Kumar KA, Garcia CRS, Chandran VR, Van Rooijen N, Zhou Y, Winzeler E, et al. Exposure of *Plasmodium* sporozoites to the intracellular concentration of potassium enhances infectivity and reduces cell passage activity. *Mol Biochem Parasitol.* 2007;156: 32–40. doi:10.1016/j.molbiopara.2007.07.004
267. Siau A, Silvie O, Franetich J-F, Yalaoui S, Marinach C, Hannoun L, et al. Temperature shift and host cell contact up-regulate sporozoite expression of *Plasmodium falciparum* genes involved in hepatocyte infection. *PLoS Pathog.* 2008;4: e1000121. doi:10.1371/journal.ppat.1000121
268. Silvie O, Franetich J-FF, Charrin S, Mueller MS, Siau A, Bodescot M, et al. A role for apical membrane antigen 1 during invasion of hepatocytes by *Plasmodium falciparum* sporozoites. *J Biol Chem.* 2004;279: 9490–6. doi:10.1074/jbc.M311331200
269. Dijk MR Van, Douradinha B, Franke-Fayard B, Heussler V, Dooren MW Van, Schaijk B Van, et al. Genetically attenuated, P36p-deficient malarial sporozoites induce protective immunity and apoptosis of infected liver cells. *Proc Natl Acad Sci U S A.* 2005;102: 12194–9. doi:10.1073/pnas.0500925102
270. Ishino T, Chinzei Y, Yuda M. Two proteins with 6-cys motifs are required for malarial parasites to commit to infection of the hepatocyte. *Mol Microbiol.* 2005;58: 1264–75. doi:10.1111/j.1365-2958.2005.04801.x
271. van Schaijk BCL, Janse CJ, van Gemert GJ, van Dijk MR, Gego A, Franetich JF, et al. Gene disruption of *Plasmodium falciparum* p52 results in attenuation of malaria liver stage development in cultured primary human hepatocytes. *PLoS One.* 2008;3. doi:10.1371/journal.pone.0003549
272. Giovannini D, Späth S, Lacroix C, Perazzi A, Bargieri D, Lagal V, et al. Independent roles of apical membrane antigen 1 and rhoptry neck proteins during host cell invasion by apicomplexa. *Cell Host Microbe.* 2011;10: 591–602. doi:10.1016/j.chom.2011.10.012
273. Yang ASP, Lopaticki S, O’Neill MT, Erickson SM, Douglas DN, Kneteman NM, et al. AMA1 and MAEBL are important for *Plasmodium falciparum* sporozoite infection of the liver. *Cell Microbiol.* 2017;19: 1–14. doi:10.1111/cmi.12745
274. Govindaswamy K, Jebiwott S, Jaijyan DK, Davidow A, Ojo KK, Van Voorhis WC, et al. Invasion of hepatocytes by *Plasmodium* sporozoites requires cGMP-dependent protein kinase and calcium dependent protein kinase 4. *Mol Microbiol.* 2016;102: 349–363. doi:10.1111/mmi.13466
275. Sinnis P, Willnow TE, Briones MRS, Herz J, Nussenzweig V. Remnant Lipoproteins Inhibit Malaria Sporozoite Invasion of Hepatocytes. *J Exp Med.* 1996;184: 945–954.
276. Silvie O, Rubinstein E, Franetich J-F, Prenant M, Belnoue E, Rénia L, et al. Hepatocyte CD81 is required for *Plasmodium falciparum* and *Plasmodium yoelii* sporozoite infectivity. *Nat Med.* 2003;9: 93–6. doi:10.1038/nm808
277. Silvie O, Greco C, Franetich JF, Dubart-Kupperschmitt A, Hannoun L, van Gemert GJ, et al. Expression of human CD81 differently affects host cell susceptibility to malaria sporozoites depending on the *Plasmodium* species. *Cell Microbiol.* 2006;8: 1134–1146. doi:10.1111/j.1462-5822.2006.00697.x
278. Foquet L, Hermsen CC, Verhoye L, Van Gemert GJ, Cortese R, Nicosia A, et al. Anti-CD81 but not anti-SR-BI blocks *Plasmodium falciparum* liver infection in a humanized mouse model. *J Antimicrob Chemother.* 2014;70: 1784–1787. doi:10.1093/jac/dkv019

279. Rodrigues CD, Hannus M, Prudêncio M, Martin C, Gonçalves L a, Portugal S, et al. Host scavenger receptor SR-BI plays a dual role in the establishment of malaria parasite liver infection. *Cell Host Microbe*. 2008;4: 271–82. doi:10.1016/j.chom.2008.07.012
280. Yalaoui S, Huby T, Franetich JF, Gego A, Rametti A, Moreau M, et al. Scavenger Receptor BI Boosts Hepatocyte Permissiveness to *Plasmodium* Infection. *Cell Host Microbe*. 2008;4: 283–292. doi:10.1016/j.chom.2008.07.013
281. Manzoni G, Marinach C, Topçu S, Briquet S, Grand M, Tolle M, et al. *Plasmodium* P36 determines host cell receptor usage during sporozoite invasion. *Elife*. 2017;6: 1–24. doi:10.7554/eLife.25903
282. Kaushansky A, Douglass AN, Arang N, Vigdorovich V, Dambrauskas N, Kain HS, et al. Malaria parasites target the hepatocyte receptor EphA2 for successful host infection. *Science*. 2015;350: 1089–1092. doi:10.1126/science.aad3318
283. Silvie O, Charrin S, Billard M, Franetich J-F, Clark KL, van Gemert G-J, et al. Cholesterol contributes to the organization of tetraspanin-enriched microdomains and to CD81-dependent infection by malaria sporozoites. *J Cell Sci*. 2006;119: 1992–2002. doi:10.1242/jcs.02911
284. Silvie O, Franetich J-F, Boucheix C, Rubinstein E, Mazier D. Alternative invasion pathways for *Plasmodium berghei* sporozoites. *Int J Parasitol*. 2007;37: 173–82. doi:10.1016/j.ijpara.2006.10.005
285. Prudêncio M, Rodrigues CD, Hannus M, Martin C, Real E, Gonçalves LA, et al. Kinome-side RNAi screen implicates at least 5 host hepatocyte kinases in *Plasmodium* sporozoite infection. *PLoS Pathog*. 2008;4. doi:10.1371/journal.ppat.1000201
286. Gonzalez V, Combe A, David V, Malmquist N a, Delorme V, Leroy C, et al. Host cell entry by apicomplexa parasites requires actin polymerization in the host cell. *Cell Host Microbe*. Elsevier Inc.; 2009;5: 259–72. doi:10.1016/j.chom.2009.01.011
287. Real E, Rodrigues L, Cabal GGG, Enguita FJFJ, Mancio-Silva L, Mello-Vieira J, et al. *Plasmodium* UIS3 sequesters host LC3 to avoid elimination by autophagy in hepatocytes. *Nat Microbiol*. 2017;3: 17–25. doi:10.1038/s41564-017-0054-x
288. Wahlgren M, Goel S, Akhouri RR. Variant surface antigens of *Plasmodium falciparum* and their roles in severe malaria. *Nat Rev Microbiol*. 2017;15: 479–491. doi:10.1038/nrmicro.2017.47
289. Laveran A. *Traité des Fièvres Palustres avec la Description des Microbes du Paludisme*. Doin O, editor. Paris; 1884.
290. Laveran A. *Du paludisme et de son Hématozoaire*. Masson G, editor. Paris: Libraire de l'Académie de Médecine; 1891.
291. Soni R, Sharma D, Bhatt TK. *Plasmodium falciparum* Secretome in Erythrocyte and Beyond. *Front Microbiol*. 2016;7: 1–10. doi:10.3389/fmicb.2016.00194
292. Smith JD, Chitnis CE, Craig AG, Roberts DJ, Hudson-Taylor DE, Peterson DS, et al. Switches in expression of *Plasmodium falciparum* var genes correlate with changes in antigenic and cytoadherent phenotypes of infected erythrocytes. *Cell*. 1995;82: 101–110. doi:10.1016/0092-8674(95)90056-X
293. Baruch DI, Pasloske BL, Singh HB, Bi X, Ma XC, Feldman M, et al. Cloning the *P. falciparum* gene encoding PfEMP1, a malarial variant antigen and adherence receptor on the surface of parasitized human erythrocytes. *Cell*. 1995;82: 77–87. doi:10.1016/0092-8674(95)90054-3
294. Chen Q, Barragan a, Fernandez V, Sundström a, Schlichtherle M, Sahlén a, et al. Identification of *Plasmodium falciparum* erythrocyte membrane protein 1 (PfEMP1) as the rosetting ligand of the malaria parasite *P. falciparum*. *J Exp Med*. 1998;187: 15–23. doi:10.1084/jem.187.1.15
295. Mills JP, Diez-Silva M, Quinn DJ, Dao M, Lang MJ, Tan KSW, et al. Effect of plasmodial RESA protein on deformability of human red blood cells harboring *Plasmodium falciparum*. *Proc Natl Acad Sci U S A*. 2007;104: 9213–9217. doi:10.1073/pnas.0703433104
296. Glenister FK, Fernandez KM, Kats LM, Hanssen E, Mohandas N, Coppel RL, et al. Functional alteration of red blood cells by a megadalton protein of *Plasmodium falciparum*. *Blood*. 2009;113:

References

- 919–928. doi:10.1182/blood-2008-05-157735
297. Homewood CA, Neame KD. Malaria and the permeability of the host erythrocyte. *Nature*. 1974;252: 718–719. doi:10.1038/252718a0
298. Ginsburg H, Krugliak M, Eidelman O, Ioav Cabantchik Z. New permeability pathways induced in membranes of *Plasmodium falciparum* infected erythrocytes. *Mol Biochem Parasitol*. 1983;8: 177–190. doi:10.1016/0166-6851(83)90008-7
299. Kutner S, Ginsburg H, Cabantchik ZI. Permeability changes in malaria (*Plasmodium falciparum*) infected human red blood cell membranes. *J Cell Physiol*. 1983;114: 245–51. doi:10.1002/jcp.1041140215
300. Gilson PR, Chisholm SA, Crabb BS, de Koning-Ward TF. Host cell remodelling in malaria parasites: a new pool of potential drug targets. *Int J Parasitol. Australian Society for Parasitology*; 2017;47: 119–127. doi:10.1016/j.ijpara.2016.06.001
301. Przyborski JM, Nyboer B, Lanzer M. Ticket to ride: export of proteins to the *Plasmodium falciparum*-infected erythrocyte. *Mol Microbiol*. 2016;101: 1–11. doi:10.1111/mmi.13380
302. Koning-ward TF De, Dixon MWA, Tilley L, Gilson PR. *Plasmodium* species: master renovators of their host cells. *Nat Rev Microbiol*. 2016;14: 494–507. doi:10.1038/nrmicro.2016.79
303. Wickham ME, Rug M, Ralph SA, Klonis N, Mcfadden GI, Tilley L, et al. Trafficking and assembly of the cytoadherence complex in *Plasmodium falciparum*-infected human erythrocytes. *EMBO J*. 2001;20: 5636–5649. doi:10.1093/emboj/20.20.5636
304. Adisa A, Rug M, Klonis N, Foley M, Cowman AF, Tilley L. The signal sequence of exported protein-1 directs the green fluorescent protein to the parasitophorous vacuole of transfected malaria parasites. *J Biol Chem*. 2003;278: 6532–6542. doi:10.1074/jbc.M207039200
305. Hanson KK, Ressurreição AS, Buchholz K, Prudêncio M, Herman-Ornelas JD, Rebelo M, et al. Torins are potent antimalarials that block replenishment of *Plasmodium* liver stage parasitophorous vacuole membrane proteins. *Proc Natl Acad Sci U S A*. 2013;110: E2838–E2847. doi:10.1073/pnas.1306097110/-/DCSupplemental.www.pnas.org/cgi/doi/10.1073/pnas.1306097110
306. Albano FR, Berman a, La Greca N, Hibbs a R, Wickham M, Foley M, et al. A homologue of Sar1p localises to a novel trafficking pathway in malaria-infected erythrocytes. *Eur J Cell Biol*. 1999;78: 453–462. doi:10.1016/S0171-9335(99)80072-7
307. Marti M, Good RT, Rug M, Knuepfer E, Cowman AF. Targeting malaria virulence and remodeling proteins to the host erythrocyte. *Science*. 2004;306: 1930–3. doi:10.1126/science.1102452
308. Hiller NL, Bhattacharjee S, van Ooij C, Liolios K, Harrison T, Lopez-Estraño C, et al. A host-targeting signal in virulence proteins reveals a secretome in malarial infection. *Science*. 2004;306: 1934–7. doi:10.1126/science.1102737
309. Sargeant TJ, Marti M, Caler E, Carlton JM, Simpson K, Speed TP, et al. Lineage-specific expansion of proteins exported to erythrocytes in malaria parasites. *Genome Biol*. 2006;7: R12. doi:10.1186/gb-2006-7-2-r12
310. Boddey J a, Hodder AN, Günther S, Gilson PR, Patsiouras H, Kapp E a, et al. An aspartyl protease directs malaria effector proteins to the host cell. *Nature*. 2010;463: 627–31. doi:10.1038/nature08728
311. Russo I, Babbitt S, Muralidharan V, Butler T, Oksman A, Goldberg DE. Plasmeprin V licenses *Plasmodium* proteins for export into the host erythrocyte. *Nature*. 2010;463: 632–6. doi:10.1038/nature08726
312. Chang HH, Falick AM, Carlton PM, Sedat JW, DeRisi JL, Marletta M a. N-terminal processing of proteins exported by malaria parasites. *Mol Biochem Parasitol*. 2008;160: 107–15. doi:10.1016/j.molbiopara.2008.04.011
313. Boddey JA, Moritz RL, Simpson RJ, Cowman AF. Role of the *Plasmodium* export element in

- trafficking parasite proteins to the infected erythrocyte. *Traffic*. 2009;10: 285–299. doi:10.1111/j.1600-0854.2008.00864.x
314. Spielmann T, Gilberger TW. Protein export in malaria parasites: do multiple export motifs add up to multiple export pathways? *Trends Parasitol*. 2010;26: 6–10. doi:10.1016/j.pt.2009.10.001
 315. Haase S, Herrmann S, Grüning C, Heiber A, Jansen PW, Langer C, et al. Sequence requirements for the export of the *Plasmodium falciparum* Maurer's clefts protein REX2. *Mol Microbiol*. 2009;71: 1003–1017. doi:10.1111/j.1365-2958.2008.06582.x
 316. Grüning C, Heiber A, Kruse F, Flemming S, Franci G, Colombo SF, et al. Uncovering common principles in protein export of malaria parasites. *Cell Host Microbe*. 2012;12: 717–29. doi:10.1016/j.chom.2012.09.010
 317. Marti M, Spielmann T. Protein export in malaria parasites: Many membranes to cross. *Curr Opin Microbiol*. Elsevier Ltd; 2013;16: 445–451. doi:10.1016/j.mib.2013.04.010
 318. Boddey JA, Carvalho TG, Hodder AN, Sargeant TJ, Sleebs BE, Marapana D, et al. Role of Plasmepsin V in Export of Diverse Protein Families from the *Plasmodium falciparum* Exportome. *Traffic*. 2013;14: 532–550. doi:10.1111/tra.12053
 319. Spielmann T, Gilberger T-W. Critical Steps in Protein Export of *Plasmodium falciparum* Blood Stages. *Trends Parasitol*. Elsevier Ltd; 2015;31: 514–25. doi:10.1016/j.pt.2015.06.010
 320. Papakrivov J, Newbold CI, Lingelbach K. A potential novel mechanism for the insertion of a membrane protein revealed by a biochemical analysis of the *Plasmodium falciparum* cytoadherence molecule PfEMP-1. *Mol Microbiol*. 2005;55: 1272–1284. doi:10.1111/j.1365-2958.2004.04468.x
 321. Riglar DT, Rogers KL, Hanssen E, Turnbull L, Bullen HE, Charnaud SC, et al. Spatial association with PTEX complexes defines regions for effector export into *Plasmodium falciparum*-infected erythrocytes. *Nat Commun*. 2013;4: 1415. doi:10.1038/ncomms2449
 322. Mesén-Ramírez P, Reinsch F, Blancke Soares A, Bergmann B, Ullrich A-K, Tenzer S, et al. Stable Translocation Intermediates Jam Global Protein Export in *Plasmodium falciparum* Parasites and Link the PTEX Component EXP2 with Translocation Activity. *PLoS Pathog*. 2016;12: e1005618. doi:10.1371/journal.ppat.1005618
 323. Bhattacharjee S, Speicher KD, Stahelin R V, Speicher DW, Haldar K. PI(3)P-independent and -dependent pathways function together in a vacuolar translocation sequence to target malarial proteins to the host erythrocyte. *Mol Biochem Parasitol*. Elsevier B.V.; 2012;185: 106–13. doi:10.1016/j.molbiopara.2012.07.004
 324. Boddey JA, O'Neill MT, Lopaticki S, Carvalho TG, Hodder AN, Nebl T, et al. Export of malaria proteins requires co-translational processing of the PEXEL motif independent of phosphatidylinositol-3-phosphate binding. *Nat Commun*. 2016;7: 10470. doi:10.1038/ncomms10470
 325. Tawk L, Chicanne G, Dubremetz JF, Richard V, Payrastra B, Vial HJ, et al. Phosphatidylinositol 3-phosphate, an essential lipid in *Plasmodium*, localizes to the food vacuole membrane and the apicoplast. *Eukaryot Cell*. 2010;9: 1519–1530. doi:10.1128/EC.00124-10
 326. Przyborski JM, Miller SK, Pfahler JM, Henrich PP, Rohrbach P, Crabb BS, et al. Trafficking of STEVOR to the Maurer's clefts in *Plasmodium falciparum*-infected erythrocytes. *EMBO J*. 2005;24: 2306–17. doi:10.1038/sj.emboj.7600720
 327. Külzer S, Gehde N, Przyborski JM. Return to sender: Use of *Plasmodium* ER retrieval sequences to study protein transport in the infected erythrocyte and predict putative ER protein families. *Parasitol Res*. 2009;104: 1535–1541. doi:10.1007/s00436-009-1397-x
 328. Gehde N, Hinrichs C, Montilla I, Charpian S, Lingelbach K, Przyborski JM. Protein unfolding is an essential requirement for transport across the parasitophorous vacuolar membrane of *Plasmodium falciparum*. *Mol Microbiol*. 2009;71: 613–628. doi:10.1111/j.1365-2958.2008.06552.x
 329. Ansorge I, Benting J, Bhakdi S, Lingelbach K. Protein sorting in *Plasmodium falciparum*-infected red blood cells permeabilized with the pore-forming protein streptolysin O. *Biochem J*. 1996;315 (Pt 1: 307–314. Available:

References

- <http://www.pubmedcentral.nih.gov/articlerender.fcgi?artid=1217187&tool=pmcentrez&rendertype=abstract>
330. de Koning-Ward TF, Gilson PR, Boddey J a, Rug M, Smith BJ, Papenfuss AT, et al. A newly discovered protein export machine in malaria parasites. *Nature*. 2009;459: 945–9. doi:10.1038/nature08104
 331. Bullen HE, Charnaud SC, Kalanon M, Riglar DT, Dekiwadia C, Kangwanrangsan N, et al. Biosynthesis, Localization, and Macromolecular Arrangement of the *Plasmodium falciparum* Translocon of Exported Proteins (PTEX). *J Biol Chem*. 2012;287: 7871–7884. doi:10.1074/jbc.M111.328591
 332. Ho C-M, Beck JR, Lai M, Cui Y, Goldberg DE, Egea PF, et al. Malaria parasite translocon structure and mechanism of effector export. *Nature*. Springer US; 2018;561: 70–75. doi:10.1038/s41586-018-0469-4
 333. Matthews K, Kalanon M, Chisholm SA, Sturm A, Goodman CD, Dixon MWA, et al. The *Plasmodium* translocon of exported proteins (PTEX) component thioredoxin-2 is important for maintaining normal blood-stage growth. *Mol Microbiol*. 2013;89: 1167–1186. doi:10.1111/mmi.12334
 334. Matz JM, Matuschewski K, Kooij TW a. Two putative protein export regulators promote *Plasmodium* blood stage development in vivo. *Mol Biochem Parasitol*. Elsevier B.V.; 2013;191: 44–52. doi:10.1016/j.molbiopara.2013.09.003
 335. Beck JR, Muralidharan V, Oksman A, Goldberg DE. PTEX component HSP101 mediates export of diverse malaria effectors into host erythrocytes. *Nature*. 2014;511: 592–595. doi:10.1038/nature13574
 336. Elsworth B, Matthews K, Nie CQ, Kalanon M, Charnaud SC, Sanders PR, et al. PTEX is an essential nexus for protein export in malaria parasites. *Nature*. 2014;511: 587–591. doi:10.1038/nature13555
 337. Costa TRD, Felisberto-Rodrigues C, Meir A, Prevost MS, Redzej A, Trokter M, et al. Secretion systems in Gram-negative bacteria: structural and mechanistic insights. *Nat Rev Microbiol*. 2015;13: 343–359. doi:10.1038/nrmicro3456
 338. Elsworth B, Sanders PR, Nebl T, Batinovic S, Kalanon M, Nie CQ, et al. Proteomic analysis reveals novel proteins associated with the *Plasmodium* protein exporter PTEX and a loss of complex stability upon truncation of the core PTEX component, PTEX150. *Cell Microbiol*. 2016;18: 1551–1569. doi:10.1111/cmi.12596
 339. Hakamada K, Watanabe H, Kawano R, Noguchi K, Yohda M. Expression and characterization of the *Plasmodium* translocon of the exported proteins component EXP2. *Biochem Biophys Res Commun*. Elsevier Ltd; 2017;482: 6–11. doi:10.1016/j.bbrc.2016.11.097
 340. Gold DA, Kaplan AD, Lis A, Bett GCL, Rosowski EE, Cirelli KM, et al. The *Toxoplasma* dense granule proteins GRA17 and GRA23 mediate the movement of small molecules between the host and the parasitophorous vacuole. *Cell Host Microbe*. Elsevier Inc.; 2015;17: 642–652. doi:10.1016/j.chom.2015.04.003
 341. Garten M, Nasamu AS, Niles JC, Zimmerberg J, Goldberg DE, Beck JR. EXP2 is a nutrient-permeable channel in the vacuolar membrane of *Plasmodium* and is essential for protein export via PTEX. *Nat Microbiol*. Springer US; 2018; doi:10.1038/s41564-018-0222-7
 342. Chisholm SA, McHugh E, Lundie R, Dixon MWA, Ghosh S, O’Keefe M, et al. Contrasting inducible knockdown of the auxiliary PTEX component PTEX88 in *P. falciparum* and *P. berghei* unmask a role in parasite virulence. *PLoS One*. 2016;11: 1–21. doi:10.1371/journal.pone.0149296
 343. Matz JM, Ingmundson A, Nunes JC, Stenzel W, Matuschewski K, Kooij TWA a, et al. In vivo function of PTEX88 in malaria parasite sequestration and virulence. *Eukaryot Cell*. 2015;14: 528–534. doi:10.1128/EC.00276-14
 344. Spielmann T, Gardiner DL, Beck HP, Trenholme KR, Kemp DJ. Organization of ETRAMPs and EXP-1 at the parasite-host cell interface of malaria parasites. *Mol Microbiol*. 2006;59: 779–794. doi:10.1111/j.1365-2958.2005.04983.x
 345. Elsworth B, Crabb BS, Gilson PR. Protein export in malaria parasites: an update. *Cell Microbiol*. 2014;16: 355–63. doi:10.1111/cmi.12261

346. Nyalwidhe J, Lingelbach K. Proteases and chaperones are the most abundant proteins in the parasitophorous vacuole of *Plasmodium falciparum*-infected erythrocytes. *Proteomics*. 2006;6: 1563–1573. doi:10.1002/pmic.200500379
347. Chu T, Lingelbach K, Przyborski JM. Genetic evidence strongly support an essential role for *Pf*VP1 in intra-erythrocytic growth of *P. falciparum*. *PLoS One*. 2011;6: 1–8. doi:10.1371/journal.pone.0018396
348. Batinovic S, McHugh E, Chisholm SA, Matthews K, Liu B, Dumont L, et al. An exported protein-interacting complex involved in the trafficking of virulence determinants in *Plasmodium*-infected erythrocytes. *Nat Commun*. 2017;8: 16044. doi:10.1038/ncomms16044
349. Offeddu V, Rauch M, Silvie O, Matuschewski K. The Plasmodium protein P113 supports efficient sporozoite to liver stage conversion in vivo. *Mol Biochem Parasitol*. Elsevier B.V.; 2014;193: 101–109. doi:10.1016/j.molbiopara.2014.03.002
350. Külzer S, Rug M, Brinkmann K, Cannon P, Cowman A, Lingelbach K, et al. Parasite-encoded Hsp40 proteins define novel mobile structures in the cytosol of the *P. falciparum*-infected erythrocyte. *Cell Microbiol*. 2010;12: 1398–420. doi:10.1111/j.1462-5822.2010.01477.x
351. Külzer S, Charnaud S, Dagan T, Riedel J, Mandal P, Pesce ER, et al. *Plasmodium falciparum*-encoded exported hsp70/hsp40 chaperone/co-chaperone complexes within the host erythrocyte. *Cell Microbiol*. 2012;14: 1784–1795. doi:10.1111/j.1462-5822.2012.01840.x
352. Grüring C, Heiber A, Kruse F, Ungefehr J, Gilberger T-W, Spielmann T. Development and host cell modifications of *Plasmodium falciparum* blood stages in four dimensions. *Nat Commun*. 2011;2: 165. doi:10.1038/ncomms1169
353. Kilian N, Dittmer M, Cyrklaff M, Ouermi D, Bisseye C, Simpore J, et al. Haemoglobin s and c affect the motion of Maurer's clefts in *Plasmodium falciparum*-infected erythrocytes. *Cell Microbiol*. 2013;15: 1111–1126. doi:10.1111/cmi.12102
354. McMillan PJ, Millet C, Batinovic S, Maiorca M, Hanssen E, Kenny S, et al. Spatial and temporal mapping of the *Pf*EMP1 export pathway in *Plasmodium falciparum*. *Cell Microbiol*. 2013;15: 1401–1418. doi:10.1111/cmi.12125
355. Lanzer M, Wickert H, Krohne G, Vincensini L, Braun Breton C. Maurer's clefts: A novel multi-functional organelle in the cytoplasm of *Plasmodium falciparum*-infected erythrocytes. *Int J Parasitol*. 2006;36: 23–36. doi:10.1016/j.ijpara.2005.10.001
356. Waterkeyn JG, Wickham ME, Davern KM, Cooke BM, Coppel RL, Reeder JC, et al. Targeted mutagenesis of *Plasmodium falciparum* erythrocyte membrane protein 3 (*Pf*EMP3) disrupts cytoadherence of malaria-infected red blood cells. *EMBO J*. 2000;19: 2813–23. doi:10.1093/emboj/19.12.2813
357. Kriek N, Tilley L, Horrocks P, Pinches R, Elford BC, Ferguson DJP, et al. Characterization of the pathway for transport of the cytoadherence- mediating protein, *Pf*EMP1, to the host cell surface in malaria parasite-infected erythrocytes. *Mol Microbiol*. 2003;50: 1215–1227. doi:10.1046/j.1365-2958.2003.03784.x
358. Knuepfer E, Rug M, Klonis N, Tilley L, Cowman AF. Trafficking of the major virulence factor to the surface of transfected *P. falciparum*-infected erythrocytes. *Blood*. 2005;105: 4078–87. doi:10.1182/blood-2004-12-4666
359. Trelka DP, Schneider TG, Reeder JC, Taraschi TF. Evidence for vesicle-mediated trafficking of parasite proteins to the host cell cytosol and erythrocyte surface membrane in *Plasmodium falciparum* infected erythrocytes. *Mol Biochem Parasitol*. 2000;106: 131–45. doi:10.1016/S0020-7519(01)00256-9
360. Cyrklaff M, Sanchez CP, Kilian N, Bisseye C, Simpore J, Frischknecht F, et al. Hemoglobins S and C interfere with actin remodeling in *Plasmodium falciparum*-infected erythrocytes. *Science*. 2011;334: 1283–6. doi:10.1126/science.1213775
361. Kilili GK, LaCount DJ. An erythrocyte cytoskeleton-binding motif in exported *Plasmodium falciparum*

References

- proteins. *Eukaryot Cell*. 2011;10: 1439–1447. doi:10.1128/EC.05180-11
362. Maier AG, Rug M, O'Neill MT, Brown M, Chakravorty S, Szestak T, et al. Exported Proteins Required for Virulence and Rigidity of *Plasmodium falciparum*-Infected Human Erythrocytes. *Cell*. Elsevier Inc.; 2008;134: 48–61. doi:10.1016/j.cell.2008.04.051
363. Vaughan AM, Mikolajczak SA, Wilson EM, Grompe M, Kaushansky A, Camargo N, et al. Complete *Plasmodium falciparum* liver-stage development in liver-chimeric mice. *J Clin Invest*. 2012;122: 3618–3628. doi:10.1172/JCI62684.3618
364. Matz JM, Goosmann C, Brinkmann V, Grütze J, Ingmundson A, Matuschewski K, et al. The *Plasmodium berghei* translocon of exported proteins reveals spatiotemporal dynamics of tubular extensions. *Sci Rep*. 2015;5: 12532. doi:10.1038/srep12532
365. Kalanon M, Bargieri D, Sturm A, Matthews K, Ghosh S, Goodman CD, et al. The *Plasmodium* translocon of exported proteins component EXP2 is critical for establishing a patent malaria infection in mice. *Cell Microbiol*. 2016;18: 399–412. doi:10.1111/cmi.12520
366. Albuquerque SS, Carret C, Grosso AR, Tarun AS, Peng X, Kappe SHII, et al. Host cell transcriptional profiling during malaria liver stage infection reveals a coordinated and sequential set of biological events. *BMC Genomics*. 2009;10: 270. doi:10.1186/1471-2164-10-270
367. Leirião P, Albuquerque SS, Corso S, Gemert G Van, Sauerwein RW, Rodriguez A, et al. HGF / MET signalling protects *Plasmodium*-infected host cells from apoptosis. 2005;7: 603–609. doi:10.1111/j.1462-5822.2005.00490.x
368. van de Sand C, Horstmann S, Schmidt A, Sturm A, Bolte S, Krueger A, et al. The liver stage of *Plasmodium berghei* inhibits host cell apoptosis. *Mol Microbiol*. 2005;58: 731–42. doi:10.1111/j.1365-2958.2005.04888.x
369. Ruivo MTG, Vera IM, Sales-Dias J, Meireles P, Gural N, Bhatia SN, et al. Host AMPK Is a Modulator of *Plasmodium* Liver Infection. *Cell Rep*. 2016;16: 2539–2545. doi:10.1016/j.celrep.2016.08.001
370. Inacio P, Zuzarte-Luis V, Ruivo MT, Falkard B, Nagaraj N, Rooijers K, et al. Parasite-induced ER stress response in hepatocytes facilitates *Plasmodium* liver stage infection. *EMBO Rep*. 2015;16: 955–964. doi:10.15252/embr.201439979
371. Meireles P, Sales-Dias J, Andrade CMC, Mello-Vieira J, Mancio-Silva L, Simas JPP, et al. GLUT1-mediated glucose uptake plays a crucial role during *Plasmodium* hepatic infection. *Cell Microbiol*. 2017;19: e12646. doi:10.1111/cmi.12646
372. Ingmundson A, Alano P, Matuschewski K, Silvestrini F. Feeling at home from arrival to departure: protein export and host cell remodelling during *Plasmodium* liver stage and gametocyte maturation. *Cell Microbiol*. 2014;16: 324–33. doi:10.1111/cmi.12251
373. Khan ZM, Ng C, Vanderberg JP. Early hepatic stages of *Plasmodium berghei*: Release of circumsporozoite protein and host cellular inflammatory response. *Infect Immun*. 1992;60: 264–270.
374. Hügel FU, Pradel G, Frevert U. Release of malaria circumsporozoite protein into the host cell cytoplasm and interaction with ribosomes. *Mol Biochem Parasitol*. 1996;81: 151–70. Available: <http://www.ncbi.nlm.nih.gov/pubmed/8898331>
375. Frevert U, Galinski MR, Hü F-U, Allon N, Schreier H, Smulevitch S, et al. Malaria circumsporozoite protein inhibits protein synthesis in mammalian cells. *EMBO J*. 1998;17: 3816–3826. doi:10.1093/emboj/17.14.3816
376. Singh AP, Buscaglia C a., Wang Q, Levay A, Nussenzweig DR, Walker JR, et al. *Plasmodium* Circumsporozoite Protein Promotes the Development of the Liver Stages of the Parasite. *Cell*. 2007;131: 492–504. doi:10.1016/j.cell.2007.09.013
377. Hamilton AJ, Suhrbier A, Nicholas J, Sinden RE. Immunoelectron microscopic localization of circumsporozoite antigen in the differentiating exoerythrocytic trophozoite of. *Cell Biol Int Rep*. 1988;12: 123–129. doi:10.1016/0309-1651(88)90126-9

378. Cockburn IA, Tse S-WW, Radtke AJ, Srinivasan P, Chen Y-CC, Sinnis P, et al. Dendritic cells and hepatocytes use distinct pathways to process protective antigen from *Plasmodium* in vivo. *PLoS Pathog.* 2011;7: e1001318. doi:10.1371/journal.ppat.1001318
379. Rennenberg A, Lehmann C, Heitmann A, Witt T, Hansen G, Nagarajan K, et al. Exoerythrocytic *Plasmodium* parasites secrete a cysteine protease inhibitor involved in sporozoite invasion and capable of blocking cell death of host hepatocytes. *PLoS Pathog.* 2010;6: e1000825. doi:10.1371/journal.ppat.1000825
380. Orito Y, Ishino T, Iwanaga S, Kaneko I, Kato T, Menard R, et al. Liver-specific protein 2: a *Plasmodium* protein exported to the hepatocyte cytoplasm and required for merozoite formation. *Mol Microbiol.* 2013;87: 66–79. doi:10.1111/mmi.12083
381. Grützke J, Rindte K, Goosmann C, Silvie O, Rauch C, Heuer D, et al. The spatiotemporal dynamics and membranous features of the *Plasmodium* liver stage tubovesicular network. *Traffic.* 2014;15: 362–382. doi:10.1111/tra.12151
382. Agop-Nersesian C, De Niz M, Niklaus L, Prado M, Eickel N, Heussler VT. Shedding of host autophagic proteins from the parasitophorous vacuolar membrane of *Plasmodium berghei*. *Sci Rep. Springer US;* 2017;7: 2191. doi:10.1038/s41598-017-02156-7
383. Hall R, McBride J, Morgan G, Tait A, Zolg JW, Walliker D, et al. Antigens of the erythrocytic stages of the human malaria parasite *Plasmodium falciparum* detected by monoclonal antibodies. *Mol Biochem Parasitol.* 1983;7: 247–265.
384. Bushell E, Gomes AR, Sanderson T, Anar B, Girling G, Herd C, et al. Functional Profiling of a *Plasmodium* Genome Reveals an Abundance of Essential Genes. *Cell. Elsevier Inc.;* 2017;170: 260–272.e8. doi:10.1016/j.cell.2017.06.030
385. Lacroix C, Giovannini D, Combe A, Bargieri DY, Spath S, Panchal D, et al. FLP/FRT-mediated conditional mutagenesis in pre-erythrocytic stages of *Plasmodium berghei*. *Nat Protoc.* 2011;6: 1412–28. doi:10.1038/nprot.2011.363
386. Combe A, Giovannini D, Carvalho TG, Spath S, Boisson B, Loussert C, et al. Clonal conditional mutagenesis in malaria parasites. *Cell Host Microbe.* 2009;5: 386–96. doi:10.1016/j.chom.2009.03.008
387. Franke-Fayard B, Trueman H, Ramesar J, Mendoza J, van der Keur M, van der Linden R, et al. A *Plasmodium berghei* reference line that constitutively expresses GFP at a high level throughout the complete life cycle. *Mol Biochem Parasitol.* 2004;137: 23–33. doi:10.1016/j.molbiopara.2004.04.007
388. Moll K, Kaneko A, Scherf A, Wahlgren M, editors. *Methods in Malaria Research* [Internet]. Sixth Edit. Manassas, VA, USA; 2013. Available: https://www.beiresources.org/portals/2/MR4/Methods_In_Malaria_Research-6th_edition.pdf
389. Yoshida N, Nussenzweig R, Potocnjak P, Nussenzweig V, Aikawa M. Hybridoma produces protective antibodies directed against the sporozoite stage of malaria parasite. *Science.* 1980;207: 71–73. doi:10.1126/science.6985745
390. Schindelin J, Arganda-Carreras I, Frise E, Kaynig V, Longair M, Pietzsch T, et al. Fiji: an open-source platform for biological-image analysis. *Nat Methods.* 2012;9: 676–82. doi:10.1038/nmeth.2019
391. Prudêncio M, Rodrigues CD, Ataíde R, Mota MM, Prudencio M, Rodrigues CD, et al. Dissecting in vitro host cell infection by *Plasmodium* sporozoites using flow cytometry. *Cell Microbiol.* 2008;10: 218–24. doi:10.1111/j.1462-5822.2007.01032.x
392. Idone V, Tam C, Goss JW, Toomre D, Pypaert M, Andrews NW. Repair of injured plasma membrane by rapid Ca²⁺-dependent endocytosis. *J Cell Biol.* 2008;180: 905–14. doi:10.1083/jcb.200708010
393. Fernandes MC, Andrade LR de, Andrews NW, Mortara RA. *Trypanosoma cruzi* trypomastigotes induce cytoskeleton modifications during HeLa cell invasion. *Mem Inst Oswaldo Cruz.* 2011;106: 1014–6. doi:10.1590/S0074-02762011000800019
394. Fernandes MC, Flannery AR, Andrews N, Mortara RA. Extracellular amastigotes of *Trypanosoma cruzi* are potent inducers of phagocytosis in mammalian cells. *Cell Microbiol.* 2013;15: 977–91.

References

- doi:10.1111/cmi.12090
395. Kennedy M, Fishbaugher ME, Vaughan AM, Patrapuvich R, Boonhok R, Yimamnuaychok N, et al. A rapid and scalable density gradient purification method for *Plasmodium* sporozoites. *Malar J*. 2012;11: 421. doi:10.1186/1475-2875-11-421
 396. Tsuji M, Mattei D, Nussenzweig RS, Eichinger D, Zavala F. Demonstration of heat-shock protein 70 in the sporozoite stage of malaria parasites. *Parasitol Res*. 1994;80: 16–21. Available: <http://www.ncbi.nlm.nih.gov/pubmed/8153120>
 397. Wiser MF, Lanners HN, Bafford RA, Favaloro JM. A novel alternate secretory pathway for the export of *Plasmodium* proteins into the host erythrocyte. *Proc Natl Acad Sci*. 1997;94: 9108–9113. doi:10.1073/pnas.94.17.9108
 398. Itoe MA, Sampaio JL, Cabal GG, Real E, Zuzarte-Luis V, March S, et al. Host Cell Phosphatidylcholine Is a Key Mediator of Malaria Parasite Survival during Liver Stage Infection. *Cell Host Microbe*. 2014;16: 778–786. doi:10.1016/j.chom.2014.11.006
 399. Ecker A, Lewis RE, Eklund EH, Jayabalasingham B, Fidock D a. Tricks in *Plasmodium*'s molecular repertoire--escaping 3'UTR excision-based conditional silencing of the chloroquine resistance transporter gene. *Int J Parasitol. Australian Society for Parasitology Inc.*; 2012;42: 969–74. doi:10.1016/j.ijpara.2012.09.003
 400. Gomes-Santos CSS, Braks J, Prudêncio M, Carret C, Gomes AR, Pain A, et al. Transition of *Plasmodium* sporozoites into liver stage-like forms is regulated by the RNA binding protein Pumilio. *PLoS Pathog*. 2011;7: e1002046. doi:10.1371/journal.ppat.1002046
 401. Mancio-Silva L, Slavic K, Grilo Ruivo MT, Grosso AR, Modrzynska KK, Vera IM, et al. Nutrient sensing modulates malaria parasite virulence. *Nature*. 2017;547: 213–216. doi:10.1038/nature23009
 402. Amino R, Giovannini D, Thiberge S, Gueirard P, Boisson B, Dubremetz J-F, et al. Host Cell Traversal Is Important for Progression of the Malaria Parasite through the Dermis to the Liver. *Cell Host Microbe*. 2008;3: 88–96. doi:10.1016/j.chom.2007.12.007
 403. Meis JFGM, Verhave JP. Exoerythrocytic Development of Malarial Parasites. *Advances in Parasitology*. 1988. pp. 1–61. doi:10.1016/S0065-308X(08)60352-8
 404. Mueller A-K, Camargo N, Kaiser K, Andorfer C, Frevert U, Matuschewski K, et al. *Plasmodium* liver stage developmental arrest by depletion of a protein at the parasite-host interface. *Proc Natl Acad Sci U S A*. 2005;102: 3022–7. doi:10.1073/pnas.0408442102
 405. Matuschewski K, Ross J, Brown SM, Kaiser K, Nussenzweig V, Kappe SHI. Infectivity-associated Changes in the Transcriptional Repertoire of the Malaria Parasite Sporozoite Stage. *J Biol Chem*. 2002;277: 41948–41953. doi:10.1074/jbc.M207315200
 406. Boucher LE, Bosch J. The apicomplexan glideosome and adhesins – Structures and function. *J Struct Biol*. Elsevier Inc.; 2015;190: 93–114. doi:10.1016/j.jsb.2015.02.008
 407. Stewart MJ, Vanderberg JP. Electron Microscopic Analysis of Circumsporozoite Protein Trail Formation by Gliding Malaria Sporozoites. *J Protozool*. 1992;39: 663–671. doi:10.1111/j.1550-7408.1992.tb04446.x
 408. Bergman LW. Myosin A tail domain interacting protein (MTIP) localizes to the inner membrane complex of *Plasmodium* sporozoites. *J Cell Sci*. 2002;116: 39–49. doi:10.1242/jcs.00194
 409. Sá E Cunha C, Nyboer B, Heiss K, Sanches-Vaz M, Fontinha D, Wiedtke E, et al. *Plasmodium berghei* EXP-1 interacts with host Apolipoprotein H during *Plasmodium* liver-stage development. *Proc Natl Acad Sci U S A*. 2017;114: E1138–E1147. doi:10.1073/pnas.1606419114
 410. Carey AF, Singer M, Bargieri D, Thiberge S, Frischknecht F, Ménard R, et al. Calcium dynamics of *Plasmodium berghei* sporozoite motility. *Cell Microbiol*. 2014;16: 768–783. doi:10.1111/cmi.12289
 411. Carruthers VB, Giddings OK, Sibley LD. Secretion of micronemal proteins is associated with *Toxoplasma* invasion of host cells. *Cell Microbiol*. 1999;1: 225–235.
 412. Risco-Castillo V, Topçu S, Son O, Briquet S, Manzoni G, Silvie O. CD81 is required for rhoptry

- discharge during host cell invasion by *Plasmodium yoelii* sporozoites. *Cell Microbiol.* 2014;16: 1533–48. doi:10.1111/cmi.12309
413. Gantt S, Persson C, Rose K, Birkett AJ, Abagyan R, Nussenzweig V. Antibodies against thrombospondin-related anonymous protein do not inhibit *Plasmodium* sporozoite infectivity in vivo. *Infect Immun.* 2000;68: 3667–3673. doi:10.1128/IAI.68.6.3667-3673.2000
414. Gouaux JE, Braha O, Hobaugh MR, Song L, Cheley S, Shustak C, et al. Subunit stoichiometry of staphylococcal alpha-hemolysin in crystals and on membranes: a heptameric transmembrane pore. *Proc Natl Acad Sci U S A.* 1994;91: 12828–31. doi:10.1073/pnas.91.26.12828
415. Song L, Hobaugh MR, Shustak C, Cheley S, Bayley H, Gouaux JE. Structure of Staphylococcal alpha - Hemolysin, a Heptameric Transmembrane Pore. *Science.* 1996;274: 1859–1865. doi:10.1126/science.274.5294.1859
416. Skals M, Jorgensen NR, Leipziger J, Praetorius HA. -Hemolysin from *Escherichia coli* uses endogenous amplification through P2X receptor activation to induce hemolysis. *Proc Natl Acad Sci.* 2009;106: 4030–4035. doi:10.1073/pnas.0807044106
417. Palmer M, Harris R, Freytag C, Kehoe M, Trantum-Jensen J, Bhakdi S. Assembly mechanism of the oligomeric streptolysin O pore: The early membrane lesion is lined by a free edge of the lipid membrane and is extended gradually during oligomerization. *EMBO J.* 1998;17: 1598–1605. doi:10.1093/emboj/17.6.1598
418. Jimah JR, Salinas ND, Sala-Rabanal M, Jones NG, Sibley LD, Nichols CG, et al. Malaria parasite CelTOS targets the inner leaflet of cell membranes for pore-dependent disruption. *Elife.* 2016;5. doi:10.7554/eLife.20621
419. Lopez JA, Susanto O, Jenkins MR, Lukoyanova N, Sutton VR, Law RHP, et al. Perforin forms transient pores on the target cell plasma membrane to facilitate rapid access of granzymes during killer cell attack. *Blood.* 2013;121: 2659–2668. doi:10.1182/blood-2012-07-446146
420. Chen T-W, Wardill TJ, Sun Y, Pulver SR, Renninger SL, Baohan A, et al. Ultrasensitive fluorescent proteins for imaging neuronal activity. *Nature.* 2013;499: 295–300. doi:10.1038/nature12354
421. Goñi FM, Alonso A. Sphingomyelinases: enzymology and membrane activity. *FEBS Lett.* 2002;531: 38–46. doi:10.1016/S0014-5793(02)03482-8
422. Tani M, Hannun YA. Analysis of membrane topology of neutral sphingomyelinase 2. *FEBS Lett.* 2007;581: 1323–1328. doi:10.1016/j.febslet.2007.02.046
423. Menck K, Sönmezer C, Worst TS, Schulz M, Dihazi GH, Streit F, et al. Neutral sphingomyelinases control extracellular vesicles budding from the plasma membrane. *J Extracell Vesicles.* Taylor & Francis; 2017;6. doi:10.1080/20013078.2017.1378056
424. Luberto C, Hassler DF, Signorelli P, Okamoto Y, Sawai H, Boros E, et al. Inhibition of tumor necrosis factor-induced cell death in MCF7 by a novel inhibitor of neutral sphingomyelinase. *J Biol Chem.* 2002;277: 41128–41139. doi:10.1074/jbc.M206747200
425. Albouz S, Vanier MT, Hauw JJ, Le Saux F, Boutry JM, Baumann N. Effect of tricyclic antidepressants on sphingomyelinase and other sphingolipid hydrolases in C6 cultured glioma cells. *Neurosci Lett.* 1983;36: 311–315. doi:10.1016/0304-3940(83)90018-6
426. Lindner SE, Swearingen KE, Harupa A, Vaughan AM, Sinnis P, Moritz RL, et al. Total and Putative Surface Proteomics of Malaria Parasite Salivary Gland Sporozoites. *Mol Cell Proteomics.* 2013;12: 1127–1143. doi:10.1074/mcp.M112.024505
427. Swearingen KE, Lindner SE, Flannery EL, Vaughan AM, Morrison RD, Patrapuvich R, et al. Proteogenomic analysis of the total and surface-exposed proteomes of *Plasmodium vivax* salivary gland sporozoites. *PLoS Neglected Tropical Diseases.* 2017. doi:10.1371/journal.pntd.0005791
428. Shin SC, Vanderberg JP, Terzakis JA. Direct infection of hepatocytes by sporozoites of *Plasmodium berghei*. *J Protozool.* 1982;29: 448–54. doi:10.1371/journal.pbio.0030192
429. Frevert U, Engelmann S, Zougbedé S, Stange J, Ng B, Matuschewski K, et al. Intravital observation of

References

- Plasmodium berghei* sporozoite infection of the liver. PLoS Biol. 2005;3: 1034–1046. doi:10.1371/journal.pbio.0030192
430. Muñoz-Planillo R, Kuffa P, Martínez-Colón G, Smith BL, Rajendiran TM, Núñez G. K⁺ Efflux Is the Common Trigger of NLRP3 Inflammasome Activation by Bacterial Toxins and Particulate Matter. *Immunity*. 2013;38: 1142–1153. doi:10.1016/j.immuni.2013.05.016
431. Aachoui Y, Sagulenko V, Miao EA, Stacey KJ. Inflammasome-mediated pyroptotic and apoptotic cell death, and defense against infection. *Curr Opin Microbiol*. Elsevier Ltd; 2013;16: 319–326. doi:10.1016/j.mib.2013.04.004
432. Panchal R, Smart M, Bowser D, Williams D, Petrou S. Pore-Forming Proteins and their Application in Biotechnology. *Curr Pharm Biotechnol*. 2002;3: 99–115. doi:10.2174/1389201023378418
433. Kaushansky A, Metzger PG, Douglass AN, Mikolajczak SA, Lakshmanan V, Kain HS, et al. Malaria parasite liver stages render host hepatocytes susceptible to mitochondria-initiated apoptosis. *Cell Death Dis*. 2013;4: e762–e762. doi:10.1038/cddis.2013.286
434. Thieleke-Matos C, Lopes da Silva M, Cabrita-Santos L, Portal MD, Rodrigues IP, Zuzarte-Luis V, et al. Host cell autophagy contributes to *Plasmodium* liver development. *Cell Microbiol*. 2016;18: 437–50. doi:10.1111/cmi.12524
435. Rodríguez A, Webster P, Ortego J, Andrews NW. Lysosomes Behave as Ca²⁺-regulated Exocytic Vesicles in Fibroblasts and Epithelial Cells. *J Cell Biol*. 1997;137: 93–104. doi:10.1083/jcb.137.1.93
436. Fox TE, Houck KL, O'Neill SM, Nagarajan M, Stover TC, Pomianowski PT, et al. Ceramide recruits and activates protein kinase C ζ (PKC ζ) within structured membrane microdomains. *J Biol Chem*. 2007;282: 12450–12457. doi:10.1074/jbc.M700082200
437. Wang G, Krishnamurthy K, Umapathy NS, Verin AD, Bieberich E. The carboxyl-terminal domain of Atypical protein kinase C ζ binds to ceramide and regulates junction formation in Epithelial cells. *J Biol Chem*. 2009;284: 14469–14475. doi:10.1074/jbc.M808909200
438. Fiory F, Oriente F, Miele C, Romano C, Trecia A, Alberobello AT, et al. Protein Kinase C- ζ and Protein Kinase B Regulate Distinct Steps of Insulin Endocytosis and Intracellular Sorting. *J Biol Chem*. 2004;279: 11137–11145. doi:10.1074/jbc.M308751200
439. Voisset C, Lavie M, Helle F, Op De Beeck A, Bilheu A, Bertrand-Michel J, et al. Ceramide enrichment of the plasma membrane induces CD81 internalization and inhibits hepatitis C virus entry. *Cell Microbiol*. 2008;10: 606–617. doi:10.1111/j.1462-5822.2007.01070.x
440. Coffey GP, Rajapaksa R, Liu R, Sharpe O, Kuo C-C, Krauss SW, et al. Engagement of CD81 induces ezrin tyrosine phosphorylation and its cellular redistribution with filamentous actin. *J Cell Sci*. 2009;122: 3137–44. doi:10.1242/jcs.045658
441. Quast T, Eppler F, Semmling V, Schild C, Homsy Y, Levy S, et al. CD81 is essential for the formation of membrane protrusions and regulates Rac1-activation in adhesion-dependent immune cell migration. *Blood*. 2011;118: 1818–1827. doi:10.1182/blood-2010-12-326595
442. Riethmüller J, Riehle A, Grassmé H, Gulbins E. Membrane rafts in host-pathogen interactions. *Biochim Biophys Acta*. 2006;1758: 2139–47. doi:10.1016/j.bbamem.2006.07.017
443. Mingorance L, Friesland M, Coto-Llerena M, Pérez-del-Pulgar S, Boix L, López-Oliva JM, et al. Selective inhibition of hepatitis c virus infection by hydroxyzine and benzotropine. *Antimicrob Agents Chemother*. 2014;58: 3451–3460. doi:10.1128/AAC.02619-14
444. Schuchman EH, Wasserstein MP. Types A and B Niemann-Pick disease. *Best Pract Res Clin Endocrinol Metab*. Elsevier; 2015;29: 237–247. doi:10.1016/j.beem.2014.10.002
445. Kolter T, Sandhoff K. Sphingolipid metabolism diseases. *Biochim Biophys Acta - Biomembr*. 2006;1758: 2057–2079. doi:10.1016/j.bbamem.2006.05.027
446. Kester M. Sphingolipid Metabolites and the Cellular Phenotype. *Trends Glycosci Glycotechnol*. 1997;9: 447–460. doi:10.4052/tigg.9.447

***Curriculum Vitae* and Publications**

João Tiago Carvalho Jordão de Mello Vieira

Young scientist with biochemistry background, team spirit, committed, willing to learn and with strong communication skills.

Personal information

Telephone	+351 919 610 295
E-mail	Joao.tiago.vieira@gmail.com
Date of birth	15 October 1989
Nationality	Portuguese

Education

Bachelor's degree in Biochemistry (2007-2010)

Courses on cell biology and metabolism, microbiology, immunology and genetics. Introduction to several experimental techniques and detection methods **Completed with 16/20 classification.**

Master's degree in Biochemistry (2010-2012)

Further study of molecular biology, immunology, biophysics and genetics Advance training in fluorescence-based techniques. **Completed with 18/20 classification (Thesis evaluated at 20/20).**

For the 2nd year of the MSc (September 2011 until October 2012) I worked on a Life Sciences research project under the guidance of Dr. Fábio Fernandes and Prof. Dr. Manuel Prieto at Biological Fluorescence group at CQFM, IST, entitled *Membranes as targets for apoptotic bile acids*.

Research Assistant in the Mota Lab (2013)

Under the supervision of Vanessa Zuzarte-Luís, I was trained in cell culture techniques, mouse handling, mosquito dissection. Moreover, I was trained in a variety of analytical techniques, such as qRT-PCR, fluorescence microscopy and flow cytometry.

PhD Student of the Mota Lab (2014-2020)

Under the supervision of Prof. Dra. Maria Mota and Dra. Vanessa Zuzarte-Luís, I performed my work on *A novel role for EXP2 in invasion of Plasmodium sporozoites*.

Publications

Mello-Vieira, J.; Enguita, F.J.; de Koning-Ward, T.F.; Zuzarte-Luís, V.; Mota, M.M.; *Plasmodium translocon component EXP2 facilitates invasion of hepatocytes*; Nat Commun (2020) *accepted*

Mota, M.M.; **Mello-Vieira, J.**; *Dispatch – Parasitism: Anopheles Mosquitoes and Plasmodium Parasites Share Resources*; Current Biology (2019) **29 (13)**: R632-R634;

Real, E.; Rodrigues, L.; Cabal, G.G.; Enguita, F.J.; Mancio-Silva, L.; **Mello-Vieira, J.**; Beatty, W.; Vera, I.M.; Zuzarte-Luís, V.; Figueira, T.N.; Mair, G.R.; Mota, M.M.; *Plasmodium UIS3 sequesters host LC3 to avoid elimination by autophagy in hepatocytes*; Nat Microbiol (2018) **3 (1)**: 17-25;

Zuzarte-Luís, V.; **Mello-Vieira, J.**; Marreiros, I.M.; Liehl, P.; Chora, Â.F.; Carret, C.K.; Carvalho, T.; Mota, M.M.; *Dietary alterations modulate susceptibility to Plasmodium infection*; Nat Microbiol (2017) **2 (12)**: 1600-1607;

Meiros, P.; Sales-Dias, J.; Andrade, C.M.; **Mello-Vieira, J.**; Mancio-Silva, L.; Simas, J.P.; Staines, H.M.; Prudêncio, M.; *GLUT1-mediated glucose uptake plays a crucial role during Plasmodium hepatic infection*; Cell Microbiol (2017) **19 (2)**: e12646;

Mello-Vieira, J.; Sousa, T.; Coutinho, A.; Fedorov, A.; Lucas, S.D.; Moreira, R.; Castro, R.E.; Rodrigues, C.M.P.; Prieto, M. And Fernandes, F.; *Cytotoxic bile acids, but not cytoprotective species, inhibit the ordering effect of cholesterol in model membranes at physiologically active concentrations*; Biochim Biophys Acta (2013) **1828 (9)**: 2152-2163.

Meetings

Talk and Poster Presentations:

Mello-Vieira, J.; Enguita, F.J.; de Koning-Ward, T.F.; Mota, M.M.; Zuzarte-Luís, V.; *The role of EXP2 during the invasion of the hepatocyte by Plasmodium sporozoite* at Molecular Parasitology Meeting 2018 – Woods Hole, USA (September 2018) – Presenter **João Mello-Vieira**

Mello-Vieira, J.; Enguita, F.J.; de Koning-Ward, T.F.; Mota, M.M.; Zuzarte-Luís, V.; *The role of EXP2 during the invasion of the hepatocyte by Plasmodium sporozoite* at TwinToInfect Spring School – Sesimbra, Portugal (March 2018) – Presenter **João Mello-Vieira**

Poster presentation:

Mello-Vieira, J.; Geurink, P.; Neefjes, J.; Ovaa, H.; Mota, M.M.; Zuzarte-Luís, V.; *Establishment of malaria liver stage infection is dependent on the ubiquitin pathway* at BioMalPar XI: Biology and Pathology of the Malaria Parasite in Heidelberg, Germany (May 2015) – Presenter **João Mello-Vieira**

Mello-Vieira, J.; Fedorov, A.; Coutinho, A.; Lucas, S.D.; Moreira, R.; Castro, R.E.; Rodrigues, C. M. P.; Prieto, M.; Fernandes, F.; *The Apoptotic Bile Acid DCA has Preference for Association to*

Liquid Disordered Lipid Domains and Inhibits the Rigidifying Effect of Cholesterol in Membranes at the Biophysical Society in Philadelphia, USA (February 2013) – Presenter Fábio Fernandes

Mello-Vieira, J.; Fedorov, A.; Coutinho, A.; Lucas, S.D.; Moreira, R.; Castro, R.E.; Rodrigues, C. M. P.; Prieto, M.; Fernandes, F.; *Lipid membranes as possible targets for apoptotic bile acids* at the IUBMB & FEBS 2012 Congress in Sevilla, Spain (September 2012) – Presenter **João Mello-Vieira**

CAML PhD Meetings:

Mello-Vieira, J.; Enguita, F.J.; de Koning-Ward, T.F.; Mota, M.M.; Zuzarte-Luís, V.; *The role of EXP2 during the invasion of the hepatocyte by Plasmodium sporozoite* at XI CAML PhD Meeting (May 2017) – Presenter **João Mello-Vieira**

Mello-Vieira, J.; de Koning-Ward, T.F.; Mota, M.M.; Zuzarte-Luís, V.; *The role of EXP2 during liver infection by Plasmodium parasites* at X CAML PhD Meeting (March 2016) – Presenter **João Mello-Vieira**

Mello-Vieira, J.; Slavic, K.; Mota, M.M.; Zuzarte-Luís, V.; *Dissecting the late stages of malaria liver infection* at IX CAML PhD Meeting (March 2015) – Presenter **João Mello-Vieira**

Mello-Vieira, J.; Mota, M.M.; Zuzarte-Luís, V.; *The role of the Plasmodium centrosome during liver stage schizogony* at VIII CAML PhD Meeting (March 2014) – Presenter **João Mello-Vieira**

Courses

Inserm Workshop on Emerging Tools in Quantitative Fluorescence Microscopy for Systems Biology (IMM, September 2011)

Nanosciences and Single Molecule Techniques (SPBf, November 2011)

Confocal Microscopy (IMM, FMUL, February 2012)

Laboratory Animal Science, certified with Felasa Category B (February 2013).

Lisbon BioMed (January and February 2014)

Statistical Tests by Ruy Ribeiro (March 2014)

Statistics for Beginners by Isabel Flores (2016)

Advanced Statistics by Isabel Flores (2017)

Curriculum Vitae and Publications

Science Management Activities

I was a member of the Organizing Committee of the IX and X editions of the CAML PhD Meeting.

I was PhD representative of the iMM PhD Students during March 2016 until March 2017.

Participated as a volunteer in the organization of the EuroXXIV, an Operation Research Congress, in Lisbon (July 2010).

Other skills and competences

Languages:

- Fluent in Portuguese (mother tongue);
- Proficient in English;
- Basic user of Spanish and German.

Computer skills:

- Accomplished user of Word, Excel and PowerPoint;
 - Proficient with ImageJ and GraphPad;
 - Basic knowledge of SPSS and Python.
-

GLUT1-mediated glucose uptake plays a crucial role during *Plasmodium* hepatic infection

Patrícia Meireles,¹ Joana Sales-Dias,^{1,#}
Carolina M. Andrade,¹ João Mello-Vieira,¹
Liliana Mancio-Silva,¹ J. Pedro Simas,¹
Henry M. Staines² and Miguel Prudêncio^{1*}

¹Instituto de Medicina Molecular, Faculdade de Medicina, Universidade de Lisboa, Lisboa, Portugal.

²Institute for Infection & Immunity, St. George's, University of London, Cranmer Terrace, London, UK.

Summary

Intracellular pathogens have evolved mechanisms to ensure their survival and development inside their host cells. Here, we show that glucose is a pivotal modulator of hepatic infection by the rodent malaria parasite *Plasmodium berghei* and that glucose uptake via the GLUT1 transporter is specifically enhanced in *P. berghei*-infected cells. We further show that ATP levels of cells containing developing parasites are decreased, which is known to enhance membrane GLUT1 activity. In addition, GLUT1 molecules are translocated to the membrane of the hepatic cell, increasing glucose uptake at later stages of infection. Chemical inhibition of GLUT1 activity leads to a decrease in glucose uptake and the consequent impairment of hepatic infection, both *in vitro* and *in vivo*. Our results reveal that changes in GLUT1 conformation and cellular localization seem to be part of an adaptive host response to maintain adequate cellular nutrition and energy levels, ensuring host cell survival and supporting *P. berghei* hepatic development.

Introduction

Glucose is the primary source of energy and a key substrate for most cells. Glucose and other carbohydrates are transported into cells by members of a family of integral membrane glucose transporter (GLUT) molecules. To date, 14 members of this family, also called the solute carrier 2A proteins, have been identified in humans, which are divided on the basis of transport characteristics and sequence similarities into several families (Classes I to III) [reviewed in (Karim *et al.*, 2012; Mueckler and Thorens, 2013)]. GLUT1 is a class I facilitative glucose transporter expressed in liver cells (Tal *et al.*, 1990) and overexpressed in various tumours (Smith, 1999). GLUT1 expression is highest in the human erythrocyte membrane, and has been shown to play a critical role in cerebral glucose uptake (Koranyi *et al.*, 1991). GLUT1 is also a receptor for the human T cell leukaemia virus (Manel *et al.*, 2003), and GLUT1-mediated glucose transport in T-cells has been shown to regulate Human immunodeficiency virus infection (Loisel-Meyer *et al.*, 2012).

Mammalian infection by the malaria parasite is initiated when *Plasmodium* sporozoites, injected through the bite of an infected mosquito, cross the endothelium of the liver sinusoids and enter the liver. Sporozoites then traverse a few hepatocytes before productively invading a final one, inside which they asymptotically differentiate into exoerythrocytic forms (EEFs) that originate thousands of red blood cell-infective merozoites (Prudencio *et al.*, 2006). Merozoites are eventually released to the bloodstream, initiating the blood stage of infection, and giving rise to malaria symptoms. The liver stage of a mammalian infection by *Plasmodium* is an obligatory uni-directional step in the parasite's progression towards the symptomatic, erythrocytic phase of its life cycle.

Blood stages of malarial parasites are dependent on glycolysis, employed as their main energy source of Adenosine triphosphate (ATP) production (Pfaller *et al.*, 1982; Vander Jagt *et al.*, 1990; Kirk *et al.*, 1996), a process that has recently been modelled for the human malaria parasite *P. falciparum* (Penkler *et al.*, 2015). Glucose has been shown to be transported from human blood plasma into the erythrocyte cytosol by GLUT1 (Hellwig and Joost, 1991), and then taken up by the parasite via a parasite-encoded facilitative hexose transporter (PfHT) (Woodrow *et al.*, 2000; Joet *et al.*, 2003), which limits the rate of glucose entry into the parasite's

Received 6 March, 2016; revised 20 June, 2016; accepted 6 July, 2016. *For correspondence. E-mail mprudencio@medicina.ulisboa.pt; Tel. +351217999513; Fax +351217999504. #Present address: Instituto de Tecnologia Química e Biológica, Oeiras, Portugal

glycolytic pathways (Tjhin *et al.*, 2013). These findings support novel chemotherapeutic interventions that target PfHT (Feistel *et al.*, 2008; Slavic *et al.*, 2011b). Studies in the rodent malaria model, *P. berghei*, further found that the orthologous hexose transporter (PbHT) is expressed not only throughout the parasite's development within the mosquito vector, but also during liver and transmission stages of *P. berghei* (Slavic *et al.*, 2010; Slavic *et al.*, 2011a). During their extensive hepatic replication, developing *Plasmodium* parasites require the availability of large amounts of nutrients and energy. The availability of appropriate amounts of glucose in infected hepatic cells is thus expected to play an essential role in the development of liver stage *Plasmodium* parasites. Inhibition of PbHT by compound 3361, a specific inhibitor of plasmodial HTs, impairs hepatic *P. berghei* development (Slavic *et al.*, 2011a), supporting the essentiality of glucose uptake for *Plasmodium* liver stages. Accordingly, a recent study established glucose concentration in the culture medium as a key factor for liver stage parasite development (Itani *et al.*, 2014).

In this study, we employed rodent *P. berghei* parasites, a well-established model of malaria infection (Prudencio *et al.*, 2011), to elucidate the uptake and utilisation of glucose by *Plasmodium* liver stages. We investigated the glucose requirements during the course of *P. berghei* development in hepatic cells as well as the host molecular receptors involved in glucose uptake by those cells. We demonstrate that *P. berghei* infection leads to intracellular ATP depletion and enhances the translocation of GLUT1 to the cell membrane of infected hepatoma cells, allowing the uptake of significantly higher amounts of glucose compared with non-infected cells. We further show that glucose plays an essential role during the liver stage of infection by the malaria parasite, modulating its liver stage development both *in vitro* and *in vivo*.

Results

Effect of glucose on P. berghei hepatic infection

In order to evaluate glucose requirements throughout the liver stage of infection, Huh7 cells, a human hepatoma cell line, were infected with luciferase-expressing *P. berghei* sporozoites in the presence of varying concentrations of glucose. Glucose concentrations ranged from 1.25 to 20 mM, which includes and expands the physiological range of glucose concentrations, 2.5 to 10 mM (Shrayyef and Gerich, 2010). Luminescence intensity, a correlate of parasite load (Ploemen *et al.*, 2009), and cell viability were measured near the end of hepatic parasite development, at 48 h post-infection (hpi). Our results show that an increase in glucose availability correlates with an increase of overall *Plasmodium* infection (Fig. 1A). In contrast, any glucose concentration below the standard medium \approx 10 mM concentration significantly impairs infection (Fig. 1A), demonstrating that glucose is required for a successful hepatic *Plasmodium* infection. Cell viability was not affected by the presence of an excess of glucose in the

medium, but decreased for 2.5 and 1.25 mM of glucose (Fig. 1A). Crucially, decreasing the glucose concentration from 10 to 5 mM significantly decreases parasite load but has no impact on cell viability.

In order to dissect how glucose influences hepatic infection, we employed an established flow cytometry-based approach that makes use of green fluorescent protein (GFP)-expressing *P. berghei* parasites to determine the number of infected cells and to measure parasite development (Prudencio *et al.*, 2008). The analysis of cells 2 h after sporozoite addition, when the invasion process is virtually completed (Prudencio *et al.*, 2008), shows that glucose concentration does not affect the ability of parasites to traverse (data not shown) or invade (Fig. 1B) cells. Conversely, when cells were analysed 48 hpi, a glucose-dependent increase in parasite development was observed (Fig. 1C). These results also showed that the number of infected cells is higher at 20 mM glucose concentration, and lower at glucose concentrations below the physiological range, suggesting that glucose availability influences the survival of infected cells. These results were further confirmed by immunofluorescence microscopy analysis, which demonstrated that parasite size is proportional to the amount of glucose in the medium and that the survival of liver stage parasites 48 hpi depends on the availability of glucose (Fig. 1D, E). In fact, at low glucose concentrations, not only are most parasites very small ($<50 \mu\text{m}^2$) but also the number of infected cells is very low. Increasing concentrations of glucose lead to higher numbers of parasites and favour parasite growth, with approximately 40% of the parasites being larger than $200 \mu\text{m}^2$ at 10 and 20 mM glucose (Fig. 1E).

Whereas hepatoma cells are highly dependent on glucose uptake for ATP production through glycolysis (Warburg *et al.*, 1927; Kroemer and Pouyssegur, 2008), primary hepatocytes are able to store glucose as glycogen and use oxidative phosphorylation to produce ATP. Accordingly, the requirements for glucose uptake by primary hepatic cells are significantly lower than those displayed by tumorigenic cells (O'Neil *et al.*, 2005). In agreement with this, we showed that the decreased cell viability noted in hepatoma cells at 2.5 and 1.25 mM glucose was not observed in primary hepatocytes, even upon complete removal of glucose. Crucially, however, our data also clearly show that overall infection of mouse primary hepatocytes by *P. berghei* is significantly decreased in the absence of glucose in the medium (Fig. S1). Overall, these results demonstrate that glucose availability plays a crucial role in the liver stage development and survival of *Plasmodium* parasites.

Glucose uptake is specifically increased in hepatic cells containing replicating P. berghei parasites

Having demonstrated a requirement for glucose during liver stage *P. berghei* development, we then sought to determine

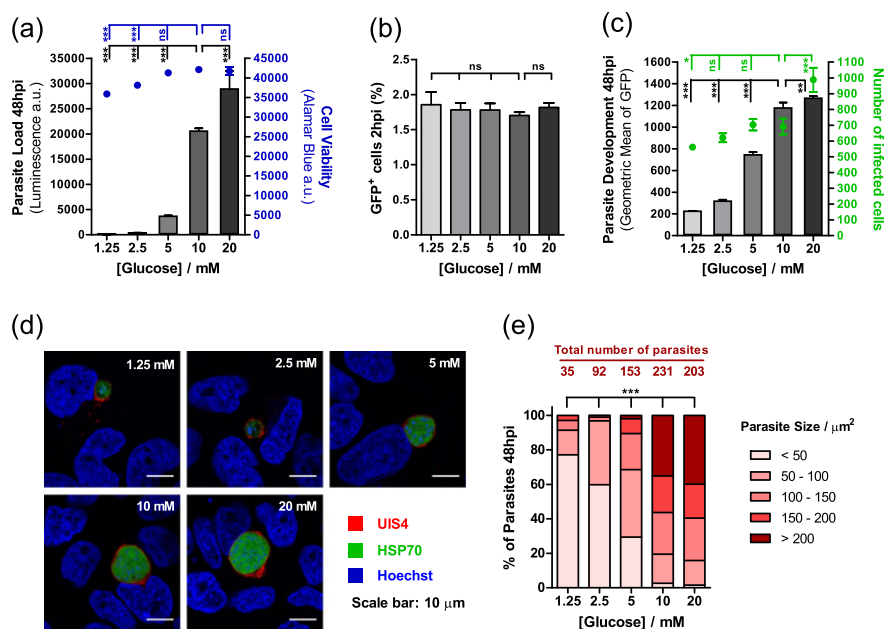


Fig. 1. Glucose availability impacts *P. berghei* hepatic infection.

A. Huh7 cells were infected with luciferase-expressing *P. berghei* sporozoites, and the culture medium was replaced 2 hpi by medium with different concentrations of glucose. Parasite load (luminescence) and cell viability were assessed after 48 h. Representative experiment out of two independent experiments. Error bars represent standard deviation (SD). One-way analysis of variance (ANOVA) with post-test Dunnett.

B. The culture medium of Huh7 cells was replaced by medium with different concentrations of glucose 1 h prior to infection with green fluorescent protein (GFP)-expressing sporozoites. Cell invasion was quantified by determining the percentage of GFP⁺ cells 2 hpi by flow cytometry. Representative experiment out of two independent experiments. Error bars represent SD. One-way ANOVA with post-test Dunnett.

C. Huh7 cells were infected with GFP-expressing *P. berghei* sporozoites, and the culture medium was replaced 2 hpi by medium with different concentrations of glucose. Parasite development and the total number of infected cells were assessed by flow cytometry by determining the fluorescence intensity and the number of GFP⁺ cells at 48 hpi, respectively. Representative experiment out of five independent experiments. Error bars represent SD. One-way ANOVA with post-test Dunnett.

D. Representative confocal images of Huh7 cells infected with sporozoites and incubated in medium with different concentrations of glucose for 48 h. Cells were immunostained with anti-UIS4 (red), which localises to the parasitophorous vacuole membrane, anti-heat shock protein (HSP)70 (green), which localises to the parasite's cytoplasm, and Hoechst (blue), a nuclear stain. Scale bar, 10 μm.

E. For each glucose concentration, the exoerythrocytic forms in the fluorescence microscopy images acquired were counted, and their area was determined. Exoerythrocytic forms were divided into five different size classes. Pool of two independent experiments. Chi-square test. ns, not significant; * $P < 0.05$, ** $P < 0.01$ and *** $P < 0.001$.

whether glucose uptake is specifically enhanced in infected cells and whether this is linked to parasite replication within these cells. To this end, we monitored by flow cytometry the uptake of a fluorescent glucose derivative, 2-NBDG (2-deoxy-2-[(7-nitro-2,1,3-benzoxadiazol-4-yl)amino]-D-glucose) (O'Neil *et al.*, 2005; Yamada *et al.*, 2007) by *P. berghei*-infected cells. Huh7 cells were incubated with 2-NBDG and analysed at different time points following addition of red fluorescence protein (RFP)-expressing *P. berghei* sporozoites. The uptake of 2-NBDG was measured as an increase in green fluorescence intensity, whereas parasite development was monitored as a function of red fluorescence intensity. The latter enables the population of cells containing replicating parasites to be distinguished from a smaller population of cells containing parasites that do not develop *in vitro* (Prudencio *et al.*, 2008) (Fig. S2). Our results clearly show that glucose uptake is highly increased in cells containing developing parasites, from 30 hpi onwards (Fig. 2A). A smaller increase in glucose uptake is also observed at around the same time in

non-infected cells and in cells containing non-developing parasites, present in the same well (Fig. 2A). Live fluorescence microscopy analysis of non-infected and infected Huh7 cells 48 hpi (Fig. S3A) confirmed that 2-NBDG fluorescence intensity is significantly higher in infected than in non-infected cells (Fig. S3B) and further revealed the uptake of 2-NBDG by the developing parasite (Fig. S3B).

Because it is known that glucose uptake may be influenced by factors such as feeding/fasting, exposure to low/high temperature, exercise, oxidative stress, several liver pathologies, such as steatosis and non-alcoholic fatty liver disease and liver infections, for example, by hepatitis C virus (Cunningham *et al.*, 1985; Pencek *et al.*, 2004; Bitar *et al.*, 2005; Bechmann *et al.*, 2012; Moore *et al.*, 2012; Vidyashankar *et al.*, 2012; Yu *et al.*, 2013), we sought to assess the specificity of the *P. berghei*-induced increase in glucose uptake by infected Huh7 cells. To this end, we measured 2-NBDG uptake by Huh7 cells subjected to conditions known to induce low-temperature stress in various types of mammalian cells (Fujita, 1999), high-temperature

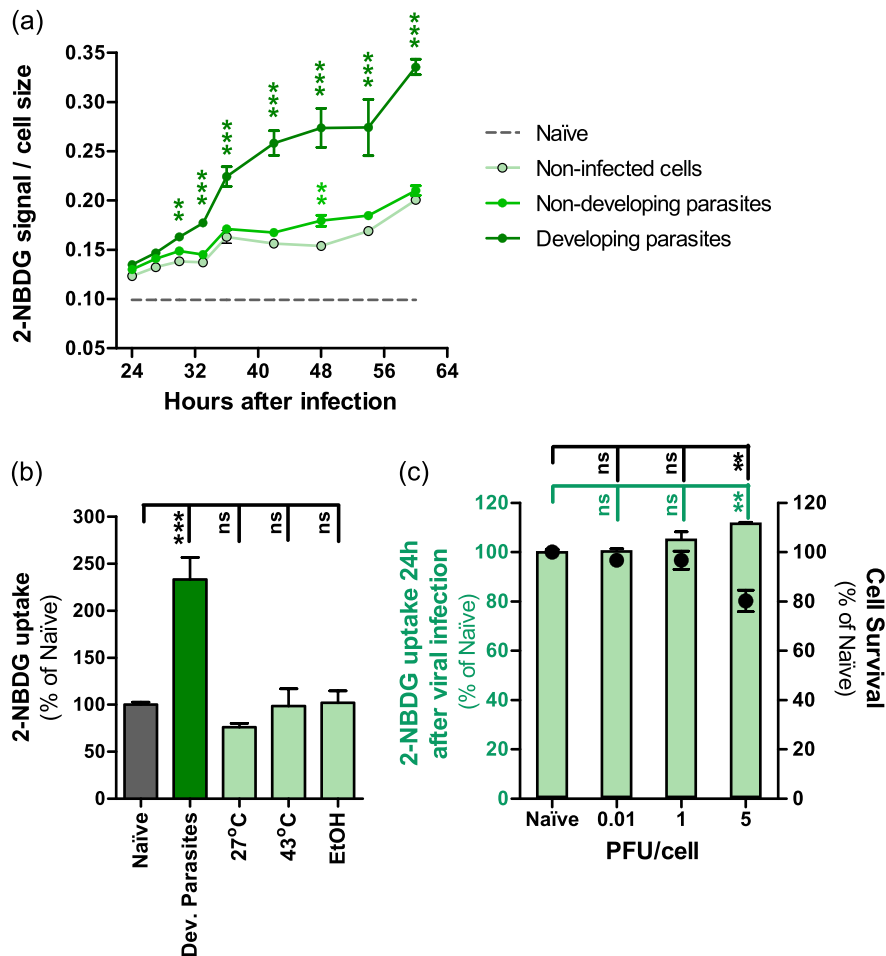


Fig. 2. Glucose uptake is specifically increased in hepatoma cells containing developing *P. berghei* parasites.

A. 2-NBDG uptake by different cell populations, normalised to cell size, at different time points of infection, assessed by flow cytometry. Error bars represent standard deviation. Two-way analysis of variance (ANOVA) with post-test Bonferroni.

B. 2-NBDG uptake by naïve Huh7 cells, cells containing developing *P. berghei* parasites at 48 hpi, and cells subjected to low-temperature, high-temperature and ethanol-induced oxidative stresses, assessed by flow cytometry. Pool of two independent experiments. Error bars represent standard deviation. One-way ANOVA with post-test Dunnett.

C. 2-NBDG uptake by naïve Huh7 cells and cells infected with MHV-68 at different multiplicity of infection, assessed by flow cytometry. Pool of two independent experiments. Error bars represent Standard error of the mean (SEM). One-way ANOVA with post-test Dunnett. ns, not significant; ** $P < 0.01$ and *** $P < 0.001$. PFU, plaque-forming unit.

stress in a chicken hepatocellular carcinoma cell line (Sun *et al.*, 2015) or oxidative stress in rat hepatocytes (Sergent *et al.*, 2005; Nourissat *et al.*, 2008) (Fig. 2B). Finally, we infected Huh7 cells with murine gammaherpesvirus 68 (MHV-68) (Collins *et al.*, 2009), and measured 2-NBDG uptake at 24 hpi and at different infection loads (Fig. 2C). The efficacy of infection was confirmed by flow cytometry employing YFP-expressing MHV-68 in a parallel experiment (Fig. S4). Our data clearly show that there was little or no effect on 2-NBDG uptake into the cells by any of the stress-inducing treatments employed, or by viral infection. This indicates that the increase in glucose uptake by *P. berghei*-infected cells is not the result of a non-specific response to stress or to infection (Fig. 2B, C). Overall, our results show that *P. berghei* development inside Huh7 leads to

a specific and marked enhancement of glucose uptake by these cells. The observed effect appears rather unique to malaria parasites, as other intracellular pathogens, such as *Toxoplasma gondii* do not depend on host-derived glucose (Blume *et al.*, 2009), and hepatitis C virus replication actually suppresses cellular glucose uptake through down-regulation of cell surface expression of glucose transporters (Kasai *et al.*, 2009).

RNA interference screen implicates GLUT1 in glucose uptake by *P. berghei*-infected hepatic cells

The results so far suggest that infection of hepatic cells by *Plasmodium* modulates the uptake of glucose by these cells, possibly through the enhancement of the activity of

membrane glucose transporters in the cell. To ascertain this, we decided to carry out a small-scale RNA interference (RNAi) screen to evaluate the effect of the down-regulation of the expression of 5 transmembrane glucose transporters upon *P. berghei* infection (Table S1). The screen included all class I GLUT genes (GLUT1-4) as well as GLUT9, a major regulator of influx in HepG2 hepatoma cells (Takanaga *et al.*, 2008).

Huh7 cells stably expressing shRNA sequences targeting the selected genes were constructed to be used throughout the RNAi screen. The screen proceeded in three consecutive steps, employing different established methods to measure hepatic infection by *P. berghei*. In the first step of the screen, three shRNA sequences were used to silence each of the selected genes and the resulting stable cell lines were infected with luciferase-expressing *P. berghei* sporozoites. Forty-eight h later, the parasite load in these cells was determined by measuring the bioluminescence of cell lysates. Each sequence was used in at least four independent experiments, and an shRNA targeting Scavenger receptor class B type I (SR-BI) was employed as a positive control for infection decrease, as this receptor has been implicated in hepatic cell invasion by *P. berghei* parasites (Rodrigues *et al.*, 2008). GLUT1 emerged as the gene whose knock-down (KD) leads to the strongest decrease in infection (Fig. 3A), with GLUT4 and GLUT9 KD yielding a more moderate effect (Fig. 3A). We then carried out the second step of the RNAi screen, where only GLUT1, GLUT4 and GLUT9 were silenced prior to infection with GFP-expressing *P. berghei* parasites. The extent of parasite development was assessed 48 h later by flow cytometry determination of GFP intensity (Prudencio *et al.*, 2008). The results showed that KD of GLUT1 leads to the strongest impairment of parasite development among the three genes assessed (Fig. 3B). Therefore, GLUT1 was selected for the final confirmation screening step using the three different shRNA sequences targeting the *GLUT1* gene and assessing parasite development by immunofluorescence microscopy (Fig. 3C). Interestingly, the imaging data demonstrated that parasite size correlates with the mRNA levels of GLUT1, suggesting that GLUT1-mediated glucose uptake is required for the parasite's development (Fig. 3C and Table S1).

To further establish a link between the uptake of glucose by GLUT1 and *Plasmodium* infection, we assessed the difference in 2-NBDG uptake between infected and non-infected Huh7 cells expressing the same three *GLUT1*-targeting shRNA sequences as earlier. This difference was drastically reduced in the GLUT1-KD stable cell lines, relative to scramble-transduced control cells, a decrease that is proportional to the extent of the down-modulation of GLUT1 (Fig. 3D). As an additional control, we assessed 2-NBDG uptake following KD of GLUT2, whose expression by Huh7 cells we confirmed (2.6 ± 0.8 -fold lower than GLUT1), and can therefore contribute to glucose uptake by these cells. Nevertheless, our results showed that, contrary to GLUT1 the down-modulation of the expression of GLUT2 does not affect

2-NBDG uptake by cells containing developing parasites (Fig. 3D). We also confirmed that GLUT1 KD does not affect glucose uptake by non-infected cells except for a small decrease in cells where the down-modulation of GLUT1 expression is most pronounced (Fig. S5).

Finally, we assessed infection, as well as 2-NBDG uptake by infected cells, in the presence of WZB117, a specific inhibitor of GLUT1-mediated glucose transport (Liu *et al.*, 2012). Our results provide a chemical validation of the genetic approach (Fig. 3), as they show a clear dose-dependent effect of WZB117 on overall *P. berghei* infection of Huh7 cells (Fig. 4A), on parasite development (Fig. 4B), and on the difference in 2-NBDG uptake between cells infected with developing parasites and non-infected cells (Fig. 4C). Additionally, we showed that *P. berghei* infection of mouse primary hepatocytes is significantly impaired by the addition of 100 μ M WZB117 to the cell culture medium (Fig. S6). Most importantly, intra-peritoneal administration of WZB117 to mouse models of *Plasmodium* infection significantly decreases the parasite load in the livers of *P. berghei*-infected mice relative to vehicle-treated control animals (Fig. 4D). Immunofluorescence microscopy analysis of liver sections of these mice (Fig. 4E) revealed a significant decrease in parasite areas (Fig. 4F) and numbers (Fig. 4G) in WZB117-treated animals. These results indicate that GLUT1 inhibition by WZB117 leads to the inhibition of the hepatic parasite's development, as well as to its decreased survival *in vivo*.

GLUT1 expression is not enhanced in Plasmodium-infected cells

Having established a role for GLUT1 in the specific uptake of glucose by infected cells, we hypothesised that *Plasmodium* infection might lead to an increase in the expression of that transporter. To address this, we compared GLUT1 expression levels in non-infected and infected Huh7 cells at 6, 30 and 48 hpi with GFP-expressing *P. berghei* parasites. Following the separation of infected and non-infected cells by fluorescence-activated cell sorting (FACS) (Albuquerque *et al.*, 2009), cells were analysed by quantitative real-time polymerase chain reaction (qPCR), employing GLUT1-specific primers (Table S2). The data showed no significant differences in GLUT1 expression between infected and non-infected cells, at the selected time points (Fig. S7). As such, we concluded that the increase in GLUT1-mediated glucose uptake by *Plasmodium*-infected cells does not result from an infection-induced enhancement of the mRNA expression of this transporter.

P. berghei development leads to cytoplasmic ATP depletion

It has been shown that GLUT1 has a cytoplasmic pocket that is postulated to allow the binding of ATP, which in turn induces conformational changes that inhibit GLUT1-mediated glucose transport (Cloherty *et al.*, 1996; Levine

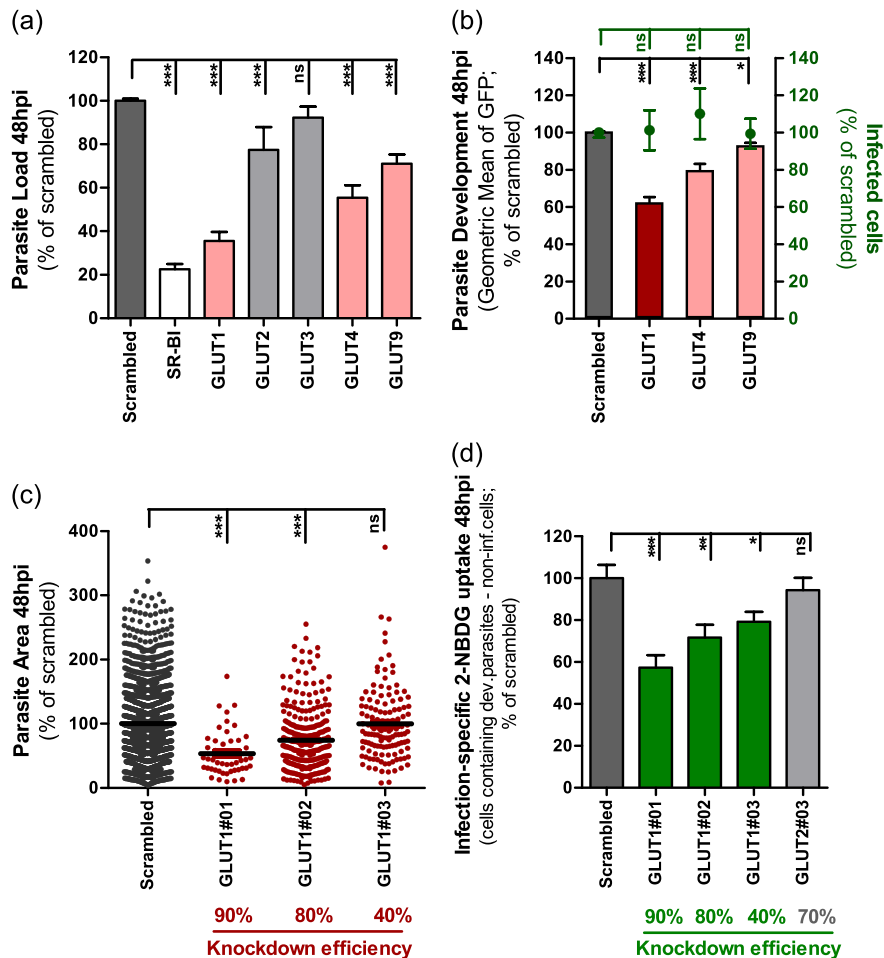


Fig. 3. GLUT1 knockdown significantly impairs *P. berghei* liver stage development and glucose uptake by *P. berghei*-infected cells. A. Huh7 cells with stable knockdown of one of five GLUT receptors were infected with luciferase-expressing *P. berghei* sporozoites and parasite load was assessed by luminescence measurement 48 h later. A scrambled shRNA sequence was used as a negative control and a cell line with stable knockdown of SR-BI as positive control. Pool of four independent experiments. Error bars represent SEM. B. Huh7 cells with the knockdown of GLUT1, GLUT4 or GLUT9 were infected with green fluorescent protein (GFP)-expressing *P. berghei* sporozoites. The percentage of infected cells and parasite development were assessed by flow cytometry at 48 hpi. Pool of three independent experiments. Error bars represent SEM. C. Quantification of the area of the EEFs in each of the three different cell lines with GLUT1 knockdown at 48 hpi by immunofluorescence microscopy. The knockdown efficiency of each shRNA sequence is indicated. Pool of three independent experiments. D. Difference of 2-NBDG uptake in the several cell lines with GLUT1 knockdown by developing parasites-containing cells and non-infected cells at 48 hpi, assessed by flow cytometry. A cell line with the knockdown of GLUT2 was used as control. Pool of four independent experiments. Error bars represent SEM. All panels: one-way analysis of variance (ANOVA) with post-test Dunnett. ns, not significant, * $P < 0.05$, ** $P < 0.01$ and *** $P < 0.001$.

et al., 1998). This modulation of GLUT1 conformation by ATP is counteracted by the binding of Adenosine monophosphate (AMP) and Adenosine diphosphate (ADP) to the same site in GLUT1 (Blodgett *et al.*, 2007). We thus wondered whether the observed increase in glucose uptake by *Plasmodium*-infected cells would correlate to a decrease in ATP levels in these cells. To investigate this, we employed a fluorescence resonance energy transfer-based indicator for ATP (ATeam), composed of the ϵ subunit of the bacterial F_0F_1 -ATP synthase sandwiched between the cyan-fluorescent proteins and Venus fluorescent proteins (CFP and Venus, respectively), which enables measurement of intracellular ATP levels as a function of the Venus/CFP ratio

(Imamura *et al.*, 2009). Using RFP-expressing *P. berghei* parasites and live fluorescence microscopy, we specifically monitored ATP levels in non-infected and infected cells at 30 and 48 hpi. Interestingly, we observed that the ATP levels of infected cells were significantly lower than those of naïve cells (Fig. 5A). In agreement with the results in Fig. 2A, which show that non-infected cells take up more 2-NBDG than naïve cells, we also detected a smaller but significant ATP reduction in the non-infected cells (Fig. 5A), when compared with naïve cells. These data indicate that liver stage parasite development results in a decrease in the ATP available inside the host cell, presumably leading to the well-described ATP/ADP/AMP-driven conformational

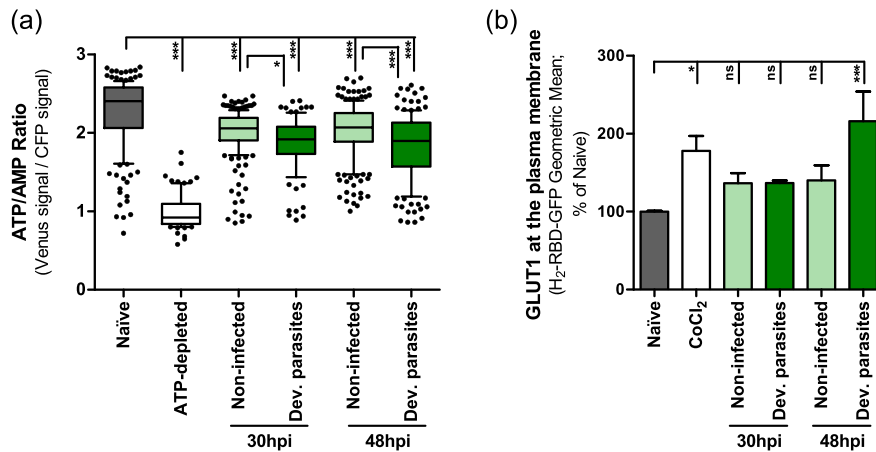


Fig. 5. *P. berghei* development inside Huh7 cells results in a decreased ATP/AMP ratio and increased GLUT1 content at the plasma membrane. A. Huh7 cells were transfected with an ATP probe, AT1.03, and infected with red fluorescent protein-expressing *P. berghei* sporozoites. Thirty and 48 hpi, the Venus/cyan-flourescent proteins (CFP) emission ratio in the cytoplasm of each individual cell (non-infected and cells containing developing parasites) was calculated from the fluorescent images acquired in both channels. Huh7 cells incubated in RPMI without glucose with 10 mM of galactose and 10 μ M of Oligomycin were used as positive controls for ATP depletion. Pool of 2 and 3 independent experiments for the 30 and 48 h time points, respectively. B. Huh7 cells were infected with red fluorescent protein-expressing sporozoites and, at 30 and 48 hpi, were incubated with the H_{RBD}-EGFP peptide that binds specifically to GLUT1 at the surface of the cells and were analysed by flow cytometry. Huh7 cells incubated overnight in complete RPMI with 250 μ M of CoCl₂ were used as positive controls. Pool of 2 and 4 independent experiments for the 30 and 48 h time points, respectively. Error bars represent SEM. Both panels: one-way ANOVA with post-test Tukey. ns, not significant; * $P < 0.05$ and *** $P < 0.001$.

glucose uptake (Fig. 2A). Overall, our data support the notion that increased glucose uptake by *P. berghei*-infected hepatic cells is mediated by GLUT1, which becomes activated by the ATP depletion and translocated into the membrane of the infected cell (Fig. 6).

Discussion

Plasmodium parasites require large amounts of nutrients for their extensive replication inside liver cells. Here, we show that glucose uptake is significantly increased in infected hepatic cells, through the enhanced action and translocation of the GLUT1 membrane transporter.

Glucose is ubiquitously used as the common currency of metabolism, and the ability to transport this hexose across

the plasma membrane is a feature of nearly all cells (Mueckler, 1994). Although GLUT2 is the major glucose transporter of hepatocytes, where it is involved in glucose uptake and release in the fed and fasted states, respectively (Thorens *et al.*, 1990; Mueckler and Thorens, 2013), GLUT1 is also present in the liver (Karim *et al.*, 2012), where it is transcribed and expressed by both periportal and perivenular hepatocytes. Of note, GLUT2 has a high capacity but a low affinity for glucose, with a K_m value (the concentration of glucose at which transport is half of its maximal value) in the order of 17 mM (Uldry *et al.*, 2002). GLUT1, on the other hand, has a higher affinity for glucose with a K_m value of ~ 3 mM (Uldry *et al.*, 2002), which is closer to that of PfHT (~ 1 mM, (Woodrow *et al.*, 2000)). Thus, it is tempting to speculate that GLUT1 is better matched to

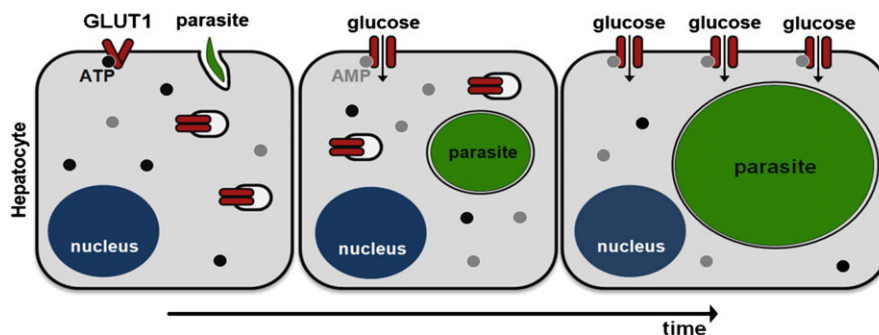


Fig. 6. Proposed model of GLUT1-mediated glucose uptake during hepatic infection by *Plasmodium*. Following the invasion of hepatic cells by *Plasmodium* parasites and the establishment of infection (left), parasites initiate a process of dramatic intracellular replication. Parasite development reduces the amount of host intracellular glucose, leading to depletion of the ATP pool and binding of ADP/AMP to GLUT1 transporters at the plasma membrane. This results in their activation (middle). At later stages of infection, GLUT1 transporters present in the host cell's cytoplasmic compartments are translocated to the cell membrane, leading to further enhancement of glucose uptake (right).

supply glucose to the parasite, especially if local glucose concentrations decrease towards the K_m of GLUT1. Interestingly, despite being expressed by all hepatocytes, membrane localization of GLUT1 under basal conditions is restricted to hepatocytes proximal to the hepatic venule (Tal *et al.*, 1990; Thorens *et al.*, 1990; Bilir *et al.*, 1993; Karim *et al.*, 2012; Mueckler and Thorens, 2013). Because the liver cell plate is perfused unidirectionally from portal to hepatic venule, the concentration of several substrates, such as oxygen and glucose, decreases as blood moves closer to the latter (Bilir *et al.*, 1993). This is consistent with the observation that GLUT1 expression is enhanced by a decrease in circulating glucose levels (Simpson *et al.*, 1999) as well as by hypoxia (Ebert *et al.*, 1995). Importantly, it has recently been shown that hypoxia enhances liver stage infection by malaria parasites, an effect that is also observed following treatment with an activator of hypoxia inducer factor-1 α (HIF-1 α) or with the hypoxia mimetic CoCl₂ (Ng *et al.*, 2014). Interestingly, increased HIF-1 α levels have been shown to upregulate expression of GLUT1 (Chen *et al.*, 2001) and CoCl₂ has been shown to enhance GLUT1 translocation to the plasma membrane ((Koseoglu and Beigi, 1999) and Fig. 5B). In this context, our results suggest that GLUT1-mediated glucose transport may provide a crucial link to explain the observed preferential infectivity of hypoxic liver cells by *Plasmodium* parasites.

The data presented here is consistent with our proposed model (Fig. 6), in which the extensive replication of liver stage parasites promotes the depletion of intracellular glucose and, consequently, of ATP. This effect is compensated for by an increase in glucose uptake that results from (i) the likely activation of GLUT1 transporters at the plasma membrane via AMP-dependent conformational changes and (ii) from GLUT1 translocation to the plasma membrane, particularly towards the end of parasite development. The significant increase in glucose uptake by infected cells likely leads to a decrease in glucose availability in the vicinity of infected cells, which may result in a similar, albeit weaker, response by neighbouring non-infected cells. In fact, these cells also display a small decrease in ATP levels, as well as some, although not statistically significant, GLUT1 translocation to the membrane (Fig. 5A,B), and a slight increase in glucose uptake from 30 hpi onwards (Fig. 2A). A question that remains open is which mechanism(s) is (are) involved in regulating GLUT1 activation and translocation into the membrane of the infected cell. It has previously been shown that enhanced glucose transport by GLUT1 transporters preexisting in the plasma membrane is associated with stimulation of AMP-activated protein kinase (AMPK) activity (Abbud *et al.*, 2000; Barnes *et al.*, 2002). On the other hand, it has been shown that GLUT1 translocation to the plasma membrane may be triggered by insulin (Egert *et al.*, 1999), in a phosphoinositide 3-kinase (PI3K)-dependent fashion (Egert *et al.*, 1999; Perrini *et al.*, 2004).

Intriguingly, neither parasite development nor glucose uptake by *P. berghei*-infected cells seem to be affected by the down-regulation of either the $\alpha 1$ and the $\alpha 2$ subunits of AMPK (Fig. S8). Likewise, addition of insulin or inhibition of PI3K with Wortmannin (Nagai *et al.*, 2011; Hsu and Yang, 2014) do not impact infection or glucose uptake by infected cells (Fig. S9). Very recently, phosphorylation of GLUT1 by protein kinase C has been shown to lead to the rapid increase in glucose uptake and enhanced cell surface localization of GLUT1 induced by TPA (Lee *et al.*, 2015). Whether a similar mechanism may be at play during *P. berghei* infection of hepatic cells is currently under investigation.

Despite the fact that, under basal conditions, GLUT1 is only localised at the membrane of perivenous hepatocytes, we showed that *in vivo* chemical inhibition of GLUT1-mediated glucose uptake has a substantial impact on the number of *P. berghei*-infected hepatocytes. There are two possible explanations for this observation. The first is that the inhibitor only hinders GLUT1-mediated glucose uptake on perivenous hepatocytes and, therefore, only has an effect on the parasites inside these hepatocytes. Alternatively, in accordance with our model, the replication of the parasite inside periportal hepatocytes could lead to a depletion of the cellular glucose pool and trigger the translocation of GLUT1 present in the endoplasmic reticulum (ER), Golgi and endosomal compartments to the plasma membrane, thereby increasing the percentage of infected hepatocytes with GLUT1 at the plasma membrane and, therefore, the number of cells targeted by the inhibitor.

The (East Rutherford, NJ, USA) liver displays the capacity to remove 30–40% of the glucose presented to it following glucose ingestion and therefore must be considered a significant site of postprandial glucose removal (Pagliassotti and Cherrington, 1992). Interestingly, a recent case–control study in Ghana found that patients with type 2 diabetes mellitus had a 46% increased risk for infection with *P. falciparum* (Danquah *et al.*, 2010). The authors of this study offer a number of possible explanations for this observation, including impaired immune responses, an increased number of infectious mosquito bites, and enhanced parasite growth in the blood of type 2 diabetes mellitus patients (Danquah *et al.*, 2010). Thus, our results suggest the possibility that the elevated amounts of circulating glucose displayed by diabetic patients may also promote parasite development in the liver, thereby contributing to the increased risk of appearance of clinically relevant malaria. Further investigation of the link between diabetes and malaria is clearly warranted by the fact that sub-Saharan Africa currently faces the world's highest increase in type 2 diabetes mellitus (Wild *et al.*, 2004).

To the best of our knowledge, this is the first report that addresses the role of glucose during hepatic infection by *Plasmodium* from a molecular point of view. It identifies

GLUT1 as a druggable target and a major player in glucose uptake by infected cells and shows that its function as a glucose transporter is modulated in cells containing replicating parasites. These findings contribute to an understanding of how hepatic host cells meet the energy demands imposed by the parasite's huge replication rate. Such an understanding may help identify strategies to control energy production by infected cells and thereby limit parasite development and survival.

Experimental procedures

Chemicals

Roswell Park Memorial Institute (RPMI) 1640, PBS pH 7.4, trypsin, fetal bovine serum (FBS), non-essential amino acids, penicillin/streptomycin, glutamine, HEPES pH 7, OptiMEM and Lipofectamine RNAiMAX were purchased from Gibco-Thermo Fisher Scientific (Waltham, MA USA). All other chemicals were obtained from Sigma-Aldrich (St. Louis, MO, USA), unless otherwise specified.

Cells

Huh7 cells, a human hepatoma cell line, were cultured in RPMI 1640 medium supplemented with 10% v/v FBS, 0.1 mM non-essential amino acids, 50 µg/ml penicillin/streptomycin, 2 mM glutamine and 1 mM HEPES (final concentrations), pH 7 and maintained at 37 °C with 5% CO₂. Mouse primary hepatocytes were cultured in William's E medium supplemented with 4% FBS, 2 mM glutamine, 1 mM HEPES and 50 µg/ml penicillin/streptomycin, and maintained at 37 °C with 5% CO₂.

Mice

C57BL/6 mice were purchased from Charles River (Lyon, France) and housed in the rodent facility of Instituto de Medicina Molecular (Lisbon, Portugal). All animal experiments were performed in strict compliance to the guidelines of our institution's animal ethics committee and the Federation of European Laboratory Animal Science Associations (FELASA).

Parasites

Green fluorescent protein (GFP)-expressing, red fluorescent protein (RFP)-expressing, or luciferase-expressing *P. berghei* ANKA sporozoites were dissected in non-supplemented RPMI medium from the salivary glands of infected female *A. stephensi* mosquitoes, bred at Instituto de Medicina Molecular, prior to being employed for *in vitro* and *in vivo* infections (Franke-Fayard *et al.*, 2004; Ploemen *et al.*, 2009).

Overall *in vitro* infection by luminescence

Overall hepatic infection was determined by measuring the luminescence intensity in Huh7 cells or mouse primary hepatocytes infected with a firefly luciferase-expressing *P. berghei* line, as previously described (Ploemen *et al.*, 2009). Briefly, Huh7 cells or mouse primary hepatocytes (1.0×10^4 and 2.0×10^4 per well, respectively)

were seeded in 96-well plates the day before infection. Sporozoite addition was followed by centrifugation at 1800 × g for 5 min and the medium was replaced approximately 2 hpi by the appropriate medium. Parasite infection load was measured 48 hpi by a bioluminescence assay (Biotium, Hayward, CA, USA) using a multiplate reader Infinite M200 (Tecan, Männedorf, Switzerland). The effect of the different treatments on cell viability was assessed by the CellTiter-Blue assay (Promega, Fitchburg, WI, USA) according to the manufacturer's protocol.

Quantification of *P. berghei* invasion and development by flow cytometry

Invasion of hepatoma cells and intracellular parasite development were assessed by determining the percentage of GFP⁺ cells 2 hpi with a GFP-expressing *P. berghei* line and by measuring the intensity of the GFP signal of the infected cells 48 hpi, respectively, as previously described (Prudencio *et al.*, 2008). Huh7 cells (5.0×10^4 per well) were seeded in 24-well plates the day before infection. The medium was replaced by the appropriate medium 1 h prior or 2 hpi, for invasion and development quantification, respectively. Cells were then collected for flow cytometry analysis at 2 h or 48 hpi, respectively, and analysed on a BD Biosciences FACScalibur (BD Biosciences, Franklin Lakes, NJ, USA). Data acquisition and analysis were carried out using the CELLQUEST (version 3.1.1 f1, BD Biosciences) and FLOWJO (version 6.4.7, Ashland, OR, USA) software packages, respectively.

Immunofluorescence imaging of *P. berghei* in Huh7 cells

For immunofluorescence microscopy analyses, cells were seeded on glass coverslips in 24-well plates and infected with sporozoites as described earlier. Forty-eight hpi, cells were rinsed with 1x PBS and fixed with 4% v/v paraformaldehyde (Santa Cruz Biotechnology, Dallas, TX, USA) for 20 min at room temperature and stored at 4 °C in PBS 1x until being stained. Cells were incubated with the permeabilization/blocking solution (0.1% v/v Triton X-100, 1% w/v bovine serum albumin in 1x PBS) for 30 min at room temperature. Parasites were stained with a parasite specific anti-Heat shock protein 70 (Hsp70) antibody (2E6; dilution 1:100) and an anti-UIS4 antibody (dilution 1:1000) for 1 h at room temperature, followed by three washes with permeabilization/blocking solution. Cells were further incubated in a 1:400 dilution of anti-mouse Alexa-Fluor 488 (Jackson ImmunoResearch Laboratories, West Grove, PA, USA) or anti-goat Alexa-Fluor 568 (Life Technologies, Carlsbad, CA, USA) secondary antibodies in the presence of a 1:1000 dilution of Hoechst 33342 (Invitrogen, Carlsbad, CA, USA) for nuclei staining. An additional three washes were carried out with permeabilization/blocking solution. Coverslips were mounted on microscope slides with Fluoromount (SouthernBiotech, Birmingham, AL, USA). Confocal images were acquired using a Zeiss LSM 710 confocal microscope (Carl Zeiss, Oberkochen, Germany). Widefield images for size determination were acquired in a Zeiss Axiovert 200 M microscope (Carl Zeiss, Oberkochen, Germany). Images were processed with IMAGEJ software (version 1.47, NIH, Bethesda, MD, USA).

Quantification of glucose uptake by flow cytometry and live microscopy

Glucose uptake into Huh7 cells was quantified by flow cytometry using a fluorescent D-glucose derivative, 2-[N-(7-nitrobenz-2-oxa-1,3-diazol-4-yl)amino]-2-deoxy-D-glucose (2-NBDG; Molecular Probes, Life Technologies) as a tracer (O'Neil *et al.*, 2005; Yamada *et al.*, 2007). Briefly, Huh7 cells (1.0×10^4 per well) were seeded in 96-well plates the day before infection with RFP-expressing *P. berghei* sporozoites. At several time points after infection, the medium was replaced by RPMI without glucose supplemented with 1 mM of glucose and 0.1 mM of 2-NBDG, and cells were incubated for 5 min at 37 °C to allow uptake (O'Neil *et al.*, 2005). Cells were then collected for flow cytometry analysis and analysed on a BD LSR Fortessa flow cytometer (BD BIOSCIENCES, Franklin Lakes, NJ, USA) with the DIVA software (version 6.2, BD BIOSCIENCES, Franklin Lakes, NJ, USA). Analysis was carried out using the FLOWJO software (version 6.4.7, FlowJo). For live microscopy, Huh7 cells (2.0×10^5) were seeded on glass bottom microwell dishes (MatTek, Ashland, MA, USA) the day before infection with RFP-expressing *P. berghei* sporozoites. At 48 hpi, the medium was replaced by RPMI without glucose supplemented with 1 mM of glucose and 0.1 mM of 2-NBDG, and cells were incubated for 30 min at 37 °C. Cells were then visualised on a 3i Marianas SDC microscope and the acquired images were processed with IMAGEJ software (version 1.47).

Temperature shocks and ethanol-induced oxidative stress

Huh7 cells (1.0×10^4 per well) were seeded in 96-well plates and incubated at 37 °C for 48 h. To induce a mild cold stress response, one of the plates was incubated at 27 °C for 1 h (Fujita, 1999). To induce a heat stress response, another plate was incubated at 43 °C for 1 h (Sun *et al.*, 2015). A control plate was maintained at 37 °C. Ethanol-induced oxidative stress was attained by incubating Huh7 cells in complete RPMI with 50 mM of ethanol for 24 h (Sergent *et al.*, 2005; Nourissat *et al.*, 2008). Following temperature shocks and ethanol-induced oxidative stress, the uptake of 2-NBDG by the cells was determined as previously described.

Viral infection-induced stress

Huh7 cells (5.0×10^4 per well) were seeded in 24-well plates and, on the following day, were infected with 0.01, 1 and 5 plaque-forming units/cell of wild type murine gammaherpesvirus 68 (MHV-68) or YFP-expressing MHV-68 (MHV-68-YFP) (Collins *et al.*, 2009). Twenty-four h later, the uptake of 2-NBDG by the MHV-68-infected cells was determined as previously described. The percentage of MHV-68-infected cells in each condition was estimated by determining the percentage of YFP⁺ cells after infection with the same amount of plaque-forming units/cell of MHV-68-YFP.

Assessment of the impact of glucose transporters on Plasmodium infection by RNA interference (RNAi)

Down-modulation of the genes encoding selected glucose transporters employed short hairpin RNAs (shRNAs). All shRNAs were purchased from the MISSION TRC library (Sigma) in the form

of bacterial glycerol stocks which were grown to obtain the purified plasmids. Each gene was targeted by using three distinct shRNAs, used individually (Table S1). For the lentiviral production, HEK 293FT cells (2.0×10^4 per well) were seeded in 96-well plates. On the following day, cells were transfected with the packaging vectors and each individual shRNA plasmid in a final concentration of 100 ng/well using the FuGENE 6 reagent (Promega), according to the manufacturer's instructions. The lentiviral particles were collected in the supernatant of these cells approximately 60 h after transfection and stored at -80 °C. For the transduction of Huh7 cells and subsequent generation of cell lines with stable knockdown of the genes of interest, cells (1.0×10^5 per well) were seeded in 12-well plates. On the following day, the medium was replaced by 400 µl of supplemented RPMI with 8 µg/ml of polybrene, on top of which were added 100 µl of lentiviral particles-containing supernatant [approximate multiplicity of infection (MOI) of 1:1] and the plates were centrifuged for 30 min at 1200 × g and 37 °C. Twenty-four hours after transduction, the medium was replaced by supplemented RPMI with 5 µg/ml of puromycin (Calbiochem) for the selection of the transduced cells which were allowed to grow for at least a week before being used for infections with luciferase-expressing or GFP-expressing *P. berghei* sporozoites to determine overall infection and parasite development by luminescence, flow cytometry and microscopy, as described earlier. Cells transduced with lentiviral particles carrying a negative control shRNA (SHC002) not targeting any annotated gene in the human genome were used as negative control. A stable cell line with the knockdown of Scavenger receptor class B type I (SR-BI) was used as positive control in the luminescence assays (Rodrigues *et al.*, 2008). The knockdown efficiency of each shRNA sequence (Table S1) was assessed by quantitative PCR (qPCR) with specific primers for each gene (Table S2).

Small interfering RNA transfection

4.0×10^4 Huh7 cells were reverse-transfected with 30 nM of target specific (human AMPK α 1: ref. L-005027-00-0005; human AMPK α 2: ref. L-005361-00-0005) or control small interfering RNA sequence pools (ON-TARGETplus SMARTpool, Dharmacon, Lafayette, CO, USA), using Lipofectamine RNAiMAX (Gibco/Invitrogen) according to the manufacturer's instructions. Twenty-four hours after transfection, the cells were infected with 3.0×10^4 GFP-expressing *P. berghei* sporozoites. Cells were collected for flow cytometry analysis at 48 hpi and analysed on a BD LSR Fortessa flow cytometer with the DIVA software (version 6.2). Analysis was carried out using the FLOWJO software (version 6.4.7, FlowJo). The efficiency of knockdown was assessed with specific primers by qPCR (Table S2).

Fluorescence-activated cell sorting of P. berghei-infected and non-infected Huh7 cells

Huh7 cells (1.0×10^5 per well) were seeded in 24-well plates and infected 24 h later with 1.0×10^5 GFP-expressing *P. berghei* sporozoites. Cells were collected at 2 hpi and FACS-sorted on a BD

FACSAria III Cell Sorter (BD Biosciences). Non-infected and GFP-expressing *P. berghei*-infected cells were gated on the basis of their different fluorescence intensity, as previously established, and collected simultaneously (Prudencio *et al.*, 2008; Albuquerque *et al.*, 2009). Immediately after FACS-sorting, both infected and non-infected cells were washed and seeded in 24-well plates at a density of 1.5×10^5 per well. Infected cells were diluted 1:1 with non-infected cells to allow replicates. Cells were then incubated until collection at 30 or 48 hpi. In the case of the 6 hpi time point, *P. berghei*-infected cells were FACS-sorted at this time, diluted 1:1 with non-infected cells, pelleted, snap-frozen and stored until RNA extraction.

RNA extraction, complementary DNA synthesis and qPCR

RNA was extracted from cultured cells using the High Pure RNA Isolation kit (Roche, Basel, Switzerland) according to the manufacturer's instructions. The amount of RNA in each sample was assessed with a NanoDrop[®] ND-1000 spectrophotometer (NanoDrop, Wilmington, DE, USA).

Complementary DNA (cDNA) was synthesised from 1 µg of RNA using the Roche cDNA synthesis kit, according to the manufacturer's instructions. The cDNA was synthesised employing the following thermocycling parameters: 25 °C for 10 min, 55 °C for 30 min, and 85 °C for 5 min. qPCR reaction was performed in a total volume of 20 µl in a ABI Prism 7500 Fast system (Applied Biosystems, Foster City, CA, USA) using the iTaq[™] Universal SYBR[®] Green kit (BioRad, Hercules, CA, USA) as follows: 50 °C for 2 min, 95 °C for 10 min, 40 cycles at 95 °C for 15 s and 60 °C for 1 min, melting stage was done at 95 °C for 15 s, 60 °C for 1 min, and 95 °C for 30 s. Primers for hypoxanthine-guanine phosphoribosyltransferase (Hprt), a well-established housekeeping gene, were used for normalisation in all experiments (Table S2). The delta-delta cycle threshold ($\Delta\Delta$ CT) relative quantification method was used for analysis of qPCR results.

In vivo WZB117 treatment, *P. berghei* sporozoite infection and quantification of parasite liver load by qPCR

Six weeks old male C57BL/6 mice were injected intraperitoneally (i.p.) with 10 mg/kg of WZB117 in PBS/DMSO 1:1 (v/v), or with vehicle alone, immediately before intravenous (i.v.) injection of 3.0×10^4 GFP-expressing *P. berghei* sporozoites (Liu *et al.*, 2012). The administration of the drug or vehicle was repeated at 15 and 30 hpi, and the livers were collected at 44 hpi and homogenised in 3 ml of denaturing solution (4 M guanidine thiocyanate; 25 mM sodium citrate pH 7, 0.5% w/v *N*-lauroylsarcosine and v/v 0.7% β mercaptoethanol in DEPC-treated water). Total RNA was extracted from the livers with the NZY Total RNA Isolation Kit (NZYTech, Lisboa, Portugal), according to the manufacturer's protocol, and converted into cDNA as described earlier. Parasite load was quantified by qPCR using primers specific to *P. berghei* 18S RNA (Table S2). Mouse Hprt expression was used for normalisation.

Immunohistochemical staining of liver sections

For microscopy, paraformaldehyde-fixed liver lobes were cut in 50 µm sections and were incubated in permeabilization/blocking

solution (1% w/v bovine serum albumin, 0.5% v/v Triton-X100 in PBS) at room temperature for 1 h, followed by a 2 h incubation at room temperature with an anti-UIS4 antibody (dilution 1:500). Slices were further incubated in a 1:300 dilution of anti-GFP-Alexa488 antibody (Invitrogen) and anti-goat Alexa-Fluor 568 (Invitrogen) in the presence of a 1:1000 dilution of Hoechst 33342 (Invitrogen) and a 1:100 dilution of Phalloidin-660 (Invitrogen) for actin staining for 1 h. After washing, slices were mounted on microscope slides with Fluoromount (SouthernBiotech). Images were acquired and processed as described above.

Determination of ATP levels inside single cells by live microscopy

Huh7 cells (2.0×10^5 cells) were seeded on glass bottom microwell dishes (MatTek). The following day, 1 µg of ATeam plasmid carrying the ATP indicator (pRSET-AT1.03) was transfected into the cells with FuGENE 6 (Roche) according to the manufacturer's instructions (Imamura *et al.*, 2009). Twenty-four hours after transfection, cells were infected with RFP-expressing *P. berghei* sporozoites and, at selected time points of infection, were visualised at 37 °C on a Zeiss LSM 710 confocal microscope as described previously (Ando *et al.*, 2012). Huh7 cells incubated for 6 h in RPMI without glucose with 10 mM of galactose and 10 µM of Oligomycin were used as positive controls for ATP depletion. Image analysis was performed using the IMAGEJ software (version 1.47). The Venus/CFP emission ratio was calculated for each cell dividing its mean intensity in the Venus channel by the mean intensity in the CFP channel.

Quantification of GLUT1 at the plasma membrane of infected cells by flow cytometry

Huh7 cells (1.0×10^4 per well) were seeded in 96-well plates and were infected with RFP-expressing *P. berghei* sporozoites on the following day. Thirty and 48 hpi, cells were detached using PBS containing 1 mM EDTA, centrifuged at 4 °C, and the cell pellet was resuspended in cold RPMI containing 10% v/v FBS. Cells were further incubated with supernatant obtained from 293T cells transfected with a vector encoding the H_{RBD}-EGFP fusion protein (dilution 1:50 in PBS with 2% v/v FBS) (Manel *et al.*, 2003; Kinet *et al.*, 2007). Following incubation at 37 °C for 30 min, cells were harvested by centrifugation, washed one time with PBS with 2% v/v FBS, resuspended in the same buffer and analysed with a BD LSR Fortessa cytometer with the DIVA software (version 6.2). Huh7 cells incubated overnight in complete RPMI with 250 µM of cobalt (II) chloride (CoCl₂) were used as positive controls (Koseoglu and Beigi, 1999). Analysis was carried out using the FLOWJO software (version 6.4.7, FlowJo).

Statistical analyses

Statistical analyses were performed using the GRAPHPAD PRISM 5 software (La Jolla, CA, USA). One-way analysis of variance, Two-way analysis of variance, Chi-Square, Mann-Whitney *U* test or Student's *t*-test were used for significance of differences observed, as indicated in each figure. ns, not significant; * $P < 0.05$, ** $P < 0.01$ and *** $P < 0.001$.

Acknowledgements

We are very grateful to Marc Sitbon and Julie Laval (Institut de Génétique Moléculaire de Montpellier CNRS-UMSF, France), and Vincent Petit and Sandra Moriceau (Metafora biosystems), for kindly providing the H_{RBD}-EGFP peptide, to Hiromi Imamura (Graduate School of Biostudies, Kyoto University, Japan) for kindly providing the pRSET-AT1.03 plasmid, to Maria M. Mota (Instituto de Medicina Molecular, Portugal) for critically reviewing the manuscript, to Marta Miranda for help with the viral infections, to Ana Parreira and Filipa Teixeira for producing the various lines of *P. berghei*-infected mosquitoes and to the bioimaging and flow cytometry facilities of iMM Lisboa for technical support.

This work was supported by the Fundação para a Ciência e Tecnologia (www.fct.pt, FCT, Portugal) through grants PTDC/SAU/MIC/117060/2010 and PTDC/SAU-MET/118199/2010 to MP and LMS, respectively. MP was sponsored by an Investigador FCT (2013) grant, PM by FCT fellowship SFRH/BD/71098/2010 and LMS by the European Community's Seventh Framework Programme (FP7/2007-2013) under grant agreement N. 242095 (EVI-MaLAR). The funders had no role in study design, data collection and interpretation, or the decision to submit the work for publication.

Conflict of interest

The authors declare no conflicts of interest.

References

- Abbud, W., Habinowski, S., Zhang, J.Z., Kendrew, J., Elkairi, F. S., Kemp, B.E., *et al.* (2000) Stimulation of AMP-activated protein kinase (AMPK) is associated with enhancement of Glut1-mediated glucose transport. *Arch Biochem Biophys* **380**: 347–352.
- Albuquerque, S.S., Carret, C., Grosso, A.R., Tarun, A.S., Peng, X., Kappe, S.H., *et al.* (2009) Host cell transcriptional profiling during malaria liver stage infection reveals a coordinated and sequential set of biological events. *BMC Genomics* **10**: 270.
- Ando, T., Imamura, H., Suzuki, R., Aizaki, H., Watanabe, T., Wakita, T., and Suzuki, T. (2012) Visualization and measurement of ATP levels in living cells replicating hepatitis C virus genome RNA. *PLoS Pathog* **8**: e1002561.
- Barnes, K., Ingram, J.C., Porras, O.H., Barros, L.F., Hudson, E. R., Fryer, L.G., *et al.* (2002) Activation of GLUT1 by metabolic and osmotic stress: potential involvement of AMP-activated protein kinase (AMPK). *J Cell Sci* **115**: 2433–2442.
- Bechmann, L.P., Hannivoort, R.A., Gerken, G., Hotamisligil, G. S., Trauner, M., and Canbay, A. (2012) The interaction of hepatic lipid and glucose metabolism in liver diseases. *J Hepatol* **56**: 952–964.
- Bilir, B.M., Gong, T.W., Kwasiborski, V., Shen, C.S., Fillmore, C. S., Berkowitz, C.M., and Gumucio, J.J. (1993) Novel control of the position-dependent expression of genes in hepatocytes. The GLUT-1 transporter. *J Biol Chem* **268**: 19776–19784.
- Bitar, M.S., Al-Saleh, E., and Al-Mulla, F. (2005) Oxidative stress-mediated alterations in glucose dynamics in a genetic animal model of type II diabetes. *Life Sci* **77**: 2552–2573.
- Blodgett, D.M., De Zutter, J.K., Levine, K.B., Karim, P., and Carruthers, A. (2007) Structural basis of GLUT1 inhibition by cytoplasmic ATP. *J Gen Physiol* **130**: 157–168.
- Blume, M., Rodriguez-Contreras, D., Landfear, S., Fleige, T., Soldati-Favre, D., Lucius, R., and Gupta, N. (2009) Host-derived glucose and its transporter in the obligate intracellular pathogen *Toxoplasma gondii* are dispensable by glutaminolysis. *Proc Natl Acad Sci U S A* **106**: 12998–13003.
- Chen, C., Pore, N., Behrooz, A., Ismail-Beigi, F., and Maity, A. (2001) Regulation of glut1 mRNA by hypoxia-inducible factor-1. Interaction between H-ras and hypoxia. *J Biol Chem* **276**: 9519–9525.
- Cloherty, E.K., Diamond, D.L., Heard, K.S., and Carruthers, A. (1996) Regulation of GLUT1-mediated sugar transport by an antiport/uniport switch mechanism. *Biochemistry* **35**: 13231–13239.
- Collins, C.M., Boss, J.M., and Speck, S.H. (2009) Identification of infected B-cell populations by using a recombinant murine gammaherpesvirus 68 expressing a fluorescent protein. *J Virol* **83**: 6484–6493.
- Cunningham, J.J., Gulino, M.A., Meara, P.A., and Bode, H.H. (1985) Enhanced hepatic insulin sensitivity and peripheral glucose uptake in cold acclimating rats. *Endocrinology* **117**: 1585–1589.
- Danquah, I., Bedu-Addo, G., and Mockenhaupt, F.P. (2010) Type 2 diabetes mellitus and increased risk for malaria infection. *Emerg Infect Dis* **16**: 1601–1604.
- Ebert, B.L., Firth, J.D., and Ratcliffe, P.J. (1995) Hypoxia and mitochondrial inhibitors regulate expression of glucose transporter-1 via distinct Cis-acting sequences. *J Biol Chem* **270**: 29083–29089.
- Egert, S., Nguyen, N., and Schwaiger, M. (1999) Myocardial glucose transporter GLUT1: translocation induced by insulin and ischemia. *J Mol Cell Cardiol* **31**: 1337–1344.
- Feistel, T., Hodson, C.A., Peyton, D.H., and Landfear, S.M. (2008) An expression system to screen for inhibitors of parasite glucose transporters. *Mol Biochem Parasitol* **162**: 71–76.
- Franke-Fayard, B., Trueman, H., Ramesar, J., Mendoza, J., van der Keur, M., van der Linden, R., *et al.* (2004) A Plasmodium berghei reference line that constitutively expresses GFP at a high level throughout the complete life cycle. *Mol Biochem Parasitol* **137**: 23–33.
- Fujita, J. (1999) Cold shock response in mammalian cells. *J Mol Microbiol Biotechnol* **1**: 243–255.
- Hellwig, B., and Joost, H.G. (1991) Differentiation of erythrocyte-(GLUT1), liver-(GLUT2), and adipocyte-type (GLUT4) glucose transporters by binding of the inhibitory ligands cytochalasin B, forskolin, dipyrindamole, and isobutylmethylxanthine. *Mol Pharmacol* **40**: 383–389.
- Hsu, P.Y., and Yang, Y.W. (2014) Gene delivery via the hybrid vector of recombinant adeno-associated virus and polyethylenimine. *Eur J Pharm Sci* **52**: 62–68.
- Imamura, H., Nhat, K.P., Togawa, H., Saito, K., Iino, R., Kato-Yamada, Y., *et al.* (2009) Visualization of ATP levels inside single living cells with fluorescence resonance energy transfer-based genetically encoded indicators. *Proc Natl Acad Sci U S A* **106**: 15651–15656.
- Itani, S., Torii, M., and Ishino, T. (2014) d-Glucose concentration is the key factor facilitating liver stage maturation of Plasmodium. *Parasitol Int* **63**: 584–590.
- Joet, T., Eckstein-Ludwig, U., Morin, C., and Krishna, S. (2003) Validation of the hexose transporter of Plasmodium falciparum as a novel drug target. *Proc Natl Acad Sci U S A* **100**: 7476–7479.

- Karim, S., Adams, D.H., and Lalor, P.F. (2012) Hepatic expression and cellular distribution of the glucose transporter family. *World J Gastroenterol* **18**: 6771–6781.
- Kasai, D., Adachi, T., Deng, L., Nagano-Fujii, M., Sada, K., Ikeda, M., et al. (2009) HCV replication suppresses cellular glucose uptake through down-regulation of cell surface expression of glucose transporters. *J Hepatol* **50**: 883–894.
- Kinet, S., Swainson, L., Lavanya, M., Mongellaz, C., Montel-Hagen, A., Craveiro, M., et al. (2007) Isolated receptor binding domains of HTLV-1 and HTLV-2 envelopes bind Glut-1 on activated CD4+ and CD8+ T cells. *Retrovirology* **4**: 31.
- Kirk, K., Horner, H.A., and Kirk, J. (1996) Glucose uptake in Plasmodium falciparum-infected erythrocytes is an equilibrative not an active process. *Mol Biochem Parasitol* **82**: 195–205.
- Koranyi, L., Bourey, R.E., James, D., Mueckler, M., Fiedorek, F. T., Jr., and Permutt, M.A. (1991) Glucose transporter gene expression in rat brain: Pretranslational changes associated with chronic insulin-induced hypoglycemia, fasting, and diabetes. *Mol Cell Neurosci* **2**: 244–252.
- Koseoglu, M.H., and Beigi, F.I. (1999) Mechanism of stimulation of glucose transport in response to inhibition of oxidative phosphorylation: analysis with myc-tagged Glut1. *Mol Cell Biochem* **194**: 109–116.
- Kroemer, G., and Pouyssegur, J. (2008) Tumor cell metabolism: cancer's Achilles' heel. *Cancer Cell* **13**: 472–482.
- Lee, E.E., Ma, J., Sacharidou, A., Mi, W., Salato, V.K., Nguyen, N., et al. (2015) A protein kinase C Phosphorylation motif in GLUT1 affects glucose transport and is mutated in GLUT1 deficiency syndrome. *Mol Cell* **58**: 845–853.
- Levine, K.B., Cloherty, E.K., Fidyk, N.J., and Carruthers, A. (1998) Structural and physiologic determinants of human erythrocyte sugar transport regulation by adenosine triphosphate. *Biochemistry* **37**: 12221–12232.
- Liu, Y., Cao, Y., Zhang, W., Bergmeier, S., Qian, Y., Akbar, H., et al. (2012) A small-molecule inhibitor of glucose transporter 1 downregulates glycolysis, induces cell-cycle arrest, and inhibits cancer cell growth *in vitro* and *in vivo*. *Mol Cancer Ther* **11**: 1672–1682.
- Loisel-Meyer, S., Swainson, L., Craveiro, M., Oburoglu, L., Mongellaz, C., Costa, C., et al. (2012) Glut1-mediated glucose transport regulates HIV infection. *Proc Natl Acad Sci U S A* **109**: 2549–2554.
- Manel, N., Kim, F.J., Kinet, S., Taylor, N., Sitbon, M., and Battini, J.L. (2003) The ubiquitous glucose transporter GLUT-1 is a receptor for HTLV. *Cell* **115**: 449–459.
- Moore, M.C., Coate, K.C., Winnick, J.J., An, Z., and Cherrington, A.D. (2012) Regulation of hepatic glucose uptake and storage *in vivo*. *Adv Nutr* **3**: 286–294.
- Mueckler, M. (1994) Facilitative glucose transporters. *Eur J Biochem* **219**: 713–725.
- Mueckler, M., and Thorens, B. (2013) The SLC2 (GLUT) family of membrane transporters. *Mol Aspects Med* **34**: 121–138.
- Nagai, T., Arai, T., Furuta, K., Sakai, K., Kudo, K., Kaneda, H., et al. (2011) Sorafenib inhibits the hepatocyte growth factor-mediated epithelial mesenchymal transition in hepatocellular carcinoma. *Mol Cancer Ther* **10**: 169–177.
- Ng, S., March, S., Galstian, A., Hanson, K., Carvalho, T., Mota, M.M., and Bhatia, S.N. (2014) Hypoxia promotes liver-stage malaria infection in primary human hepatocytes *in vitro*. *Dis Model Mech* **7**: 215–224.
- Nourissat, P., Travert, M., Chevanne, M., Tekpli, X., Rebillard, A., Le Moigne-Muller, G., et al. (2008) Ethanol induces oxidative stress in primary rat hepatocytes through the early involvement of lipid raft clustering. *Hepatology* **47**: 59–70.
- O'Neil, R.G., Wu, L., and Mullani, N. (2005) Uptake of a fluorescent deoxyglucose analog (2-NBDG) in tumor cells. *Mol Imaging Biol* **7**: 388–392.
- Pagliassotti, M.J., and Cherrington, A.D. (1992) Regulation of net hepatic glucose uptake *in vivo*. *Annu Rev Physiol* **54**: 847–860.
- Pencek, R.R., James, F.D., Lacy, D.B., Jabbour, K., Williams, P. E., Fueger, P.T., and Wasserman, D.H. (2004) Exercise-induced changes in insulin and glucagon are not required for enhanced hepatic glucose uptake after exercise but influence the fate of glucose within the liver. *Diabetes* **53**: 3041–3047.
- Penkler, G., du Toit, F., Adams, W., Rautenbach, M., Palm, D. C., van Niekerk, D.D., and Snoep, J.L. (2015) Construction and validation of a detailed kinetic model of glycolysis in Plasmodium falciparum. *FEBS J* **282**: 1481–1511.
- Perrini, S., Natalicchio, A., Laviola, L., Belsanti, G., Montrone, C., Cignarelli, A., et al. (2004) Dehydroepiandrosterone stimulates glucose uptake in human and murine adipocytes by inducing GLUT1 and GLUT4 translocation to the plasma membrane. *Diabetes* **53**: 41–52.
- Pfaller, M.A., Krogstad, D.J., Parquette, A.R., and Nguyen-Dinh, P. (1982) Plasmodium falciparum: stage-specific lactate production in synchronized cultures. *Exp Parasitol* **54**: 391–396.
- Ploemen, I.H., Prudencio, M., Douradinha, B.G., Ramesar, J., Fonager, J., van Gemert, G.J., et al. (2009) Visualisation and quantitative analysis of the rodent malaria liver stage by real time imaging. *PLoS One* **4**: e7881.
- Prudencio, M., Mota, M.M., and Mendes, A.M. (2011) A toolbox to study liver stage malaria. *Trends Parasitol* **27**: 565–574.
- Prudencio, M., Rodrigues, C.D., Ataíde, R., and Mota, M.M. (2008) Dissecting *in vitro* host cell infection by Plasmodium sporozoites using flow cytometry. *Cell Microbiol* **10**: 218–224.
- Prudencio, M., Rodriguez, A., and Mota, M.M. (2006) The silent path to thousands of merozoites: the Plasmodium liver stage. *Nat Rev Microbiol* **4**: 849–856.
- Rodrigues, C.D., Hannus, M., Prudencio, M., Martin, C., Goncalves, L.A., Portugal, S., et al. (2008) Host scavenger receptor SR-BI plays a dual role in the establishment of malaria parasite liver infection. *Cell Host Microbe* **4**: 271–282.
- Sergent, O., Pereira, M., Belhomme, C., Chevanne, M., Huc, L., and Lagadic-Gossman, D. (2005) Role for membrane fluidity in ethanol-induced oxidative stress of primary rat hepatocytes. *J Pharmacol Exp Ther* **313**: 104–111.
- Shrayyef, M.Z., and Gerich, J.E. (2010) Normal glucose homeostasis. In *Principles of Diabetes Mellitus*. Poretzky, L. (ed). Springer, Berlin, Germany.
- Simpson, I.A., Appel, N.M., Hokari, M., Oki, J., Holman, G.D., Maher, F., et al. (1999) Blood-brain barrier glucose transporter: effects of hypo- and hyperglycemia revisited. *J Neurochem* **72**: 238–247.
- Slavic, K., Delves, M.J., Prudencio, M., Talman, A.M., Straschil, U., Derbyshire, E.T., et al. (2011a) Use of a selective inhibitor to define the chemotherapeutic potential of the plasmodial hexose transporter in different stages of the parasite's life cycle. *Antimicrob Agents Chemother* **55**: 2824–2830.
- Slavic, K., Krishna, S., Derbyshire, E.T., and Staines, H.M. (2011b) Plasmodial sugar transporters as anti-malarial

- drug targets and comparisons with other protozoa. *Malar J* **10**: 165.
- Slavic, K., Straschil, U., Reininger, L., Doerig, C., Morin, C., Tewari, R., and Krishna, S. (2010) Life cycle studies of the hexose transporter of Plasmodium species and genetic validation of their essentiality. *Mol Microbiol* **75**: 1402–1413.
- Smith, T.A. (1999) Facilitative glucose transporter expression in human cancer tissue. *Br J Biomed Sci* **56**: 285–292.
- Sun, L., Lamont, S.J., Cooksey, A.M., McCarthy, F., Tudor, C. O., Vijay-Shanker, K., et al. (2015) Transcriptome response to heat stress in a chicken hepatocellular carcinoma cell line. *Cell Stress Chaperones* **20**: 939–950.
- Takanaga, H., Chaudhuri, B., and Frommer, W.B. (2008) GLUT1 and GLUT9 as major contributors to glucose influx in HepG2 cells identified by a high sensitivity intramolecular FRET glucose sensor. *Biochim Biophys Acta* **1778**: 1091–1099.
- Tal, M., Schneider, D.L., Thorens, B., and Lodish, H.F. (1990) Restricted expression of the erythroid/brain glucose transporter isoform to perivenous hepatocytes in rats. Modulation by glucose. *J Clin Invest* **86**: 986–992.
- Thorens, B., Cheng, Z.Q., Brown, D., and Lodish, H.F. (1990) Liver glucose transporter: a basolateral protein in hepatocytes and intestine and kidney cells. *Am J Physiol* **259**: C279–285.
- Tjhin, E.T., Staines, H.M., van Schalkwyk, D.A., Krishna, S., and Saliba, K.J. (2013) Studies with the Plasmodium falciparum hexokinase reveal that PfHT limits the rate of glucose entry into glycolysis. *FEBS Lett* **587**: 3182–3187.
- Uldry, M., Ibberson, M., Hosokawa, M., and Thorens, B. (2002) GLUT2 is a high affinity glucosamine transporter. *FEBS Lett* **524**: 199–203.
- Vander Jagt, D.L., Hunsaker, L.A., Campos, N.M., and Baack, B.R. (1990) D-lactate production in erythrocytes infected with Plasmodium falciparum. *Mol Biochem Parasitol* **42**: 277–284.
- Vidyashankar, S., Sharath Kumar, L.M., Barooah, V., Sandeep Varma, R., Nandakumar, K.S., and Patki, P.S. (2012) Liv.52 up-regulates cellular antioxidants and increase glucose uptake to circumvent oleic acid induced hepatic steatosis in HepG2 cells. *Phytomedicine* **19**: 1156–1165.
- Warburg, O., Wind, F., and Negelein, E. (1927) The Metabolism of Tumors in the Body. *J Gen Physiol* **8**: 519–530.
- Wild, S., Roglic, G., Green, A., Sicree, R., and King, H. (2004) Global prevalence of diabetes: estimates for the year 2000 and projections for 2030. *Diabetes Care* **27**: 1047–1053.
- Woodrow, C.J., Burchmore, R.J., and Krishna, S. (2000) Hexose permeation pathways in Plasmodium falciparum-infected erythrocytes. *Proc Natl Acad Sci U S A* **97**: 9931–9936.
- Yamada, K., Saito, M., Matsuoka, H., and Inagaki, N. (2007) A real-time method of imaging glucose uptake in single, living mammalian cells. *Nat Protoc* **2**: 753–762.
- Yu, J.W., Sun, L.J., Liu, W., Zhao, Y.H., Kang, P., and Yan, B.Z. (2013) Hepatitis C virus core protein induces hepatic metabolism disorders through down-regulation of the SIRT1-AMPK signaling pathway. *Int J Infect Dis* **17**: e539–545.

Supporting information

Additional supporting information may be found in the online version of this article at the publisher's web-site:

Fig. S1. Glucose availability impacts *P. berghei* infection *ex vivo*. (A) Mouse primary hepatocytes were infected with luciferase-expressing *P. berghei* sporozoites and the culture medium was replaced 2 hpi by medium with different concentrations of glucose. Parasite load (luminescence) and cell viability were assessed 48 hpi. Pool of 3 independent experiments. Error bars represent SEM. One-way ANOVA with post-test Dunnett. (B) Mouse primary hepatocytes were infected with GFP-expressing *P. berghei* sporozoites and the culture medium was replaced by medium with different concentrations of glucose 2 hpi. Parasite development and the total number of infected cells were assessed at 48 hpi by flow cytometry by determining the fluorescence intensity and the number of GFP⁺ cells, respectively. One experiment. One-way ANOVA with post-test Dunnett. Error bars represent SD. ns - not significant, * $P < 0.05$, ** $P < 0.01$ and *** $P < 0.001$.

Fig. S2. Gating strategy to determine 2-NBDG uptake and parasite development by flow cytometry. Huh7 cells were infected with RFP-expressing *P. berghei* sporozoites and incubated with 2-NBDG-containing medium at different time points of infection. Dot plot represents non-infected and infected (RFP⁺) cells of one replicate from the 48 h time point. Left histogram shows the different fluorescence intensity displayed by non-developing (RFP^{low}) and developing (RFP^{high}) parasites. Right histogram exemplifies the 2-NBDG uptake by the different cell populations (non-infected, non-developing and developing parasites), assessed as an increased fluorescence intensity in the green channel.

Fig. S3. *P. berghei*-infected Huh7 cells and developing parasites uptake more 2-NBDG than non-infected and naïve cells. Huh7 cells were infected with RFP-expressing *P. berghei* sporozoites and incubated for 30 min with 2-NBDG-containing medium at 48 hpi. (A) Representative images of *P. berghei*-infected Huh7 cells with or without incubation with 2-NBDG. A non-infected cell, an infected cell and a parasite are outlined in yellow, pink and red, respectively. Scale bar, 20 μm . (B) Quantification of 2-NBDG uptake by naïve (grey bar), non-infected cells (yellow bar), infected cells (pink bar) and developing parasites (red bar), as assessed by live fluorescence microscopy. Representative experiment out of 2 independent experiments. One-way ANOVA with post-test Bonferroni and two-tailed Mann-Whitney test, respectively. Error bars represent SD. *** $P < 0.001$.

Fig. S4. Quantification of the percentage of MHV-68-YFP-infected cells by flow cytometry. Percentage of YFP⁺ cells 24 hpi with different loads of MHV-68-YFP.

Fig. S5. 2-NBDG uptake by non-infected Huh7 cells with GLUT1 knockdown. 2-NBDG uptake by non-infected cells of the different cell lines with GLUT1 knockdown at 48 hpi, assessed by flow cytometry. Pool of 4 independent experiments. Error bars represent SEM. One-way ANOVA with post-test Dunnett. ns - not significant and *** $P < 0.001$.

Fig. S6. Chemical inhibition of GLUT1-mediated glucose transport by WZB117 affects *P. berghei* hepatic infection *ex vivo*. (A) Mouse primary hepatocytes were infected with luciferase-expressing *P. berghei* sporozoites and 2 h later the culture

medium was replaced by medium containing WZB117. Parasite load (luminescence) and cell viability were assessed at 48 hpi. Pool of 2 independent experiments. Error bars represent SEM. One-way ANOVA with post-test Dunnett. (B) Mouse primary hepatocytes were infected with GFP-expressing *P. berghei* sporozoites and 2 h later the culture medium was replaced by medium containing WZB117. Parasite development was assessed by flow cytometry at 48 hpi. Error bars represent SD. One-way ANOVA with post-test Dunnett. ns - not significant, * $P < 0.05$, ** $P < 0.01$ and *** $P < 0.001$.

Fig. S7. GLUT1 expression is not altered in *P. berghei*-infected cells. qPCR quantification of GLUT1 transcriptional expression in FACS-sorted infected and non-infected Huh7 cells. Each time point represents a pool of 2 independent sorting experiments. Error bars represent SD. Two-tailed Mann-Whitney test. ns - not significant.

Fig. S8. Increased GLUT1-dependent glucose uptake into *P. berghei*-infected cells is independent of AMPK. (A) Knockdown efficiency upon transfection in Huh7 cells of the siRNAs used against the $\alpha 1$ and $\alpha 2$ subunits of AMPK. (B) Huh7 cells with the knockdown of $\alpha 1$ or/and $\alpha 2$ subunits of AMPK were infected with GFP-expressing *P. berghei* sporozoites and parasite development was assessed by flow cytometry at 48 hpi. Pool of 2 independent experiments. Error bars represent SD. One-way

ANOVA with post-test Dunnett. (C) 2-NBDG uptake at 48 hpi by developing parasites-containing cells with the knockdown of $\alpha 1$ or/and $\alpha 2$ subunits of AMPK, assessed by flow cytometry. Representative experiment out of 2 independent experiments. Error bars represent SD. One-way ANOVA with post-test Dunnett. ns - not significant, *** $p < 0.001$.

Fig. S9. PI3K stimulation or inhibition does not impact *P. berghei* infection of Huh7 cells neither does it alter glucose uptake by infected cells. Huh7 cells were infected with luciferase-expressing *P. berghei* sporozoites and 2 h later were treated with different concentrations of (A) insulin or (B) Wortmannin. Parasite load (luminescence) was assessed after 48 h. Representative experiment out of 2 and pool of 3 independent experiments, respectively. Error bars represent SD. To evaluate possible effects on glucose uptake, Huh7 cells were infected with RFP-expressing *P. berghei* sporozoites and the treatment with different concentrations of insulin (C) and Wortmannin (D) was initiated 2 hpi. 2-NBDG uptake by developing parasites-containing cells was assessed at 48 hpi by flow cytometry. Pool of 2 independent experiments for both insulin and Wortmannin. Error bars represent SD. All panels: one-way ANOVA with post-test Dunnett. ns - not significant.

Table S1. List of shRNA sequences used, with the corresponding knockdowns.

Table S2. List of primer sequences.

Dietary alterations modulate susceptibility to *Plasmodium* infection

Vanessa Zuzarte-Luís^{1*}, João Mello-Vieira¹, Inês M. Marreiros¹, Peter Liehl¹, Ângelo F. Chora¹, Céline K. Carret^{1,2}, Tânia Carvalho¹ and Maria M. Mota^{1*}

The relevance of genetic factors in conferring protection to severe malaria has been demonstrated, as in the case of sickle cell trait and G6PD deficiency¹. However, it remains unknown whether environmental components, such as dietary or metabolic variations, can contribute to the outcome of infection². Here, we show that administration of a high-fat diet to mice for a period as short as 4 days impairs *Plasmodium* liver infection by over 90%. *Plasmodium* sporozoites can successfully invade and initiate replication but die inside hepatocytes, thereby are unable to cause severe disease. Transcriptional analyses combined with genetic and chemical approaches reveal that this impairment of infection is mediated by oxidative stress. We show that reactive oxygen species, probably spawned from fatty acid β -oxidation, directly impact *Plasmodium* survival inside hepatocytes, and parasite load can be rescued by exogenous administration of the antioxidant N-acetylcysteine or the β -oxidation inhibitor etomoxir. Together, these data reveal that acute and transient dietary alterations markedly impact the establishment of a *Plasmodium* infection and disease outcome.

Lipids are extremely versatile molecules that are used for energy production, as building blocks of cell membranes and as intracellular transport vesicles, as well as signalling molecules. Perturbations in lipid networks are at the heart of many disorders, such as metabolic, inflammatory and neurodegenerative diseases, as well as cancer³. Mechanistically, the direct interaction between lipids and inflammatory processes has become evident, as lipids can directly activate innate immune receptors and lipid catabolism can induce the production of oxidative-free radicals^{4, 5}. The outcome of a diverse array of viral, bacterial and parasitic infections can also be modulated by lipids⁶, either by fulfilling immediate needs of the pathogen lifestyle or by influencing pathogen-sensing and host-response mechanisms.

Malaria, an infectious disease caused by *Plasmodium* parasites while infecting red blood cells (RBCs), is still one of the most devastating diseases in the world, killing a child every 2 minutes. Prior to infecting RBCs, *Plasmodium* parasites must infect a hepatocyte and undergo a period of remarkable division and expansion, termed schizogony, to become an exoerythrocytic form (EEF)⁷. The extreme replication rate of *Plasmodium* parasites inside hepatocytes must impose a high demand for lipids. Indeed, studies by us and others have shown that the parasite relies heavily on the scavenging of host and environmental lipids^{8, 9}.

To evaluate the impact of dietary lipids in the establishment and course of *Plasmodium* infection, we subjected C57BL/6J mice to a

high-fat diet (HFD) (36% energy from fat) prior to (2 days before) or concomitant with a *Plasmodium berghei* sporozoite infection. The data show that, when compared to mice fed on a regular diet (RD), administration of HFD for 2 or 4 days causes a significant reduction in *Plasmodium* parasite liver load (Fig. 1a), impacting the course of subsequent blood stage infection. Indeed, when infection was allowed to progress to the blood stage, we observe a delay in onset of parasitaemia, with 27% of the HFD-fed mice remaining negative for circulating parasites up 20 days after infection initiated by mosquito bite (Fig. 1b, left panel). None of the mice fed an HFD showed signs of severe disease, namely the lethal neurological syndrome referred to as experimental cerebral malaria, resulting in an extended overall survival when compared to mice fed an RD (Fig. 1b right panel and Supplementary Fig. 1a). It is noteworthy that, as previously reported¹⁰, this short-term (4 days) HFD regimen leads to mild increase in hepatic enzymes and serum total cholesterol levels without affecting body weight, food and water consumption or glucose metabolism (Table 1 and Supplementary Fig. 1b). Nevertheless, 4 days of HFD are sufficient to cause a significant increase in liver lipid content without severe hepatic vacuolization. Hepatocytes display increased number and size of optically empty vacuoles and positive for Oil Red O (ORO) compatible with early microvesicular lipidosis (Fig. 1c,d).

Having such an acute effect of short-term HFD administration on *Plasmodium* liver infection, we next asked whether this would last after termination of the HFD regimen. To that end, mice were subjected to 4 days of HFD followed by 2 or 4 days of RD, the latter regimen being sufficient to restore the biochemical parameters and hepatocellular lipidosis (Supplementary Table 1, Fig. 1e and Supplementary Fig. 1c). The results indicate that 4 days of RD following 4 days of HFD completely restores parasite liver load (Fig. 1f). Our data so far shows that short-term HFD administration acutely and transiently reduces *Plasmodium* liver stage infection, impacting on the course of blood infection and progression to severe disease.

We next wanted to clarify whether the impairment of *Plasmodium* liver stage infection caused by HFD occurs during early stages of liver invasion, as previously suggested¹¹, or later during parasite development inside the hepatocyte. Time course analysis shows that the impact of HFD on infection is not significant during early stages of infection, namely after sporozoite invasion (6 hours) or at the beginning of parasite replication (24 hours), but becomes evident at later stages of parasite development (48 hours) (Fig. 2a and Supplementary Fig. 2a). Detailed microscopic examination of liver sections from mice on HFD versus RD, 48 hours after infection,

¹Instituto de Medicina Molecular, Faculdade de Medicina, Universidade de Lisboa, 1649-028 Lisboa, Portugal. Present address: ²EMBO, Meyerhofstrasse 1, 69117 Heidelberg, Germany. João Mello-Vieira and Inês M. Marreiros contributed equally to this work. *e-mail: vluis@medicina.ulisboa.pt; mmota@medicina.ulisboa.pt

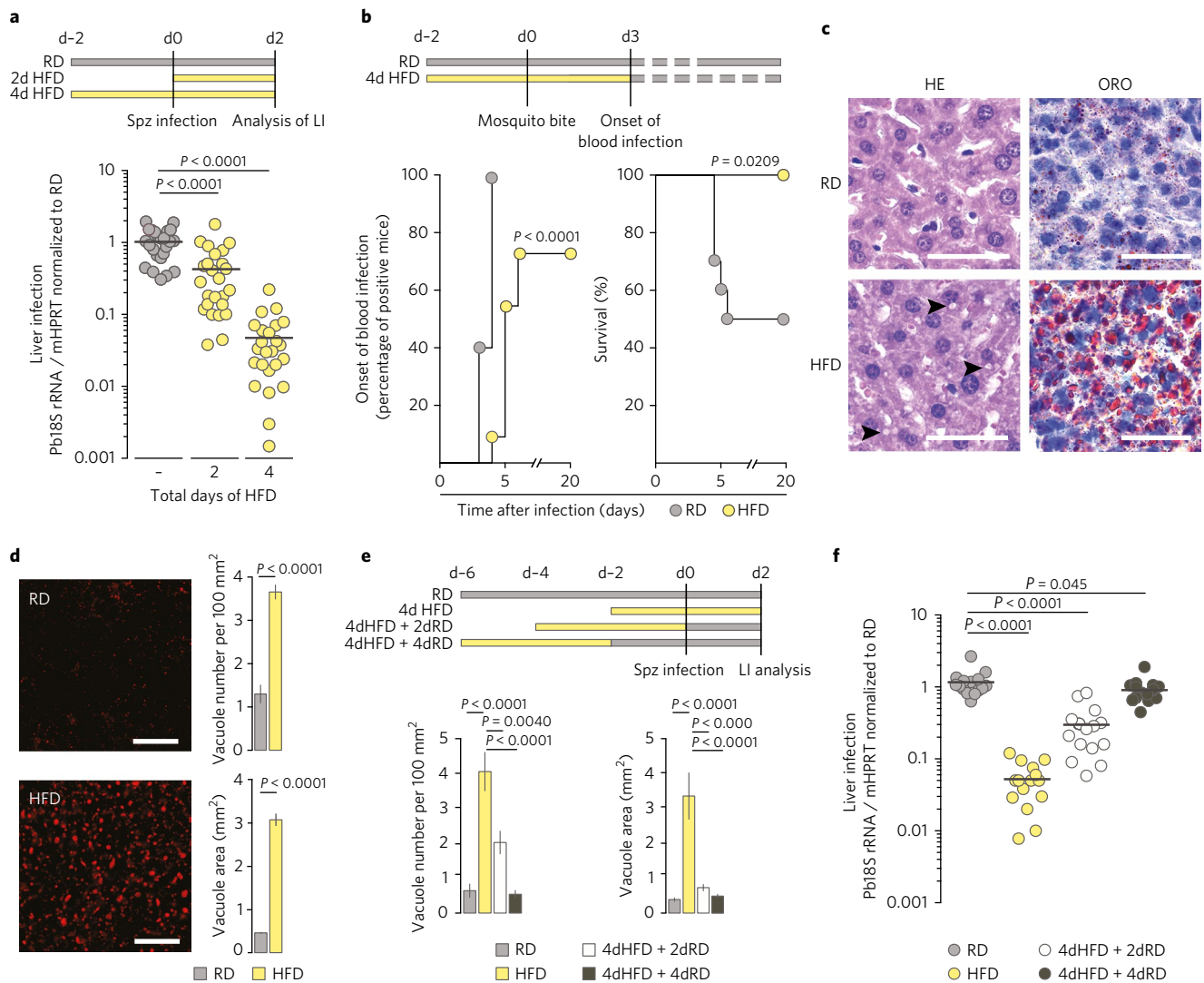


Fig. 1 | Short-term HFD administration impacts *Plasmodium* infection. **a**, Liver parasite load quantified by RT-qPCR in mice fed with RD or HFD for 2 days or 4 days ($n=25$ in each experimental group). **b**, Percentage of mice exhibiting blood infection (left panel) and percentage of survival from experimental cerebral malaria (right panel) upon infection by mosquito bite (RD, $n=10$; HFD, $n=11$). P values for survival and parasitaemia curves were determined using the log-rank Mantel-Cox Chi-squared test. **c**, Representative microphotographs of liver sections of RD- and HFD-fed mice stained with HE and ORO. Arrowheads point to lipid-laden vacuoles present in the hepatocytes of HFD-fed mice. Scale bars, $50\ \mu\text{m}$. **d**, Representative microphotographs (left panel) and correspondent quantification of the number and size of ORO-positive vacuoles (graphs) in livers of mice fed an RD or an HFD for 4 days. Scale bars, $50\ \mu\text{m}$. $n=5$ in each experimental group. **e**, Quantification of number and size of ORO-positive vacuoles in livers of mice fed on RD, HFD for 4 days and HFD for 4 days followed by 2 or 4 days of RD. $n=5$ in each experimental group. **f**, Liver parasite load quantified by RT-qPCR in mice fed with RD, HFD for 4 days and HFD for 4 days followed by 2 or 4 days of RD. $n=15$ in each experimental group. **a, d-f**, Data are represented as mean \pm s.e.m. P values were determined using the non-parametric two-tailed Mann-Whitney test. LI, liver infection; Spz, sporozoite.

revealed a strong and significant decrease in number of infected hepatocytes along with a decrease in EEF size (Fig. 2b,c). Together, the data show that the HFD-mediated effect on the establishment of *Plasmodium* infection and disease onset is caused by a marked reduction in the number of parasites in the liver.

We and others have noticed the association of liver-infiltrated inflammatory cells with infected hepatocytes and possible parasite clearance^{12, 13}. Further, diet-induced metabolic inflammation has been widely described for both the adipose tissue and the liver¹⁴. In agreement with these, histopathology analysis of several organs of mice fed an HFD for 4 days displays increased inflammatory cell infiltration exclusively in the liver, consisting of small foci rich in macrophages and granulocytes, with multifocal distribution throughout the liver parenchyma (Fig. 2d, arrowheads).

This contrasts with the absent-to-minimal inflammatory cell infiltration seen in RD-fed mice (Fig. 2d,e). Flow cytometry analysis of liver and spleen corroborated this finding, as significantly higher numbers of infiltrated myeloid cells, consisting mostly of macrophages and granulocytes, are observed in livers (Fig. 2f) but not in the spleen (Supplementary Fig. 2b) of mice fed an HFD for 4 days, when compared to mice fed an RD. However, association of inflammatory cell foci with infected hepatocytes, analysed at a time point preceding parasite disappearance, is similar between mice fed on RD or HFD (Supplementary Fig. 2c-e). Furthermore, antibody-mediated neutrophil depletion does not rescue *Plasmodium* infection impairment caused by HFD (Supplementary Fig. 2f) and neither does administration of HFD to mice genetically deficient for *Myd88*^{-/-} (Fig. 2g), an essential adaptor protein for Toll-like receptor

Table 1 | Body weight, food and water consumption, energy intake and serum biochemistry of non-infected mice fed on RD and 4 days of HFD

	RD	4d HFD
Body weight variation (g)	0.62 ± 0.40	0.38 ± 0.21 ^a
Liver weight (g per g bw)	0.05 ± 0.01	0.05 ± 0.004
Daily water consumption (g)	4.06 ± 0.25	3.74 ± 0.65
Daily food consumption (g)	3.59 ± 0.20	3.00 ± 0.45 ^a
Daily gross energy intake (MJ)	0.059 ± 0.003	0.058 ± 0.009
Daily metabolizable energy intake (MJ)	0.046 ± 0.003	0.050 ± 0.007
Serum parameters		
ALT (U per L)	48.3 ± 14.77	182.3 ± 50.49 ^a
AST (U per L)	86.2 ± 33.97	179.2 ± 91.28
Triglycerides (mg per dL)	137.79 ± 43.02	89.14 ± 26.07 ^a
Total cholesterol (mg per dL)	97.86 ± 20.22	172.52 ± 29.92 ^a
LDL (mg per dL)	35.63 ± 29.76	74.33 ± 64.09 ^a
HDL (mg per dL)	39.86 ± 16.66	52.39 ± 34.87

Data are represented as mean ± s.d.; n = 20 in each experimental group. P values (see Supplementary Table 3) were determined using the non-parametric two-tailed Mann-Whitney test. Bw, body weight; ALT, alanine aminotransferase; AST, aspartate aminotransferase; LDL, low-density lipoprotein; HDL, high-density lipoprotein. ^aSignificantly different from RD.

signalling and critical for the long-term HFD-induced accumulation of myeloid cells in the liver¹⁵. Importantly, the impairment of *Plasmodium* liver infection caused by HFD occurs in *Myd88*^{-/-} mice in spite of the lack of hepatic accumulation of macrophages and granulocytes (Fig. 2h). Altogether, these data exclude the participation of infiltrated myeloid cells in the impairment of *Plasmodium* liver infection caused by HFD.

Finally, administration of HFD to mice genetically deficient for natural killer T cells, inflammasome regulators, type I IFN and cytokines/receptors, as well as T, B and natural killer cells and innate lymphoid cells, still results in the impairment of *Plasmodium* liver infection similar to wild-type mice (Supplementary Fig. 3). Since these represent the most important innate and adaptive immune determinants, many of which have been implicated in HFD-induced inflammation¹⁶ or are known to impact *Plasmodium* liver infection^{12,13}, our data do not support a role for immune-mediated inflammation in the impairment of *Plasmodium* liver infection caused by HFD.

To gain mechanistic insight into how HFD leads to parasite elimination, we performed an unbiased transcriptomic analysis of livers of uninfected mice under HFD or RD regimens. The analysis revealed 430 differentially expressed transcripts of which 108 were at least twofold altered (Supplementary Table 2). In accordance with what has been reported after long-term HFD regimens⁵, gene ontology analysis revealed an enrichment in genes involved in oxidative stress upon short-term HFD administration (Fig. 3a). We confirmed that, indeed, 4 days of HFD administration led to differential expression (DE) of oxidative stress markers in the liver (Fig. 3b), significantly altered hepatic glutathione (GSH) levels (Supplementary Fig. 4a) and accumulation of reactive oxygen species (ROS) in hepatocytes (Fig. 3c and Supplementary Fig. 4b). Interestingly, histopathologic and immunofluorescence analyses of parasites at a time preceding elimination revealed that although parasitophorous vacuole membrane integrity is preserved (Supplementary Fig. 4d,e), thereby excluding this as the cause of parasite elimination^{9,17}, EEFs developing inside hepatocytes of HFD-fed mice often have an altered morphology including an irregular contour and abnormal nuclei (Fig. 3d) suggestive of parasite death inside the host cell. Thus, we sought to determine

whether ROS could directly impact parasite survival or development inside hepatocytes. Due to the unstable configuration of ROS, the HFD-induced ROS are not sustained after hepatocyte isolation and consequently the HFD-induced phenotype is not observed *ex vivo* (Supplementary Fig. 4b,c). As such, we used piperlongumine (PL) to induce ROS in HepG2 cells (Supplementary Fig. 5a)¹⁸. The results show that PL strongly affects parasite survival without affecting cell viability (Fig. 3e and Supplementary Fig. 5b,c) and this effect is fully reverted upon addition of the antioxidant N-acetylcysteine (NAC; Fig. 3e and Supplementary Fig. 5b,c). We then assessed whether antioxidant treatment could rescue *Plasmodium* liver stage impairment caused by HFD *in vivo*. Administration of NAC is sufficient to restore the expression levels of the oxidative stress markers (Fig. 3f) and the hepatic GSH levels (Supplementary Fig. 6a) as well as prevent the HFD-induced production of ROS (Fig. 3g). Most importantly, NAC treatment fully restores *Plasmodium* liver stage infection (Fig. 3h; and the same is true for a different antioxidant compound, S-adenosylmethionine, Supplementary Fig. 6b). Consequently, mice fed an HFD and treated with NAC develop similar blood stage infection levels (Supplementary Fig. 6c). Fatty acid oxidation has been pointed out as the main source of ROS in long-term HFD administration models¹⁹. Thus, to interrogate mitochondrial β -oxidation as the source of ROS in our model we used the inhibitor etomoxir²⁰. The results show that treatment with etomoxir prevents the HFD-induced production of ROS (Fig. 3i) and restores *Plasmodium* liver stage infection as well as gene expression (Fig. 3j and Supplementary Fig. 6d), suggesting that fatty acids from lipid droplets accumulated in hepatocytes of HFD-fed mice are oxidized in the mitochondria, maybe to serve as a source of energy, resulting in ROS production and parasite elimination. Altogether, the data demonstrate that HFD-induced ROS impact the host susceptibility to *Plasmodium* infection and disease.

The establishment and progression of an infection is more than just the consequence of a random encounter between a pathogen and its host. It depends on many factors including the density and virulence of the pathogen and the susceptibility of the host. The coevolution of different pathogens with their hosts led to the development of many host protective strategies as well as pathogen survival and evasion mechanisms. In the case of malaria, the development of immune-evasion strategies by *Plasmodium*, such as antigenic variation, occurred concomitantly with the acquisition of several host-protective genetic traits, such as haemoglobinopathies (HbS, HbC, HbE) and G6PD deficiency^{1,21}. Notably, sympatric populations with different lifestyles, such as dietary habits, but exposed to the same risk of malaria infection present differences in susceptibility to malaria (for a review see²), suggesting that environmental components must play an important role in disease. Surprisingly, while the association between several genetic traits and disease susceptibility is well established, the role of environmental factors such as nutrient availability has only recently started to be tackled using caloric restriction models. In this regard, it has been shown that restriction of food intake modulates host T-cell response, preventing neuropathology in experimental cerebral malaria²², and *Plasmodium* blood-stage parasites actively respond to host caloric restriction through transcriptome, multiplication rate and virulence rearrangements²³. We now show that short-term HFD administration significantly reduces *Plasmodium* liver stage infection, despite inducing only mild alterations in hepatic physiological and metabolic parameters. Transcriptomic data followed by functional assays identified HFD-induced ROS as the mechanism mediating the impairment of *Plasmodium* liver infection. Altogether, these observations show that nutrient availability and dietary habits strongly impact both the establishment and the course of a malaria infection. Remarkably, this occurs by interfering with both host and parasite pathways during different stages of infection.

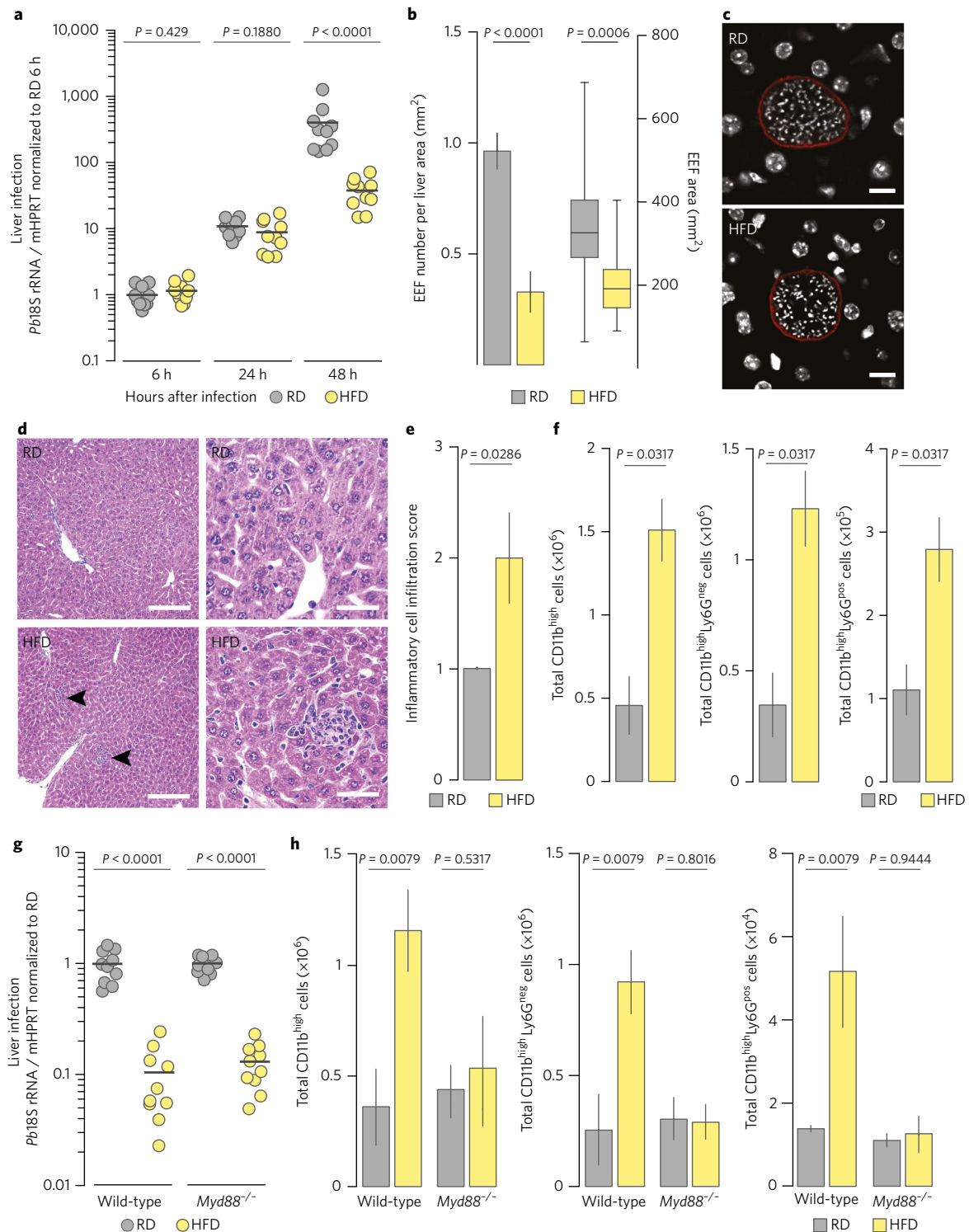


Fig. 2 | Plasmodium infection impairment is not mediated by immune cells. a, Liver parasite load quantified by RT-qPCR in mice fed with RD or HFD and analysed at 6, 24 and 48 h after infection. $n = 10$ in each experimental group. **b**, Quantification of the number (bars representing mean \pm s.e.m.) and size (min to max boxplot) of EEFs present in livers of mice fed on RD or HFD (RD, $n = 8$; HFD, $n = 8$). **c**, Representative microphotographs of EEF size quantified in **b**. Scale bars, 10 μm . **d**, Representative microphotographs of HE-stained liver sections of non-infected mice fed on RD or HFD. Arrowheads point to inflammatory cell foci scattered in the parenchyma, composed of granulocytes and macrophages, evident in the right-side panel at higher magnification. Scale bars: left panel, 200 μm ; right panel, 50 μm . **e**, Hepatic inflammatory cell infiltration score in livers of non-infected mice fed on RD or HFD (RD, $n = 4$; HFD, $n = 4$). **f**, Absolute numbers of liver-infiltrated myeloid cells ($\text{CD11b}^{\text{high}}$), macrophages ($\text{CD11b}^{\text{high}}\text{Ly6G}^{\text{neg}}$) and granulocytes ($\text{CD11b}^{\text{high}}\text{Ly6G}^{\text{pos}}$) analysed by flow cytometry in RD- and HFD-fed mice (RD, $n = 5$; HFD, $n = 5$). **g**, Liver parasite load quantified by RT-qPCR in wild-type and *Myd88*^{-/-} mice fed with RD or HFD ($n = 10$ in each experimental group). **h**, Absolute numbers of liver-infiltrated myeloid cells ($\text{CD11b}^{\text{high}}$), macrophages ($\text{CD11b}^{\text{high}}\text{Ly6G}^{\text{neg}}$) and granulocytes ($\text{CD11b}^{\text{high}}\text{Ly6G}^{\text{pos}}$) analysed by flow cytometry in wild-type and *Myd88*^{-/-} mice fed on RD and HFD ($n = 5$ in each experimental group). **a, e-h**, Data are represented as mean \pm s.e.m. **a, b, e-h**, P values were determined using the non-parametric two-tailed Mann-Whitney test.

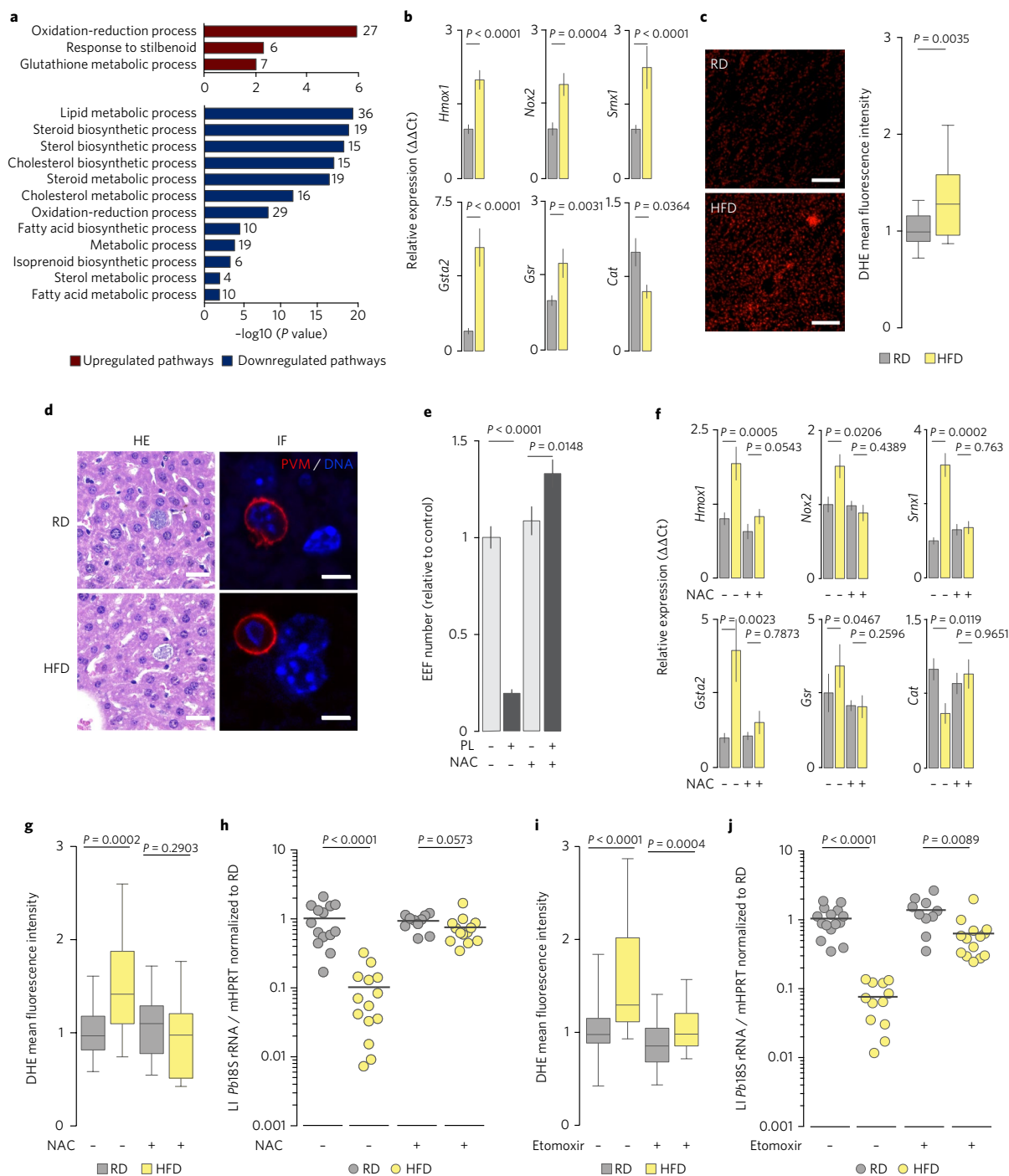


Fig. 3 | *Plasmodium* elimination is caused by hepatic ROS. **a**, Gene enrichment analysis of transcriptomic data from livers of non-infected mice, fed on RD or HFD, showing up- (red) and downregulated (blue) pathways with specification of the number of altered genes belonging to each pathway (RD, $n = 3$; HFD, $n = 3$). **b**, Relative expression of oxidative stress-related genes in livers of non-infected mice, fed on RD or HFD (RD, $n = 15$; HFD, $n = 15$). **c**, Representative microphotographs of liver sections stained with DHE and corresponding quantification of ROS levels (graph) in livers of RD- and HFD-fed mice. Scale bars, 100 μm. RD, $n = 5$; HFD, $n = 5$. **d**, Representative microphotographs of *Plasmodium* EEFs with altered morphology and irregular contour (HE), and with altered nuclei morphology (IF), developing in hepatocytes from HFD-fed mice when compared with EEFs developing inside hepatocytes from RD-fed mice. Scale bars: HE, 25 μm; IF, 5 μm. **e**, Quantification of the number of EEFs developing inside HepG2 cells 48 h after infection, treated with 2.5 μM PL alone or combined with 0.5 mM NAC, starting 2 h after infection. Data are representative of three independent experiments. **f-g**, Analysis of relative expression of oxidative stress-related genes (**f**) and ROS production (**g**) in livers of mice fed on RD or HFD, and supplemented with NAC in drinking water (1 g per 100 mL) starting the day before administration of HFD (**f**, $n = 10$ in each experimental group; **g**, $n = 5$ in each experimental group). **h**, Liver parasite load quantified by RT-qPCR in mice fed on RD or HFD and supplemented with NAC (1 g per 100 mL) in drinking water. $n = 14$ in each experimental group. **i**, Quantification of ROS production in livers of mice fed on RD or HFD and treated with etomoxir (Eto) (15 mg per kg of body weight, intraperitoneally). $n = 5$ in each experimental group. **j**, Liver parasite load quantified by RT-qPCR in mice fed with RD or HFD and treated with etomoxir (15 mg per kg of body weight, intraperitoneally) (RD, $n = 15$; HFD, $n = 12$; RD Eto, $n = 10$; HFD Eto, $n = 14$). **b, c, e-j**, Data are represented as mean \pm s.e.m. All P values were determined using the non-parametric two-tailed Mann-Whitney test. IF, immunofluorescence. PVM, parasitophorous vacuole membrane.

Importantly, while the susceptibility of intraerythrocytic *Plasmodium* parasites to ROS and the protective role of the RBC antioxidant mechanisms have been addressed, only indirect evidences have linked ROS with intra-hepatic developing *Plasmodium* parasites^{24, 25}. We now show for the first time that ROS induction in hepatocytes leads to a decrease in parasite numbers, and although it remains to be shown whether such decrease is due to direct parasite killing or elimination of the infected hepatocyte, our in vitro data show that ROS-mediated parasite elimination occurs in conditions where cell viability is preserved. Interestingly, oxidative stress is the hallmark of most disorders associated with the protective genetic traits such as G6PD-deficiency and all the haemoglobinopathies^{26, 27}. In light of our results, it is tempting to hypothesize that the resistance mechanism associated with such disorders starts in the liver with ROS-mediated impairment of liver stage infection. Indisputably, we show that antioxidant therapy or pharmacological inhibition of mitochondrial β -oxidation largely restores *Plasmodium* infection. It would, however, be interesting to challenge genetic models possessing either increased (deficient for G6PD, superoxide dismutases, catalase or glutathione synthetase) or decreased (deficient for NADPH-oxidases) ROS levels to further dissect the mechanism of ROS-mediated protection against *Plasmodium* infection.

Dietary habits are changing across the globe, including in malaria endemic regions²⁸. Although there is a rising concern about the spread of metabolic disorders, there is far less consensus on the implications of such lifestyle alterations on the establishment and progression of infectious diseases.

Our study emphasizes the concept that metabolic fluctuations, caused by alterations in dietary habits, strongly impact the course of malaria infection. Interestingly, such mechanisms may already be acting in malaria endemic regions. Natural resistance to malaria has been reported for the Fulani ethnic group. Although numerous hypotheses have been formulated (based on humoral or cytokine responses and genetic polymorphisms, among others; reviewed in²⁹) we still lack a clear and definitive explanation for this protection. The Fulani diverge from other sympatric non-resistant populations mainly in their dietary habits. The Fulani diet is rich in saturated fats derived from dairy products and cooking oils such as palm oil and butter oil³⁰. Whether these dietary habits and metabolic characteristics are at the basis of the resistance is for the moment unknown.

Our data clearly establish that acute and transient disruption of host metabolic homeostasis can dramatically change host susceptibility to infection and determine the outcome of disease. It is therefore our conviction that the strategies aiming to control infectious diseases must take into account alterations in populations' dietary habits.

Methods

Mice, diets and treatments. All mice used in this study were housed in the facilities of the Instituto de Medicina Molecular, four to five per cage, and allowed free access to water and food. C57BL/6J wild-type mice were purchased from Charles River Laboratories (L'Arbresle, France). *Myd88*^{-/-}, *Ifnar1*^{-/-}, *Ifn γ R*^{-/-} and *Rag2*^{-/-} were bred in specific pathogen-free facilities at the Instituto Gulbenkian de Ciéncia in Oeiras. *Caspase-3*^{-/-} and *Rag2*^{-/-}*yc*^{-/-} were bred in specific pathogen-free facilities at the Instituto de Medicina Molecular. *Il1 α / β* ^{-/-} mice were a kind gift from A. Zychlinsky. *Ja18*^{-/-}, *Nlrp3*^{-/-}, *Asc*^{-/-} and *Caspase-1*^{-/-} were a kind gift from K. Fitzgerald. Male mice 6 weeks of age were used in all experiments using exclusively wild-type mice. In the experiments using genetically deficient mouse lines, due to the limited availability of animals, both male and female mice 6 to 8 weeks of age were used. In such experiments wild-type C57BL/6J male and/or female mice, 6 to 8 weeks of age, were used to match gender and age of the genetically deficient mice. Mice were randomly assigned to different experimental groups. Blinding was not possible as mice under HFD exhibit a clear difference in fur oiliness due to regular grooming upon contact with the HFD. All experiments were approved by the animal ethics committee at Instituto de Medicina Molecular and performed in strict compliance with the guidelines of national and European regulations. HFD, composed of 15.8% fat, 1.25% cholesterol and 0.5% Na-choleate (S0031-S710), and the RD (1534-30 SM) were purchased from SSniff (Soest, Germany; detailed composition presented in Supplementary Fig. 7). NAC was administered in drinking water at 1 g per 100 mL, starting the day before the HFD and changed daily. S-adenosylmethionine (in saline) was administered through

intraperitoneal injection at 75 mg per kg of body weight every 12 h, starting 12 h before the HFD. Etomoxir (in saline) was administered through intraperitoneal injection at 15 mg per kg of body weight every 2 days, starting 12 h before the HFD. Neutrophil depleting antibody (clone 1A8; BioXCell, New Hampshire, USA) was administered intravenously (250 μ g per mouse) 1 day prior to HFD administration and on the day of sporozoite infection.

Parasite lines, liver infection and blood infection. *P. berghei* sporozoites were obtained through dissection of the salivary glands of infected female *Anopheles stephensi* mosquitoes bred at the Instituto de Medicina Molecular. The following parasite lines were used: *P. berghei* ANKA expressing GFP (259cl2) and *P. berghei* ANKA expressing luciferase (676m1cl1). Mouse infection was performed by intravenous injection of 2×10^4 *P. berghei* sporozoites or, in specified experiments, by mosquito bite (one infected mosquito per mouse). Liver parasite load was quantified by RT-qPCR in total liver extracts or by microscopy analysis of liver sections, at the indicated time after infection. In specific experiments, liver infection was allowed to progress to the blood stage of infection. The onset of blood parasitaemia was determined by luminescence assay, using 1 μ l of blood collected from the tail vein, as described in³¹.

Histology. For histopathology analysis, mice were sacrificed by CO₂ narcosis and the organs (intestine, kidney, adrenal, testis, pancreas, lung, spleen, adipose tissue and heart) were harvested, fixed in 10% neutral buffered formalin and processed for haematoxylin and eosin (HE) as indicated below for the liver. The liver was harvested and processed as follows. The right segment of the medial lobe was fixed in 10% neutral buffered formalin and embedded in paraffin, and sections were cut at 4 μ m and stained with HE. Sections were analysed by a pathologist blinded to experimental groups in a Leica DM2000 microscope coupled to a Leica MC170 camera. HE-stained sections were assessed for routine histopathology analysis, which included: (1) the evaluation of hepatocellular changes and inflammatory cell infiltration (cell type and distribution), diagnosed according to previously published criteria³²; (2) inflammatory cell infiltration scoring using a 5-point severity scale, with 0 set as absent, 1 as minimal, 2 as mild, 3 as moderate and 4 as marked; and (3) identifying infected hepatocytes at 36 h after infection and assessing their association with the inflammatory foci. This was performed by measuring the minimal distance between each infected hepatocyte and the nearest inflammatory foci, using the NDP.view2 software (Hamamatsu, Hamamatsu City, Japan) in slides digitally scanned in the Hamamatsu NanoZoomerSQ.

For histochemistry of lipids by ORO staining (Sigma, St. Louis, USA) and quantification of ROS by dihydroethidium staining (DHE; Thermo Fisher Scientific, Waltham, USA), the left lobe was frozen in O.C.T. compound (Sakura Finetek, Tokyo, Japan) and cryo-sections were cut at 14 μ m. Liver sections were incubated with 0.2% ORO in 60% isopropanol for 30 min at room temperature³³, or with 10 μ M DHE in PBS for 30 min at 37°C³⁴. ORO and DHE-stained sections were imaged using a motorized wide field fluorescence microscope, Zeiss Axio Observer. Images of liver sections were randomly acquired using the ZEN 2 software (Zeiss, Oberkochen, Germany) and then analysed on ImageJ for quantification of ORO-vesicle number and size and DHE fluorescence intensity.

For the analysis of parasite EEF number and size, the left segment of the median lobe was fixed with 4% PFA (2 h, room temperature) and sectioned into 40 μ m-thick sections, using the Vibratome VT 1000 S (Leica Microsystems, Wetzlar, Germany). Liver sections, permeabilized and blocked with PBS 1% BSA and 0.3% Triton-100 for 45 min, were incubated with primary antibody anti-*Pb*UIS4 (1:1,000; goat polyclonal; SicGen, Cantanhede, Portugal) followed by incubation with a secondary antibody, donkey anti-goat Alexa Fluor 568-conjugated (1:400; Jackson ImmunoResearch Laboratories, Baltimore, USA) and Hoechst 33342 (1:1,000; Invitrogen, Carlsbad, USA). All antibody incubations were performed at room temperature for 1 h. Stained liver slices were mounted on microscope slides with Fluoromount (SouthernBiotech, Birmingham, USA) and imaged using a motorized wide field fluorescence microscope, Zeiss Axio Observer. Images of liver sections were randomly acquired using the ZEN 2 software (Zeiss) and analysed on ImageJ for quantification of EEF number and area (as proxy for parasite development), defined by the staining of a parasitophorous vacuole membrane resident protein, UIS4. Representative microphotographs of *P. berghei* EEFs were acquired on Zeiss confocal microscope LSM 710.

Serum biochemistry and glucose tolerance test. Blood was collected terminally by cardiocentesis, and serum activity of AST (aspartate aminotransferase) and ALT (alanine aminotransferase) and concentrations of triglycerides, total cholesterol, LDL and HDL were measured in RD and HFD-fed mice (DNAtch, Lisboa, Portugal). For glucose tolerance test (GTT), mice were fasted for 8 h; glucose (1 g per kg body weight) was injected intraperitoneally and blood glucose level was measured using OneTouch Ultra glucose meter prior to, and 15, 30, 60 and 90 min after, glucose injection.

Liver non-parenchymal cell (NPC) and spleen cell isolation and flow cytometry. Livers were dissociated in a PBS solution containing DNase (2 U per ml) and filtered through a 70 μ m filter. Spleens were dissociated in PBS solution with 2% foetal bovine serum (FBS) and filtered through a 70 μ m filter. NPCs were purified by centrifugation using a 35% Percoll (Sigma) solution. Isolated NPCs and spleen cells were washed, after which RBC were lysed. Immunophenotyping was

performed after blocking with mouse Ab anti-FcγIII/II receptor (clone 93), using anti-mouse CD11b (clone M1/70) and Ly-6G (clone RB6-8C5) antibodies (both eBioscience, San Diego, USA). Dead cells were excluded using the Live-Dead Fixable Aqua Dead Cell Staining kit (Molecular Probes, Eugene, USA). Total cell number was determined by flow cytometry using a fixed number of latex beads (Beckman Coulter, Brea, USA) coacquired with a pre-established volume of the cellular suspension. Fluorescence was measured using the LSR Fortessa 1 (BD Biosciences, San Jose, USA) and data was analysed using FlowJo software.

Transcription profiling. Total RNA from whole livers of non-infected mice fed on RD and non-infected mice fed on HFD was extracted using RNeasy Mini kit (Qiagen, Hilden, Germany), following the manufacturer's instructions. Three biological replicates were analysed for each group. RNA quality and quantity were assessed on a Bioanalyser nanochip (Agilent, Santa Clara, USA). Total RNA was reverse transcribed and end-labelled as antisense RNA using the GeneChip WT Amplified Double-Stranded cDNA Synthesis Kit and the GeneChip WT Terminal Labeling Kit as recommended by Affymetrix. Hybridisation to an Affymetrix Mouse Gene 1.0 ST Array was carried out at 45 °C for 16 h under rotation (60 rpm). Arrays were washed on an Affymetrix FS450 and scanned using an Affymetrix Genechip Scanner 3000 7G. Fluorescence intensities were background adjusted, quantile normalised and median polished into expression values using the robust multi-array averaging program RMA 5 in R/Bioconductor suite 6 (software package: affy 7). To assess significance and DE, the RD group was compared to the HFD group, and out of 35,513 main probe sets represented on the array 430 transcripts were classified as significant (*P* value adjusted for multiple testing > 0, Supplementary Table 1), with 108 being DE at a log fold change > 2 (software packages: limma 8 and gplots). Gene Ontology Biological Process enrichment analysis was performed using DAVID 6.8.

RNA, cDNA and RT-qPCR. Whole livers were homogenized in 3 ml denaturing solution (4 M guanidine thiocyanate; 25 mM sodium citrate pH 7; 0.5% *N*-laurylsarcosine and 0.7% β mercaptoethanol, in DEPC-treated water). RNA was extracted using RNeasy Mini kit (Qiagen). cDNA was synthesized using Transcriptor First Strand cDNA Synthesis kit (Roche). Gene expression analysis was performed using kits from Applied Biosystems. For analysis, the expression levels of all target genes were normalized against hypoxanthine guanine phosphoribosyltransferase (*Hprt*) housekeeping gene (ΔCt). Gene expression values were then calculated based on the ΔΔCt method, using the mean of the control group as the calibrator to which all other samples were compared. The oligonucleotide primers used in qPCR experiments were:

mHprt- CATTATGCCGAGGATTGGGA; AATCCAGCAGGTCAGCAAAG
mHmx1- GTCTCTGCAGGGGCAGTATC; TGCTCGAATGAACACTCTGG
mNox2- TGCAGTGCTATCATCAAGC; CTTTCTCAGGGTTCCAGTG
mSrx1- AGTAGTAGTCGCCACCCTGG; AGAGCCTGGTGGACACGAT
mGsta2- TTGAAGTAGTGAAGCACGGG; ATTGGGAGCTGAGTGGAGAA
mGsr- ATCGTGCATGAATCCGAGT; GGTGGTGGAGAGTCAACAAGC
mCat- TCAGGGCCGCTTTTGCCT; ACTCGAGCGCGGTAGGGACA
Pb18S rRNA- AAGCATTAAATAAAGCGAATACATCTTAC;
 GGAGATTGGT TTTGACGTTTATGTG

GSH quantification. Quantification of hepatic GSH was performed in freshly dissected livers using the OxiSelect™ Total Glutathione (GSSG/GSH) Assay Kit (Cell Biolabs, San Diego, USA) according to the manufacturer's instructions.

Hepatoma cells, in vitro infections and treatments. HepG2 cells were obtained from the American Type Culture Collection (ATCC): The Global Bioresources Center (ATCC HB-8065). General information about this cell line, including the results of authentication by short tandem repeat profiling, can be found here: https://www.lgcstandards-atcc.org/Products/All/HB-8065.aspx?geo_country=ro. Throughout the duration of this study the cell line was tested for mycoplasma contamination using the VenorGeM OneStep – Mycoplasma Detection Kit for conventional PCR (Minerva Biolabs, Berlin, Germany) and no evidence of contamination was ever found.

HepG2 cells were maintained in DMEM medium supplemented with FBS, 50 µg per mL penicillin/streptomycin and 2 mM glutamine (all Gibco) at 37 °C with 5% CO₂. Twenty-four hours prior to infection, cells were seeded on glass coverslips in 24-well culture plates at a density of 65,000 cells per well. Cells were infected with freshly dissected *P. berghei* sporozoites (3 × 10⁴ per well) in supplemented medium containing Fungizone (1 µg per mL, Gibco). In specified experimental conditions, NAC (0.5 mM, water soluble) and/or increasing concentrations of PL (0.1–10 µM, DMSO soluble) were added to the culture medium.

To confirm the induction of ROS by PL, cells were incubated with 0.5 mM DHE for 30 min at 37 °C and analysed using a microplate reader (excitation: 535 nm and emission: 635 nm). Cell viability was analysed using cell titre blue according to the manufacturer's instructions.

To determine the effect of PL (±NAC) in *P. berghei* infection in vitro, cells were infected with *P. berghei* sporozoites and 2 h after infection compounds were added to the culture medium. Infection was allowed to progress for 48 h after which

coverslips were fixed in 4% PFA (10 min, RT) and permeabilized and blocked with 0.2% saponin, 1% BSA. For immunostaining, samples were incubated for 2 h, RT, with primary antibody anti-*Pb*UIS4 (1:1,000; goat polyclonal, SicGen) followed by incubation for 1 h, RT, with a secondary antibody donkey anti-goat Alexa Fluor 568-conjugated (1:400; Jackson ImmunoResearch Laboratories) and Hoechst 33342 (1:1,000, Invitrogen). The coverslips were then mounted on microscope slides with Fluoromount (SouthernBiotech) and imaged using a motorized wide field fluorescence microscope, Zeiss Axio Observer. Images were randomly acquired using the ZEN 2 software (Zeiss) and analysed on ImageJ for quantification of EEF number and size, as previously determined for mouse liver sections.

Mouse primary hepatocytes, ex vivo infection and ROS detection. Mouse primary hepatocytes were isolated using a modified two-step perfusion protocol followed by a Percoll purification step^{35,36}. Briefly, mice were sacrificed by CO₂ narcosis and immediately processed for cannulation of the portal vein using a 26-gauge needle. The inferior vena cava was cut to allow fluid to drain. Liver perfusion medium was perfused at 8–9 mL per min for 10 min, followed by liver digestion medium also at a rate of 8–9 mL per min for 10 min. Intermittent clamping of the inferior vena cava (3 s clamp every 30 s) was performed during liver digestion medium perfusion to improve tissue digestion. After digestion, the liver was excised and the cells were liberated by tearing and shaking of the liver with forceps. The cell suspension was then sequentially filtered through a 100 µm and a 70 µm cell strainer and spun at 50 g for 3 min. The cell pellet was resuspended in Williams's Medium E with 10% FBS and carefully overlaid on a 60% Percoll solution (1:1). The cell suspension was fractionated by centrifugation at 750 g for 20 min, without a break, at 20 °C. Viable hepatocytes deposited in the pellet were washed with Williams's Medium E with 10% FBS, spun at 50 g for 3 min and resuspended in complete Williams's Medium E (supplemented with 4% FBS and 1% penicillin/streptomycin). Viability and yield were assessed using trypan blue. Viable hepatocytes were plated on collagen-coated 96-well plates (20,000 cells per well) for infection with 10⁴ *P. berghei* sporozoites. Parasite load was quantified by RT-qPCR as previously described. For ROS level determination, freshly isolated hepatocytes in suspension were incubated with 0.5 mM DHE for 30 min at 37 °C and analysed using a microplate reader (excitation: 535 nm and emission: 635 nm). Given the labile nature of ROS, the time elapsed from hepatocyte isolation to DHE assay is critical and was kept to a minimum.

Statistics. Significance was calculated using different tests on the GraphPad (Prism) 5.0 software. Statistical differences between two groups were analysed using the non-parametric two-tailed Mann-Whitney test. Survival and parasitaemia curves were analysed using the Log-rank Mantel-Cox Chi-squared test and glucose tolerance results were analysed using a two-way analysis of variance. Significance was considered for *P* values below 0.05. Complete statistics can be found in Supplementary Table 3. Biological replicates (*n*) indicated in figure legends refer to the number of mice. Sample sizes were chosen on the basis of historical data; no statistical methods were used to predetermine sample size.

Data availability. The transcriptomic data generated during the current study are available in the Gene Express Omnibus and can be accessed through the GEO accession code: [GSE94867](https://www.ncbi.nlm.nih.gov/geo/query/acc.cgi?acc=GSE94867). The list of genes resultant from the analysis of the differential expression is available as Supplementary Table 2.

Received: 21 February 2017; Accepted: 14 August 2017;
 Published online: 25 September 2017

References

- Karlsson, E. K., Kwiatkowski, D. P. & Sabeti, P. C. Natural selection and infectious disease in human populations. *Nat. Rev. Genet.* **15**, 379–393 (2014).
- Traoré, K., Arama, C., Médebielle, M., Doumbo, O. & Picot, S. Do advanced glycation end-products play a role in malaria susceptibility? *Parasite* **23**, 15 (2016).
- Wymann, M. P. & Schreiner, R. Lipid signalling in disease. *Nat. Rev. Mol. Cell Biol.* **9**, 162–176 (2008).
- Medzhitov, R. Toll-like receptors and innate immunity. *Nat. Rev. Immunol.* **1**, 135–145 (2001).
- Matsuzawa-Nagata, N. et al. Increased oxidative stress precedes the onset of high-fat diet-induced insulin resistance and obesity. *Metabolism* **57**, 1071–1077 (2008).
- Wenk, M. R. Lipidomics of host–pathogen interactions. *FEBS Lett.* **580**, 5541–5551 (2006).
- Prudêncio, M., Rodriguez, A. & Mota, M. M. The silent path to thousands of merozoites: the *Plasmodium* liver stage. *Nat. Rev. Microbiol.* **4**, 849–856 (2006).
- Deschermeier, C. et al. Mitochondrial lipoic acid scavenging is essential for *Plasmodium berghei* liver stage development. *Cell. Microbiol.* **14**, 416–430 (2012).
- Itoe, M. A. et al. Host cell phosphatidylcholine is a key mediator of malaria parasite survival during liver stage infection. *Cell Host Microbe* **16**, 778–786 (2014).

10. Wiedemann, M. S. et al. Short-term HFD does not alter lipolytic function of adipocytes. *Adipocyte* **3**, 115–120 (2014).
11. Sinnis, P., Willnow, T. E., Briones, M. R. S. & Herzfl, J. Remnant lipoproteins inhibit malaria sporozoite invasion of hepatocytes. *J. Exp. Med.* **184**, 945–954 (1996).
12. Liehl, P. & Mota, M. M. Innate recognition of malarial parasites by mammalian hosts. *Int. J. Parasitol.* **42**, 557–566 (2012).
13. Mota, M. M. & Rodriguez, A. (eds) *Malaria: Immune Response to Infection and Vaccination* (Springer, Cham, 2017).
14. Lyons, C. L., Kennedy, E. B. & Roche, H. M. Metabolic inflammation-differential modulation by dietary constituents. *Nutrients* **8**, E247 (2016).
15. Deng, Z. et al. Immature myeloid cells induced by a high-fat diet contribute to liver inflammation. *Hepatology* **50**, 1412–1420 (2009).
16. Fritsche, K. L. The science of fatty acids and inflammation. *Adv. Nutr.* **6**, 293S–301S (2015).
17. Hanson, K. K. et al. Torins are potent antimalarials that block replenishment of *Plasmodium* liver stage parasitophorous vacuole membrane proteins. *Proc. Natl. Acad. Sci. USA* **110**, E2838–E2847 (2013).
18. Raj, L. et al. Selective killing of cancer cells by a small molecule targeting the stress response to ROS. *Nature* **475**, 231–234 (2011).
19. Cardoso, A. R., Kakimoto, P. A. H. B. & Kowaltowski, A. J. Diet-sensitive sources of reactive oxygen species in liver mitochondria: role of very long chain acyl-CoA dehydrogenases. *PLoS ONE* <http://doi.org/10.1371/journal.pone.0077088> (2013).
20. Luiken, J. J. F. P. et al. Etomoxir-induced partial carnitine palmitoyltransferase-I (CPT-I) inhibition *in vivo* does not alter cardiac long-chain fatty acid uptake and oxidation rates. *Biochem. J.* **419**, 447–455 (2009).
21. Kwiatkowski, D. P. P. How malaria has affected the human genome and what human genetics can teach us about malaria. *Am. J. Hum. Genet.* **77**, 171–190 (2005).
22. Mejia, P. et al. Dietary restriction protects against experimental cerebral malaria via leptin modulation and T-cell mTORC1 suppression. *Nat. Commun.* **6**, 6050 (2015).
23. Mancio-Silva, L. et al. Nutrient sensing modulates malaria parasite virulence. *Nature* **547**, 213–216 (2017).
24. Miller, J. L., Harupa, A., Kappe, S. H. I. & Mikolajczak, S. A. *Plasmodium yoelii* macrophage migration inhibitory factor is necessary for efficient liver-stage development. *Infect. Immun.* **80**, 1399–1407 (2012).
25. Ng, S. et al. Hypoxia promotes liver-stage malaria infection in primary human hepatocytes *in vitro*. *Dis. Model. Mech.* **7**, 215–224 (2014).
26. Cappellini, M. & Fiorelli, G. Glucose-6-phosphate dehydrogenase deficiency. *Lancet* **371**, 64–74 (2008).
27. Voskou, S., Aslan, M., Fanis, P., Phylactides, M. & Kleanthous, M. Oxidative stress in beta-thalassaemia and sickle cell disease. *Redox Biol.* **6**, 226–239 (2015).
28. NCD Risk Factor Collaboration (NCD-RisC). et al. Trends in adult body-mass index in 200 countries from 1975 to 2014: a pooled analysis of 1698 population-based measurement studies with 19.2 million participants. *Lancet* **387**, 1377–1396 (2016).
29. Arama, C. et al. Ethnic differences in susceptibility to malaria: what have we learned from immuno-epidemiological studies in West Africa? *Acta Tropica* **146**, 152–156 (2015).
30. Glew, R. H. et al. Lipid profiles and trans fatty acids in serum phospholipids of semi-nomadic fulani in Northern Nigeria. *J. Heal. Popul. Nutr.* **28**, 159–166 (2010).
31. Zuzarte-Luis, V., Sales-Dias, J. & Mota, M. M. Simple, sensitive and quantitative bioluminescence assay for determination of malaria pre-patent period. *Malar. J.* **13**, 15 (2014).
32. Thoolen, B. et al. Proliferative and nonproliferative lesions of the rat and mouse hepatobiliary system. *Toxicol. Pathol.* **38**, 5S–81S (2010).
33. van Goor, H., Gerrits, P. O. & Grond, J. The application of lipid-soluble stains in plastic-embedded sections. *Histochemistry* **85**, 251–253 (1986).
34. Umemura, A. et al. Liver damage, inflammation, and enhanced tumorigenesis after persistent mTORC1 inhibition. *Cell Metab.* **20**, 133–144 (2014).
35. Zhang, W. et al. PCB 126 and other dioxin-like PCBs specifically suppress hepatic PEPCK expression via the aryl hydrocarbon receptor. *PLoS ONE* **7**, e37103 (2012).
36. Gonçalves, L. A., Vigário, A. M. & Penha-Gonçalves, C. Improved isolation of murine hepatocytes for *in vitro* malaria liver stage studies. *Malar. J.* **6**, 169 (2007).

Acknowledgements

The authors would like to thank A. Parreira for mosquito and sporozoite production; iMM's rodent facility and histology unit; A.M. Vigário, A. Pamplona and S. Portugal for discussion; A.M. Vigário, I. Bento and I. Vera for critical reading of the manuscript. This work was supported by Fundação para a Ciência e Tecnologia (Portugal) through grant EXCL/IMI-MIC/0056/2012 and the ERC (agreement No. 311502) to M.M.M. V.Z.-L. was sponsored by EMBO (ALTF 357-2009) and FCT (BPD-81953-2011).

Author contributions

V.Z.-L. and M.M.M. conceived and designed the study and wrote the manuscript. V.Z.-L., J.M.-V., I.M.M., P.L. and A.F.C. performed the experiments, acquired the data, performed data analysis and interpreted results. V.Z.-L. and C.K.C. performed transcriptome data analysis. T.C. performed histology data analysis. All authors read, edited and approved the final manuscript.

Competing interests

The authors declare no competing financial interests.

Additional information

Supplementary information is available for this paper at doi:10.1038/s41564-017-0025-2.

Reprints and permissions information is available at www.nature.com/reprints.

Correspondence and requests for materials should be addressed to V.Z. or M.M.M.

Publisher's note: Springer Nature remains neutral with regard to jurisdictional claims in published maps and institutional affiliations.

Life Sciences Reporting Summary

Nature Research wishes to improve the reproducibility of the work that we publish. This form is intended for publication with all accepted life science papers and provides structure for consistency and transparency in reporting. Every life science submission will use this form; some list items might not apply to an individual manuscript, but all fields must be completed for clarity.

For further information on the points included in this form, see [Reporting Life Sciences Research](#). For further information on Nature Research policies, including our [data availability policy](#), see [Authors & Referees](#) and the [Editorial Policy Checklist](#).

► Experimental design

1. Sample size

Describe how sample size was determined.

No statistical methods were used to pre-determine sample size. Methods section, line 657. The sample size is specified in each figure legend and in supplementary table 3.

2. Data exclusions

Describe any data exclusions.

No data were excluded from the analysis.

3. Replication

Describe whether the experimental findings were reliably reproduced.

All attempts of replication were successful.

4. Randomization

Describe how samples/organisms/participants were allocated into experimental groups.

Animals were randomly assign to different experimental groups. Methods section, line 431. Microscopy analysis was performed in randomly acquired images. Methods section, line 490, 504 and 616.

5. Blinding

Describe whether the investigators were blinded to group allocation during data collection and/or analysis.

No blinding was performed except for the histological analysis, which were scored blindly. Methods section, line 432 and 471.

Note: all studies involving animals and/or human research participants must disclose whether blinding and randomization were used.

6. Statistical parameters

For all figures and tables that use statistical methods, confirm that the following items are present in relevant figure legends (or in the Methods section if additional space is needed).

- | | |
|-------------------------------------|--|
| n/a | Confirmed |
| <input type="checkbox"/> | <input checked="" type="checkbox"/> The <u>exact sample size</u> (n) for each experimental group/condition, given as a discrete number and unit of measurement (animals, litters, cultures, etc.) |
| <input type="checkbox"/> | <input checked="" type="checkbox"/> A description of how samples were collected, noting whether measurements were taken from distinct samples or whether the same sample was measured repeatedly |
| <input type="checkbox"/> | <input checked="" type="checkbox"/> A statement indicating how many times each experiment was replicated |
| <input type="checkbox"/> | <input checked="" type="checkbox"/> The statistical test(s) used and whether they are one- or two-sided (note: only common tests should be described solely by name; more complex techniques should be described in the Methods section) |
| <input checked="" type="checkbox"/> | <input type="checkbox"/> A description of any assumptions or corrections, such as an adjustment for multiple comparisons |
| <input type="checkbox"/> | <input checked="" type="checkbox"/> The test results (e.g. P values) given as exact values whenever possible and with confidence intervals noted |
| <input type="checkbox"/> | <input checked="" type="checkbox"/> A clear description of statistics including <u>central tendency</u> (e.g. median, mean) and <u>variation</u> (e.g. standard deviation, interquartile range) |
| <input type="checkbox"/> | <input checked="" type="checkbox"/> Clearly defined error bars |

See the web collection on [statistics for biologists](#) for further resources and guidance.

► Software

Policy information about [availability of computer code](#)

7. Software

Describe the software used to analyze the data in this study.

To analyze transcriptomic data R/Bioconductor suite 6 (package: affy 7) was used.
To analyze microscopy images, ImageJ software (version 1.51n) was used.
To analyze qPCR data, QuantStudio Real-Time PCR software (version 1.1) was used.
For statistical analysis, GraphPad Prism software (version 5) was used.
For data presentation Adobe Illustrator (version CS4) was used.

For manuscripts utilizing custom algorithms or software that are central to the paper but not yet described in the published literature, software must be made available to editors and reviewers upon request. We strongly encourage code deposition in a community repository (e.g. GitHub). *Nature Methods* [guidance for providing algorithms and software for publication](#) provides further information on this topic.

► Materials and reagents

Policy information about [availability of materials](#)

8. Materials availability

Indicate whether there are restrictions on availability of unique materials or if these materials are only available for distribution by a for-profit company.

All materials are readily available from standard commercial sources.

9. Antibodies

Describe the antibodies used and how they were validated for use in the system under study (i.e. assay and species).

References of antibodies included in Methods section, namely in Histology and NPCs isolation and flow cytometry sections.

10. Eukaryotic cell lines

a. State the source of each eukaryotic cell line used.

ATCC. Methods section, line 584.

b. Describe the method of cell line authentication used.

STR DNA profiling. Methods section, line 587.

c. Report whether the cell lines were tested for mycoplasma contamination.

The cell lines used were tested for mycoplasma contamination. Methods section, line 589.

d. If any of the cell lines used are listed in the database of commonly misidentified cell lines maintained by [ICLAC](#), provide a scientific rationale for their use.

No commonly misidentified cell lines were used in this study.

► Animals and human research participants

Policy information about [studies involving animals](#); when reporting animal research, follow the [ARRIVE guidelines](#)

11. Description of research animals

Provide details on animals and/or animal-derived materials used in the study.

Methods section: "Mice, Diets and Treatments".

Policy information about [studies involving human research participants](#)

12. Description of human research participants

Describe the covariate-relevant population characteristics of the human research participants.

The study did not involve human research participants.

Plasmodium UIS3 sequesters host LC3 to avoid elimination by autophagy in hepatocytes

Eliana Real¹, Lénia Rodrigues¹, Ghislain G. Cabal¹, Francisco J. Enguita¹, Liliana Mancio-Silva¹, João Mello-Vieira¹, Wandy Beatty², Iset M. Vera¹, Vanessa Zuzarte-Luís¹, Tiago N. Figueira¹, Gunnar R. Mair^{3,4} and Maria M. Mota^{1*}

The causative agent of malaria, *Plasmodium*, replicates inside a membrane-bound parasitophorous vacuole (PV), which shields this intracellular parasite from the cytosol of the host cell¹. One common threat for intracellular pathogens is the homeostatic process of autophagy, through which cells capture unwanted intracellular material for lysosomal degradation². During the liver stage of a malaria infection, *Plasmodium* parasites are targeted by the autophagy machinery of the host cell, and the PV membrane (PVM) becomes decorated with several autophagy markers, including LC3 (microtubule-associated protein 1 light chain 3)^{3,4}. Here we show that *Plasmodium berghei* parasites infecting hepatic cells rely on the PVM transmembrane protein UIS3 to avoid elimination by host-cell-mediated autophagy. We found that UIS3 binds host LC3 through a non-canonical interaction with a specialized surface on LC3 where host proteins with essential functions during autophagy also bind. UIS3 acts as a bona fide autophagy inhibitor by competing with host LC3-interacting proteins for LC3 binding. Our work identifies UIS3, one of the most promising candidates for a genetically attenuated vaccine against malaria⁵, as a unique and potent mediator of autophagy evasion in *Plasmodium*. We propose that the protein-protein interaction between UIS3 and host LC3 represents a target for antimalarial drug development.

One key function of microtubule-associated protein 1 light chain 3 (LC3) is to facilitate the delivery of autophagosomal membranes to lysosomes⁶. Intriguingly, most LC3-decorated hepatic parasites seem to escape this fate^{3,4}. This implies that *Plasmodium* exo-erythrocytic forms (EEFs) actively disrupt the autophagic flux to avoid the deleterious effects of fusing the vacuole with lysosomes. The parasitophorous vacuole membrane (PVM) is ideally positioned to carry out this task, and several genetic studies point to the critical contribution of PVM-resident proteins to parasite survival^{5,7,8}. Nevertheless, a putative autophagy subversion activity in *Plasmodium* has yet to be discovered. Of the few PVM proteins identified thus far, UIS3, has the greatest impact on *Plasmodium* survival inside host hepatocytes^{5,9}. Parasites lacking UIS3 (*uis3*(-)) infect host cells, but disappear rapidly thereafter and fail to complete development⁵. To determine whether UIS3 influences *Plasmodium*'s susceptibility to host autophagy, we allowed *uis3*(+) and *uis3*(-) *P. berghei* parasites to infect HepG2 cells that had been depleted of Atg5 or Rab7 to arrest the autophagic flux in early (LC3 membrane conjugation) and late (lysosomal fusion) stages, respectively^{10,11} (Fig. 1a and Supplementary

Fig. 1a,b). Consistent with previous reports⁵, *uis3*(-) parasites were virtually undetectable in control HepG2 cells, and the few hepatic schizonts observed 65 h after infection did not express MSP1, the merozoite surface marker seen in fully mature *uis3*(+) parasites (Fig. 1b,c and Supplementary Fig. 1c). Strikingly, depletion of Atg5 or Rab7 in HepG2 cells was sufficient to fully revert the phenotype of *uis3*(-) mutants to a wild-type one (Fig. 1b,c and Supplementary Fig. 1c). With the autophagy flux of the host cell arrested, *uis3*(-) parasites behaved in the same way as their *uis3*(+) counterparts with respect to schizont abundance as well as MSP1 expression (Fig. 1b,c and Supplementary Fig. 1c). Parasites that complete the liver stage successfully induce the release of blood-infective merozoite-filled sacs (merosomes) from infected cells¹². To test the viability of the *uis3*(-) progeny released by HepG2-infected cells, we collected the cell culture supernatants (HepG2 SN) 65 h after infection, inoculated them into mice and monitored the onset of blood-stage infection by collecting blood samples daily (Fig. 1a). HepG2 SN from Atg5- or Rab7-depleted cells infected with *uis3*(-) mutants caused patent blood-stage infections within 4–5 days of mice inoculation, similar to mice inoculated with HepG2 SN derived from *uis3*(+)-infected cells (Fig. 1d–f). In stark contrast, HepG2 SN collected from control *uis3*(-) infected cells did not cause infection in mice (Fig. 1d–f). Thus, loss of autophagy during the liver stage fully restores *uis3*(-) infectivity. Additionally, the survival rates of *uis3*(-) and *uis3*(+) parasites in Atg3, Atg5 or Atg7 knockout mouse embryonic fibroblasts (MEFs) were also identical, whereas few *uis3*(-) mutants survived in wild-type MEFs (Fig. 1g). To obtain additional evidence that *uis3*(-) parasites are removed by host autophagy, newly invaded hepatoma cells were treated with chloroquine (CQ), a lysosomotropic alkalinizing agent that impairs the lysosomal degradation of autophagic cargo. CQ treatment, like genetic impairment of autophagy, rescued *uis3*(-) mutants (Fig. 1h). On rare occasions we were able to observe *uis3*(-) parasites that exhibited distinctive signs of having undergone fusion with LAMP1-positive lysosomes, most prominently, the presence of LAMP1 within the vacuole and loss of the PVM marker, UIS4 (Supplementary Fig. 1d). Thus, we conclude that *uis3*(-) mutants normally fail to establish liver-stage infections because they are promptly eliminated by host autophagy and that the critical function of UIS3 is to protect *Plasmodium* from this innate defence mechanism.

Next, we aimed to elucidate how UIS3 interferes with host autophagy. To that end, we complemented *uis3*(-) parasites with the UIS3 gene fused C-terminally to c-Myc (this parasite line will be referred

¹Instituto de Medicina Molecular, Faculdade de Medicina, Universidade de Lisboa, Lisboa, Portugal. ²Department of Molecular Microbiology, Center for Infectious Disease Research, Washington University School of Medicine, St Louis, MO, USA. ³Parasitology Department of Infectious Diseases, University of Heidelberg Medical School, Heidelberg, Germany. ⁴Present address: College of Veterinary Medicine, Iowa State University, Ames, IA, USA. Eliana Real and Lénia Rodrigues contributed equally to this work. *e-mail: mmota@medicina.ulisboa.pt

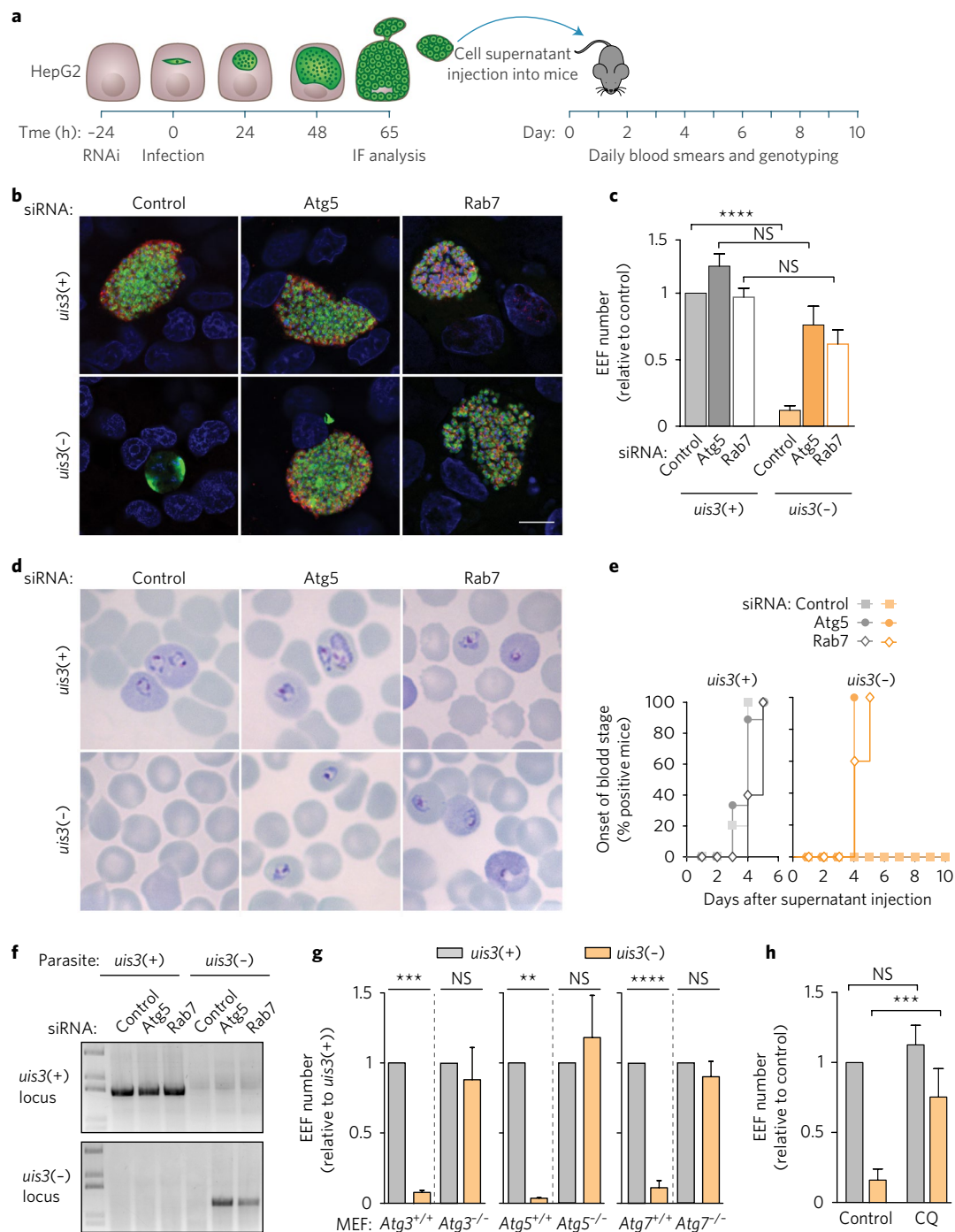


Fig. 1 | *Plasmodium* UIS3 protects liver-stage parasites from host autophagy. **a**, Timeline of HepG2 infection and cell supernatant (HepG2 SN) transfer into C57BL/6 mice. **b, c**, HepG2 cells treated with siRNAs to silence Atg5 or Rab7 expression and infected with *uis3*(+) or *uis3*(-) parasites were fixed 65 h after infection and immunostained with anti-MSP1 (red), anti-PbHsp70 (green) and Hoechst (blue). Panel **b** shows differentiated progeny surrounded by a ring of MSP1. Scale bar, 10 μ m. Panel **c** shows the number of exo-erythrocytic forms (EEFs), quantified by immunofluorescence (IF) microscopy. Mean \pm s.e.m. of pooled replicates from two (Atg5, Rab7) to four (control) independent experiments normalized to the control. **d**, Representative images of Giemsa-stained blood smears from C57BL/6 mice 10 days after receiving the indicated HepG2 SN. **e**, Onset of blood-stage parasitaemia following inoculation of C57BL/6 mice with the indicated HepG2 SN. Animals that received control *uis3*(-) HepG2 SN remained parasite free up to 30 days after inoculation. Data represent the per cent of mice (out of 5 to 10; two independent experiments) with positive blood smears. **f**, Genotype of blood-stage parasites collected 10 days after mice inoculation with the indicated HepG2 SN. Wild-type and knockout *uis3* genomic loci were amplified with specific primer sets. One representative mouse from each experimental group is shown. **g**, Control (Atg3^{+/+}, Atg5^{+/+}, Atg7^{+/+}) and autophagy-deficient MEFs (Atg3^{-/-}, Atg5^{-/-} and Atg7^{-/-}) were infected with *uis3*(+) or *uis3*(-) parasites, fixed at 48 h and labelled with anti-PbHsp70 and Hoechst. EEF numbers were quantified by microscopy and normalized to the *uis3*(+) control of each cell line. Bars represent mean \pm s.e.m. of five independent experiments. **h**, Huh7 cells treated with chloroquine (CQ) from 1 h to 24 h after infection with *uis3*(+) or *uis3*(-) parasites were immunostained with anti-PbUIS4, anti-PbHsp70 and Hoechst. The numbers of EEFs were quantified by microscopy in three independent experiments. Statistical significance was assessed using non-parametric two-tailed Mann-Whitney test. NS, $P > 0.05$; ** $P < 0.01$; *** $P < 0.001$; **** $P < 0.0001$.

to as *uis3-myc*) (Supplementary Fig. 2). Immunofluorescence analysis of liver-stage schizonts revealed that UIS3-myc co-localized with host LC3 and UIS4 to the PVM (Fig. 2a,b and Supplementary Fig. 3a,b). Of note, immuno-electron microscopy showed LC3 in direct association with the PVM, with no evidence of autophagosomal double membranes—a hallmark of canonical autophagy—forming around the PV (Fig. 2c). Prompted by these observations, we asked whether UIS3 might form a molecular complex with LC3. We allowed *uis3-myc* parasites to infect HeLa cells stably expressing

GFP-LC3 and, 24 h after infection, proceeded to immunoprecipitate UIS3-myc. Strikingly, GFP-LC3 was found to co-immunoprecipitate with UIS3 (Fig. 2d). We further confirmed this association in *P. berghei*-infected mouse primary hepatocytes (Supplementary Fig. 3c), thus ruling out the possibility of a potential artefact linked to GFP-LC3 over-expression. LC3 immunoprecipitation could not be detected in cells infected with *uis3(-)* mutants, which do not express UIS3 (Fig. 2d and Supplementary Fig. 3c). Next, we used recombinant UIS3 and LC3 to test whether the two proteins directly

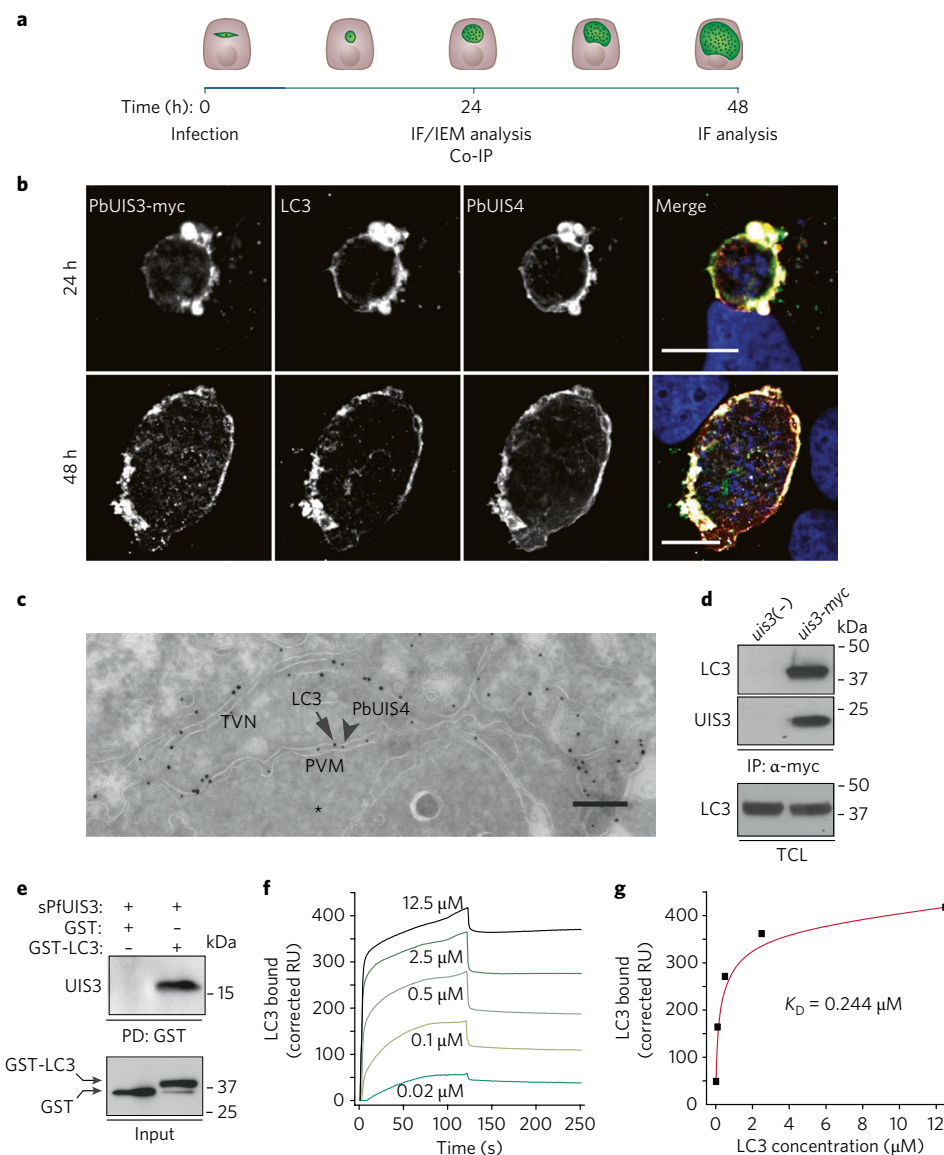


Fig. 2 | Plasmodium UIS3 binds to host LC3. **a**, Timeline of in vitro infection and analysis. **b**, Representative confocal images (two independent experiments) of Huh7 cells infected with *P. berghei* expressing UIS3-myc (*uis3-myc*). Cells were fixed 24 h (top) and 48 h (bottom) after infection and immunostained with anti-myc (white), anti-UIS4 (red), anti-LC3 (green) and Hoescht (blue). Scale bars, 10 μ m. **c**, Representative immunoelectron microscopy (IEM) micrograph of the host-parasite interface in a Huh7 cell 24 h after infection with *P. berghei*. PbUIS4 and host LC3 are shown labelled with 12 nm (arrowhead) and 18 nm (arrow) gold particles, respectively. The EEF cytosol is marked with an asterisk. The PbUIS4-positive structures correspond to the PVM and tubular-vesicular network (TVN) of the parasite. Scale bar, 200 nm. Seventeen randomly selected cells were analysed. **d**, Lysates of GFP-LC3 HeLa cells infected with *uis3-myc* or *uis3(-)* *P. berghei* were immunoprecipitated with anti-myc. Analysis of the precipitates was carried out by western blot with anti-LC3 and anti-myc antibodies (top and middle panels). Total cell lysates (TCL) were immunoblotted with anti-LC3 (bottom panel). **e**, Purified GST or GST-LC3 were used as bait to pull down recombinant His-tagged sPfUIS3. Pull-down fractions were immunoblotted with anti-GST and anti-His antibodies. One of four independent experiments is shown (**d,e**). **f**, Binding of GST-LC3 to sPfUIS3 immobilized on a sensor chip was analysed by surface plasmon resonance (SPR). The indicated concentrations of GST-LC3 were perfused over the sPfUIS3-coated sensor. Normalized response sensorgrams were calculated by subtracting the unspecific binding contribution of the same molar concentrations of GST alone. **g**, SPR response units (RU) at equilibrium plotted as a function of LC3 concentration. The dissociation constant of the interaction, K_D , is shown.

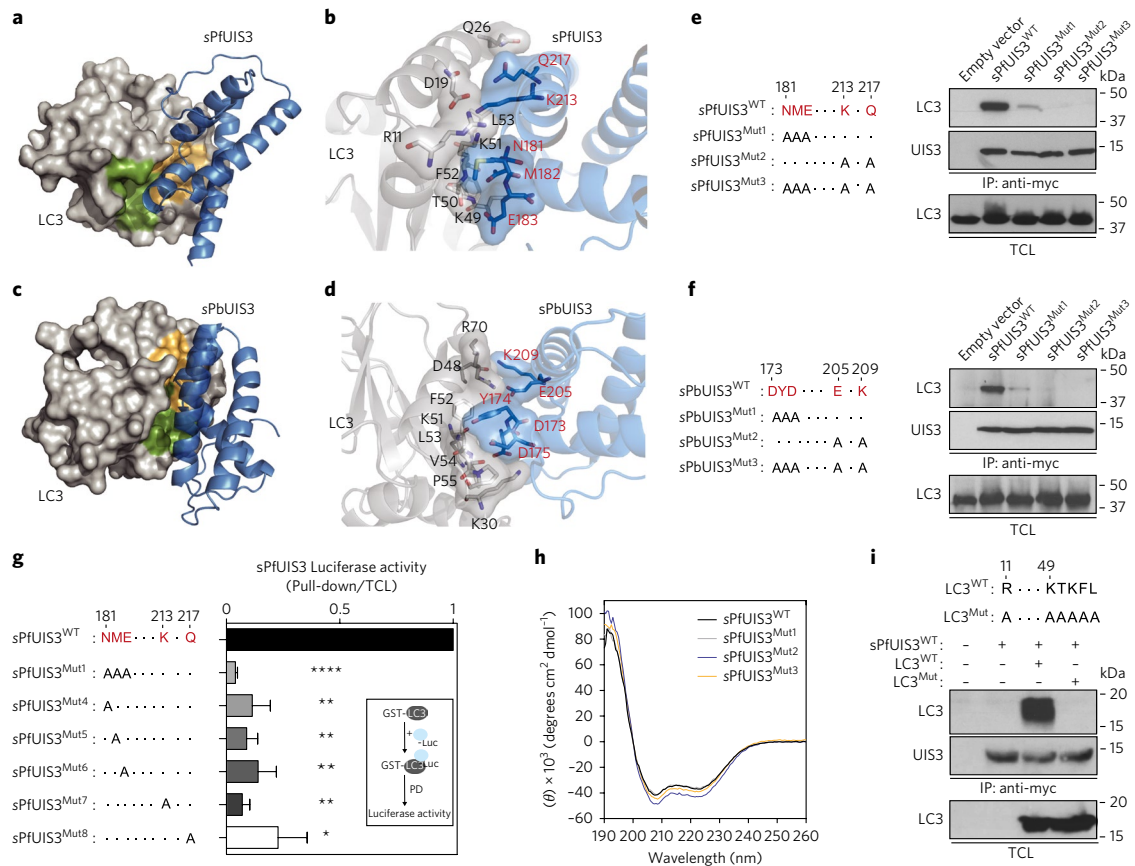


Fig. 3 | Non-canonical binding of *Plasmodium* UIS3 to the LIR pocket of LC3. **a–d**, Representations of the putative complex between the soluble domain of UIS3 and LC3 obtained by molecular docking. The LC3 areas depicted in green and orange represent the two hydrophobic pockets responsible for the recognition of LIR motifs and overlap significantly with the surface recognized by UIS3 (Supplementary Fig. 5d,e). All key interacting amino acids are highlighted in black (LC3) and red (UIS3). *P. falciparum* (**a,b**) and *P. berghei* complexes (**c,d**) are shown. **e,f**, Lysates of GFP-LC3 HeLa cells expressing the indicated sPfUIS3 (**e**) or sPbUIS3 (**f**) myc-tagged proteins (amino acid substitutions shown on the left) were immunoprecipitated with anti-myc. Precipitates were analysed by western blot with anti-LC3 (top panels) and anti-myc (middle panels). TCL were immunoblotted with anti-LC3 (bottom panels). **g**, Relative contribution of single amino acid substitutions (shown on the left) to the binding of luciferase-tagged sPfUIS3 to recombinant GST-LC3. Inset: outline of the pull-down assay. The average + s.e.m. of two independent experiments is shown. **h**, CD spectra of sPfUIS3 recombinant proteins (wild-type and indicated mutants). Each spectrum is the average of 10 technical replicates, corrected for the buffer background. **i**, Immunoprecipitation of myc-tagged sPfUIS3^{WT} from HeLa cell lysates co-expressing the indicated HA-tagged LC3 proteins (amino acid substitutions shown on top). Precipitates were probed with anti-HA (top panel) and anti-myc (middle panel). The bottom panel shows the levels of LC3 in TLC. One representative immunoblot of at least three independent experiments is shown in **e, f** and **i**. Statistical significance was assessed using an unpaired two-tailed *t*-test. **P* < 0.05; ***P* < 0.01; ****P* < 0.0001.

associate. Full-length UIS3 comprises a signal peptide, a short intravacuolar N-terminal domain, a transmembrane anchor and a C-terminal domain that spans residues 83–229 and is predicted to be exposed to the host cytosol. Previous studies reported that the C-terminal domain of *P. falciparum* UIS3 is prone to dimerization, but undergoes proteolytic cleavage in solution, yielding a stable and soluble monomeric fragment consisting of residues 130–229 (hereafter referred to as soluble UIS3, sPfUIS3)¹³. Using recombinant GST-LC3, we were able to pull down recombinant His-tagged sPfUIS3 (Fig. 2e). The dissociation constant (K_D) for the complex measured by surface plasmon resonance was 0.244 μ M (Fig. 2f,g). Despite being co-localized with both UIS3 and UIS4 on the PVM, LC3 was shown to co-immunoprecipitate with sPbUIS3, but not with the corresponding C-terminal domain of PbUIS4 (Supplementary Fig. 3d). We also did not observe co-immunoprecipitation of L-FABP with recombinant sPfUIS3 (Supplementary Fig. 3e), in line with previous work suggesting that the reported interaction between the C terminus of *Plasmodium yoelii* UIS3 and mouse L-FABP (ref. 14) might be species-specific¹⁵. Collectively, these data demonstrate that

the distal C-terminal subdomain of UIS3, spanning amino acids 130–229, binds to LC3 directly. Our data establish that UIS3 forms a molecular complex with LC3, but the association of LC3 with the PVM was found to be host-driven (two core components of the LC3 conjugation system, Atg3 and Atg5, were shown to be essential and independent of UIS3 (Supplementary Fig. 4a–d). In contrast, neither ULK1, the AMPK-regulated autophagy-initiating kinase, nor the autophagy receptors p62 and NDP52, all previously implicated in xenophagy¹⁶, were required (Supplementary Fig. 4e–g). This is consistent with recent reports highlighting the role of Atg5 and the lack of involvement of the autophagy-initiation complex in targeting LC3 to the PVM (refs. 3,17). LC3 association with the PVM was also unaffected by reactive oxygen species (ROS) scavengers (Supplementary Fig. 4h,i), implying that the host response against *Plasmodium* is mechanistically unrelated to LC3-associated phagocytosis (LAP). LAP has been described as a microbicidal pathway wherein elements of the LC3 conjugation system transfer LC3 in a ROS-dependent manner to pathogen-containing phagosomes¹⁸. Intriguingly, the pathway leading to *Plasmodium* targeting by autophagy appears to

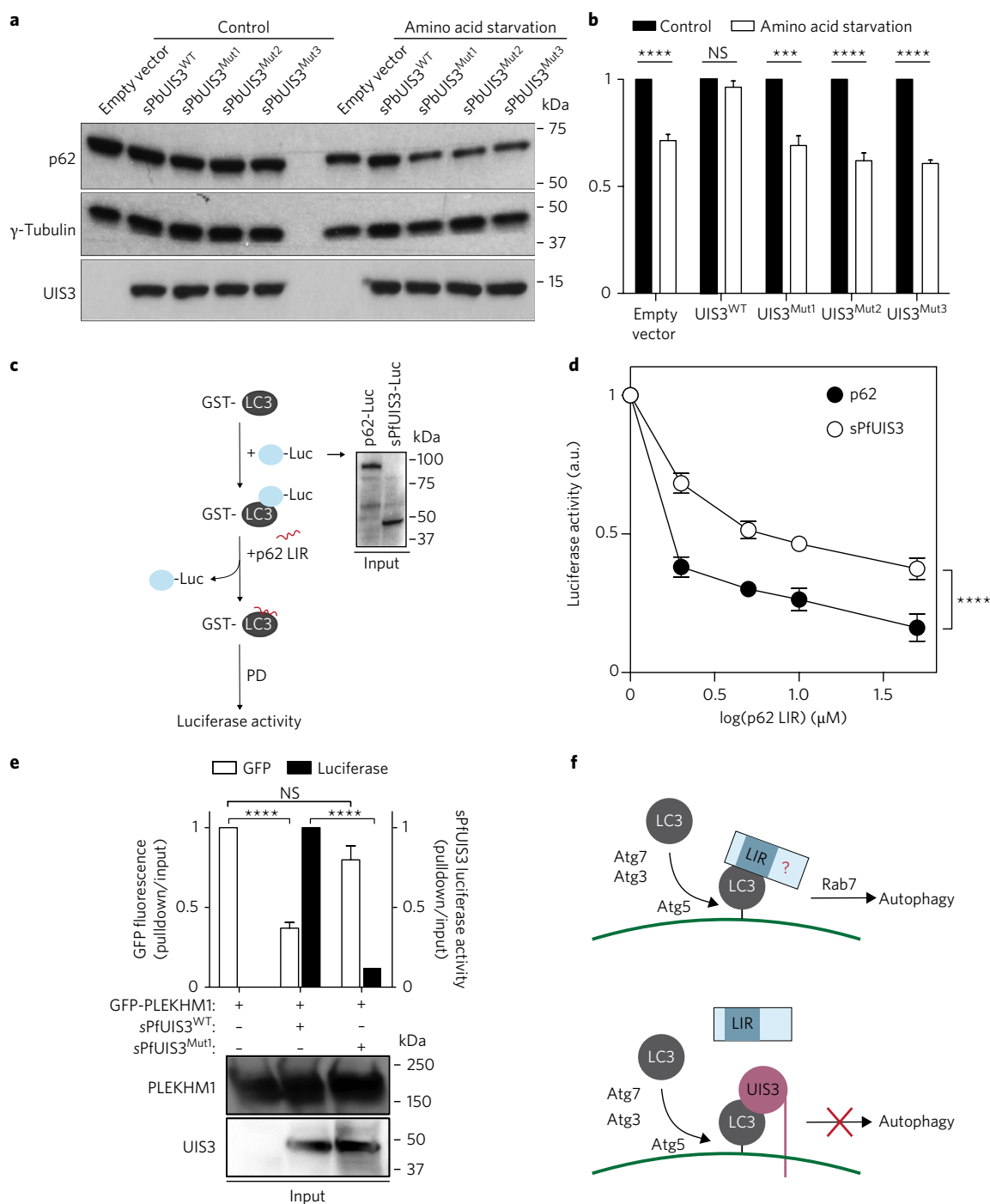


Fig. 4 | UIS3 acts as a bona fide autophagy inhibitor by competing with host LC3-interacting proteins for LC3 binding. **a**, Western blot analysis of p62 levels in HeLa cells expressing the indicated sPbUIS3 proteins and kept for 8 h in complete (control) or amino-acid-depleted medium (amino acid starvation). Whole-cell lysates were analysed by western blot for p62, tubulin and UIS3-myc. Immunoblots representative of five independent experiments are shown. **b**, The levels of p62 before and after amino acid starvation were calculated as the ratio of p62 to tubulin. Bars represent mean + s.e.m. of five independent experiments. **c**, Outline of LUMIER competition assay. The assay measures the amount of p62 LIR peptide necessary to displace luciferase-tagged p62 or sPbUIS3 from their complexes with recombinant GST-LC3. Inset: input levels (detected with anti-*Renilla* luciferase) of luciferase-tagged p62 and sPbUIS3 in one (of three) representative experiments. **d**, Binding of luciferase-tagged p62 or sPbUIS3 to recombinant GST-LC3 in the presence of the indicated concentrations of p62 LIR. The mean + s.e.m. of three independent experiments is shown. For the data points corresponding to 2 and 5 μM of p62 LIR, $n = 2$. **e**, Recombinant GST-LC3 was used to pull down extracts of HEK 293T cells co-transfected with the indicated plasmids. The ratio of PLEKHM1 and sPbUIS3 in the pull-down versus input was calculated from the GFP and luminescence signals of each fraction. The bottom panels show the levels of PLEKHM1 and UIS3 in the input extract. Bars represent average + s.e.m. of three independent experiments. Statistical significance was assessed using unpaired two-tailed *t*-tests in **b** and **e** and two-way ANOVA in **d**. NS, $P > 0.05$; *** $P < 0.001$; **** $P < 0.0001$. **f**, Summary of the observed effects of *Plasmodium* UIS3 on host autophagy. Antiplasmodial autophagy depends on the LC3 conjugation machinery and on lysosome-associated Rab7, with unidentified LIR-motif proteins mediating one or several steps leading to lysosomal fusion. The C terminus of UIS3 binds to the LIR-docking site on LC3, rendering the site inaccessible for autophagy-promoting interactions.

be inhibited by ULK1. Indeed, we observed significantly higher levels of PVM-associated LC3 upon knockdown of ULK1 expression (Supplementary Fig. 4f). These results confirm the unconventional nature of the host autophagy response against *Plasmodium* and imply that the association of LC3 to the PVM precedes the UIS3–LC3 interaction.

Whereas LC3 binding partners typically contain an LC3-interacting region (LIR) with the consensus sequence W/F-x-x-I/L/V (refs 19,20), UIS3 lacks this canonical LIR (Supplementary Fig. 5a). To gain further insight on the specific mode of binding of UIS3 to LC3, we modelled the three-dimensional structure of the putative complex between sPfUIS3 or sPbUIS3 and LC3 using a molecular docking algorithm and the published X-ray structures of sPfUIS3 (ref. 13) and LC3B (ref. 21) (Fig. 3a–d and Supplementary Fig. 5). Our *in silico* analysis predicted that the interaction is likely to be driven by a flexible turn between helices $\alpha 2$ and $\alpha 3$ of UIS3 (N181, M182 and E183 in *P. falciparum* UIS3) and the $\beta 2$ strand of LC3 (Fig. 3a,b). The complex appears also to be stabilized by polar interactions involving K213 and Q217 (Fig. 3b). In the *P. berghei* complex, the residues located in equivalent positions are D173, Y174 and D175, with E205 and K209 stabilizing the complex through electrostatic interactions (Fig. 3c,d). To validate these predictions, we substituted the above amino acids for alanine to measure the effect of the substitutions on UIS3 binding to LC3. Simultaneous or individual mutations on all five residues abolished the interaction of sPfUIS3 with LC3 (Fig. 3e,g). Similarly, alanine substitutions of the equivalent positions in sPbUIS3 abrogated binding to LC3 almost completely (Fig. 3f). Of note, the circular dichroism (CD) spectra of recombinant sPfUIS3 proteins harbouring the above mutations did not reveal any significant effect of the amino acid substitutions on protein conformation (Fig. 3h). Detailed analysis of the predicted LC3–UIS3 complexes from *P. berghei* and *P. falciparum* (Fig. 3a–d and Supplementary Fig. 5d,e) indicated that the LC3 surface where UIS3 putatively binds coincides with the surface recognized by autophagy proteins containing canonical LIR motifs, such as p62 (refs 19,20,22). Mutations of key residues in this LIR-binding LC3 surface to alanine abolished the interaction between sPfUIS3 and LC3 (Fig. 3i), as predicted. Thus, although UIS3 lacks a canonical LIR, our data demonstrate that the LIR-binding surface of LC3 can accommodate this atypical interaction.

Because UIS3 and canonical LIR motifs interact with the same region of LC3, we next hypothesized that UIS3 might interfere with the binding of LIR-containing proteins to LC3, thus interrupting the autophagic flux. To examine whether the UIS3–LC3 interaction represents a physiological autophagy subversion mechanism, we quantified the impact of heterologous UIS3 expression on the autophagic flux of HeLa cells. As a readout for autophagy, we monitored p62 degradation in response to amino acid starvation^{23,24}. Strikingly, sPbUIS3^{WT} inhibited the degradation of p62 induced by amino acid depletion, whereas UIS3 mutants had no effect (Fig. 4a,b). The data demonstrates that binding of UIS3 to LC3 disrupts the autophagic flux, hinting at the possibility that UIS3 functions as an autophagy inhibitor, through a hindrance effect on the LC3 surface. To explore this hypothesis, we set up a LUMIER-based competition assay²⁵ in which sPfUIS3 or p62 was complexed to GST–LC3 and subsequently incubated with increasing concentrations of the p62 LIR (ref. 22) (Fig. 4c). We found that higher concentrations of p62 LIR were necessary to disrupt the UIS3–LC3 complex compared to p62–LC3 (Fig. 4d). This is consistent with the lower K_D measured for the UIS3–LC3 interaction (Fig. 2g) compared to similar measurements for canonical LIR sequences²⁶. To determine how pervasive the UIS3 hindrance effect was, we examined the impact of sPfUIS3 on the association between the LIR-containing Rab7 effector PLEKHM1 (ref. 27) and recombinant GST–LC3. When sPfUIS3^{WT} and PLEKHM1 were co-expressed, LC3 pull-downs were significantly depleted of PLEKHM1 and enriched in UIS3, whereas

mutations that reduced the affinity of UIS3 for LC3 restored the PLEKHM1–LC3 association (Fig. 4e). Taken together, these observations not only demonstrate that *Plasmodium* UIS3 antagonizes LIR-mediated LC3 interactions by binding to a conserved LIR-interacting surface on LC3, but they also confirm UIS3 as a *bona fide* autophagy inhibitor.

In this study, we show that *Plasmodium* parasites escape autophagy by engaging host LC3 in an inhibitory interaction with the cytosolic domain of the PVM transmembrane protein UIS3. Our observations demonstrate that UIS3 competitively inhibits the binding of LIR-containing host proteins to the LIR-docking surface of LC3. This strongly suggests that the UIS3-mediated protection against antiplasmodial autophagy is a direct consequence of LC3 being sequestered into UIS3–LC3 complexes on the PVM (Fig. 4f and Supplementary Fig. 6). Although UIS3 is necessary to avert the potential deleterious effects of the association of LC3 to the PVM, whether *Plasmodium* succeeds in evading autophagy probably depends on how much of the PVM-associated LC3 is bound by UIS3. This, in turn, is determined by the levels of UIS3 expression and the robustness of the antiplasmodial response, both of which may diverge significantly between individual parasites and hosts, and could explain the vulnerability of *P. berghei* parasites to autophagy observed in previous reports^{3,4}.

Evidence that interferon (IFN)- γ enhances LC3 recruitment onto the PVM of *Plasmodium vivax*, causing parasite elimination²⁸, supports the idea that host autophagy may be chemically enhanced to suppress the protective effect of UIS3 expression. Repurposing autophagy-inducing drugs for malaria prophylaxis might thus be a safe and cost-effective way of breaking the transmission cycle in endemic areas. Whether clinically available autophagy inducers activate the non-canonical autophagy pathway targeting *Plasmodium* in hepatic cells remains to be determined. Of note, neither metformin nor rapamycin, two of the best known autophagy-inducing drugs, affect the number of infected cells *in vitro* or *in vivo*^{3,8,29}, supporting our observations that antiplasmodial autophagy is mechanistically distinct from the AMPK- and mTOR-regulated canonical autophagy pathway.

Recent reports underscored the risk of breakthrough infections in mice immunized with a *uis3(-)* *P. berghei* ANKA whole-organism vaccine³⁰. The data presented here suggest that host genetic or metabolic factors compromising the autophagy response might be the cause of such breakthrough infections. Although insufficiently safe on its own, UIS3 deletion is likely to improve the safety of any genetically attenuated whole-organism vaccine against malaria by enhancing the susceptibility of hepatic parasites to host autophagy. Additionally, with the spread of drug resistance casting a shadow over malaria eradication efforts, the protein–protein interaction between UIS3 and LC3 constitutes a promising new target for tailored pharmacological interventions aiming at controlling *Plasmodium* liver infection and disease.

Methods

Chemicals. RPMI 1640, DMEM, EBSS and other cell culture reagents were purchased from Gibco Invitrogen. All chemicals were from Sigma-Aldrich, unless specified otherwise. Lipofectamine (Invitrogen) was used for transfection of HepG2 cells. siRNAs were transfected using Lipofectamine RNAiMAX in OptiMEM (Invitrogen).

Cell lines. Huh7, HepG2 and HEK 293T (ATCC) cells were cultured under standard conditions in RPMI 1640 (Huh7) or DMEM (HepG2 and HEK 293T) medium supplemented with 10% FCS, 1% non-essential amino acids (RPMI 1640), 1% glutamine, 1% penicillin/streptomycin, and 1% HEPES. Mouse embryonic fibroblasts (MEFs) were obtained from the Riken BioResource Center (*Atg5^{+/+}* (RCB2710) and *Atg5^{-/-}* (RCB2711))³¹, M. Komatsu, Tokyo Metropolitan Institute of Medical Science (*Atg3^{+/+}* and *Atg3^{-/-}*)³² and T. Finkel, NIH National Heart, Lung, and Blood Institute (*Atg7^{+/+}* and *Atg7^{-/-}*)³³. HeLa cells expressing GFP-LC3 were a gift from T. Hyman, MPI-CBG. MEFs and HeLa cells were maintained in DMEM supplemented as before. MEFs were validated through quantitative reverse transcription PCR (qRT-PCR) and HeLa cells were tested for the expression of

GFP-LC3 by western blot. All cell lines were routinely tested for mycoplasma contamination.

Mice. All mice used in this study were C57BL/6J males, between 6 and 8 weeks of age, housed in the animal facility of the Instituto de Medicina Molecular in Lisbon. All protocols were approved by the internal animal care committee of the Instituto de Medicina Molecular and were performed according to national and European regulations.

Mouse primary hepatocytes. Mouse primary hepatocytes were isolated using a modified two-step perfusion protocol followed by a Percoll purification step^{34,35}. Briefly, mice were sacrificed by CO₂ inhalation and immediately processed for cannulation of the portal vein using a 26-gauge needle. Next, the inferior vena cava (IVC) was cut to allow fluid to drain. Liver perfusion medium (LPM) was perfused at 8–9 ml min⁻¹ for 10 min, followed by liver digestion medium (LDM), also at a rate of 8–9 ml min⁻¹ for 10 min. Intermittent clamping of the IVC (3 s clamp every 30 s) was performed during LDM perfusion to improve tissue digestion. After digestion, the liver was excised and the cells were liberated by tearing and shaking of the liver with forceps. The cell suspension was then sequentially filtered through a 100 µm and a 70 µm cell strainer and spun at 50g for 3 min. The cell pellet was resuspended in Williams's Medium E with 10% of fetal calf serum (FBS) and carefully overlaid on a 60% Percoll solution (1:1). The cell suspension was fractionated by centrifugation at 750g for 20 min, without break, at 20 °C. Viable hepatocytes deposited in the pellet were washed with Williams's Medium E with 10% FBS, spun at 50g for 3 min and resuspended in complete Williams's Medium E (supplemented with 4% FBS and 1% penicillin/streptomycin). Viability and yield were assessed by trypan blue staining. Viable hepatocytes were plated on collagen-coated 24-well plates.

RNAi. HepG2 cells were reverse-transfected with target-specific SMARTpool siRNA pools, as previously described³⁶. Non-targeting SMARTpool siRNA was used as a negative control (Dharmacon, GE Healthcare). The efficiency of knockdown was assessed 48 h after transfection by qRT-PCR using kits from Applied Biosystems. Gene expression levels were normalized against those of hypoxanthine guanine phosphoribosyltransferase (Hprt1). The primer pairs used for qRT-PCR reactions are listed in Supplementary Table 3.

Parasite lines. *P. berghei* sporozoites were obtained through dissection of the salivary glands of infected female *Anopheles stephensi* mosquitoes bred at the Instituto de Medicina Molecular. The following parasite lines were used: GFP-expressing *P. berghei* ANKA (259cl2, Leiden Malaria Research Group), *uis3(-)*³⁷, *uis3(+)* and *uis3-myc P. berghei* NK65 (generated for this study).

Plasmodium transfection. *P. berghei uis3-myc* and *uis3(+)* were obtained by complementing the *uis3(-)* parasite line via single crossover recombination as described in Supplementary Fig. 2. Transfection was carried out by electroporation of purified schizonts as previously described³⁷. Parasites were selected with WR99210 (provided by Jacobus Pharmaceuticals) for four consecutive days, collected on day 10 post-transfection and genotyped by PCR with the primers listed in Supplementary Table 2.

Infections. Hepatoma cells, MEFs and mouse primary hepatocytes were plated on 24-well culture plates at a density of 65,000, 50,000 and 120,000 cells per well, respectively. Cells were infected with freshly dissected *P. berghei* sporozoites (30,000 per well) 1 day after seeding and processed for analysis at 24 h or 48 h. siRNA-treated HepG2 cells were infected with *uis3(+)* or *uis3(-)* sporozoites 36 h after siRNA transfection and cultured for another 65 h in standard medium supplemented with 0.3% Fungizone. At 65 h, the entire volume of cell culture medium (HepG2 SN) in each well was collected and immediately inoculated into mice (1 well for each animal). The onset of blood-stage parasitaemia was monitored through Giemsa-stained thin blood smears by two unblinded independent observers. The smears were analysed daily from day 1 to day 10 after inoculation, when most animals suffered from hyperparasitaemia and had to be killed. On day 10, parasite genomic DNA was extracted from the blood of each experimental animal for parasite genotyping. The primer pairs used to probe the *uis3* wild-type and knockout genomic loci are listed in Supplementary Table 2. For ROS-scavenging experiments, Huh7 cells were incubated for 2 h in complete medium supplemented with 20 mM *N*-acetylcysteine (NAC), before sporozoite addition. Chloroquine (50 µM) was added to hepatoma cells 1 h after sporozoite infection.

Plasmids. The plasmids used in this study are listed in Supplementary Table 1. All *Plasmodium* sequences (except single point mutants) and human LC3B were chemically synthesized and subcloned into pCMV-Myc-N or pCMV-HA-N expression vectors (Clontech) using the EcoRI and KpnI restriction sites (GeneArt, Invitrogen). The *Renilla* luciferase sequence was chemically synthesized (GeneArt, Invitrogen) and subcloned into pCMV-MYC-sPfUIS3 using the EcoRI restriction site. Single point mutants of sPfUIS3 were obtained by site-directed mutagenesis using the primers listed in Supplementary Table 4 and the

QuickChange II site-directed mutagenesis kit (Agilent Technologies), following the manufacturer's instructions. For production of His6-sPfUIS3 (WT and mutants), the soluble domain of *P. falciparum* UIS3 was amplified from pCMV-MYC-sPfUIS3 (forward primer: 5'CATGGGATCCATGGAGCAGAAGCTG3'; reverse primer: 5'CCGGGTCTCGAGTCAGTTCTCTTCT3) and cloned into pET28a (Novagen). All plasmids were verified by sequencing. *Plasmodium* sequences were optimized for expression in mammalian cells.

Immunofluorescence. Cells plated on glass coverslips were fixed in 4% paraformaldehyde (ChemCruz) for 10 min at room temperature (RT) and permeabilized/blocked with a solution of 0.2% saponin-1% BSA. For immunostaining, samples were incubated with primary antibodies diluted in blocking solution (2 h, RT), washed with PBS, incubated for 1 h at RT with AlexaFluor-conjugated secondary antibodies (Jackson ImmunoResearch Laboratories) and Hoechst 33342 (Invitrogen) and washed again. The coverslips were then mounted on microscope slides with Fluoromount (SouthernBiotech). The following primary antibodies were used for confocal microscopy: LC3 (mouse monoclonal, MBL, M152-3), c-Myc (mouse monoclonal, MBL, M192-3), PbHSP70 (2E6³⁸), PbUIS4³⁹ (goat polyclonal, SicGen, AB0042-200), LAMP1 (rabbit polyclonal, Sigma, L1418) and PbMSP1²⁹ (rabbit polyclonal, GenScript, custom-made). All images were acquired on Zeiss confocal microscopes (LSM 510 META or LSM 710) and processed in ImageJ. For co-localization analysis, the region of interest (ROI) corresponding to the PVM was defined by thresholding the UIS4 signal, after which the Manders coefficients M1 and M2 within the ROI were calculated using the Colocalisation Threshold plugin from ImageJ. For infection quantification by microscopy, parasites were detected with anti-PbHSP70 (2E6) and anti-PbMSP1 on a Zeiss Axiovert 200M wide-field microscope equipped with an automated stage. All images (42 per coverslip) were processed and analysed using ImageJ.

Immuno-EM. Huh7 cells were fixed 24 h after infection with 4% paraformaldehyde-0.05% glutaraldehyde in 100 mM PIPES-0.5 mM MgCl₂ (pH 7.2) for 1 h at 4 °C and processed as described previously³⁹. Sections were stained with antibodies against human LC3 (mouse monoclonal, MBL, M152-3) and UIS4 (goat polyclonal, SicGen, AB0042-200), followed by gold-conjugated secondary antibodies (Jackson ImmunoResearch Laboratories), and viewed on a JEOL 1200 EX transmission electron microscope (JEOL).

Molecular docking of UIS3-LC3 complexes. Homology models of the UIS3 soluble domains belonging to different *Plasmodium* species and human LC3 were built with the Phyre2 server (<http://www.sbg.bio.ic.ac.uk/phyre2/html/page.cgi?id=index>) using the crystal structures of *P. falciparum* UIS3 (PDB code: 2VWA) and LC3B (PDB code: 2ZJD) as reference models. The quality of the homology models obtained was improved by atomic coordinate refinement using a two-step atomic-level energy refinement protocol implemented in ModRefiner software⁴⁰. Experimental and homology-derived protein coordinates were then used to construct models of the human and mouse UIS3-LC3 complexes by flexible molecular docking with the Swarmdock algorithm⁴¹. LC3 proteins were considered as receptors and UIS3 as ligands. For each complex, an initial set of 100 ligand starting positions was generated in the space around the receptor, being further optimized by energy minimization. The top 10 docking solutions were ranked by increasing free energy and submitted to an additional energy minimization cycle by conjugated gradient during 1,000 steps with GROMACS⁴², to avoid potential steric clashes between contact atoms. Visual inspection and cross comparison between the docking results obtained for the human and mouse complex showed a conserved pattern of molecular orientations for the top five docking solutions. Consensus residues involved in UIS3-LC3 interactions in the best docking solution were determined using CONS-COCOMAPS application⁴³ and graphically represented with LigPlot+ software⁴⁴.

Co-immunoprecipitation. HeLa cells expressing GFP-LC3 were transfected with plasmids encoding c-Myc or HA fusion proteins (Supplementary Table 1) on 10 cm dishes and collected 48 h after transfection in lysis buffer (0.5% NP-40, 150 mM NaCl, 10 mM Tris-Cl pH 7.4, 0.5 mM EDTA) supplemented with Complete protease inhibitor and PhosStop phosphatase inhibitor cocktails (Roche). On some experiments, HeLa cells were co-transfected with both myc-UIS3 and HA-tagged LC3. c-Myc- and HA-tagged proteins were purified from total cell lysates using the c-Myc-tagged protein mild purification kit and the HA-tagged protein purification kit, respectively, according to the manufacturer's instructions (MBL). GFP-LC3 was immunoprecipitated from total cell lysates using GFP-Trap coupled to agarose beads (Chromotek). For immunoprecipitation of parasite-encoded UIS3-myc from infected cells, HeLa cells or mouse primary hepatocytes were lysed 24 h after infection with *uis3-myc P. berghei* and total cell lysates were processed as described above. Co-immunoprecipitated proteins and total cell lysates were analysed by western blot using antibodies against LC3 (rabbit polyclonal, MBL, PM036) and c-Myc (mouse monoclonal, MBL, M192-3) or HA tags (mouse monoclonal, Biologend, 901503) to detect UIS3 or UIS4, followed by HRP-conjugated secondary antibodies (Jackson ImmunoResearch Laboratories). Immunoblots were developed using Luminata Crescendo Western HRP substrate reagent (Merck Millipore).

Expression and purification of recombinant proteins. *Escherichia coli* BL21 cells were transformed with GST-His-tagged LC3 or GST-His bacterial expression vectors. After overnight culture in Luria-Bertani (LB) broth, cells were diluted 1/100 in fresh medium to an optical density (OD) of ~0.7 and incubated with 0.3 mM IPTG for 5 h to induce expression of the recombinant proteins. All cultures were performed at 37 °C with vigorous shaking. For expression of His-tagged sPflUIS3^{WT}, *E. coli* BL21 C43 bacteria were used. Cells grown overnight in LB broth were diluted 1/100 in fresh medium to an OD of ~1.2. Recombinant protein expression was induced by the addition 0.3 mM IPTG and overnight culture at 25 °C. His-tagged sPflUIS3 mutants were expressed in *E. coli* BL21 bacteria. Overnight cell cultures were diluted 1/100 in LB supplemented with NZY auto-induction reagent (NZYTech). Recombinant His-tagged proteins were initially purified by metal chelating affinity chromatography using His-Trap Ni-containing columns (GE Healthcare) connected to an AKTA Explorer chromatographic system (GE Healthcare). The His-trap column (1 ml bed volume) was equilibrated with sodium phosphate buffer pH 6.8 containing 1 M NaCl and 25 mM imidazole before protein injection. His-tagged proteins were eluted by a linear gradient of imidazole from 25–500 mM in the same phosphate buffer. Fractions containing protein were collected and pooled and further polished by size exclusion chromatography purification using a Sephadex S-200 column (GE Healthcare) eluted with PBS. Fractions containing protein were analysed by SDS-PAGE, concentrated by ultrafiltration and stored at –80 °C in PBS buffer containing 15% glycerol.

Interaction between recombinant proteins. Recombinant sPflUIS3 (5 µg) was incubated with recombinant GST-His6-LC3 (10 µg) or with GST-His6 (5 µg), pre-adsorbed to glutathione beads in lysis buffer (150 mM NaCl, 20 mM Tris-HCl (pH 7.4), 0.1% Triton-X100, 5% glycerol, 5 mM EDTA and Complete protease inhibitors (Roche)). After washing, the complex was eluted in lysis buffer supplemented with 10 mM reduced L-glutathione (Sigma-Aldrich) and analysed by western blot with antibodies against LC3 (rabbit polyclonal, MBL, PM036) and c-Myc (mouse monoclonal, MBL, M192-3).

Surface plasmon resonance. Recombinant sPflUIS3 was immobilized on a Biacore CM5 chip surface following standard protocols provided by the manufacturer (GE Healthcare). In brief, recombinant sPflUIS3 was chemically immobilized via amine coupling to the free carboxyl groups on the CM5 chip through standard NHS (N-hydroxysuccinimide) and EDC (N-ethyl-N'-(dimethylaminopropyl) carbodiimide) activation procedures. Recombinant GST-His-LC3 dissolved in PBS buffer was injected over the immobilized sPflUIS3 at various concentrations to generate affinity sensorgrams that were collected in a single-cycle mode with no regeneration between sample injections. Unspecific binding was monitored by injecting recombinant GST-His protein over the sPflUIS3-coated chip under the same conditions. Normalized response sensorgrams were calculated by subtracting the unspecific binding contribution of the same molar concentrations of GST protein alone. All biosensor data processing and analysis and K_D calculations were performed using the Biacore T100 Evaluation Software (GE Healthcare version 2.01). For K_D calculation, a monovalent interaction model was assumed, with both proteins interacting with 1:1 stoichiometry.

Circular dichroism. Recombinant His-tagged sPflUIS3 proteins (wild type and mutants) used for circular dichroism were purified using a modification of the already described protocol, where the elution buffer of the size exclusion chromatography was substituted by 50 mM sodium phosphate, 200 mM NaF, pH 7.5. CD spectra of sPflUIS3 variants were collected between 190 and 260 nm in a JASCO J-815 spectropolarimeter (Tokyo, Japan) using 1 mm quartz cells from Hellma Analytics. Experiments were performed at 25 °C. Each CD spectrum corresponds to the average of 10 technical replicates, corrected for the buffer background contribution. Mean molar residue ellipticity values, $[\theta]$, were determined through the relationship⁴⁵

$$[\theta] = \frac{\theta}{Nlc}$$

where θ is the observed ellipticity, N is the number of amino acid residues in each protein, l is the quartz cell optical path length and c is the protein molar concentration.

Autophagy induction and p62 degradation assay. HeLa cells were changed from normal growth medium to EBSS to induce amino acid starvation-dependent autophagy. After 7 h, cells were collected in Laemmli buffer and analysed by western blot with antibodies against p62 (rabbit polyclonal, Sigma-Aldrich, P0067) and gamma-tubulin (mouse monoclonal, Sigma-Aldrich, T5326). The levels of p62 were measured by quantifying the ratio of p62 to tubulin signals with ImageJ.

LUMIER competition assay. HEK 293T cells transiently transfected with Luc-p62 or Luc-sPflUIS3 expressing plasmids (Supplementary Table 1) were lysed 24 h post-transfection in LUMIER lysis buffer (150 mM NaCl, 20 mM Tris-HCl (pH 7.4), 0.1% Triton-X100, 5% glycerol, 5 mM EDTA and Complete protease inhibitors (Roche))²⁵. The *Renilla* luciferase activity associated with each cell lysate

was assessed using the *Renilla* Luciferase Assay System (Promega). Equivalent saturating amounts of luciferase-tagged p62 or sPflUIS3 cell lysates were incubated with recombinant GST-His6-LC3B (500 ng), pre-adsorbed to glutathione beads. After washing away unbound protein, the precipitates were incubated with increasing concentrations of synthetic p62 LIR peptide (SGGDDDWTHLSSK) for 1 h with rotation, followed by elution in lysis buffer supplemented with 10 mM reduced L-glutathione (Sigma-Aldrich). The *Renilla* luciferase activity associated with LC3 after elution was quantified as described above using Tecan's Infinite 200M multiplate reader. The expression of luciferase-tagged p62 or sPflUIS3 was additionally detected with an anti-*Renilla* luciferase antibody (Abcam).

LUMIER/GFP assay. HEK 293T cells transiently transfected with PLEKHM1-GFP⁴⁶ and co-transfected with empty plasmid, Luc-sPflUIS3^{WT} or Luc-sPflUIS3^{Mut1} (Supplementary Table 1) were lysed 24 h post-transfection in LUMIER lysis buffer (150 mM NaCl, 20 mM Tris-HCl (pH 7.4), 0.1% Triton-X100, 5% glycerol, 5 mM EDTA and Complete protease inhibitors (Roche)). The cell lysates were incubated with recombinant GST-His6-LC3B (500 ng), pre-adsorbed to glutathione beads, for 2 h at 4 °C, with rotation. After washing away unbound proteins, pull-downs were eluted in lysis buffer supplemented with 10 mM reduced L-glutathione. GFP (excitation 420 nm, emission 520 nm) and *Renilla* luciferase activity associated with LC3 in each experimental condition were quantified using Tecan's Infinite 200M multiplate reader.

Statistical analysis. Data are expressed as means + s.e.m. Statistically significant differences between two different groups were determined using non-parametric two-tailed-Mann-Whitney test, unpaired two-tailed *t*-test or two-way ANOVA, as indicated. *P* values < 0.05 were considered statistically significant. Significances are represented in the figures as follows: NS, *P* > 0.05; **P* < 0.05; ***P* < 0.01; ****P* < 0.001; *****P* < 0.0001. All tests were carried out in GraphPad Prism. The experiments were not randomized. Sample sizes on mice experiments were chosen on the basis of historical data, and no statistical methods were used to predetermine sample size.

Life Sciences Reporting Summary. Further information on experimental design and reagents is available in the Life Sciences Reporting Summary.

Data availability. The data supporting the findings of this study are available within the paper and its Supplementary Information.

Received: 7 December 2016; Accepted: 5 October 2017;

Published online: 06 November 2017

References

- Liehl, P., Zuzarte-Luis, V. & Mota, M. M. Unveiling the pathogen behind the vacuole. *Nat. Rev. Microbiol.* **13**, 589–598 (2015).
- Gomes, L. C. & Dikic, I. Autophagy in antimicrobial immunity. *Mol. Cell* **54**, 224–233 (2014).
- Prado, M. et al. Long-term live imaging reveals cytosolic immune responses of host hepatocytes against *Plasmodium* infection and parasite escape mechanisms. *Autophagy* **11**, 1561–1579 (2015).
- Thieleke-Matos, C. et al. Host cell autophagy contributes to *Plasmodium* liver development. *Cell. Microbiol.* **18**, 437–450 (2016).
- Mueller, A.-K., Labaied, M., Kappe, S. H. I. & Matuschewski, K. Genetically modified *Plasmodium* parasites as a protective experimental malaria vaccine. *Nature* **433**, 164–167 (2005).
- Shen, H.-M. & Mizushima, N. At the end of the autophagic road: an emerging understanding of lysosomal functions in autophagy. *Trends Biochem. Sci.* **39**, 61–71 (2014).
- Mueller, A.-K. et al. *Plasmodium* liver stage developmental arrest by depletion of a protein at the parasite–host interface. *Proc. Natl Acad. Sci. USA* **102**, 3022–3027 (2005).
- Hanson, K. K. et al. Torins are potent antimalarials that block replenishment of *Plasmodium* liver stage parasitophorous vacuole membrane proteins. *Proc. Natl Acad. Sci. USA* **110**, E2838–E2847 (2013).
- Spielmann, T., Montagna, G. N., Hecht, L. & Matuschewski, K. Molecular make-up of the *Plasmodium* parasitophorous vacuolar membrane. *Int. J. Med. Microbiol.* **302**, 179–186 (2012).
- Mizushima, N. et al. Dissection of autophagosome formation using Apg5-deficient mouse embryonic stem cells. *J. Cell Biol.* **152**, 657–667 (2001).
- Ganley, I. G., Wong, P.-M., Gammoh, N. & Jiang, X. Distinct autophagosomal-lysosomal fusion mechanism revealed by thapsigargin-induced autophagy arrest. *Mol. Cell* **42**, 731–743 (2011).
- Sturm, A. et al. Alteration of the parasite plasma membrane and the parasitophorous vacuole membrane during exo-erythrocytic development of malaria parasites. *Protist* **160**, 51–63 (2009).
- Sharma, A., Yogavel, M., Akhouri, R. R., Gill, J. & Sharma, A. Crystal structure of soluble domain of malaria sporozoite protein UIS3 in complex with lipid. *J. Biol. Chem.* **283**, 24077–24088 (2008).

14. Mikolajczak, S. A., Jacobs-Lorena, V., MacKellar, D. C., Camargo, N. & Kappe, S. H. I. L-FABP is a critical host factor for successful malaria liver stage development. *Int. J. Parasitol.* **37**, 483–489 (2007).
15. Favretto, F., Assfalg, M., Molinari, H. & D'Onofrio, M. Evidence from NMR interaction studies challenges the hypothesis of direct lipid transfer from L-FABP to malaria sporozoite protein UIS3. *Prot. Sci.* **22**, 133–138 (2013).
16. Farré, J.-C. & Subramani, S. Mechanistic insights into selective autophagy pathways: lessons from yeast. *Nat. Rev. Mol. Cell Biol.* **17**, 537–552 (2016).
17. Wacker, R. et al. LC3-association with the parasitophorous vacuole membrane of *Plasmodium berghei* liver stages follows a noncanonical autophagy pathway. *Cell. Microbiol.* **19**, e12754 (2017).
18. Martinez, J. et al. Molecular characterization of LC3-associated phagocytosis reveals distinct roles for Rubicon, NOX2 and autophagy proteins. *Nat. Cell Biol.* **17**, 893–906 (2015).
19. Noda, N. N., Ohsumi, Y. & Inagaki, F. Atg8-family interacting motif crucial for selective autophagy. *FEBS Lett.* **584**, 1379–1385 (2010).
20. Birgisdottir, Á. B., Lamark, T. & Johansen, T. The LIR motif—crucial for selective autophagy. *J. Cell Sci.* **126**, 3237–3247 (2013).
21. Ichimura, Y. et al. Structural basis for sorting mechanism of p62 in selective autophagy. *J. Biol. Chem.* **283**, 22847–22857 (2008).
22. Pankiv, S. et al. p62/SQSTM1 binds directly to Atg8/LC3 to facilitate degradation of ubiquitinated protein aggregates by autophagy. *J. Biol. Chem.* **282**, 24131–24145 (2007).
23. Mizushima, N., Yoshimori, T. & Levine, B. Methods in mammalian autophagy research. *Cell* **140**, 313–326 (2010).
24. Klionsky, D., Abdalla, F. & Abeliovich, H. Guidelines for the use and interpretation of assays for monitoring autophagy. *Autophagy* **8**, 445–544 (2012).
25. Barrios-Rodiles, M. et al. High-throughput mapping of a dynamic signaling network in mammalian cells. *Science* **307**, 1621–1625 (2005).
26. Zaffagnini, G. & Martens, S. Mechanisms of selective autophagy. *J. Mol. Biol.* **428**, 1714–1724 (2016).
27. McEwan, D. G. et al. PLEKHM1 regulates autophagosome–lysosome fusion through HOPS complex and LC3/GABARAP proteins. *Mol. Cell* **57**, 39–54 (2015).
28. Boonhok, R. et al. LAP-like process as an immune mechanism downstream of IFN- γ in control of the human malaria *Plasmodium vivax* liver stage. *Proc. Natl Acad. Sci. USA* **113**, E3519–E3528 (2016).
29. Ruivo, M. T. G. et al. Host AMPK is a modulator of *Plasmodium* liver infection. *Cell Rep.* **16**, 2539–2545 (2016).
30. Kumar, H. et al. Protective efficacy and safety of liver stage attenuated malaria parasites. *Sci. Rep.* **6**, 26824 (2016).
31. Kuma, A. et al. The role of autophagy during the early neonatal starvation period. *Nature* **432**, 1032–1036 (2004).
32. Sou, Y. et al. The Atg8 conjugation system is indispensable for proper development of autophagic isolation membranes in mice. *Mol. Biol. Cell* **19**, 4762–4775 (2008).
33. Lee, I. H. et al. Atg7 modulates p53 activity to regulate cell cycle and survival during metabolic stress. *Science* **336**, 225–228 (2012).
34. Zhang, W. et al. PCB 126 and other dioxin-like PCBs specifically suppress hepatic PEPCK expression via the aryl hydrocarbon receptor. *PLoS ONE* **7**, e37103 (2012).
35. Gonçalves, L. A., Vigário, A. M. & Penha-Gonçalves, C. Improved isolation of murine hepatocytes for in vitro malaria liver stage studies. *Malar. J.* **6**, 169 (2007).
36. Itoe, M. A. A. et al. Host cell phosphatidylcholine is a key mediator of malaria parasite survival during liver stage infection. *Cell Host Microbe* **16**, 778–786 (2014).
37. Janse, C. J., Ramesar, J. & Waters, A. P. High-efficiency transfection and drug selection of genetically transformed blood stages of the rodent malaria parasite *Plasmodium berghei*. *Nat. Protoc.* **1**, 346–356 (2006).
38. Tsuji, M., Mattei, D., Nussenzweig, R. S., Eichinger, D. & Zavala, F. Demonstration of heat-shock protein 70 in the sporozoite stage of malaria parasites. *Parasitol. Res.* **80**, 16–21 (1994).
39. Fentress, S. J. et al. Phosphorylation of immunity-related GTPases by a *Toxoplasma gondii*-secreted kinase promotes macrophage survival and virulence. *Cell Host Microbe* **8**, 484–495 (2010).
40. Xu, D. & Zhang, Y. Improving the physical realism and structural accuracy of protein models by a two-step atomic-level energy minimization. *Biophys. J.* **101**, 2525–2534 (2011).
41. Torchala, M., Moal, I. H., Chaleil, R. A. G., Fernandez-Recio, J. & Bates, P. A. SwarmDock: a server for flexible protein–protein docking. *Bioinformatics* **29**, 807–809 (2013).
42. Pronk, S. et al. GROMACS 4.5: a high-throughput and highly parallel open source molecular simulation toolkit. *Bioinformatics* **29**, 845–854 (2013).
43. Vangone, A., Oliva, R. & Cavallo, L. CONS-COCOMAPS: a novel tool to measure and visualize the conservation of inter-residue contacts in multiple docking solutions. *BMC Bioinformatics* **13**(Suppl. 4), S19 (2012).
44. Laskowski, R. A. & Swindells, M. B. LigPlot+: multiple ligand–protein interaction diagrams for drug discovery. *J. Chem. Inf. Model.* **51**, 2778–2786 (2011).
45. Kelly, S. M., Jess, T. J. & Price, N. C. How to study proteins by circular dichroism. *Biochim. Biophys. Acta* **1751**, 119–139 (2005).
46. Van Wesenbeeck, L. et al. Involvement of PLEKHM1 in osteoclastic vesicular transport and osteopetrosis in incisors absent rats and humans. *J. Clin. Invest.* **117**, 919–930 (2007).

Acknowledgements

The authors thank M. Komatsu (Tokyo Metropolitan Institute of Medical Science) for providing Atg3 MEFs, T. Finkel (NIH National Heart, Lung, and Blood Institute) for the Atg7 MEFs, F. Randow (MRC Laboratory of Molecular Biology) for the gift of p62-luciferase and GST-LC3 expression plasmids, Jacobus Pharmaceuticals for the WR99210 compound, A. Parreira for producing *P. berghei*-infected *Anopheles* mosquitoes, and S. Marques and K. Slavic for their help with parasite cloning. This work was supported by grants from the European Research Council (ERC-2012-StG_311502 to M.M.M.), Fundação para a Ciência e Tecnologia (EXCL/IMI-MIC/0056/2012 to M.M.M. and PTDC/IMI-MICC/1568/2012 to G.G.C.) and Institut Mérieux (MRG_20052016 to M.M.M.). E.R. was the recipient of EMBO (ALTF 949-2008) and FCT (SFRH/BPD/68709/2010) fellowships. L.R. is the recipient of FCT fellowship SFRH/BPD/111323/2015. G.G.C. was sponsored by Marie Curie (PIEF-GA-2009-235864) and FCT (SFRH/BPD/74151/2010) fellowships. L.M.S. was supported by the European Community's Seventh Framework Programme (FP7/2007-2013) under grant agreement no. 242095 (EVI-MalaR). V.Z.L. was sponsored by EMBO (ALTF 357-2009) and FCT (BPD-81953-2011) fellowships. I.M.V. and J.M.-V. were supported by NIH (1F32A11042-5 021) and FCT (SFRH/BD/52226/2013) fellowships, respectively.

Author contributions

E.R. and M.M.M. conceived and led the study and wrote the manuscript. E.R., L.R., G.G.C. and J.M.-V. performed the experiments, acquired the data, performed data analysis and interpreted results. F.J.E. performed molecular docking, protein purification and SPR analysis. Animal experimentation was conducted by L.M.-S., L.R., I.M.V. and V.Z.-L. W.B. performed electron microscopy analysis. Circular dichroism was performed by T.N.F. G.R.M. constructed plasmids for parasite transfections. All authors read and approved the final manuscript.

Competing interests

The authors declare no competing financial interests.

Additional information

Supplementary information is available for this paper at <https://doi.org/10.1038/s41564-017-0054-x>.

Reprints and permissions information is available at www.nature.com/reprints.

Correspondence and requests for materials should be addressed to M.M.M.

Publisher's note: Springer Nature remains neutral with regard to jurisdictional claims in published maps and institutional affiliations.

Life Sciences Reporting Summary

Nature Research wishes to improve the reproducibility of the work that we publish. This form is intended for publication with all accepted life science papers and provides structure for consistency and transparency in reporting. Every life science submission will use this form; some list items might not apply to an individual manuscript, but all fields must be completed for clarity.

For further information on the points included in this form, see Reporting Life Sciences Research. For further information on Nature Research policies, including our data availability policy, see Authors & Referees and the Editorial Policy Checklist.

▶ Experimental design

1. Sample size

Describe how sample size was determined.

No statistical methods were used to pre-determine sample size. The sample size is specified in each figure legend and in Supplementary Table 5.

2. Data exclusions

Describe any data exclusions.

No data were excluded from the analysis.

3. Replication

Describe whether the experimental findings were reliably reproduced.

All attempts at replication were successful.

4. Randomization

Describe how samples/organisms/participants were allocated into experimental groups.

Microscopy analysis were performed on randomly acquired images. Mice were randomly assigned to each experimental group.

5. Blinding

Describe whether the investigators were blinded to group allocation during data collection and/or analysis.

No blinding was performed.

Note: all studies involving animals and/or human research participants must disclose whether blinding and randomization were used.

6. Statistical parameters

For all figures and tables that use statistical methods, confirm that the following items are present in relevant figure legends (or in the Methods section if additional space is needed).

- | n/a | Confirmed |
|--------------------------|--|
| <input type="checkbox"/> | <input checked="" type="checkbox"/> The <u>exact sample size</u> (n) for each experimental group/condition, given as a discrete number and unit of measurement (animals, litters, cultures, etc.) |
| <input type="checkbox"/> | <input checked="" type="checkbox"/> A description of how samples were collected, noting whether measurements were taken from distinct samples or whether the same sample was measured repeatedly |
| <input type="checkbox"/> | <input checked="" type="checkbox"/> A statement indicating how many times each experiment was replicated |
| <input type="checkbox"/> | <input checked="" type="checkbox"/> The statistical test(s) used and whether they are one- or two-sided (note: only common tests should be described solely by name; more complex techniques should be described in the Methods section) |
| <input type="checkbox"/> | <input checked="" type="checkbox"/> A description of any assumptions or corrections, such as an adjustment for multiple comparisons |
| <input type="checkbox"/> | <input checked="" type="checkbox"/> The test results (e.g. P values) given as exact values whenever possible and with confidence intervals noted |
| <input type="checkbox"/> | <input checked="" type="checkbox"/> A clear description of statistics including <u>central tendency</u> (e.g. median, mean) and <u>variation</u> (e.g. standard deviation, interquartile range) |
| <input type="checkbox"/> | <input checked="" type="checkbox"/> Clearly defined error bars |

See the web collection on statistics for biologists for further resources and guidance.

► Software

Policy information about availability of computer code

7. Software

Describe the software used to analyze the data in this study.

Software used to analyze data is specified in methods section, pages 6-12.

For manuscripts utilizing custom algorithms or software that are central to the paper but not yet described in the published literature, software must be made available to editors and reviewers upon request. We strongly encourage code deposition in a community repository (e.g. GitHub). *Nature Methods* guidance for providing algorithms and software for publication provides further information on this topic.

► Materials and reagents

Policy information about availability of materials

8. Materials availability

Indicate whether there are restrictions on availability of unique materials or if these materials are only available for distribution by a for-profit company.

All materials are available from standard commercial sources.

9. Antibodies

Describe the antibodies used and how they were validated for use in the system under study (i.e. assay and species).

References for all antibodies are provided in the Methods sections "Immunofluorescence", "Immuno-EM", "Co-Immunoprecipitation", and "Autophagy induction and p62 degradation assay", pages 9, 10 and 11 respectively.

10. Eukaryotic cell lines

a. State the source of each eukaryotic cell line used.

Cell line source is referenced in Methods section "Cell Lines", page 7, and "Parasite lines", page 8.

b. Describe the method of cell line authentication used.

Authentication was performed as described in Methods section "Cell Lines", page 7.

c. Report whether the cell lines were tested for mycoplasma contamination.

Cell lines were routinely tested for mycoplasma contamination, as specified in Methods section "Cell Lines", page 7.

d. If any of the cell lines used are listed in the database of commonly misidentified cell lines maintained by ICLAC, provide a scientific rationale for their use.

No commonly misidentified cell lines were used in this study.

► Animals and human research participants

Policy information about studies involving animals; when reporting animal research, follow the ARRIVE guidelines

11. Description of research animals

Provide details on animals and/or animal-derived materials used in the study.

Details on animals used is provided in Methods section "Mice" and "Mouse primary hepatocytes", page 7.

Policy information about studies involving human research participants

12. Description of human research participants

Describe the covariate-relevant population characteristics of the human research participants.

No human participants were used in this study.

3. Conklin, E.G. (1912). Cell size and nuclear size. *J. Exp. Zool.* **12**, 1–98.
4. Kellenberger, E., Ryter, A., and Séchaud, J. (1958). Electron microscope study of DNA-containing plasmids: II. Vegetative and mature phage DNA as compared with normal bacterial nucleoids in different physiological states. *J. Cell Biol.* **4**, 671–678.
5. Mason, D.J., and Powelson, D.M. (1956). Nuclear division as observed in live bacteria by a new technique. *J. Bacteriol.* **71**, 474–479.
6. Viollier, P.H., Thanbichler, M., McGrath, P.T., West, L., Meewan, M., McAdams, H.H., and Shapiro, L. (2004). Rapid and sequential movement of individual chromosomal loci to specific subcellular locations during bacterial DNA replication. *Proc. Natl. Acad. Sci. USA* **101**, 9257–9262.
7. Gray, W.T., Govers, S.K., Xiang, Y., Parry, B.R., Campos, M., Kim, S., and Jacobs-Wagner, C. (2019). Nucleoid size scaling and intracellular organization of translation across bacteria. *Cell* **177**, 1632–1648.
8. Wu, F., Swain, P., Kuijpers, L., Zheng, X., Felter, K., Guurink, M., Solari, J., Jun, S., Shimizu, T.S., Chaudhuri, D., *et al.* (2019). Cell boundary confinement sets the size and position of the *E. coli* chromosome. *Curr. Biol.* **29**, 2131–2144.
9. Rafelski, S.M., Viana, M.P., Zhang, Y., Chan, Y.-H.M., Thorn, K.S., Yam, P., Fung, J.C., Li, H., Costa, L.d.F., and Marshall, W.F. (2012). Mitochondrial network size scaling in budding yeast. *Science* **338**, 822–824.
10. Sengupta, D., and Linstedt, A.D. (2011). Control of organelle size: the Golgi complex. *Annu. Rev. Cell Dev. Biol.* **27**, 57–77.
11. Lioy, V.S., Cournac, A., Marbouty, M., Duigou, S., Mozziconacci, J., Espéli, O., Boccard, F., and Koszul, R. (2018). Multiscale structuring of the *E. coli* chromosome by nucleoid-associated and condensin proteins. *Cell* **172**, 771–783.
12. Le, T.B., Imakaev, M.V., Mirny, L.A., and Laub, M.T. (2013). High-resolution mapping of the spatial organization of a bacterial chromosome. *Science* **342**, 731–734.
13. Mondal, J., Bratton, B.P., Li, Y., Yethiraj, A., and Weisshaar, J.C. (2011). Entropy-based mechanism of ribosome-nucleoid segregation in *E. coli* cells. *Biophys. J.* **100**, 2605–2613.
14. Zimmerman, S.B., and Trach, S.O. (1991). Estimation of macromolecule concentrations and excluded volume effects for the cytoplasm of *Escherichia coli*. *J. Mol. Biol.* **222**, 599–620.
15. Parry, B.R., Surovtsev, I.V., Cabeen, M.T., O’Hern, C.S., Dufresne, E.R., and Jacobs-Wagner, C. (2014). The bacterial cytoplasm has glass-like properties and is fluidized by metabolic activity. *Cell* **156**, 183–194.
16. Nonejuie, P., Burkart, M., Pogliano, K., and Pogliano, J. (2013). Bacterial cytological profiling rapidly identifies the cellular pathways targeted by antibacterial molecules. *Proc. Natl. Acad. Sci. USA* **110**, 16169–16174.

Parasitism: *Anopheles* Mosquitoes and *Plasmodium* Parasites Share Resources

Maria M. Mota* and João Mello-Vieira

Instituto de Medicina Molecular João Lobo Antunes, Faculdade de Medicina, Universidade de Lisboa, Av. Prof. Egas Moniz, 1649-028, Lisboa, Portugal

*Correspondence: mmota@medicina.ulisboa.pt
<https://doi.org/10.1016/j.cub.2019.05.030>

Female *Anopheles* mosquitoes are the definitive hosts of *Plasmodium* parasites. A new study has found that successful establishment and development of *Plasmodium* in the *Anopheles* midgut requires mosquito oogenesis, without affecting egg production.

Female *Anopheles* mosquitoes are the definitive hosts of *Plasmodium* parasites, the causative agents of malaria. Mosquitoes become infected when they ingest a blood meal from a human carrying *Plasmodium* gametocytes, the sexual-stage parasite cells responsible for malaria parasite transmission. Shortly after the parasite is ingested, it crosses the mosquito’s midgut epithelium and encysts in the outer layer of the midgut, developing into an oocyst [1]. These oocysts develop for one to two weeks, growing, maturing and differentiating into hundreds of new sporozoites that can be injected into the next human host when the mosquito takes a new blood meal [1].

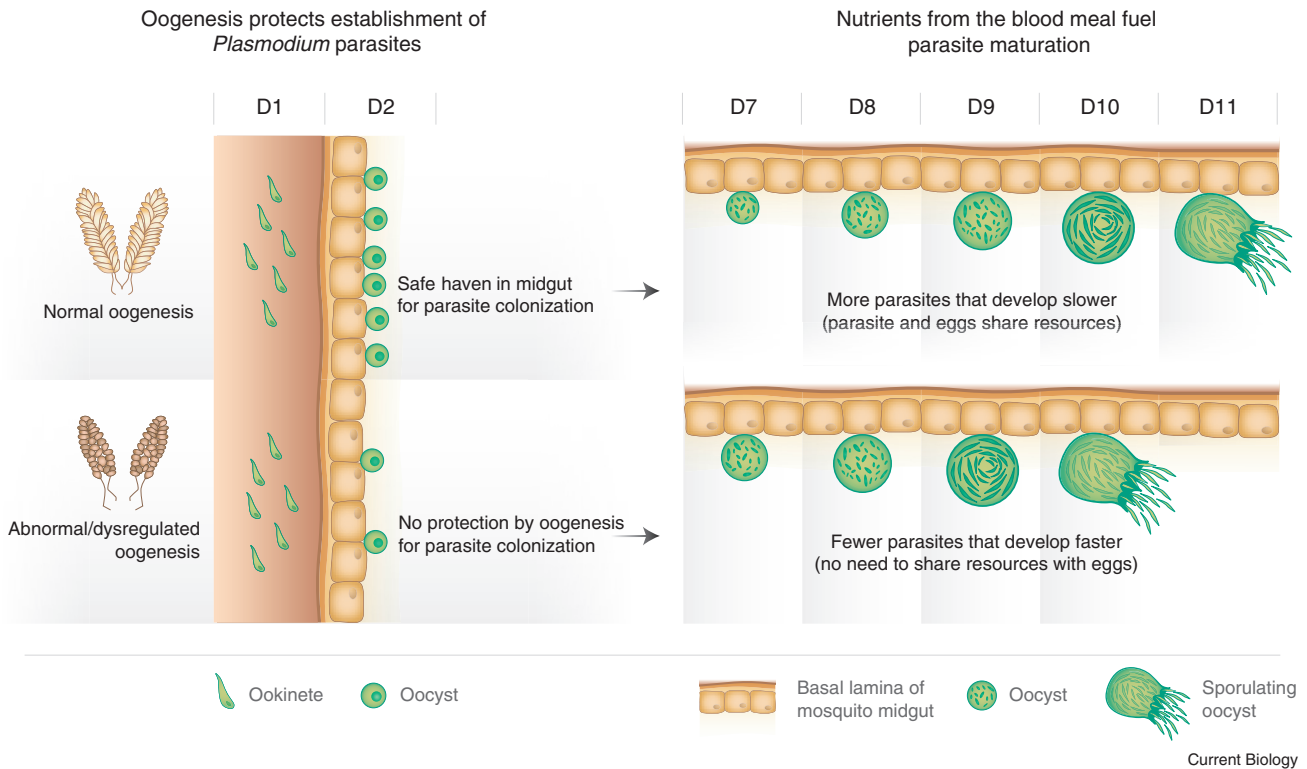
Importantly, although all adult *Anopheles* mosquitoes eat the nectar of

plants to get sugar, which provides enough nourishment for both males and females to live, females also take blood meals from animals to gather the necessary nutrients (including proteins) to produce eggs (reviewed in [2]). Nutrients from the blood are incorporated into eggs, which develop in the ovaries 2–3 days after blood feeding. Thus, when a mosquito bites a human that is carrying *Plasmodium* gametocytes, egg development and parasite maturation occur simultaneously. Since *Plasmodium* parasites take up nutrients from the mosquito to develop [3], it has been postulated that infection by *Plasmodium* should affect female reproductive fitness [4]. Remarkably, a new study by Werling, Shaw, Itoe and colleagues, recently published in *Cell*, shows that *Plasmodium*

falciparum parasites require mosquito oogenesis to survive in the midgut without affecting female reproductive fitness [5], implying a less parasitic and more commensal *Plasmodium–Anopheles* relationship.

To study the effect of parasite development on mosquito reproductive fitness, the authors first noticed that there is a positive correlation between the number of eggs produced by a female *Anopheles gambiae* and the number of *P. falciparum* oocysts it is infected with. Indeed, when Werling and colleagues used mosquitoes depleted of their germ line, which present underdeveloped ovaries, only one third the number of parasites were observed in the midgut, as compared to control mosquitoes





Current Biology

Figure 1. *Anopheles* oogenesis determines *Plasmodium* parasite survival in the midgut and nutrients are shared between developing parasites and mosquito eggs.

Oogenic signals protect *Plasmodium* parasites from elimination in the mosquito midgut during their transition from ookinete to oocyst (left panel, top line). Eggs and *Plasmodium* oocysts share nutrients from the blood meal, and oocysts mature within 11 days of mosquito infection (right panel, top line). When oogenesis is dysregulated, *Plasmodium* parasites struggle to colonize the midgut as they are eliminated by an as yet unknown mechanism (left panel, middle line). However, the lack of egg development allows *Plasmodium* parasites to mature faster, as more nutrients are available for oocyst growth (right panel, middle line).

(Figure 1, left panel). Moreover, the authors found that oocyst numbers were regulated by the ovarian hormone 20-hydroxyecdysone (20E). Yet, if the parasite infects the midgut of the mosquito, why are the ovaries and an ovarian hormone important for its establishment?

The 20E hormone is known to signal through nuclear receptors EcR and USP [6], changing the transcriptional profile in the ovaries and causing cells in this organ to take up more nutrients, particularly lipids, via the lipid shuttle lipophorin (the insect version of the mammalian lipoproteins) [7]. Therefore, the authors proceeded to knock down both nuclear receptors and observed that oocyst number dropped (Figure 1, left panel). As expected, lipophorin expression was deregulated, and the abundance of lipids in midguts increased when EcR was silenced.

Interestingly, the oocysts that escaped this bottleneck developed faster and gave

rise to sporozoites sooner, leading the authors to postulate that the higher abundance of lipids in the midgut might be driving the faster development of the surviving oocysts (Figure 1, right panel). To confirm this, the authors impaired lipolysis in the mosquito, increasing the levels of total lipids in the midgut, and observed that this led to faster development of oocysts. In both EcR-silenced mosquitoes and mosquitoes with increased levels of neutral lipids, parasites reached the salivary glands one day earlier than in control mosquitoes (Figure 1, right panel). Importantly, these premature parasites seemed to be as infectious to human hepatocytes as those from control mosquitoes, suggesting a dual impact of mosquito oogenesis on *Plasmodium*'s successful establishment in the mosquito: in the case of reduced oogenesis, the fewer *Plasmodium* oocysts that survive in the midgut develop faster and thus the blood meal must provide nutrients to fuel parasite development.

The mechanisms by which parasite numbers are reduced in the absence of mosquito oogenesis are still unclear. The authors show that this elimination is not dependent on the mosquito's complement system, one of the better-characterized mechanisms of *Plasmodium*-parasite clearance known to happen in this host [8]. Thus, other hypotheses can be put forth to explain this observation: for example, oogenesis may inhibit other immune mechanisms capable of efficiently eliminating parasites. Alternatively, parasites may die due to rate limiting quantities of a given nutrient or an excess of a particular toxin. The authors note that this is an extremely fast mechanism — when oogenesis processes are affected, the number of oocysts (but not their prevalence) is significantly decreased as early as two days after the blood meal. It would be interesting to determine whether strategies that impair mosquito oogenesis would completely block parasite transmission in field settings, where the

number of oocysts that colonize a midgut is generally believed to be lower than in laboratory conditions.

Additionally, whatever parasite-killing mechanism may be at play, it is inhibited during oogenesis. Once this mechanism is identified, it will be critical to test whether it also impacts mosquito oogenesis. If not, any anti-malarial strategy employing this mechanism would reduce *Plasmodium* numbers without accelerating *P. falciparum* transmission.

On the other hand, an anti-malarial strategy targeting the mosquito's oogenesis program *per se* may come at a cost, as it would lead to faster parasite development and earlier transmission. This is particularly relevant because female mosquitoes have a short life span, not more than 2–3 weeks in the field, and so any accelerated growth by the parasite (which usually takes 10–14 days to develop) would lead to increased transmission even if numbers of transmissible parasites are lower.

Faster growth occurs because, when egg development is impaired, *Plasmodium* oocysts can use excess mosquito resources. Importantly, although it accelerates growth, an excess of nutrients does not increase the number of sporozoites produced per oocyst, suggesting that *Plasmodium* oocysts have a pre-determined number of sporozoites they can generate, and that this number cannot be exceeded. This is likely a consequence of 30 million years of co-evolution [9], which have shaped the oocyst's developmental process to be as silent as possible, so as not to affect the mosquito's reproductive fitness and to consequently maintain the population of vectors needed for the perpetuation of the parasite's life cycle. Ultimately, *Plasmodium* oocysts act less as parasites and more as commensal organisms.

These results are surprising because it has long been suggested that parasitic infections of vectors would impose a reproductive cost for the mosquito [4]. With these results, the authors show that the number of *Plasmodium* parasites and the development of mosquito eggs are linked in a commensal relationship [5]. The mosquito does not lose its reproductive fitness in spite of the presence of *Plasmodium* parasites, which benefit two-fold from the oogenesis process — for protection and for resources.

Although, by definition, parasitism means that one species — the parasite — exploits a second species — the host — to obtain food, housing, or protection while causing harm to the host, it is not in the parasite's best interest to weaken its host to a point that it cannot support the parasite anymore. The study by Werling, Shaw, Itoe *et al.* suggests that *Plasmodium*–*Anopheles* interactions are the product of an evolutionary process that may have progressed from a typical parasitic association into a commensal one.

REFERENCES

1. Bennink, S., Kiesow, M.J., and Pradel, G. (2016). The development of malaria parasites in the mosquito midgut. *Cell. Microbiol.* 18, 905–918.
2. Mitchell, S.N., and Catteruccia, F. (2017). Anopheline reproductive biology: Impacts on vectorial capacity and potential avenues for malaria control. *Cold Spring Harb. Perspect. Med.* 7, 14.
3. Costa, G., Gildenhard, M., Eldering, M., Lindquist, R.L., Hauser, A.E., Sauerwein, R., Goosmann, C., Brinkmann, V., Carrillo-Bustamante, P., and Levashina, E.A. (2018). Non-competitive resource exploitation within mosquito shapes within-host malaria infectivity and virulence. *Nat. Commun.* 9, 3474.
4. Schwenke, R.A., Lazzaro, B.P., and Wolfner, M.F. (2015). Reproduction–immunity trade-offs in insects. *Annu. Rev. Entomol.* 61, 239–256.
5. Werling, K., Shaw, W.R., Itoe, M.A., Westervelt, K.A., Marcenac, P., Paton, D.G., Peng, D., Singh, N., Smidler, A.L., South, A., *et al.* (2019). Steroid hormone function controls non-competitive *Plasmodium* development in *Anopheles*. *Cell* 177, 315–325.
6. Bai, H., Gelman, D.B., and Palli, S.R. (2010). Mode of action of methoprene in affecting female reproduction in the African malaria mosquito, *Anopheles gambiae*. *Pest Manag. Sci.* 66, 936–943.
7. Atella, G.C., Silva-Neto, M.A.C., Golodne, D.M., Arefin, S., and Shahabuddin, M. (2006). *Anopheles gambiae* lipophorin: Characterization and role in lipid transport to developing oocyte. *Insect Biochem. Mol. Biol.* 36, 375–386.
8. Blandin, S., Shiao, S.H., Moita, L.F., Janse, C.J., Waters, A.P., Kafatos, F.C., and Levashina, E.A. (2004). Complement-like protein TEP1 is a determinant of vectorial capacity in the malaria vector *Anopheles gambiae*. *Cell* 116, 661–670.
9. Hayakawa, T., Culleton, R., Otani, H., Horii, T., and Tanabe, K. (2008). Big bang in the evolution of extant malaria parasites. *Mol. Biol. Evol.* 25, 2233–2239.

Vision: Dialogues between Deep Networks and the Brain

Charles E. Connor

Department of Neuroscience, Krieger Mind/Brain Institute, Johns Hopkins University, Baltimore, MD 21218, USA

Correspondence: connor@jhu.edu

<https://doi.org/10.1016/j.cub.2019.05.072>





Two new papers show how deep neural networks interacting with the brain can generate visual images that drive surprisingly strong neural responses. These images are tantalizing reflections of visual information in the brain.

Artificial intelligence (AI) has been revolutionized in recent years by 'deep networks': artificial neural networks, realized in computers, with multiple layers — which define the network 'depth' — of processing units that transform input information into output solutions [1]. They learn to produce desired outputs through back-

propagation, a method of adjusting connection weights between units to minimize output errors. Deep networks have been around for a long time [2], but recent advances in processing power have allowed them to smash through longstanding AI challenges like object recognition and master-level Go play. One of the most powerful learning



Plasmodium translocon component EXP2 facilitates hepatocyte invasion

João Mello-Vieira ¹, Francisco J. Enguita¹, Tania F. de Koning-Ward ², Vanessa Zuzarte-Luís ¹✉ & Maria M. Mota ¹✉

Plasmodium parasites possess a translocon that exports parasite proteins into the infected erythrocyte. Although the translocon components are also expressed during the mosquito and liver stage of infection, their function remains unexplored. Here, using a combination of genetic and chemical assays, we show that the translocon component Exported Protein 2 (EXP2) is critical for invasion of hepatocytes. EXP2 is a pore-forming protein that is secreted from the sporozoite upon contact with the host cell milieu. EXP2-deficient sporozoites are impaired in invasion, which can be rescued by the exogenous administration of recombinant EXP2 and alpha-hemolysin (an *S. aureus* pore-forming protein), as well as by acid sphingomyelinase. The latter, together with the negative impact of chemical and genetic inhibition of acid sphingomyelinase on invasion, reveals that EXP2 pore-forming activity induces hepatocyte membrane repair, which plays a key role in parasite invasion. Overall, our findings establish a novel and critical function for EXP2 that leads to an active participation of the host cell in *Plasmodium* sporozoite invasion, challenging the current view of the establishment of liver stage infection.

¹Instituto de Medicina Molecular João Lobo Antunes, Faculdade de Medicina, Universidade de Lisboa, 1649-028 Lisboa, Portugal. ²School of Medicine, Deakin University, Waurn Ponds, Geelong, Australia. ✉email: vluis@medicina.ulisboa.pt; mmota@medicina.ulisboa.pt

An obligatory step of infection by *Plasmodium* parasites, the causative agents of malaria, is the invasion of host hepatocytes that involves both parasite and host proteins¹. However, the mechanism by which *Plasmodium* sporozoites enter hepatocytes remains elusive¹. The major sporozoite surface protein, circumsporozoite protein (CSP), must undergo conformational changes and cleavage², likely mediated by *Plasmodium* cysteine proteases. Another surface protein, the thrombospondin-related anonymous protein (TRAP), which is connected to the actin machinery of the parasite, propels the parasite into the hepatocyte³. The hepatocyte membrane receptors scavenger receptor class B type I (SR-BI)^{4,5} or CD81⁶ are also involved, with CD81 being potentially important for the discharge of parasite invasive proteins⁷. The *Plasmodium* 6-cys protein p36⁸, has been shown to be important for binding to these host cell receptors⁹. Other host proteins, the ephrin type-A receptor 2^{10,11} and the protein kinase C zeta (PKC ζ)^{12,13} have also been associated with invasion, yet their distinct roles in the invasion process are still unknown. Noteworthy, for years, the prevailing view of *Plasmodium* sporozoite invasion implied that the host cell does not play an active role during parasite entry^{14–16}, a concept only challenged by the observation that host actin reorganizes around the invading sporozoite^{17,18}.

Exported Protein 2 (EXP2) is a parasite pore-forming protein located at the parasitophorous vacuole membrane (PVM) of both liver and blood stage parasites^{19,20}, whose structure has recently been solved²¹. During the blood stage of infection, EXP2 and four other parasite proteins are part of the translocon complex²², crucial for exporting parasite proteins to the cytosol of the erythrocyte^{23,24}. Besides being engaged in protein translocation, recent reports have demonstrated that the EXP2 pore, independent of the other translocon components²⁵, might also serve as a nutrient channel through which solutes flow between the host cell and the vacuole surrounding the parasite^{26,27}. In the liver stage, although EXP2 deficiency leads to a significant decrease in parasite burden²⁸, its function remains unexplored.

In this work, we use an EXP2 conditional knockout parasite line to study its role during the liver stage of infection. We observe that the lack of EXP2 in the sporozoite stage leads to a decrease in the ability of sporozoites to invade hepatocytes. In fact, EXP2 is detected in sporozoites and is secreted upon stimulation, similarly to other proteins involved in invasion. Our hypothesis is that EXP2 is triggering the host membrane-repair pathway and we observe that the host protein acid sphingomyelinase, critical for this repair process, is also important for sporozoite invasion of hepatocytes. Our results uncover a surprising and critical function of EXP2 in triggering an active response by the hepatocyte, which is key for sporozoite invasion and establishment in the host cell.

Results

Conditional knockout of the EXP2 gene in the sporozoite leads to a decrease in the number of infected cells. To study the function of EXP2 during the liver stage of infection, we used an EXP2 conditional knockout parasite line (EXP2 cKO) based on the flippase recombinase and flippase recognition targets (FLP/FRT) system²⁹. In this system, the FLP recombinase expression is controlled either by the TRAP or the Upregulated in Infectious Sporozoite 4 (UIS4) promoter and mediates excision of the FRT sequences flanking the EXP2 3' UTR, starting at the sporozoite stage of *Plasmodium berghei*. As a control, we used the parental EXP2 FRT parasites lacking the FLP recombinase (WT)²⁸. To assess the efficiency of the conditional deletion system, the excision of the EXP2 3' UTR was quantified by quantitative polymerase chain reaction (qPCR) in sporozoite genomic DNA.

In the parasite line where the FLP expression is controlled by the TRAP promoter excision was very inefficient, with only $26 \pm 12\%$ of EXP2 cKO sporozoites showing an excised EXP2 locus ($p = 0.1429$, Fig. 1a). However, when the UIS4 promoter was used we observed that $45 \pm 4\%$ of EXP2 cKO sporozoites showed an excised EXP2 locus ($p = 0.0286$, Fig. 1a). We selected the UIS4 promoter-induced EXP2 cKO line to be used in subsequent experiments.

The lack of EXP2 protein in sporozoites, the consequence of locus excision, was analyzed in the UIS4 parasite line by microscopy and compared with control WT parasites. We observed that the population of EXP2 cKO sporozoites comprised of sporozoites without the EXP2 protein (EXP2 negative, $42 \pm 7\%$, Fig. 1b, bottom line) and sporozoites with detectable EXP2 protein (EXP2 positive, $58 \pm 5\%$, Fig. 1b middle line), in a proportion similar to that obtained by qPCR. Noteworthy, the EXP2 cKO sporozoite population showed a variety of EXP2 intensity values, ranging from the levels observed in the negative control (unstained) to those observed in WT sporozoites (Supplementary Fig. 1a–b). This suggests that the timing of excision of the EXP2 gene locus varies within the sporozoite population.

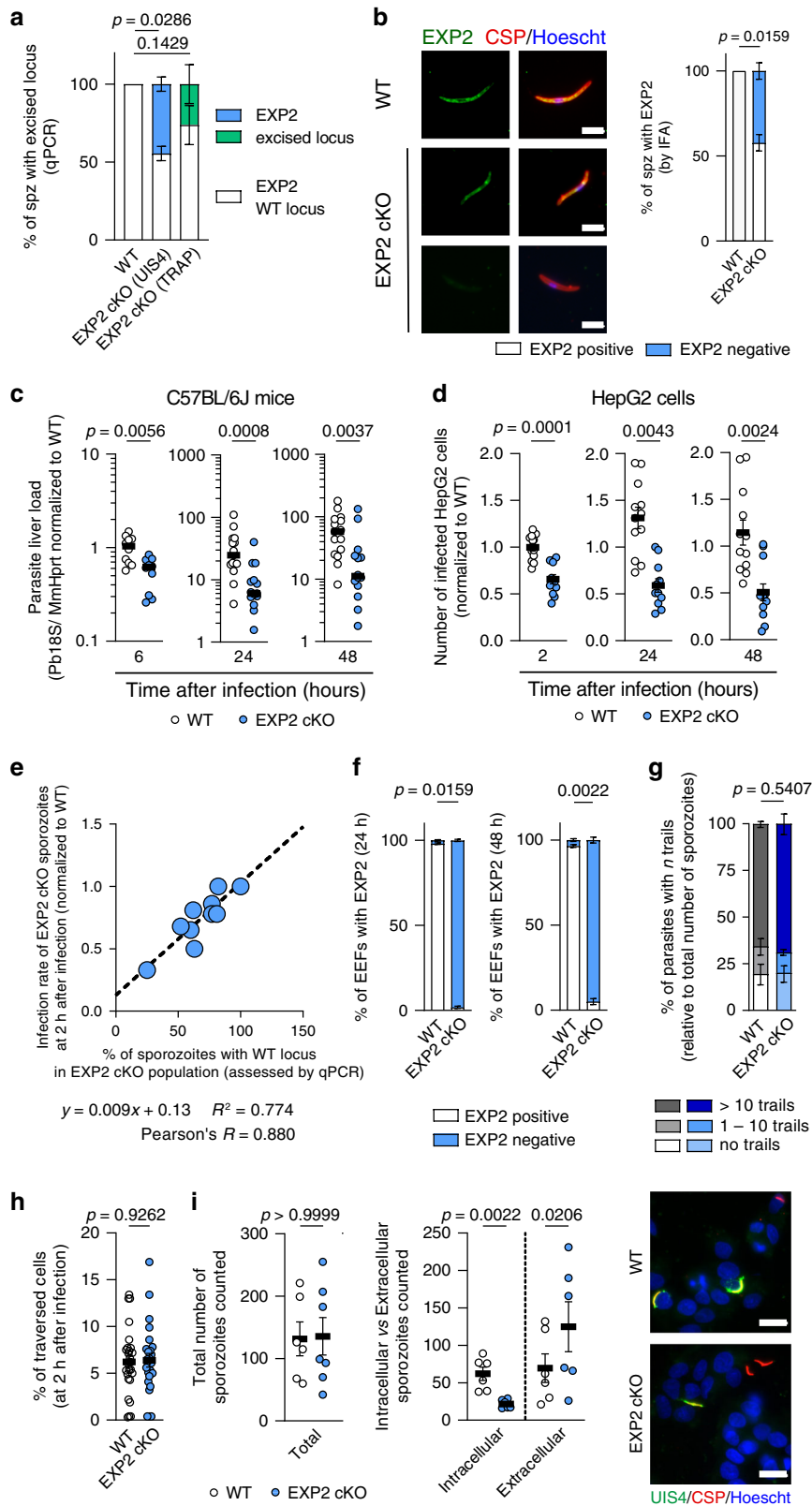
To evaluate how the lack of EXP2 impacts liver stage development we infected C57Bl/6 mice with EXP2 cKO sporozoites. When compared with WT parasites, infection with EXP2 cKO sporozoites resulted in a decreased parasite liver load, starting at 6 hours (h) after infection, as detected by qRT-PCR ($57 \pm 7\%$, $p = 0.0056$, Fig. 1c). This decrease was maintained throughout liver stage development ($71 \pm 6\%$ at 24 h, $p = 0.0008$; $62 \pm 10\%$ at 48 h, $p = 0.0037$; Fig. 1c).

Next, we infected HepG2 cells with WT or EXP2 cKO sporozoites and analyzed the number of exoerythrocytic forms (EEFs) and their size by immunofluorescence assay (IFA). Detailed microscopic analysis of HepG2 cells revealed that the number of cells infected with EXP2 cKO sporozoites is reduced at 2 h after infection, when compared with the control parental line ($46 \pm 6\%$, $p = 0.0001$). Once again, this decrease was maintained throughout infection ($47 \pm 5\%$ and $46 \pm 4\%$ at 24 and 48 h after infection, $p = 0.0043$; $p = 0.0024$, respectively, Fig. 1d). Parasite development was not affected (Supplementary Fig. 1c). Notably, the translocon activity during the liver stage is yet to be observed, which might explain why liver stage development is not affected by the lack of EXP2.

Importantly, the early and stable reduction in the number of infected cells at 2 h after infection correlates with the extent of excision of the EXP2 locus at the sporozoite stage (Pearson's $R = 0.880$, Fig. 1e). Conversely, EXP2 expression does not seem to be necessary for the ensuing development, as it was detected in $<3\%$ of the remaining EXP2 cKO EEFs, all of which developed normally ($2 \pm 1\%$ at 24 h, $p = 0.0159$; $3 \pm 3\%$ at 48 h, $p = 0.0022$; Fig. 1f and Supplementary Fig. 1d). The increase of the excision rate throughout EEF development can be explained by the fact that the UIS4 promoter is kept active during the liver stage of infection, allowing for more expression of the FLP recombinase and further excision of the EXP2 3' UTR.

Altogether, these results show that EXP2 is critical for the early establishment of hepatocyte infection by *P. berghei* sporozoites.

EXP2 cKO parasites are impaired in the invasion of hepatocytes. Such an early phenotype suggests that EXP2 is important for liver colonization. To successfully establish in the liver, sporozoites use gliding motility to traverse through several host cells prior to invading hepatocytes³⁰. Our results show that EXP2 cKO sporozoites glide and traverse similarly to the WT parasites (Fig. 1g–h, respectively). To assess if EXP2 cKO sporozoites were able to infect cells, we performed in-and-out staining at 2 h after



infection. We stained for the sporozoite protein CSP to count the total number of parasites and for the PVM marker UIS4 to assess the number of invaded parasites. We observed that WT and EXP2 cKO sporozoites adhered to cells similarly based on CSP staining (comparable absolute number of sporozoites counted, Fig. 1i). However, EXP2 cKO sporozoites were more predominantly found outside cells ($76 \pm 21\%$, $p = 0.0206$) when compared with

WT sporozoites by UIS4 staining ($49 \pm 13\%$, $p = 0.0022$), evidencing a defect in hepatocyte invasion (Fig. 1i).

EXP2 is relocated and discharged by the sporozoite upon contact with the host cell milieu. Given the invasion phenotype of EXP2 cKO sporozoites, we next sought to characterize EXP2

Fig. 1 EXP2 deletion hinders invasion of hepatocytes. **a** Percentage of sporozoites with WT EXP2 (white) or excised locus (shaded bars) determined by qPCR in WT and EXP2 (UIS4 (blue) or TRAP (green) promoter mediated) cKO sporozoites. ($N = 4$ independent experiments). **b** Micrographs of WT or EXP2 cKO sporozoites, stained with mouse α PfEXP2 (green), α PbCSP (red), Hoechst (blue). Scale bar: 5 μ m. Percentage of sporozoites classified as EXP2-positive (white) and EXP2-negative (blue) by immunofluorescence ($N = 7$). **c** Parasite liver load in mice infected with WT (white) or EXP2 cKO (blue) sporozoites by qPCR ($N = 2$ or 3 totaling 10 or 15 mice for 6 h or other timepoints, respectively, normalized to 6 h). **d** Number of cells infected with WT (white) or EXP2 cKO (blue) sporozoites analyzed by immunofluorescence ($>30,000$ cells analyzed, $N = 4$ or 5 totaling 12 or 15 replicates for 2 h or other timepoints, respectively, normalized to 2 h). **e** Percentage of WT parasites in EXP2 cKO sporozoite population versus number of infected HepG2 cells at 2 h after infection (blue). Proportion of EXP2-positive parasites assessed by qPCR, proportion of invaded parasites quantified by immunofluorescence ($N = 10$ totaling 10 and 30 replicates for excision and invasion rates, respectively). **f** Proportion of EEFs classified as EXP2-positive (white) and EXP2-negative (blue) by immunofluorescence. ($N = 3$). **g** Percentage of WT (gray-shaded) or EXP2 cKO (blue-shaded) sporozoites with CSP trails by immunofluorescence. Sporozoites scored as having 0, between 1 and 10 or >10 trails. ($N = 3$). **h** Percentage of traversed HepG2 cells by WT (white) or EXP2 cKO (blue) sporozoites, assessed by Flow Cytometry. ($>10,000$ cells analyzed, $N = 8$ totaling 27 and 26 replicates for WT and EXP2 cKO, respectively). **i** Total number of WT (white) or EXP2 cKO (blue) sporozoites (CSP staining), intracellular sporozoites (both UIS4 and CSP) and extracellular sporozoites (only CSP) at 2 h after infection. Micrographs of WT or EXP2 cKO sporozoites at same time point, stained with α PbUIS4 (green), α PbCSP (red), Hoechst (blue). Scale bar: 10 μ m. ($N = 3$ totaling 6 and 7 replicates for WT and EXP2 cKO, respectively). Results shown as mean \pm SEM, two-tailed Mann-Whitney U test was applied for p values in all panels except for **e**, where correlation and linear regression was performed.

expression and localization in sporozoites. To that end, the localization of EXP2 in freshly dissected *P. berghei* sporozoites was assessed by immuno-EM and we observed that EXP2 is distributed throughout the parasite cell body, frequently observed inside vesicles (Fig. 2a). Micronemes and rhoptries are the most characterized types of vesicles found in *Plasmodium* sporozoites, which contain proteins that participate in the invasion process³¹. We sought to colocalize EXP2 with proteins reported to be present in those organelles, such as TRAP (present in micronemes)³², RON4 (present in rhoptries)⁷ and UIS4 (in still unidentified vesicles)^{33,34}. We did not observe colocalization of EXP2 with any of the proteins tested, in freshly dissected sporozoites (Fig. 2b).

Apicomplexan parasites are known to secrete proteins important for the invasion process³⁵. To address whether EXP2 is also mobilized during invasion, sporozoites were incubated in medium with fetal calf serum (FCS) at 37 °C, a combination that simulates the host milieu conditions and shown to prime sporozoites for invasion^{36–38}. Western Blot (WB) analysis of sporozoites pellet and the supernatant fractions after sporozoite activation (incubation with FCS at 37 °C) showed EXP2, but not the intracellular ER-marker BiP, in the supernatant fraction of activated sporozoites (Fig. 2c). This shows that EXP2 is discharged to the medium upon activation.

The results so far imply that EXP2 relocation and secretion is important for the invasion of hepatocytes. If this hypothesis is correct, the addition of exogenous EXP2 would rescue the invasion impairment of EXP2 cKO sporozoites. Indeed, addition of exogenous recombinant *Plasmodium falciparum* EXP2 (rPfEXP2)³⁹ to the culture medium restores the invasion capacity of EXP2 cKO sporozoites (Fig. 2d). Interestingly, this rescue only occurs when rPfEXP2 is added to the culture 1 h after sporozoite incubation and not when rPfEXP2 is added to the cells concomitantly with the sporozoites ($44 \pm 8\%$, $p < 0.0001$, Fig. 2d) nor if added to sporozoites prior to incubation with cells ($43 \pm 10\%$, $p = 0.0022$, Supplementary Fig. 2a).

We sought to understand why EXP2 is needed at 1 h after the sporozoite incubation and not earlier. It has been reported that *Plasmodium* sporozoites begin productive invasion only 1 h after being in contact with cells⁴⁰. We observe that this is also true for spect1 KO sporozoites that are incapable of cell traversal (Supplementary Fig. 2b), suggesting that *Plasmodium* sporozoites require a “waiting period”, not related with cell traversal, of ~1 hour, before invading hepatocytes. Interestingly, transcriptomic analysis of activated sporozoites showed EXP2 upregulation starting at 1 h after incubation at 37 °C⁴¹. Indeed, we observed a peak of EXP2 mRNA expression at 1 h after infection (Fig. 2e). This behavior is specific to EXP2 but not of other invasion-related

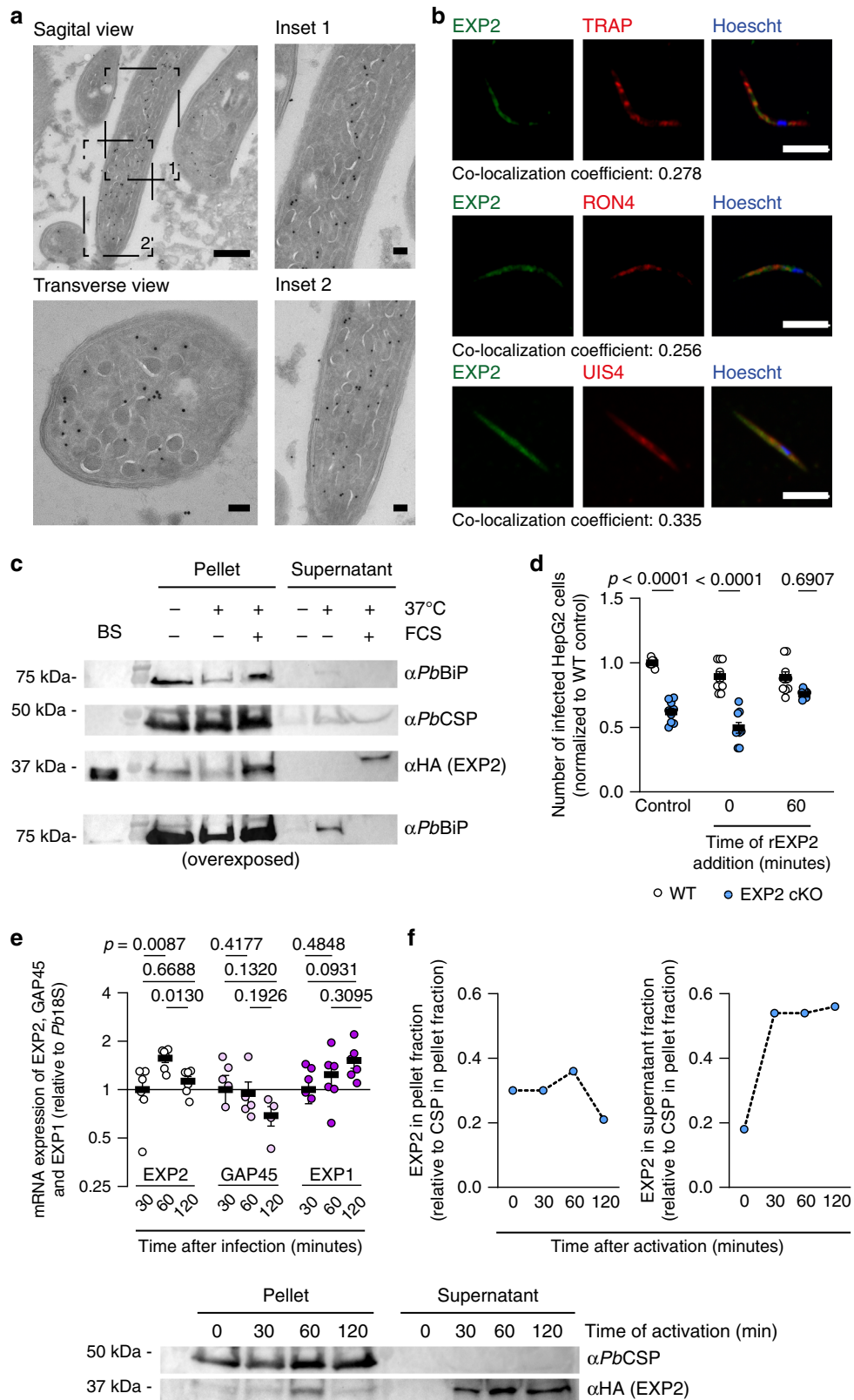
genes, such as, Glideosome-associated Protein 45 (GAP45), which showed a tendency to be down-regulated (Fig. 2e), nor that of the liver stage PVM-resident Exported Protein 1 (EXP1), which showed a tendency to be upregulated during invasion (Fig. 2e). In *P. falciparum*, EXP2 was found to be continuously upregulated until 2 h after incubation of sporozoites with cells⁴¹, although traversal has been shown to take longer in *P. falciparum*⁴² than in rodent *Plasmodium* parasites⁴⁰. At 2 h after infection, *P. falciparum* is still actively traversing cells⁴². It remains to be tested whether *P. falciparum* EXP2 mRNA decreases after invasion is completed (3–4 h after incubation with cells).

We next sought to examine if the secretion of the EXP2 protein follows the invasion kinetics. Importantly, we observed continuous secretion of EXP2 to the surrounding medium starting at 30 minutes after sporozoite activation and increasing until 2 h after activation (Fig. 2f). These results show that the temporal dynamics of EXP2 expression and secretion accompanies the invasion kinetics observed in *P. berghei* sporozoites.

To complement the previous experiment, we tested if rPfEXP2 has the ability to interact with cellular membranes. For this, we incubated rPfEXP2 with HepG2 cells, collected the cellular medium and we assayed this conditioned medium for the presence of rPfEXP2 by WB. In cells treated with 1 nM of rPfEXP2, we observed a decrease in rPfEXP2 concentration in the supernatant already at 5 min after cells are exposed to the protein (Supplementary Fig. 2c). This decrease is consistent with previous observations for other pore-forming proteins⁴³, which are readily absorbed by cells. The fact that not all the protein is internalized, and the remaining rPfEXP2 is not absorbed by the cells in the following hour, suggests that cells become non responsive to the action of rPfEXP2.

Remarkably, EXP2 is never detected in sporozoites immediately after invasion (Supplementary Fig. 2d). This behavior has been reported for other proteins important for sporozoite invasion, RON4 and AMA1^{7,36}, suggesting that EXP2 might be degraded or completely discharged during the invasion process. Altogether, these data strengthen the role of EXP2 during invasion of the hepatocyte.

EXP2 pore-forming activity induces a membrane-repair pathway, facilitating invasion of sporozoites. Ad both native and recombinant PfEXP2 protein are known to form pores in membranes^{21,39} we wondered if the function of EXP2 during invasion is related to its pore-forming ability. Indeed, EXP2 cKO invasion defect can be rescued by both rPfEXP2 and the recombinant pore-forming protein from *S. aureus*, α -hemolysin (α -HL) in a similar range of concentrations (Fig. 3a–b). Notably, the pore



formed by α -HL is similar to that formed by EXP2, both are heptamers^{21,44} and create a pore with 1 nm of diameter^{21,45}. Importantly, the invasion defect of the EXP2 cKO sporozoites could not be reverted by the *S. pyogenes* pore-forming protein streptolysin O (SLO, Supplementary Fig. 3a) added in a similar concentration. SLO is known to form pores of 25–30 nm in

diameter⁴⁶, 10–30 times wider than the pore of EXP2²¹ and of α -HL⁴⁵.

Host plasma membrane wounding has been previously implicated as a critical step for invasion of *Trypanosoma cruzi* parasites and can also be triggered by the addition of pore-forming toxins to mammalian cells⁴⁷. *T. cruzi*-induced host cell

Fig. 2 EXP2 is present in the sporozoite and is translocated to the membrane and secreted after activation. **a** Immuno-electron microscopy of sporozoites, stained with rabbit α PfEXP2. Scale bar: 500 nm and 100 nm in insets and transverse views. Representative image of three independent experiments. **b** Micrographs of permeabilized sporozoites stained with α PfEXP2 (green), α PbTRAP (microneme protein), α PbRON4 (rhostry protein), or α PbUIS4 (dense granule protein) (all in red) and the DNA dye Hoechst (blue). For EXP2 co-staining with TRAP and UIS4, mouse α PfEXP2 was used. For co-staining with RON4, rabbit α PfEXP2 was used. Scale bar: 5 μ m. (>50 sporozoites analyzed per experiment, $N = 3$ independent experiments). Shown below each panel is the colocalization coefficient between EXP2 and the corresponding protein. **c** Western blot analysis of secreted EXP2 protein. PbEXP2-HA sporozoites were incubated for 30 min, at 4 °C (–), at 37 °C (+) and in the presence or absence of FCS. Sporozoites were pelleted and both pellet and supernatant were assayed for the presence of PbEXP2-HA, PbCSP (membrane protein of the sporozoite) and PbBiP (ER-resident protein). Lysates of a mixed blood stage infection of PbEXP2-HA were used as control. Representative images of three independent WB. **d** Number of infected cells at 2 h after infection, infected with WT (white) or EXP2 cKO sporozoites (blue), after treatment with 10 nM rEXP2 concomitantly with sporozoite addition to cells or at 1 h after infection ($N = 3$ independent experiments totaling nine replicates). **e** mRNA expression of invasion-related genes of *P. berghei* at different timepoints during infection, normalized to Pb18S. EXP2 (white), GAP45 (light pink), and EXP1 (dark pink) ($N = 2$ independent experiments totaling six replicates). **f** Quantification of EXP2 secretion by sporozoites following activation with FCS at 37 °C throughout time. The amount of EXP2 (blue) in pellet or supernatant fractions for each experiment, was normalized to the amount of CSP in the pellet fraction at the respective time point. Protein extraction was performed immediately after sporozoites were removed from incubation (as in Fig. 2c) and secretion was quantified by WB. Representative images of two independent WB. Results in **d** and **e** shown as mean \pm SEM, two-tailed Mann-Whitney *U* test was applied for *p* values.

wounding results in Ca^{2+} influx and consequently exocytosis of lysosomes that deliver acid sphingomyelinase (aSMase) to host plasma membrane, generating ceramide on the outer leaflet of the plasma membrane to facilitate PV formation and internalization of the parasite⁴⁸. We now hypothesize that similarly to *T. cruzi*, *Plasmodium* sporozoites (via EXP2) induce pores in the host cell plasma membrane resulting in Ca^{2+} influx, key for invasion.

The diameter of the EXP2 pore is of 1 nm²¹, and it would be wide enough to fit small ions, such as calcium and potassium, the most abundant ions on the outside and inside of mammalian cells, respectively. To assess if rPfEXP2 would allow for the passage of ions we transfected HepG2 cells with the intracellular calcium-sensitive reporter Gcamp6f⁴⁹ or the potassium fluorescent sensor GEPII⁵⁰. Treatment of Gcamp6f-transfected cells with rPfEXP2 resulted in an increase in Gcamp6f fluorescence, reflecting an influx of Ca^{2+} (Fig. 3c). In cells transfected with GEPII and treated with rPfEXP2, the fluorescence of the reporter protein decreased, suggesting that potassium is leaking out of the cell (Fig. 3d). It is noteworthy that the concentration of rPfEXP2 in these experiments was 100 nM, ten times higher than that used for the rescue experiments. In the context of invasion, smaller concentrations of rEXP2 might cause local ion changes in the cell that are enough to induce the necessary mechanisms for sporozoite invasion, but not sufficient to induce changes in global ion concentrations.

The next step in the membrane-repair pathway involves the release of host aSMase and its activity in the outer leaflet of the plasma membrane of the hepatocyte. Indeed, when aSMase was inhibited by desipramine^{51,52}, *P. berghei* sporozoite invasion was impaired ($\text{IC}_{50} = 15 \pm 2 \mu\text{M}$) (Fig. 3e). Noteworthy, inhibition of neutral SMase, by GW4869, did not block *P. berghei* sporozoite invasion (Fig. 3e). To further establish host aSMase as a key protein during the invasion process, we proceeded to knockdown its expression using short-hairpin RNA (shRNA). The decrease in aSMase expression by the shRNA ($36 \pm 10\%$, $p = 0.0022$, Supplementary Fig. 3b), resulted in a decrease in *P. berghei* invasion ($56 \pm 17\%$, $p = 0.0022$, Fig. 3f). This effect was counteracted by the addition of recombinant acid SMase from *B. cereus* (Fig. 3f). Remarkably, exogenous addition of recombinant aSMase also rescued the invasion impairment exhibited by EXP2 cKO sporozoites (Fig. 3g).

Altogether, our data show that *Plasmodium* sporozoites secrete EXP2 upon stimulation and that recombinant EXP2 can lead to the formation of pores in the hepatocyte plasma membrane. Both exogenous EXP2 and acid SMase can rescue the invasion impairment of EXP2 cKO sporozoites, suggesting that sporozoites

hijack the host membrane-repair pathway, to facilitate invasion of the host cell.

Discussion

EXP2 is expressed throughout the *Plasmodium* life cycle^{19,20} but has been mostly studied during the blood stages. This protein is found in the dense granules of merozoites⁵³, which are discharged after the invasion of the erythrocyte is complete. Inside this cell, the parasite relies on EXP2 and the other components of the translocon complex to remodel the erythrocyte with its own proteins²². This remodeling is necessary for nutrient acquisition and immune system evasion by the parasite (reviewed in ref. 54). Beside its association with the translocon complex, EXP2 also exists in regions of the PVM of blood stage parasites without the other translocon components²⁵, suggesting that EXP2 might have an additional function. Indeed, a recent study suggests that EXP2 contributes to the exchange of small molecules across the PVM, such as amino acids and glucosamine²⁷. It seems that these two functions of EXP2 might be influenced by the RON3 protein⁵⁵ by a mechanism that is still not understood. Although reports suggest that EXP2 is not involved in erythrocyte invasion⁵³, we show here that hepatocyte invasion by sporozoites is mediated by EXP2. These data imply not only that *Plasmodium* uses distinct mechanisms to invade hepatocytes and erythrocytes as previously suggested¹⁸, but also that the same parasite molecule plays divergent functions in different stages of infection.

For the invasion of hepatocytes, one hypothesis is that EXP2 is secreted from the sporozoite to the hepatocyte membrane, creating pores that generate ion fluxes, which in turn trigger the release of host aSMase and induces endocytosis, facilitating parasite invasion (Fig. 4). This is in agreement with recent findings showing that *Plasmodium* sporozoites trigger exocytosis of host lysosomes, to facilitate invasion⁵⁶. Notably, other pathogens including another eukaryotic parasite, *T. cruzi*⁴⁸, but also the bacteria *Listeria monocytogenes*⁵⁷ and *Neisseria gonorrhoeae*⁵⁸ as well as human adenoviruses⁵⁹ have also been reported to invade cells by hijacking host cell plasma membrane-repair pathways resulting in ceramide generation. These ceramide membrane domains have been shown to bind and activate PKC ζ ⁶⁰, a kinase that activates endocytosis⁶¹, and that has been previously identified as a positive modulator of *P. berghei* invasion¹² and establishment¹³. Moreover, ceramide generation increases the rigidity of the plasma membrane, leading to the aggregation of host cell receptors, namely CD81⁶². CD81 has been shown to be essential for invasion of *P. falciparum* and *P. yoelii*⁶, possibly by inducing rhostry discharge and moving junction formation⁷.

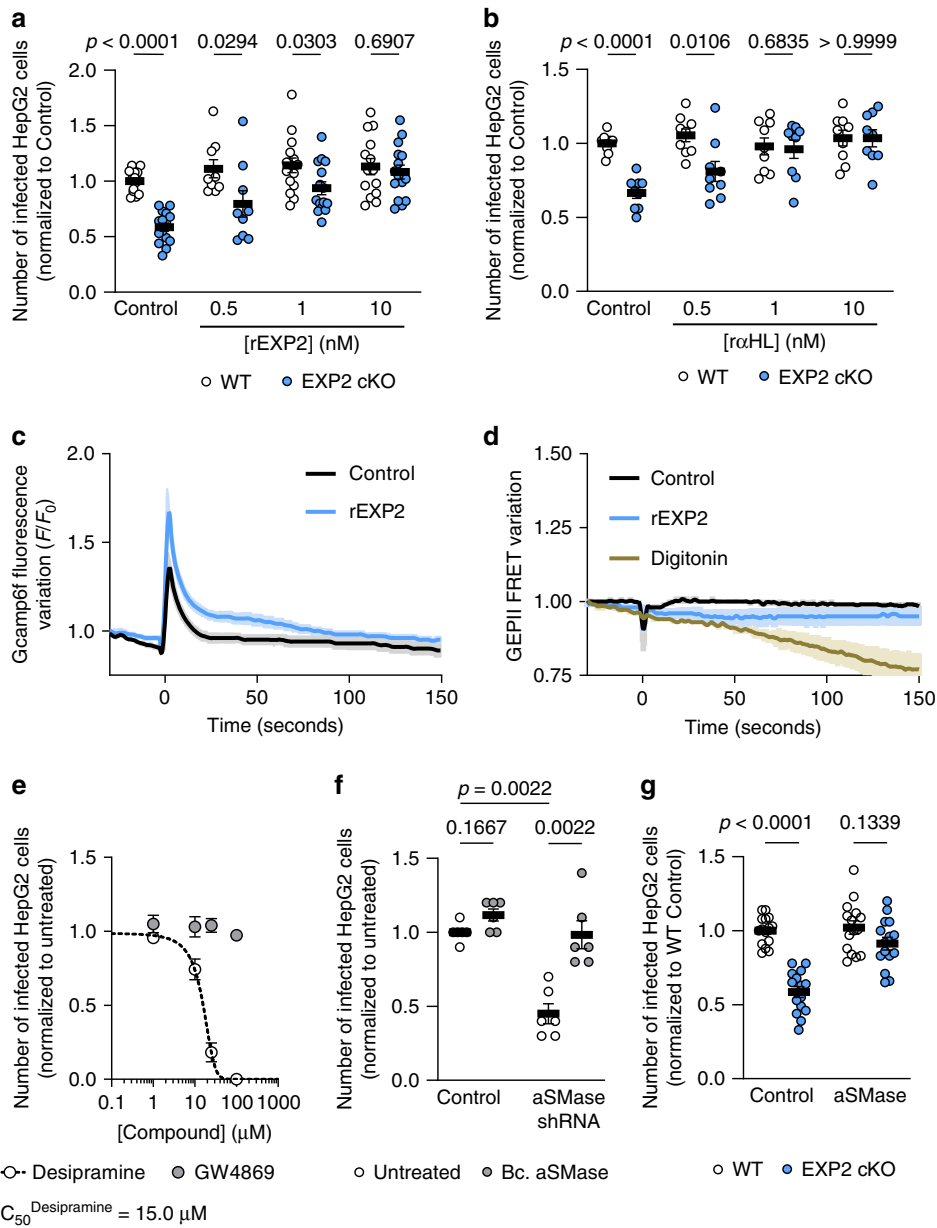


Fig. 3 Hepatocyte membrane repair is important for invasion of *Plasmodium* sporozoites. **a** Number of infected cells at 2 h after infection, infected with WT (white) or EXP2 cKO sporozoites (blue), after addition of rPfEXP2 at 1 h after infection ($N = 5$ independent experiments totaling 15 replicates for all concentrations except for 0.5 nM, where $N = 3$ independent experiments totaling nine replicates were performed). **b** Number of infected cells at 2 h after infection, infected with WT (white) or EXP2 cKO sporozoites (blue), after addition of r α -HL at 1 h after infection ($N = 3$ independent experiments totaling nine replicates). **c** Calcium uptake by cells measured using Gcamp6f fluorescent protein, through time after addition (at time 0 s) of 100 nM rPfEXP2 (blue line) or vehicle control (black line) ($N = 3$ independent experiments, >75 total cells imaged per condition). **d** Potassium efflux by cells measured using GEPII fluorescent protein, through time after addition (at time 0 s) of 100 nM rPfEXP2 (blue line), 50 μ M of Digitonin (brown line, permeabilizes cellular membranes) or vehicle control (black line) ($N = 2$ independent experiments, >50 cells imaged per condition). **e** Number of infected cells at 2 h after infection by GFP-expressing sporozoites in the presence of desipramine (acid SMase inhibitor, white) or GW4869 (neutral SMase inhibitor, gray) ($N = 3$ independent experiments totaling nine replicates). **f** Number of infected cells at 2 h after infection by GFP-expressing sporozoites after knockdown of aSMase by shRNA, in the absence (white) or presence of 10 μ U/mL of recombinant acid SMase from *Bacillus cereus* (gray). ($N = 3$ independent experiments totaling nine replicates). **g** Number of infected cells at 2 h after infection, infected with WT (white) or EXP2 cKO sporozoites (blue), after treatment with 10 μ U/mL of recombinant aSMase added at 1 h after infection. ($N = 5$ independent experiments totaling 15 replicates). Results are shown as mean \pm SEM, two-tailed Mann-Whitney U test was applied for p values in all panels except for **c**, **d**. **c**, **d** Lines represent the average of the mean fluorescence intensity and shaded areas the 95% confidence intervals for each time point. Dose-inhibition curve in **e** was generated and IC_{50} value was estimated from the fitted curve.

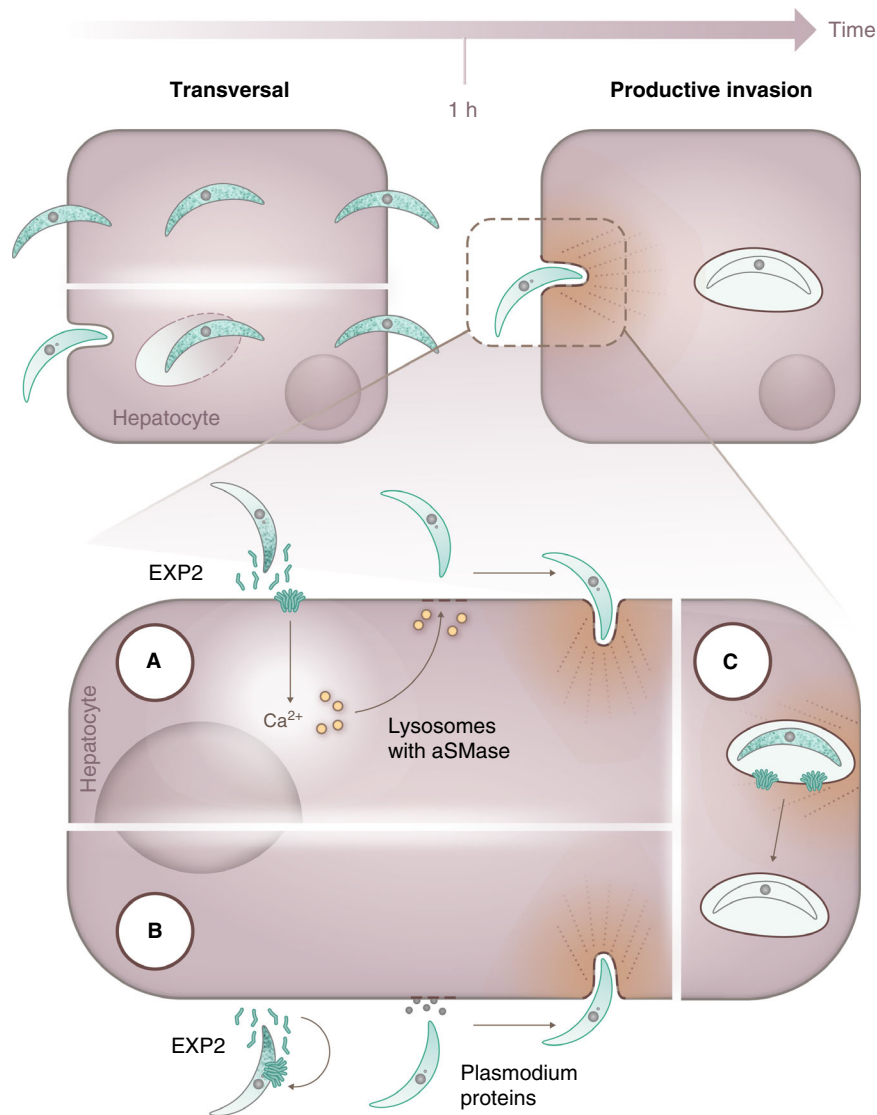


Fig. 4 Model for the action of *Plasmodium berghei* EXP2. *Plasmodium berghei* sporozoites, after reaching the liver, traverse hepatocytes before invading the final one inside which they will replicate. Once they encounter the definitive hepatocyte, and stimulated for ~1 hour by the host cell milieu conditions (increase in temperature and presence of mammalian serum components), sporozoites secrete the pore-forming protein EXP2. **a** EXP2 might create pores at the membrane of hepatocytes, allowing the influx of calcium, leading to the activity of host aSMase that facilitates the invasion of the hepatocyte by the sporozoite. **b** Alternatively, EXP2 might bind to the sporozoite membrane, inducing a calcium influx in the sporozoite, which triggers the release of rhoptry and other proteins, allowing for the sporozoite to invade the hepatocyte. **c** Another possibility is that EXP2 is discharged by the sporozoite during vacuole formation, similarly to what happens during the blood stage, being critical for the survival of the sporozoite during the initial stages of hepatocyte infection.

Importantly, increasing the rigidity of the membrane facilitates the invasion of hepatocytes by sporozoites by clustering CD81 at the membrane of the hepatocyte⁶³. As such, the hijack of the membrane-repair pathway by *Plasmodium* sporozoites might lead to both aggregation of host cell receptors essential for invasion as well as a trigger for endocytosis via PKCζ.

We cannot exclude that EXP2 secretion might also create pores at the surface of the sporozoite, leading to the increase of intracellular calcium in the sporozoite, triggering the release of more invasion proteins. Nonetheless, this EXP2-induced calcium increase would need to be timed with the expression of other invasion proteins, as the addition of rPfEXP2 to unactivated sporozoites does not rescue the invasion capacity of EXP2 cKO (Fig. 4).

On the other hand, our sporozoite secretion assay does not allow us to distinguish between pre-invasion and post-invasion release. As such, it is also possible that EXP2 might be

incorporated in the nascent PVM, not being required for the invasion process itself but for vacuole integrity and parasite maturation during the few minutes/hours after the parasite has sealed the PVM, similarly to what happens during the blood stage of *Plasmodium* infection. Given that we rescue the invasion defect with another pore-forming protein from a different pathogen, this suggests that the role for EXP2 in this maturation process can be attributed to its pore-forming ability. Noteworthy, the action of EXP2 in this scenario would be transient, as we do not detect EXP2 in the PVM following invasion of the hepatocyte. Moreover, parasites lacking EXP2 would still need to escape this immature vacuole and leave the hepatocyte, as EXP2 cKO sporozoites are found preferably outside cells. In essence, in this scenario, EXP2 could be a parasite factor that transforms a transient vacuole into a definitive one, a concept that has been put forward recently⁴⁰.

Interestingly, our data also show that the invasion process of *Plasmodium* sporozoites requires a waiting period before the parasite commits to invasion of the hepatocyte. This has been observed before⁴⁰ and possibly correlates with the synthesis and secretion of invasion proteins, such as P36⁸ and likely EXP2. In fact, sporozoites have been shown to possess a mechanism of translational repression, which prevents the production of liver stage proteins when the sporozoite is in the mosquito salivary glands⁶⁴. Importantly, EXP2 was found to be upregulated in the absence of the mRNA binding protein Puf2, a parasite protein responsible for this process⁶⁴. It is possible that this waiting period correlates with the release of a regulator of sporozoite invasion from translation repression, which initiates transcription of the EXP2 gene. In fact, addition of rPfEXP2 to sporozoites before this waiting period is complete does not rescue the defect of EXP2 cKO. This suggests that this waiting period is sporozoite-intrinsic and that premature presence of EXP2 does not accelerate it. Sporozoite invasion likely requires the timely expression and secretion of a number of parasite proteins, including EXP2. Particularly, we think that this waiting period could occur in the dermis, where sporozoites are deposited during the mosquito bite, to avoid infection of skin cells, where parasite development is less productive⁶⁵. Indeed, it has been shown that sporozoites can remain in the dermis for up to 1 hour after being deposited by the mosquito bite⁶⁶, a time frame consistent with that observed by us and others⁴⁰.

Finally, we also observed that the lack of EXP2 does not seem to affect EEF development. This observation contrasts with the essential role of EXP2 in the blood stages. Notably, the translocon activity during the liver stage is yet to be observed. In fact, a study showed that a green fluorescent reporter protein, which is exported by the translocon during the blood stage of infection, is retained in the parasite during the liver stage²⁸. Moreover HSP101, the ATPase that powers the translocon and unfolds cargo⁶⁷, is not expressed during the liver stage^{19,28}. This suggests that protein export during the liver stage might function independently of EXP2 and the translocon.

Overall, we suggest that by forcing the host cell to respond to the membrane damage caused by EXP2, the hepatocyte has an active role in *Plasmodium* sporozoite invasion. Importantly, although EXP2 has divergent functions throughout *Plasmodium* life cycle, our findings point to the convergent evolution of different intracellular pathogens, which have developed similar strategies to take advantage of cellular responses to membrane damage, hitchhiking their way into the host cell.

Methods

Mice. Male C57BL/6J and BALB/c wild-type mice, aged 6–8 weeks, were purchased from Charles River Laboratories (Saint-Germain-sur-l'Arbresle, France). Mice were housed in the facilities of the iMM João Lobo Antunes (iMM JLA), in specific pathogen-free environment and given water and food ad libitum. Mice are kept in 22–24 °C and 45–65% humidity in a 14h-light/10h-dark cycle. All in vivo protocols were approved by the ORBEA committee of the iMM JLA and were performed according to national and European regulations.

Sporozoite production. The following parasite lines were used in this study: GFP-expressing *P. berghei* ANKA (clone 259c12); *P. berghei* NK65 EXP2 FRT (WT), *P. berghei* NK65 EXP2 FRT UIS4 FLP Recombinase (EXP2 cKO), *P. berghei* NK65 EXP2 FRT TRAP FLP Recombinase and *P. berghei* NK65 EXP2-HA. The first was a kind gift from Chris Janse from Leiden University Medical Center from Leiden, The Netherlands, whereas the other lines were generated in the laboratory of Tania de Koning-Ward from Deakin University, Australia, and are described in a previous study that also outlines the protocol used to achieve excision of the EXP2 3' UTR²⁸. Parasites were stored in frozen blood vials, containing 10⁷ blood stage parasites, and kept at –80 °C in our laboratory. To achieve sporozoites, 10⁷ infected red blood cells were injected intra-peritoneally into a BALB/c wild-type mouse. After 5 days of infection, exflagellation of the male gametes in the blood of infected mice was observed under a light microscope. If more than five events per field of view were observed, the infected mouse was used to feed naive *Anopheles*

stephensi mosquitos, bred in the insectary of the iMM JLA, for 30 min. For the *P. berghei* NK65 EXP2 FRT TRAP FLP Recombinase parasite line, infected mosquitos were placed at 25 °C 18 days after the mosquito bite, to enhance the activity of the recombinase²⁹. In total, 22–35 days after the mosquito blood meal, salivary glands containing *P. berghei* sporozoites, were dissected from infected female *Anopheles stephensi* mosquitoes into simple Dulbecco's Modified Eagles Medium (DMEM, Gibco, Thermo Fisher Scientific, Waltham, MA, USA) and collected into an Eppendorf tube (Eppendorf, Hamburg, Germany). Salivary glands were smashed with a plastic pestle and filtered through a 40-µm Falcon cell-strainer (Thermo Fisher Scientific) to release sporozoites. Sporozoites were counted using a hemocytometer (Marienfeld Superior, Lauda-Königshofen, Germany).

Hepatoma cells. HepG2 cells (obtained from ATCC, Manassas, VA, USA) were cultured at 37 °C, with a 5% CO₂ atmosphere, in DMEM (Gibco), supplemented with 10% FCS (Gibco), 1% glutamine (Gibco) and 1% penicillin/streptomycin (Gibco). Cells were seeded onto no. 1 grade 12 mm diameter glass coverslips (VWR, Radnor, PA, USA) in 24-well plates (Thermo Fisher Scientific) or onto black glass-bottom 96-well plates (Greiner, Kremsmünster, Austria). After plating, cells were incubated at 37 °C, with a 5% CO₂ atmosphere.

Recombinant EXP2 protein production and purification. Plasmid for recombinant EXP2 protein (rEXP2) production was a kind gift from Professor Masafumi Yohda from Tokyo University of Agriculture and Technology from Tokyo, Japan³⁹. In brief, the plasmid pGEX-3X-HRV 3C-EXP2 containing a truncated version of the EXP2 protein fused to Glutathione S-transferase (GST) and an HRV 3C protease cleavage site to excise the affinity tag, was transformed into *E. coli* B21, a gift from the laboratory of Gonçalo Bernardes at iMM JLA. Transformed bacteria were grown in LB broth supplemented with 100 µg/mL ampicillin at 37 °C and when the optical density (OD₆₀₀) of the culture reached 0.5, the protein expression was induced with isopropyl β-D-1-thiogalactopyranoside to a final concentration of 0.5 mM, and further incubated for 24 h at 18 °C, after which they were pelleted by centrifugation.

The pelleted bacteria were resuspended in the PBS containing 137 mM NaCl (Sigma); 2.7 mM KCl (Sigma); 1 mM EDTA (Sigma), and 0.15 mM phenylmethylsulfonyl fluoride (Sigma) and disrupted by sonication. Cell debris was eliminated by centrifugation at 14,000 × g, the supernatant collected and filtered through a membrane with the 0.45 µm pore size and incubated with 0.05% N-dodecyl-β-D-maltopyranoside (DDM, Sigma) at 4 °C for 1 h prior to loading onto a 1 mL GST Hitrap FF column (GE Healthcare, Chicago, IL, USA). The column was then washed with a 10-fold volume of washing buffer (PBS with 0.02% DDM). To release rEXP2, HRV 3 C protease (Takara Bio, Shiga, Japan) in 50 mM Tris-HCl, 200 mM NaCl and 0.02% DDM was applied to the column. After a 16 h incubation at 4 °C, rEXP2 was eluted from the column with PBS buffer. All the purification steps were performed in an AKTA Explorer chromatographic system (GE Healthcare, Chicago, IL, USA). rEXP2 concentration was estimated using Pierce BCA Protein Assay Kit (Thermo Fisher Scientific).

Calcium imaging using Gcamp6f. HepG2 cells were transfected with Gcamp6f calcium reporter fluorescent plasmid (Addgene Plasmid #40755, Watertown, MA, USA, a gift from Mafalda Pimentel at iMM JLA) using FuGene 6 HD (Promega, Madison, WI, USA) and OptiMEM (Gibco). In total, 48 h after transfection, cells were imaged in Zeiss Cell Observer widefield fluorescent microscope for 3 min, using ZEN 2 software (Blue version). After an initial 30 s of imaging, the appropriate concentration of rEXP2 or vehicle control was added to the culture medium and cells were imaged for another 150 s. Fluorescence signal through time was normalized to the fluorescence at time –30s (F_i/F₋₃₀).

Potassium imaging using GEPII sensor. HepG2 cells were transfected with GEPII potassium reporter fluorescent plasmid (NGFI, Graz, Austria) using FuGene 6 HD (Promega, Madison, WI, USA) and OptiMEM (Gibco). In total, 48 h after transfection, cells were imaged in Zeiss LSM 710 confocal fluorescent microscope for 3 min, using ZEN 2 software (Blue version). After an initial 30 s of imaging, the appropriate concentration of rEXP2, digitonin or vehicle control was added to the culture medium and cells were imaged for another 150 s. Cells were excited using the 405 nm laser and fluorescence was collected using the following bandwidths: 420–480 nm for CFP channel and 500–700 nm for FRET channel. To calculate the FRET ratio, the intensity of the FRET channel was divided by the intensity of the CFP channel through time. These values were further normalized to the fluorescence at time –30s (F_i/F₋₃₀).

Chemicals and proteins. Desipramine, recombinant α-hemolysin (α-HL) from *Staphylococcus aureus*, recombinant streptolysin O (SLO), Digitonin and recombinant acid Sphingomyelinase (aSMase) from *Bacillus cereus* was purchased from Sigma (Kawasaki, Japan).

Liver infection and parasite burden determination. For sporozoite infections, mice were injected with 2 × 10⁴ sporozoites, in 200 µL of DMEM via intravenous injection. At different timepoints after sporozoite infection (6, 24, 48 h after

infection), livers of infected mice were collected into 3 mL of denaturing solution (4 M guanidium thiocyanate (Sigma), 25 mM sodium citrate (Sigma), 0.5% sarcosyl (Sigma) in MilliQ water treated with DEPC (Sigma)). Livers were then mechanically homogenized using 1 mm diameter silica beads (BioSpec Products, Bartlesville, OK, USA) in MiniBeadBeater homogenizer (BioSpec Products) for 2 min. After mechanical disruption of the tissue, 100 μ L of homogenate was used to extract RNA, using NZY Total RNA Isolation Kit (NZYTech, Lisboa, Portugal), as per manufacturer's instructions. In all, 1 μ g of extracted RNA was converted into cDNA using NZY First-Strand cDNA Synthesis Kit (NZYTech), as per manufacturer's instructions. cDNA was then used for quantitative Polymerase Chain Reaction (qPCR), by measuring the abundance of *Pb18s* RNA, compared with *MmHprt* RNA using either ViiA 7 (384-well plates, using QuantStudio, v1.3 software) or 7500Fast (96-well plates, using 7500Fast, v2.3 software) Real-Time PCR Systems (Thermo Fisher Scientific) using iTaq Universal SYBR Green Supermix (Bio-Rad Laboratories, Hercules, CA, USA). Analysis of results was performed using the $\Delta\Delta C_T$ method after export of C_T values from the collection softwares:

$$\Delta C_t = C_t^{\text{Gene of interest}} - C_t^{\text{Housekeeping}} \quad (1)$$

$$\Delta\Delta C_t = \Delta C_t^{\text{Experimental}} - \Delta C_t^{\text{Control}} \quad (2)$$

$$\text{Relative Gene expression} = 2^{[\Delta\Delta C_t]} \quad (3)$$

Primers used for liver load determination:

Pb18s – forward primer: AAGCATTAATAAAGCGAATACATCCTTAC

Pb18s – reverse primer: GGAGATTGGTTTTGACGTTTATGTG

MmHprt – forward primer: TTTGCTGACTGCTGGATTAC

MmHprt – reverse primer: CAAGACATTCTTCCAGTTAAAGTTG

Infection of cells. To infect cells, the required number of sporozoites were suspended in complete DMEM and incubated with cells and centrifuged for 5 min at 1 600 \times g. Cells were incubated for 2 hours at 37 °C, with a 5% CO₂ atmosphere, after which the medium was replaced with complete DMEM supplemented with 0.3% Fungizone (Gibco). For some experiments, compounds or rEXP2 protein was added during infection. These materials were either added to the cells concomitantly with sporozoites or added to the cells 1 hour after the sporozoites, as described in the figure legends.

Expression of parasite genes during invasion. After sporozoites and cells were incubated for the appropriate amount of time, mRNA from samples was extracted using NZY Total RNA Isolation Kit (NZYTech), as per manufacturer's instructions. In all, 1 μ g of extracted RNA was converted into cDNA using NZY First-Strand cDNA Synthesis Kit (NZYTech), as per manufacturer's instructions. cDNA was then used for qPCR, by measuring the abundance of *PbEXP2*, *PbEXP1* and *PbGAP45* was compared with *Pb18s* RNA using either ViiA 7 (384-well plates, using QuantStudio software, v1.3) or 7500Fast (96-well plates, using 7500Fast software, v2.3) Real-Time PCR Systems (Thermo Fisher Scientific) using iTaq Universal SYBR Green Supermix (Bio-Rad Laboratories, Hercules, CA, USA). Analysis of results was performed using the $\Delta\Delta C_T$ method as described above.

Primers used for determination of expression of *Plasmodium* invasion genes:

Pb18s – forward primer: AAGCATTAATAAAGCGAATACATCCTTAC

Pb18s – reverse primer: GGAGATTGGTTTTGACGTTTATGTG

PbEXP2 – forward primer: ACGATCCAGGTTTGATTTG

PbEXP2 – reverse primer: TGGTAATAGTGGGACATTC

PbGAP45 – forward primer: GTGGAGTAGTCTTTAAGG

PbGAP45 – reverse primer: GTGGAGTAGTCTTTAAGG

PbEXP1 – forward primer: AGGGAAGACATCCATCCAAATTTGG

PbEXP1 – reverse primer: TGAAGATTGGCATGTTAAGTGGTG

IFA of hepatoma cells. To process cells and parasites for IFA, experiments were performed either on black glass-bottom 96-well plates or on no. 1 grade 12 mm diameter glass coverslips. Cells and parasites were fixed at the appropriate time point in 4% paraformaldehyde (Santa Cruz Biotechnology, Dallas, TX, USA) for 10–20 min at room temperature. Cell and parasite fixed material were then blocked and permeabilized with 5% bovine serum albumin (BSA, NZYTech), 0.2% saponin (Sigma) in PBS for at least 30 min at room temperature. Cells and parasites were stained with the appropriate primary antibodies (diluted in 5% BSA, 0.2% saponin in PBS) for 2 h at room temperature in a humid chamber. Samples were washed three times with PBS for 10 min. After washing, samples were stained with appropriate fluorescent secondary antibodies (Thermo Fisher Scientific) (diluted 1:300 in 5% BSA 0.2% saponin in PBS) and with 1 mg/mL Hoechst 33342 (Thermo Fisher Scientific) for 1 hr at room temperature in a humid chamber. Stained samples were washed three times with PBS for 10 min. After the final wash, coverslips were mounted on glass slides using a drop of Fluoromount-G (Thermo Fisher Scientific). If black glass-bottom 96-well plates were being used, 50 μ L of Fluoromount G was placed on the stained well.

For in and out experiments, fixed samples were incubated with α *PbCSP* antibody before permeabilization was performed, to stain parasites that would be outside cells. After incubation with α *PbCSP* antibody, samples were washed with

PBS and were permeabilized and blocked using 5% BSA, 0.2% saponin in PBS. After permeabilization, samples were incubated with α *PbUIS4* antibody and the staining progressed as explained above. More than 40 sporozoites were imaged per replicate per parasite line.

For time-course analysis, samples were imaged using either Leica DM5000B (Leica, Wetzlar, Germany), Zeiss Axiovert 200 M or Zeiss Cell Observer (Zeiss, Oberkochen, Germany), which are all widefield fluorescence microscopes, using a \times 20 dry objective. Data were collected using Leica DFC Twain (v7.7.1), Metamorph (v7.7.9.0), and ZEN 2 (Blue version), respectively.

The primary antibodies used were goat α *PbUIS4* (1:1000 dilution, Siggen, Cantanhede, Portugal); mouse α *PbCSP* (1:1000 dilution, clone 3D11, Malaria Research and Reference Reagent Resource Center, MR4, BEI Resources, ATCC); mouse α *PfEXP2*⁶⁸ (1:500 dilution, clone 7.7, The European Malaria Reagent Repository, Edinburgh, Scotland, UK); rabbit α *PfEXP2*⁵³ (1:500 dilution, a kind gift from the laboratory of Brendan Crabb).

Sporozoite staining. To stain for sporozoite proteins, 5×10^4 freshly dissected sporozoites were incubated in DMEM medium or DMEM containing 10% FCS at 37 °C on glass coverslips. After 30 min of incubation, sporozoites were fixed in 4% paraformaldehyde for 10–20 min at room temperature. Fixed sporozoites were permeabilized using ice-cold methanol for 5 min at –20 °C. After washing, sporozoites were blocked and stained as described above. Coverslips were imaged using Zeiss LSM 710 confocal laser point-scanning fluorescence microscope (using ZEN 2 software, Blue edition), using \times 63 or \times 100 oil objective. The primary antibodies used were goat α *PbUIS4* (1:500 dilution, Siggen, Cantanhede, Portugal); mouse α *PbCSP* (1:1000 dilution, clone 3D11, MR4); mouse α *PfEXP2* (1:300 dilution, clone 7.7, The European Malaria Reagent Repository, Edinburgh, Scotland, UK); rabbit α *PfEXP2* (1:300 dilution, a kind gift from the laboratory of Brendan Crabb⁵³) and rabbit α *PbTRAP* (1:1000 dilution, a kind gift from the laboratory of Joana Tavares⁶⁹) and mouse α *PbRON4* (1:300 dilution, a kind gift from the laboratory of Maryse Lebrun⁷⁰).

For colocalization experiments, the plug-in Coloc 2 from FIJI image analysis software was used.

Quantification of EXP2-positive and EXP2-negative sporozoites in EXP2 cKO sporozoite population. To distinguish which sporozoites would be EXP2-sufficient and EXP2-deficient, immunofluorescence analysis was performed in WT or EXP2 cKO freshly dissected sporozoites stained with α EXP2 antibody. To assess the background fluorescence intensity of the staining, we also imaged sporozoites that were not stained with α EXP2 antibody. This allowed us to create a cutoff value for the intensity of EXP2 staining, below which EXP2 cKO sporozoites would be considered as EXP2-deficient (see Supplementary Fig. 1a–b) for an example of how sporozoites were analyzed). More than 50 sporozoites or EEFs were imaged per replicate per parasite line.

Gliding assay. For gliding assays, 5×10^4 sporozoites were incubated in complete DMEM medium at 37 °C on glass coverslips. After 30 min of incubation, sporozoites were fixed in 4% paraformaldehyde for 10–20 min at room temperature. Fixed sporozoites were blocked as described above and only stained with α CSP antibody (1:1000 dilution, clone 3D11) and an anti-mouse secondary antibody (1:300 dilution) and Hoechst. Coverslips were imaged using a Leica DM5000B widefield fluorescence microscope and \times 40 dry objective, using Leica DFC Twain (v7.7.1) software. Since CSP is shed in a circular fashion during sporozoite gliding, sporozoite motility can be quantified by counting the circles of CSP (termed trails) produced by each individual sporozoite. Sporozoites were divided into three groups (no trails; 1–10 trails; >10 trails) based on the number of trails that it displayed (see Supplementary Fig. 1e for an example of how sporozoites were separated between these groups). More than 75 sporozoites were imaged per replicate per parasite line.

Flow cytometry analysis of cell traversal. To quantify the level of traversal, HepG2 cells and sporozoites were incubated in the presence of 0.5 mg/mL of 10 kDa Dextran-Rhodamine (Thermo Fisher Scientific) in complete DMEM at 37 °C. The dextran molecule is passively taken up by cells that have been traversed and is detected because of the Rhodamine dye, which has Excitation/Emission maxima at 570/590 nm. Data collection was performed using BD Accuri C6 cytometer (Franklin Lakes, New Jersey, USA) and Accuri C6 software (v1.0.264.21) software was used. Data analysis was performed using FlowJo X software (FlowJo LLC, Ashland, OR, USA) (see Supplementary Fig. 1f for the gating strategy used).

Sporozoite genomic DNA purification. After dissection from salivary glands, sporozoites were pelleted by centrifugation in a table top centrifuge (Eppendorf) at maximum speed for 15 min. Genomic DNA was purified using NZY Blood gDNA Isolation kit (NZYTech). Gene abundance in sporozoite genomic DNA was analyzed using either ViiA 7 (384-well plates, using QuantStudio v1.3 software) or 7500Fast (96-well plates using 7500Fast v2.3 software) Real-Time PCR Systems (Thermo Fisher Scientific) using iTaq Universal SYBR Green Supermix (Bio-Rad). Analysis of results was performed using the $\Delta\Delta C_T$ method described above.

Primers used for assessing EXP2 recombination/excision:

Pbdlfr – forward primer: GTTGGTTCGCTAACTGCATC

Pbdhfr – reverse primer: CTGTTTACCTTCTACTGAAGAGG

Pbbsp70 – forward primer: TGCAGCAGATAATCAAACCTC

Pbbsp70 – reverse primer: ACTTCAATTTGTGGAACACC

Blood stage parasite protein isolation. For preparation of samples from blood stages, BALB/c mice were infected with *P. berghei* NK65 EXP2-HA (*PbEXP2-HA*) and parasites multiplied until reaching a parasitemia of ~10%. Mice were sacrificed using isoflurane (Abbott Laboratories, Lake Bluff, IL, USA) overdose and blood was removed by heart puncture. Red blood cells were suspended in PBS and pelleted by centrifugation at 450 × g for 5 min without brake. Pelleted red blood cells were lysed using 0.05% Saponin containing cOmplete Protease Inhibitor Cocktail (Sigma) in PBS for 5 min of ice. Parasites were pelleted at 2500 × g for 5 min and were lysed in 500 µL of radioimmunoprecipitation assay (RIPA) buffer with 1% sodium dodecyl sulphate (SDS) for 1 h on ice.

Sporozoite secretion assay. Sporozoites were dissected as described above and purified using 17% Accudenz solution⁷¹, where dissected sporozoites were placed on top of a 17% Accudenz solution and were centrifuged for 20 min at 2500 × g at room temperature. In all, 1 mL of the top fraction was removed and centrifuged at 20,000 × g for 10 min. Pelleted sporozoites were resuspended in simple DMEM and counted. In all, 2 × 10⁵ sporozoites were then transferred into a tube that would be kept on ice or at 37 °C, with or without 10% FCS. After 30 to 120 min of incubation, sporozoites were pelleted again by centrifuging at 20,000 × g for 10 min. Supernatants was separated from the pelleted sporozoites and sporozoites were lysed with RIPA buffer with 1% SDS for 1 h on ice. RIPA buffer comprised 50 mM Tris-HCl (NZYTech), 150 mM NaCl (Sigma), 5 mM EDTA (Sigma), 10 mM NaF (Sigma), 1% Triton X-100 (USB Corporation, Cleveland, OH, USA), 0.5% sodium deoxycholate (AppliChem, Maryland Heights, MO, USA). Following lysis, NuPAGE loading dye (Thermo Fisher Scientific) and β-mercaptoethanol (to a final concentration of 10%, Sigma) were added to all samples. Samples were boiled for 15 min at 95 °C.

WB analysis. Samples were separated in 10% Acrylamide gels and transferred to 0.2 µm pore-sized Nitrocellulose membranes (Bio-Rad). Membranes were placed inside Falcon tubes and blocked with 5% skim milk (Nestle, Vevey, Switzerland) overnight at 4 °C, on a tube roller. Membranes were then incubated with the appropriate primary antibodies, diluted in 5% skim milk, for 1 hour at room temperature. Membranes were washed with 0.1% Tween 20 (Sigma) in PBS, three times for 10 minutes. Membranes were then incubated with the appropriate secondary antibodies, conjugated to Horseradish peroxidase diluted in 5% skim milk, for 1 hour at room temperature, after which they were washed again three times for 10 minutes. WB were revealed using Amersham ECL Prime Blotting Detection Reagent (GE Healthcare) on the ChemiDoc XRS + system (Bio-Rad) using ImageLab software (v5.2.1). The primary antibodies used were rabbit αHA tag (1:1000 dilution, clone C29F4, Cell Signaling Technology, Danvers, MA, USA); mouse αPbCSP (1:5000 dilution, clone 3D11, MR4) and rabbit αPbBiP (1:1000 dilution, GenScript Biotech. Corp, New Jersey, NJ, USA). The secondary antibodies used were goat anti-mouse IgG F(ab')₂, polyclonal antibody horseradish peroxidase (HRP) conjugate (1:5000 dilution, Enzo Life Sciences, Lausen, Switzerland); anti-rabbit IgG, HRP-linked antibody (1:3000 dilution, Cell Signaling Technology).

To assess the amount of secreted EXP2 protein, the intensity of the EXP2 band in the supernatant fraction was normalized to the intensity of the CSP band intensity at the respective time point in the pellet fraction. These values were further normalized to the ratio of EXP2/CSP in the pellet fraction at time zero (no stimulation).

All membranes used for this manuscript are presented in Supplementary Fig. 4.

Acid sphingomyelinase knockdown. Acid sphingomyelinase (gene name SMPD1) and Scramble short-hairpin RNAs were obtained from Mission shRNA (Sigma). In all, 800 ng/well of shRNAs were mixed with OptiMEM (Thermo Fisher Scientific) containing 0.3% Lipofectamine RNAiMax (Thermo Fisher Scientific) and added to 100,000 HepG2 cells. Cells were infected with sporozoites 48 hours after transfection. Samples were fixed 2 hours after infection and were stained as described above.

To assess the amount of knockdown of acid sphingomyelinase, mRNA was collected from uninfected cells, lysed at the time of infection. To quantify the amount of acid sphingomyelinase RNA, RNA was extracted using NZY Total RNA Isolation Kit, following manufacturer's instructions. 1 µg of extracted RNA was converted into cDNA using NZY First-Strand cDNA Synthesis Kit (NZYTech), as per manufacturer's instructions. cDNA was then used for qPCR, by measuring the abundance of *HuSMPD1* RNA, compared with *HuHPRT* RNA using either ViiA 7 (384-well plates, using QuantStudio v1.3 software) or 7500Fast (96-well plates, using 7500Fast v2.3 software) Real-Time PCR Systems (Thermo Fisher Scientific) using iTaq Universal SYBR Green Supermix (Bio-Rad Laboratories, Hercules, CA, USA). Analysis of results was performed using the ΔΔC_T method described above.

Primers used to assess aSMase knockdown:

HsHPRT – forward primer: TTTGCTGACCTGCTGGATTAC

HsHPRT – reverse primer: CAAGACATCTTCCAGTTAAAGTTG

HuSMPD1 – forward primer: GGCCACATTTGGGAAAGTT

HuSMPD1 – reverse primer: TTCACCGGATGATCTTGCCT

Electron microscopy. Immuno-electron microscopy of purified parasites was performed according to Tokuyasu technique. In brief, the pellet was chemically fixed in 0.1 M phosphate buffer containing 2% formaldehyde and 0.2% glutaraldehyde, embedded in food-grade gelatine and cryopreserved in 2.3 M sucrose. Gelatine blocks were shaped in cubes and froze in liquid nitrogen and sectioned at –110 °C using a cryo-ultramicrotome (UC7 and FC7, Leica) to generate 70 nm sections. Sections were collected and thawed in a mixture of 2.3 M sucrose and 2% methylcellulose. Immuno-labeling was done in 1% bovine serum albumin and 0.8% gelatine from cold water fish skin in PBS with rabbit αEXP2 primary antibody (1:500 dilution) and 15 nm gold coupled Protein A (CMC Utrecht, The Netherlands, 1:50 dilution). After immuno-labeling, the sections were stained and mounted in a mixture of 3% (aq.) uranyl acetate and 2% methylcellulose. Images were recorded using a Hitachi H-7650 electron microscope (Hitachi, Tokyo, Japan) at 100 kV acceleration.

Image analysis. All immunofluorescence images were processed using FIJI software (version 1.52i) and macros written for each analysis to automate it. For WB images, the software ImageLab was used (version 5.2.1)

Flow cytometry analysis. Flow cytometry data were analyzed using FlowJo version X software (FlowJo LLC, Ashland, OR, USA).

Statistical analysis. Statistical analysis was performed using GraphPad Prism 5 software (GraphPad, La Jolla, CA). Mann-Whitney *U* test was used to assess significance of differences observed between two groups and non-linear regression was performed to assess Desipramine inhibitory effects on invasion. Raw data and a description of statistical tests used is provided in Supplementary Information. Plots and figures were prepared using Adobe Illustrator (version CS4).

Reporting summary. Further information on research design is available in the Nature Research Reporting Summary linked to this article.

Data availability

Replicates of WBs are provided in Supplementary Fig. 4. All other data are available from the authors upon reasonable request. Source data are provided with this paper.

Received: 3 May 2020; Accepted: 8 October 2020;

Published online: 06 November 2020

References

- Vaughan, A. M. & Kappe, S. H. I. Malaria parasite liver infection and exoerythrocytic biology. *Cold Spring Harb. Perspect. Med.* **7**, a025486 (2017).
- Coppi, A., Pinzon-Ortiz, C., Hutter, C. & Sinnis, P. The Plasmodium circumsporozoite protein is proteolytically processed during cell invasion. *J. Exp. Med.* **201**, 27–33 (2005).
- Bosch, J. et al. Aldolase provides an unusual binding site for thrombospondin-related anonymous protein in the invasion machinery of the malaria parasite. *Proc. Natl Acad. Sci. USA* **104**, 7015–7020 (2007).
- Rodrigues, C. D. et al. Host scavenger receptor SR-BI plays a dual role in the establishment of malaria parasite liver infection. *Cell Host Microbe* **4**, 271–282 (2008).
- Yalaoui, S. et al. Scavenger receptor BI boosts hepatocyte permissiveness to plasmodium infection. *Cell Host Microbe* **4**, 283–292 (2008).
- Silvie, O. et al. Hepatocyte CD81 is required for Plasmodium falciparum and Plasmodium yoelii sporozoite infectivity. *Nat. Med.* **9**, 93–96 (2003).
- Risco-Castillo, V. et al. CD81 is required for prophylactic discharge during host cell invasion by Plasmodium yoelii sporozoites. *Cell Microbiol.* **16**, 1533–1548 (2014).
- Ishino, T., Chinzei, Y. & Yuda, M. Two proteins with 6-cys motifs are required for malarial parasites to commit to infection of the hepatocyte. *Mol. Microbiol.* **58**, 1264–1275 (2005).
- Manzoni, G. et al. Plasmodium P36 determines host cell receptor usage during sporozoite invasion. *Elife* **6**, 1–24 (2017).
- Kaushansky, A. et al. Malaria parasites target the hepatocyte receptor EphA2 for successful host infection. *Science* **350**, 1089–1092 (2015).
- Langlois, A.-C., Marinach, C., Manzoni, G. & Silvie, O. Plasmodium sporozoites can invade hepatocytic cells independently of the ephrin receptor A2. *PLoS ONE* **13**, 1–13 (2018).
- Prudêncio, M. et al. Kinome-side RNAi screen implicates at least 5 host hepatocyte kinases in Plasmodium sporozoite infection. *PLoS Pathog.* **4**, e1000201 (2008).
- Bando, H. et al. CXCR4 regulates Plasmodium development in mouse and human hepatocytes. *J. Exp. Med.* **216**, 1733–1748 (2019).

14. Morisaki, J. H., Heuser, J. E. & Sibley, L. D. Invasion of *Toxoplasma gondii* occurs by active penetration of the host cell. *J. Cell Sci.* **108**, 2457–2464 (1995).
15. Dobrowolski, J. M. & Sibley, L. D. *Toxoplasma* invasion of mammalian cells is powered by the actin cytoskeleton of the parasite. *Cell* **84**, 933–939 (1996).
16. Sibley, L. D. Intracellular parasite invasion strategies. *Science* **304**, 248–253 (2004).
17. Gonzalez, V. et al. Host cell entry by apicomplexa parasites requires actin polymerization in the host cell. *Cell Host Microbe* **5**, 259–272 (2009).
18. Bargieri, D. et al. Host cell invasion by apicomplexan parasites: the junction conundrum. *PLoS Pathog.* **10**, 1–9 (2014).
19. Matz, J. M. et al. The *Plasmodium berghei* translocon of exported proteins reveals spatiotemporal dynamics of tubular extensions. *Sci. Rep.* **5**, 12532 (2015).
20. Matthews, K. et al. The *Plasmodium* translocon of exported proteins (PTEX) component thioredoxin-2 is important for maintaining normal blood-stage growth. *Mol. Microbiol.* **89**, 1167–1186 (2013).
21. Ho, C.-M. et al. Malaria parasite translocon structure and mechanism of effector export. *Nature* **561**, 70–75 (2018).
22. de Koning-Ward, T. F. et al. A newly discovered protein export machine in malaria parasites. *Nature* **459**, 945–949 (2009).
23. Elsworth, B. et al. PTEX is an essential nexus for protein export in malaria parasites. *Nature* **511**, 587–591 (2014).
24. Beck, J. R., Muralidharan, V., Oksman, A. & Goldberg, D. E. PTEX component HSP101 mediates export of diverse malaria effectors into host erythrocytes. *Nature* **511**, 592–595 (2014).
25. Riglar, D. T. et al. Spatial association with PTEX complexes defines regions for effector export into *Plasmodium falciparum*-infected erythrocytes. *Nat. Commun.* **4**, 1415 (2013).
26. Gold, D. A. et al. The *Toxoplasma* dense granule proteins GRA17 and GRA23 mediate the movement of small molecules between the host and the parasitophorous vacuole. *Cell Host Microbe* **17**, 642–652 (2015).
27. Garten, M. et al. EXP2 is a nutrient-permeable channel in the vacuolar membrane of *Plasmodium* and is essential for protein export via PTEX. *Nat. Microbiol.* **3**, 1090–1098 (2018).
28. Kalanon, M. et al. The *Plasmodium* translocon of exported proteins component EXP2 is critical for establishing a patent malaria infection in mice. *Cell. Microbiol.* **18**, 399–412 (2016).
29. Lacroix, C. et al. FLP/FRT-mediated conditional mutagenesis in pre-erythrocytic stages of *Plasmodium berghei*. *Nat. Protoc.* **6**, 1412–1428 (2011).
30. Mota, M. M. et al. Migration of *Plasmodium* sporozoites through cells before infection. *Science* **291**, 141–144 (2001).
31. Frischknecht, F. & Matuschewski, K. *Plasmodium* sporozoite biology. *Cold Spring Harb. Perspect. Med.* **7**, a025478 (2017).
32. Sultan, A. A. et al. TRAP is necessary for gliding motility and infectivity of *Plasmodium* sporozoites. *Cell* **90**, 511–522 (1997).
33. Mueller, A.-K. et al. *Plasmodium* liver stage developmental arrest by depletion of a protein at the parasite-host interface. *Proc. Natl. Acad. Sci. USA* **102**, 3022–3027 (2005).
34. Hanson, K. K. et al. Torins are potent antimalarials that block replenishment of *Plasmodium* liver stage parasitophorous vacuole membrane proteins. *Proc. Natl. Acad. Sci. USA* **110**, E2838–E2847 (2013).
35. Sharma, P. & Chitnis, C. E. Key molecular events during host cell invasion by Apicomplexan pathogens. *Curr. Opin. Microbiol.* **16**, 432–437 (2013).
36. Silvie, O. et al. A role for apical membrane antigen 1 during invasion of hepatocytes by *Plasmodium falciparum* sporozoites. *J. Biol. Chem.* **279**, 9490–9496 (2004).
37. Annoura, T. et al. Two *Plasmodium* 6-Cys family-related proteins have distinct and critical roles in liver-stage development. *FASEB J.* **28**, 2158–2170 (2014).
38. Coppi, A. et al. Heparan sulfate proteoglycans provide a signal to *Plasmodium* sporozoites to stop migrating and productively invade host cells. *Cell Host Microbe* **2**, 316–327 (2007).
39. Hakamada, K., Watanabe, H., Kawano, R., Noguchi, K. & Yohda, M. Expression and characterization of the *Plasmodium* translocon of the exported proteins component EXP2. *Biochem. Biophys. Res. Commun.* **482**, 6–11 (2017).
40. Risco-Castillo, V. et al. Malaria sporozoites traverse host cells within transient vacuoles. *Cell Host Microbe* **18**, 593–603 (2015).
41. Siau, A. et al. Temperature shift and host cell contact up-regulate sporozoite expression of *Plasmodium falciparum* genes involved in hepatocyte infection. *PLoS Pathog.* **4**, e1000121 (2008).
42. Yang, A. S. P. et al. Cell traversal activity is important for *Plasmodium falciparum* liver infection in humanized mice. *Cell Rep.* **18**, 3105–3116 (2017).
43. Castro-Gomes, T., Corrotte, M., Tam, C. & Andrews, N. W. Plasma membrane repair is regulated extracellularly by proteases released from lysosomes. *PLoS ONE* **11**, 1–26 (2016).
44. Gouaux, J. E. et al. Subunit stoichiometry of staphylococcal alpha-hemolysin in crystals and on membranes: a heptameric transmembrane pore. *Proc. Natl. Acad. Sci. USA* **91**, 12828–12831 (1994).
45. Füssle, R. et al. On the mechanism of membrane damage by *Staphylococcus aureus* alpha-toxin. *J. Cell Biol.* **91**, 83–94 (1981).
46. Bhakdi, S., Tranum-Jensen, J. & Sziegoleit, A. Mechanism of membrane damage by streptolysin-O. *Infect. Immun.* **47**, 52–60 (1985).
47. Fernandes, M. C. & Andrews, N. W. Host cell invasion by *Trypanosoma cruzi*: a unique strategy that promotes persistence. *FEMS Microbiol. Rev.* **36**, 734–747 (2012).
48. Fernandes, M. C. et al. *Trypanosoma cruzi* subverts the sphingomyelinase-mediated plasma membrane repair pathway for cell invasion. *J. Exp. Med.* **208**, 909–921 (2011).
49. Chen, T.-W. et al. Ultrasensitive fluorescent proteins for imaging neuronal activity. *Nature* **499**, 295–300 (2013).
50. Bischof, H. et al. Novel genetically encoded fluorescent probes enable real-time detection of potassium in vitro and in vivo. *Nat. Commun.* **8**, 1–11 (2017).
51. Albouz, S. et al. Effect of tricyclic antidepressants on sphingomyelinase and other sphingolipid hydrolases in C6 cultured glioma cells. *Neurosci. Lett.* **36**, 311–315 (1983).
52. Yoshida, Y. et al. Reduction of acid sphingomyelinase activity in human fibroblasts induced by AY-9944 and other cationic amphiphilic drugs1. *J. Biochem.* **98**, 1669–1679 (1985).
53. Bullen, H. E. et al. Biosynthesis, localization, and macromolecular arrangement of the *Plasmodium falciparum* translocon of exported proteins (PTEX). *J. Biol. Chem.* **287**, 7871–7884 (2012).
54. Koning-ward, T. F. De, Dixon, M. W. A., Tilley, L. & Gilson, P. R. *Plasmodium* species: master renovators of their host cells. *Nat. Rev. Microbiol.* **14**, 494–507 (2016).
55. Low, L. M. et al. Deletion of *Plasmodium falciparum* protein RON3 affects the functional translocation of exported proteins and glucose uptake. *MBio* **10**, 1–11 (2019).
56. Vijayan, K. et al. *Plasmodium* secretion induces hepatocyte lysosome exocytosis promotes parasite entry. *iScience* **21**, 603–611 (2019).
57. Lam, J. G. T. et al. Host cell perforation by listeriolysin O (LLO) activates a Ca²⁺-dependent cPKC/Rac1/Arp2/3 signaling pathway that promotes *Listeria monocytogenes* internalization independently of membrane resealing. *Mol. Biol. Cell* **29**, 270–284 (2018).
58. Grassmé, H. et al. Acidic sphingomyelinase mediates entry of *N. gonorrhoeae* into nonphagocytic cells. *Cell* **91**, 605–615 (1997).
59. Luisoni, S. et al. Co-option of membrane wounding enables virus penetration into cells. *Cell Host Microbe* **18**, 75–85 (2015).
60. Fox, T. E. et al. Ceramide recruits and activates protein kinase C ζ (PKC ζ) within structured membrane microdomains. *J. Biol. Chem.* **282**, 12450–12457 (2007).
61. Fiory, F. et al. Protein kinase C- ζ and protein kinase B regulate distinct steps of insulin endocytosis and intracellular sorting. *J. Biol. Chem.* **279**, 11137–11145 (2004).
62. Voisset, C. et al. Ceramide enrichment of the plasma membrane induces CD81 internalization and inhibits hepatitis C virus entry. *Cell. Microbiol.* **10**, 606–617 (2008).
63. Silvie, O. et al. Cholesterol contributes to the organization of tetraspanin-enriched microdomains and to CD81-dependent infection by malaria sporozoites. *J. Cell Sci.* **119**, 1992–2002 (2006).
64. Gomes-Santos, C. S. S. et al. Transition of *Plasmodium* sporozoites into liver stage-like forms is regulated by the RNA binding protein Pumilio. *PLoS Pathog.* **7**, e1002046 (2011).
65. Gueirard, P. et al. Development of the malaria parasite in the skin of the mammalian host. *Proc. Natl. Acad. Sci.* **107**, 18640–18645 (2010).
66. Yamauchi, L. M., Coppi, A., Snounou, G. & Sinnis, P. *Plasmodium* sporozoites trickle out of the injection site. *Cell Microbiol.* **9**, 1215–1222 (2007).
67. Matthews, K. M., Kalanon, M. & de Koning-Ward, T. F. Uncoupling the threading and unfolding actions of *Plasmodium* HSP101 reveals differences in export between soluble and insoluble proteins. *MBio* **10**, 1–18 (2019).
68. Hall, R. et al. Antigens of the erythrocytic stages of the human malaria parasite *Plasmodium falciparum* detected by monoclonal antibodies. *Mol. Biochem. Parasitol.* **7**, 247–265 (1983).
69. Matuschewski, K., Nunes, A. C., Nussenzweig, V. & Ménard, R. *Plasmodium* sporozoite invasion into insect and mammalian cells is directed by the same dual binding system. *EMBO J.* **21**, 1597–1606 (2002).
70. Suarez, C. et al. A lipid-binding protein mediates rhoptry discharge and invasion in *Plasmodium falciparum* and *Toxoplasma gondii* parasites. *Nat. Commun.* **10**, 4041 (2019).
71. Kennedy, M. et al. A rapid and scalable density gradient purification method for *Plasmodium* sporozoites. *Malar. J.* **11**, 421 (2012).

Acknowledgements

We thank Ana Parreira for producing *P. berghei*-infected *Anopheles* mosquitoes, Andreia Pinto for the Electron Microscopy work, the Rodent, Flow Cytometry and (especially)

Bioimaging Facilities of iMM JLA, Masafumi Yodha for the recombinant EXP2 plasmid, Mafalda Pimentel for the Gcamp6f plasmid, Joana Tavares for the α PbTRAP antibody, Maryse Lebrun and Margarida Ruivo for the α PbRON4 antibody and Paul Gilson for the Rb α PbEXP2 antibody. Funding: This work was supported by grants from the Fundação para a Ciência e Tecnologia (PTDC/BIM-MEC/1342/2014 to M.M.M.) and Institut Mérieux (MRG_20052016 to M.M.M.). V.Z.-L. and J.M.-V. were sponsored by FCT fellowships (SFRH/BPD/81953/2011 and SFRH/BD/52226/2013, respectively).

Author contributions

Conceptualization: J.M.-V., T.d.K.-W., V.Z.-L., M.M.M.; investigation: J.M.-V.; resources: F.J.E., T.d.K.-W.; writing—original draft: J.M.-V., T.d.K.-W., V.Z.-L., M.M.M.; writing—review and editing: J.M.-V., F.J.E., T.d.K.-W., V.Z.-L., M.M.M.; supervision: T.d.K.-W., V.Z.-L., M.M.M.; funding acquisition: V.Z.-L., M.M.M.

Competing interests

Authors declare no competing interests.

Additional information

Supplementary information is available for this paper at <https://doi.org/10.1038/s41467-020-19492-4>.

Correspondence and requests for materials should be addressed to V.Z.-L. or M.M.M.

Peer review information *Nature Communications* thanks Jake Baum, Louis Miller and the other, anonymous, reviewer(s) for their contribution to the peer review of this work. Peer reviewer reports are available.

Reprints and permission information is available at <http://www.nature.com/reprints>

Publisher's note Springer Nature remains neutral with regard to jurisdictional claims in published maps and institutional affiliations.



Open Access This article is licensed under a Creative Commons Attribution 4.0 International License, which permits use, sharing, adaptation, distribution and reproduction in any medium or format, as long as you give appropriate credit to the original author(s) and the source, provide a link to the Creative Commons license, and indicate if changes were made. The images or other third party material in this article are included in the article's Creative Commons license, unless indicated otherwise in a credit line to the material. If material is not included in the article's Creative Commons license and your intended use is not permitted by statutory regulation or exceeds the permitted use, you will need to obtain permission directly from the copyright holder. To view a copy of this license, visit <http://creativecommons.org/licenses/by/4.0/>.

© The Author(s) 2020